NONLINEAR OPTICAL INTERACTION IN PHOTONIC STRUCTURES

LEE CHOO YONG

FACULTY OF SCIENCE
UNIVERSITY OF MALAYA
KUALA LUMPUR

2013

NONLINEAR OPTICAL INTERACTION IN PHOTONIC STRUCTURES

LEE CHOO YONG

THESIS SUBMITTED IN FULFILMENT
OF THE REQUIREMENTS
FOR THE DEGREE OF DOCTOR OF PHILOSOPHY

FACULTY OF SCIENCE
UNIVERSITY OF MALAYA
KUALA LUMPUR

2013

UNIVERSITI MALAYA

ORIGINAL LITERARY WORK DECLARATION

Name of Candidate: LEE CHOO YONG (I.C. No.:770924-07-5987)

Registration/Matrix No.: SHC100040

Name of Degree: Doctor of Philosophy

Title of Thesis ("this Work"): Nonlinear Optical Interaction in Photonic Structures

Field of Study: Laser and Quantum Optics

I do solemnly and sincerely declare that:

(1) I am the sole author/writer of this Work;
(2) This work is original;
(3) Any use of any work in which copyright exists was done by way of fair dealing and for permitted purposes and any excerpt or extract from, or reference to or reproduction of any copyright work has been disclosed expressly and sufficiently and the title of the Work and its authorship have been acknowledged in this Work;
(4) I do not have any actual knowledge nor do I ought reasonably to know that the making of this work constitutes an infringement of any copyright work;
(5) I hereby assign all and every rights in the copyright to this Work to the University of Malaya ("UM"), who henceforth shall be owner of the copyright in this Work and that any reproduction or use in any form or by any means whatsoever is prohibited without the written consent of UM having been first had and obtained;
(6) I am fully aware that if in the course of making this Work I have infringed any copyright whether intentionally or otherwise, I may be subject to legal action or any other action as may be determined by UM.

Candidate's Signature 26.12.2013
Date

Subscribed and solemnly declared before,

Witness's Signature Date

Name: Dr. C.H. Raymond Ooi
Designation: Associate Professor

ABSTRACT

In this thesis, we investigate second harmonic generation (SHG) in nonlinear 1 dimensional (1D) bilayer periodic photonic crystal with various microstructure designs. The transfer matrix is used to model propagation of fundamental field (FF) and second harmonic field inside photonic crystal and numerical simulations are studied.

Firstly, we investigate SHG caused by interaction between continuous wave and dielectric magnetic photonic crystal. For nondispersive material, constant and real permittivity and permeability are used being good approximation for frequency far away from the resonant region. We find interesting features in the SH fields versus pump frequency and relative thickness of the bilayers for the same real value of permittivity and permeability but with different signs. Negative permeability is a substitute to periodical poling, giving stronger SH signal when one of the layers has negative refractive index. For certain parameters, backward and forward SH signals can be generated over a broad frequency range. For dispersive material, around resonant region, the FF spectra show more predictable features of bandgap and transparency windows. SH spectra show irregular patterns that depend on the magnetic and dielectric resonances of each layer. The results provide insights for designing efficient nonlinear photonics devices with dieletric-magnetic materials like efficient frequency converter.

Secondly, ultrashort pulse propagation and SHG in photonic crystal with superconducting layer is studied by using a combination of Fourier transform and transfer matrix for arbitary pulse propagation. Two fluid model is used to describe electromagnetic propagation in the superconducting layer at nonzero temperature. The focus is on temperature dependence and negative index using superconducting layer and magnetic materials when the superconducting transition frequency is close the magnetic resonance. At low temperature, the superconducting layer provides higher SHG conversion efficiency. Interesting features observed include output pump and second harmonic pulses that could be strongly modulated with the transmitted pulses being delayed by slow light effect. The result demonstrates a new mechanism for reshaping and converting short pulse by combining resonant multiple scattering and nonlinear optical process.

ABSTRAK

Dalam tesis ini, kami menyiasat penjanaan harmonik kedua (SHG) dalam kristal fotonik dua lapis berkala taklinear dengan pelbagai rekabentuk struktur mikro. Matrik pemindahan digunakan untuk memodel perambatan medan asas (FF) dan medan harmonik kedua (SH) dalam kristal fotonik dan simulasi berangka telah dikaji.

Pertamanya, kami menyiasat SHG disebabkan oleh interaksi gelombang berterusan dengan kristal fotonik dieletrik bermagnet. Bagi bahan tidak berserak, kebolehtelapan dan ketelusan malar nyata digunakan sebagai penghampiran yang baik untuk frekuensi jauh daripada rantau resonan. Kami mendapati ciri-ciri menarik dalam medan SH berbanding frekuensi pam dan ketebalan relatif dua lapis untuk kebolehtelapan dan ketelusan mempunyai nilai sama tetapi dengan tanda berlainan. Kebolehtelapan negatif ialah pengganti kepada pengutuban berkala, memberi isyarat SH yang kuat apabila satu daripada lapisan mempunyai indeks biasan negatif. Bagi parameter tertentu, isyarat SH ke belakang dan ke depan boleh dijanakan bagi linkungan frekuensi yang luas. Bagi bahan berserak, sekitar rantau resonan, spectra FF menunjuk ciri-ciri jurang jalur dan tetingkap ketelusan yang lebih mudah dijangkai. Bagaimanapun, spectra SH menunjukkan corak tidak teratur yang bersandar kepada resonan magnet dan dielectrik bagi setiap lapisan. Keputusan ini memberi gambaran untuk merekabentuk peranti fotonik tidak linear dengan bahan bermagnet, contohnya penukar frekuensi tidak linear yang cekap.

Keduanya, perambatan denyutan ultra pendek dalam kristal fotonik taklinear dikaji dengan menggunakan gabungan penjelmaan Fourier dan matrik pemindahan yang sah untuk perambatan denyutan sembarangan. Model dua bendalir diguna untuk menghuraikan perambatan denyutan dalam lapisan superkonduktor pada suhu bukan sifar. Tumpuan diberi kepada kesandaran suhu dan indek biasan negatif dan bahan magnet apabila frekuensi peralihan superkonduktor menghampiri resonan magnet. Pada suhu rendah, lapisan superkonduktor memberi kecekapan pengubahan SHG yang lebih tinggi. Ciri-ciri menarik diperhatikan ialah pam output dan denyutan SH yang boleh dimodulatkan dengan denyutan terambat adalah dilambatkan oleh kesan cahaya perlahan. Keputusan menunjukkan mekanisme yang baru untuk membentuk semula dan menukar denyutan pendek dengan menggabungkan penyelerakan resonan berganda dan proses optik tidak linear.

ACKNOWLEDGEMENTS

Firstly, I would like to express my heartfelt appreciation and gratitude to my thesis supervisor Assoc. Prof. C.H. Raymond Ooi whose great patience in his guidance and support throughout my doctorate training enabled me to develop an understanding of the subject as well as important principles of life. I must thank to members in Quantum and Laser Science group, Low K.C., Ho W.L., Khoo Y.Y., Nor Hazmin, Tan K.S. and Ng K.S. for their help during my study in Universiti Malaya. Many thanks are due to family for everything. Finally, my special gratitude is directed to my beloved wife May Pau for her patience, understanding and support; and also to my wonderful daughter Wen Zhu for her cheerful smile. Both of you have couloured my life.

Dedicated to Buddha Amitabha and my beloved family

PUBLICATIONS

JOURNAL PUBLICATIONS

1. Ooi, C. H. R. and Lee, C. Y. (2013). Nonlinear photonic crystal: effects of negative refractive indices and dispersion in the resonant region. *J. Opt. 15* (5) 055102

2. Ooi, C. H. R. and Lee, C. Y. (2013). Ultrashort pulse propagation and nonlinear frequency conversion in superconducting and magnetic photonic crystal. *Appl. Phys. B 112* (2) 193-201

CONFERENCE PUBLICATIONS

1. Lee, C. Y. and Ooi, C. H. R. (2012). Nonlinear photonic crystal with negative index materials. In IEEE 3rd International Conference on Photonics (p. 336-340). Penang, Malaysia: IEEE

TABLE OF CONTENTS

LIST OF FIGURES

LIST OF TABLES

LIST OF APPENDICES

CHAPTER 1

INTRODUCTION

1.1 Introduction

1.1.1 Overview

Light is understood to exhibit duality which are wave like and particle like (photon) characteristics as formulated in de Broglie hypothesis. The relationship of wavelength (λ) and momentum $(p)$of photon is expressed as

$$\lambda = \frac{h}{p} \tag{1.1}$$

where h is Planck constant. The detail qualitative analysis of microscopic light matter interaction requires understanding of quantum mechanic (Scully & Zubairy, 1997; Paul, 2004). However, classical wave propagation and Maxwell equations are adequate to model and investigate interaction between light and matter from macroscopic perspective (Sharmal, 2006). In this thesis, the interaction of photon in nonlinear optical medium would be investigated from classical physics stand point. Light consists of time varying electric and magnetic fields where their vectors **E** and **H** with same frequency ω are perpendicular to each other and also propagation vector **k** as shown in Figure 1.1. When the electric field vector **E** lies in one plane only, the light is plane polarized.

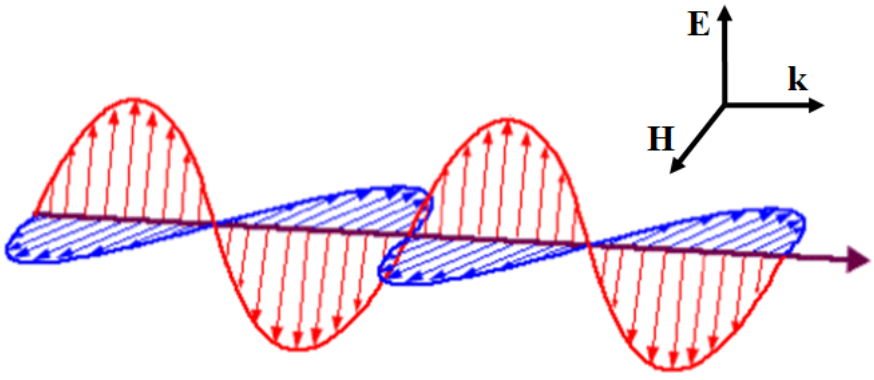

Figure 1.1: Electromagentic wave propagation with **E**, **H** and **k**.

The frequency and wave length of light spectrum are illustrated in Table 1.1 and Figure 1.2 (http://www.pas.rochester.edu/~blackman/ast104/spectrum.html). Light travels at light speed c, the relationship between frequency f and wavelength λ is

$$c = f\lambda \tag{1.2}$$

the energy of the photon for the region is

$$E = \frac{hc}{\lambda} \tag{1.3}$$

as we could see, the energy of photon increases with respect to frequency.

Table 1.1: Spectrum of light

Region	Frequency (Hz)	Wavelength (cm)	Energy (eV)
Gamma rays	$> 3 \times 10^{19}$	$< 10^{-9}$	$> 10^{5}$
X rays	$3 \times 10^{17} - 3 \times 10^{19}$	$10^{-7} - 10^{-9}$	$10^{3} - 10^{5}$
Ultraviolet	$7.5 \times 10^{14} - 3 \times 10^{17}$	$4 \times 10^{-5} - 10^{-7}$	$3 - 10^{3}$
Visible	$4.3 \times 10^{14} - 7.5 \times 10^{14}$	$7 \times 10^{-5} - 4 \times 10^{-5}$	$2 - 3$
Infrared	$3 \times 10^{12} - 4.3 \times 10^{14}$	$0.01 - 7 \times 10^{-5}$	$0.01 - 2$
Microwaves	$3 \times 10^{9} - 3 \times 10^{12}$	$10 - 0.01$	$10^{-5} - 0.01$
Radio frequency	$< 3 \times 10^{9}$	> 10	$< 10^{-5}$

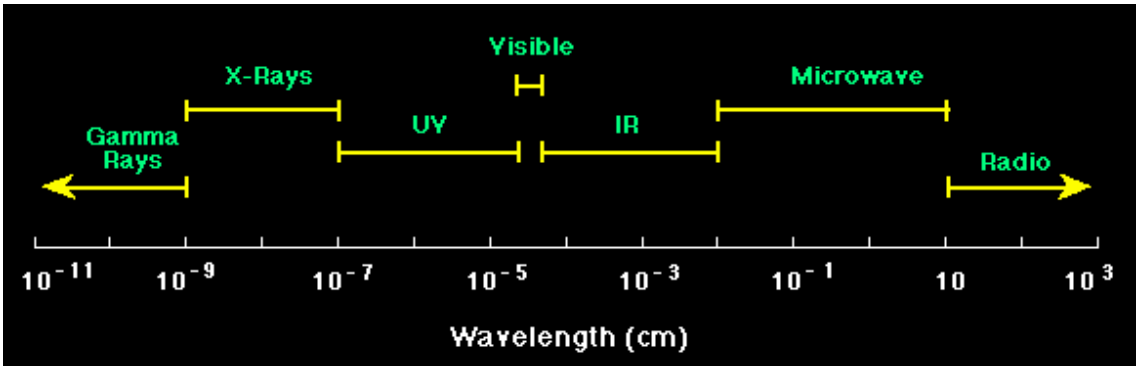

Figure 1.2: Light spectrum chart

Optical fiber uses wavelengths that are close to near infrared region which are normally known as telecommunication wavelengths, typically 850nm, 1310nm and 1550nm

and laser is used for transmission window at 1550nm (Roychoudhuri, 2008). Various methods have been used to generate photons at telecommunication wavelengths (Maywar, Nakano, & Agrawal, 2000; Usuki et al., 2006; Y. Z. Xu, Ren, Wang, Zhang, & Huang, 2007; Feng, Tian, Li, & Zhang, 2008; Arahira, Namekata, Kishimoto, Yaegashi, & Inoue, 2011; Ikuta et al., 2011). Besides that, Pliska *et al* investigated SHG at telecommunication wavelengths (Pliska et al., 2000). Before invention of laser, optical mediums are assumed to exhibit linear effect only when light wave propagates through. Superposition principle is used to predict characteristics of waveform when two or more light waves are propagating through the optical medium. The frequency of light does not change when it propagates through optical medium, besides that, refractive index and absorption coefficient are also constant for optical medium. The invention of laser in 1960's (Maiman, 1960) opened up the study of nonlinear optics. Amstrong *et al* presented both qualitative and quantitative analysis on light wave interaction in nonlinear dielectric medium (Amstrong, Bloembergen, Drucuing, & Pershan, 1962). Discovery of second harmonic generation (SHG) in 1960s (Franken, Hill, & Weinreich, 1961) leads to rapid development of nonlinear optics. They propagated ruby laser beam at 6942 Å through a quartz crystal and detected ultraviolet light at 3941 Å. Laser could operate in two modes which are continuous wave (CW) and short pulse. CW is considered as monochromatic and represented by a plane wave. In most of the applications, short pulse is used because it possesses extremely high intensity hence profoundly modify optical properties of medium.

Photonic crystal (PC) is periodic dielectric medium that could control propagation of light like semiconductor device control flow of electrons (Joannopoulos, Johnson, Winn, & Meade, 2008). In 1987, Sajeev John demonstrated strong localization of photon in engineered dielectric superlattice structure (Sajeev, 1987). In the same year, Yablonovitch also suggested the formation of electromagnetic bandgap in periodic dielectric structure caused by dispersion (Yablonovitch, 1987). When light propagates inside periodic material, it reflects at each interface of the dielectric layer with different refractive index, this phenomenon is known as Bragg scattering. This interference of light wave propagation leads to total reflection at certain frequency range. This region that prohibits wave propagation is known as photonic bandgap. Various nonlinear responses of light and PC as optical medium has been extensively studied to develop optical fiber (Agrawal, 1995;

Ferreira, 2011). In fact, the light wave band gap also exists in nature which is found in butterfly wings (Ghiradella, 1991; Argyros et al., 2002; Parker, 2002; Biro et al., 2003). The periodically ridge patterns on the wings reflect light which is seen by human eye.

Negative refractive index is one of the ground breaking finding in optics. The material that exhibits negative refractive index is often known as metamaterial or left handed material (LHM) whilst conventional material with normal refractive index is known as right handed material. Negative refraction in strongly refractive index modulated photonic crystal near band edge has been predicted in certain frequency range which is known as negative index state (Notomi, 2000). Gralak *et al* also predicted negative refraction in highly dispersive photonic crystal (Gralak, Enoch, & Tayeb, 2000). However, negative refraction demonstrated in the mentioned works should not be confused with metamaterials that uses negative permeability and permittivity to achieve negative refractive index. Contribution of Veselago and Pendry shall not be forgotten when we come into this topic (Boardman, 2011). Veselago started the theory of simultaneous negative permeability and permittivity that would result negative refractive index in 1968 (V. G. Veselago, 1968), however that theory has not been further explored due to unavailable nature material that exhibits neither negative permeability nor negative permittivity at that point of time. Only after 40 years, negative permeability is proven feasible with split ring resonator (SRR) that induce negative permeability around the magnetic resonance and also thin wire array that induce negative permittivity around dielectric resonance (Pendry & Smith, 1991).

The propagation of wave in layered media is extensively discussed by Yeh (Yeh, 1988). There are few methods being used to perform numerical simulation of electromagnetic wave propagation inside nonlinear optical medium like photonic crystal such as plane wave method (Leung & Liu, 1990; S. Guo & Sacharia, 2003), finite difference time domain (FDTD) (Kosmidou & Tsiboukis, 2003; Lavrinenko et al., 2004) and transfer matrix method (TMM). FDTD employs Yee cell which is much more complicated for programming (Yee, 1966). The 2×2 matrix in a generic form could be used to model coherent, partially coherent and interference in multilayer optical system (Katsidis & Siapkas, 2002). Tangential continuity of electric field in thin film optical medium is the fundamental principle which allows 2×1 vector matrix that describes forward and backward electric fields in particular layer to be connected with adjacent vector matrix

by introducing propagation matrix which describes phase change and dynamical matrix which describes refractive index change respectively. Hence, for period of N, multiplication of matrices is used to compute the reflectance and transmittance of light for the entire optical medium. Analytical expression of electromagnetic wave propagation equation in multi layer optical fibers with clearly identified **E** and **H** components demonstrated by Rahman *et al* is also useful for understanding the complicated propagation scenarios (Rahman, Choudhury, Kumar, & Yusoff, 2009).

In this thesis, a theoretical model of 1 dimensional finite periodic bilayer photonic crystal is developed by using transfer matrix with Maxwell equation and wave progagation equation. TMM for CW propagation is in space and time domain meanwhile TMM for ultrashort pulse is in space and frequency domain. Frankly speaking, the approach used for both CW and ultrashort pulse is the same although they are in different domain. The transfer matrix is developed step by step by taking complex electric field amplitudes for both FF and SH, change of phase and refractive index so that it is capable to compute the transmission and reflection in precise manner. Matlab is the programing language being used to simulate the results.

1.1.2 Motivation of the Research and Thesis Outline

The objectives of this thesis are to systematically develop transfer matrix for investigating propagation of fundamental field and SHG from interaction of (i) metamaterial PC with CW laser beam and (ii) superconducting magnetic PC with ultrashort pulse laser beam. The metamaterials have become of great interest because of its unique features and also potential applications such as cloaking device (Schurig et al., 2006; H. Chen, Wu, Zhang, & Kong, 2007; Guven, Saenz, Gonzalo, Ozbay, & Tretyakov, 2008; Smolyaninov, Smolyaninova, Kildishev, & Shalaev, 2009; Dong, Zheng, Lai, Wang, & Chan, 2011), filter (C. M. Lee, Shim, Moon, & Seo, 2012), waveguide (Fu, Zhang, & Tanner, 2002), polarization control of light (J. Hao et al., 2007, 2009; J. M. Hao, Qiu, & Zhou, 2010; Sun, He, Hao, & Zhou, 2011) and sensor (T. Chen, Li, & Sun, 2012; Kenanakis et al., 2012). The development of metamaterial PC is important to realize new optical properties at optical wavelength (Soukoulis, Linden, & Wegener, 2007; Shalaev, 2007; Ozbay, 2010) to enhance optical technology for the benefit of mankind (Soukoulis & Wegener,

2011). The nonlinear optical interaction between laser beam and metamaterial PC has also been extensively studied (Denz, Flach, & Kivshar, 2008). Hence, we are motivated to investigate SHG from PC with metamaterial. Chapter 2 outlines literature review of thesis, basic principles of nonlinear optics such as Maxwell equations, parametric processes, phase matching, transfer matrix, negative refractive index and features of photonic crystal are discussed to provide overview and foundation for development work in this thesis.

Next, in Chapter 3, detailed steps for transfer matrix development to model electric fields of FF and SH in dielectric photonic crystal with effective permeability μ_{eff} and effective permittivity ε_{eff} are discussed. μ_{eff} is adapted in the magnetic field equation so that it is included to describe change of refractive index. The first step of transfer matrix development is to write the electric field E in the function of forward and backward complex amplitudes. Next step is to use Maxwell equation to derive magnetic field H. Hence, a vector matrix with E and H for individual layer is obtained. Maxwell boundary condition is used to examine continuity of E and H fields at interface between layers. From there, the basic transfer matrix that connects two layers is developed. This matrix would be used to develope single period transfer matrix and the final transfer matrix for N period is obtained by using recursion relationship. The effective permittivity induced by metamaterial is taken into consideration in the simulation. In this chapter, transmission and reflection spectra for FF and SH are investigated and discussed for interaction between CW and photonic crystal. The real μ_{eff} and ε_{eff} are used to simulate FF and SH for frequency region far away from magnetic and dielectric resonance. Meanwhile, band structures for FF and SH fields with complex μ_{eff} and ε_{eff} are also being investigated.

In chapter 4, the same approach is used to develop transfer matrix in frequency domain to model interaction between ultrashort pulse and photonic crystal with superconductor layer. We consider photonic crystal has frequency dependent complex effective permeability μ_{eff} and employ two fluid model to describe conductivity σ of superconductor layer. The dieletric function ε_{eff} of superconductor is in function of conductivity σ. The pulse propagation inside photonic crystal is investigated. In chapter 5, the conclusion based on the works presented in this thesis is drawn. The works in this thesis have been published in well known ISI Journal of Optics (chapter 3) and Applied Physics B (chapter 4).

CHAPTER 2

LITERATURE REVIEW

2.1 Nonlinear Susceptibility

Nonlinear optics is the study of phenomenon caused by nonlinear interaction between light and material (Bloembergen, 1992). In early years, nonlinear optical interaction observed is spontaneous Raman effect discovered by Sir C.V. Raman in 1928 (Rajinder, 2002). This effect is the result of incident light (frequency ω_p) interacting with scattering medium to scatter lights with different frequencies (ω_S and ω_a) by excitation from incident light where ω_a is the anti-Stoke component higher than ω_p and ω_S is the Stoke component lower than ω_p. Sir C.V. Raman was awarded Nobel prize for this ground breaking discovery in 1930. However, this spontaneous Raman effect is weak process because only a very small fraction (approximately 1 in 10^6) of scattered photons are excited in to either ω_S or ω_a. The laser invented in 1960s with intensity in order of $10^8 \mathrm{Vm}^{-1}$ which is strong enough and comparable to characteristic atomic field strength could induce strong photoionization that lead to nonlinear optical interaction. This is proven when laser is pumped onto Raman medium is observed in which 10% of laser energy is converted to Stoke component, this is known as stimulated Raman scattering. Schematics of both spontaneous and stimulated Raman scattering are shown in Figure 2.1.

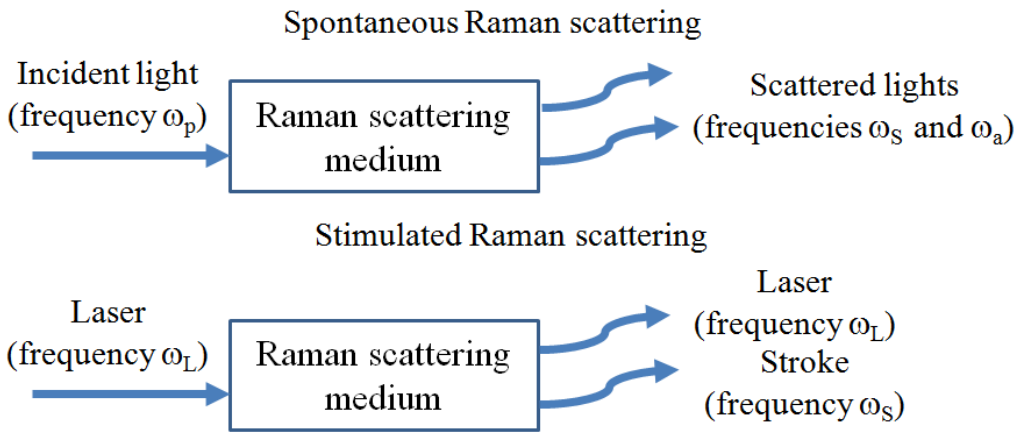

Figure 2.1: Spontaneous and stimulated Raman scattering.

This field entered new era when second harmonic generation (SHG) realized in 1960s (Franken et al., 1961). They propagated ruby laser beam at 6942 Å through a quartz crystal and detected ultraviolet light at 3941 Å. This SHG is also known as frequency doubling as it creates new light with frequency twice of the incident light. When electric field is applied to medium, positive and negative charges inside each atom are displaced from the equilibrium positions. This process is known as polarization. In dielectric material, polarization is proportional to electric field strength. Polarization induced in optical medium and electric field strength are important parameters in nonlinear optics. For linear optics, relationship of polarization $\mathbf{P}^{(1)}(\omega)$ and electric field strength $\mathbf{E}(\omega)$ in frequency domain is

$$P_i^{(1)}(\omega) = \sum_j \chi_{ij}^{(1)} E_j(\omega) \tag{2.1}$$

where $\chi_{ij}^{(1)}$ is linear susceptibility. In medium with nonlinear optical response, we could write total polarization $P_i(\omega)$, subscripts represent cartesion components.

$$P_i(\omega) = \sum_j \chi_{ij}^{(1)} E_j(\omega) + \sum_{jk} \chi_{ijk}^{(2)} E_j(\omega) E_k(\omega) + \sum_{jkl} \chi_{ijkl}^{(3)} E_j(\omega) E_k(\omega) E_l(\omega) + \ldots \tag{2.2}$$

where $\chi^{(n)}$ is a tensor of order $(n+1)$ that represents n-th order of optical susceptibility. As seen from Equation 2.2, we include $P_i^{(2)}(\omega)$ and $P_i^{(3)}(\omega)$ which are known as second and third order nonlinear polarization respectively

$$P_i^{(2)}(\omega) = \sum_{jk} \chi_{ijk}^{(2)} E_j(\omega) E_k(\omega) \tag{2.3}$$

$$P_i^{(3)}(\omega) = \sum_{jkl} \chi_{ijkl}^{(3)} E_j(\omega) E_k(\omega) E_l(\omega) \tag{2.4}$$

where $\chi_{ijk}^{(2)}$ and $\chi_{ijkl}^{(3)}$ are second and third order nonlinear optical susceptibilities. The linear susceptibility $\chi_{ij}^{(1)}$ gives rise to linear response like reflection and absorption, the second order nonlinear susceptibility $\chi_{ijk}^{(2)}$ gives rise to sum, difference, SH generation and optical rectification, and the third order nonlinear susceptibility $\chi_{ijkl}^{(3)}$ gives rise to Kerr effect and four wave mixing. In general, we could express polarization as

$$\mathbf{P}(\omega) = \mathbf{P}^{(1)}(\omega) + \mathbf{P}^{NL}(\omega)$$

where $\mathbf{P}^{NL}(\omega)$ is nonlinear polarization. In time domain, polarization is time varying process and convolution relationship applies to $\mathbf{P}(\mathbf{r},t)$ and $\mathbf{E}(\mathbf{r},t)$. The time domain

linear polarization is

$$\begin{aligned}\mathbf{P}^{(1)}(\mathbf{r},t) &= \int_{-\infty}^{\infty}\chi^{(1)}(t-\tau)\,\mathbf{E}(\mathbf{r},t)\,d\tau \\ &= \int_{-\infty}^{\infty}\chi^{(1)}(\tau)\,\mathbf{E}(\mathbf{r},t-\tau)\,d\tau\end{aligned} \tag{2.5}$$

and second order polarization

$$\begin{aligned}\mathbf{P}^{(2)}(\mathbf{r},t) &= \int_{-\infty}^{\infty}\int_{-\infty}^{\infty}\chi^{(2)}(t-\tau_1,t-\tau_2)\,\mathbf{E}(\mathbf{r},\tau_1)\,\mathbf{E}(\mathbf{r},\tau_2)\,d\tau_1 d\tau_2 \\ &= \int_{-\infty}^{\infty}\int_{-\infty}^{\infty}\chi^{(2)}(\tau_1,\tau_2)\,\mathbf{E}(\mathbf{r},t-\tau_1)\,\mathbf{E}(\mathbf{r},t-\tau_2)\,d\tau_1 d\tau_2\end{aligned} \tag{2.6}$$

and third order polarization

$$\begin{aligned}\mathbf{P}^{(3)}(\mathbf{r},t) &= \int_{-\infty}^{\infty}\int_{-\infty}^{\infty}\int_{-\infty}^{\infty}\chi^{(3)}(t-\tau_1,t-\tau_2,t-\tau_3) \\ &\qquad \mathbf{E}(\mathbf{r},\tau_1)\,\mathbf{E}(\mathbf{r},\tau_2)\,\mathbf{E}(\mathbf{r},\tau_3)\,d\tau_1 d\tau_2 d\tau_3 \\ &= \int_{-\infty}^{\infty}\int_{-\infty}^{\infty}\int_{-\infty}^{\infty}\chi^{(3)}(\tau_1,\tau_2,\tau_3)\,\mathbf{E}(\mathbf{r},t-\tau_1)\,\mathbf{E}(\mathbf{r},t-\tau_2) \\ &\qquad \mathbf{E}(\mathbf{r},t-\tau_3)\,d\tau_1 d\tau_2 d\tau_3\end{aligned} \tag{2.7}$$

2.2 Maxwell Equations in Nonlinear Medium

Laser beam comprises electric field and magnetic field that oscillating at very high rate which is in the order of 10^{13} to 10^{15} Hz where magnetic field is perpendicular to electric field. The velocity of electromagnetic wave in free space is

$$c = \frac{1}{\sqrt{\varepsilon_0\mu_0}} \tag{2.8}$$

where ε_0 and μ_0 are free space permittivity and permeability.

From classical electomagnetic theory, we could use Maxwell equations (SI unit) (Cook, 1975; Neviere, Popov, Reinisch, & Vitrant, 2000) to describe propagation of monochromatic laser beam with angular frequency ω with space and time domain electric field $\mathbf{E}(\mathbf{r},t)$, magnetic field $\mathbf{H}(\mathbf{r},t)$, electric flux density $\mathbf{D}(\mathbf{r},t)$ and magnetic flux density $\mathbf{B}(\mathbf{r},t)$ inside optical medium. Consider electric field consists of complex field envelope and time harmonic dependence

$$\mathbf{E}(\mathbf{r},t) = \mathbf{A}(\mathbf{r},t)\,e^{-i\omega t} \tag{2.9}$$

where $\mathbf{A}(\mathbf{r},t)$ is slowly varying complex amplitude of the field.

$$\nabla \times \mathbf{E}(\mathbf{r},t) = -\frac{\partial \mathbf{B}(\mathbf{r},t)}{\partial t} \tag{2.10}$$

$$\nabla \times \mathbf{H}(\mathbf{r},t) = \mathbf{J}(\mathbf{r},t) + \frac{\partial \mathbf{D}(\mathbf{r},t)}{\partial t} \tag{2.11}$$

$$\nabla \cdot \mathbf{D}(\mathbf{r},t) = \rho_f(\mathbf{r},t) \tag{2.12}$$

$$\nabla \cdot \mathbf{B}(\mathbf{r},t) = 0 \tag{2.13}$$

$$\nabla \times \mathbf{B}(\mathbf{r},t) = \varepsilon_0 \mu_0 \frac{\partial \mathbf{E}(\mathbf{r},t)}{\partial t} + \mu_0 \mathbf{J}(\mathbf{r},t) \tag{2.14}$$

$$\nabla \cdot \mathbf{E}(\mathbf{r},t) = \frac{\rho(\mathbf{r},t)}{\varepsilon_0} \tag{2.15}$$

where $\rho_f(\mathbf{r},t)$ is free charge density, $\rho(\mathbf{r},t)$ is charge density and $\mathbf{J}(\mathbf{r},t)$ is electric current. Assume the medium which has no free charge and current,

$$\rho_f(\mathbf{r},t) = 0$$

$$\mathbf{J}(\mathbf{r},t) = 0$$

therefore, Equations 2.11, 2.12 and 2.14 are reduced to

$$\nabla \times \mathbf{H}(\mathbf{r},t) = \frac{\partial \mathbf{D}(\mathbf{r},t)}{\partial t} \tag{2.16}$$

$$\nabla \cdot \mathbf{D}(\mathbf{r},t) = 0 \tag{2.17}$$

$$\nabla \times \mathbf{B}(\mathbf{r},t) = \varepsilon_0 \mu_0 \frac{\partial \mathbf{E}(\mathbf{r},t)}{\partial t} \tag{2.18}$$

Equation 2.10 is deduced from Faraday law which means time varying magnetic field produces electric field, Equation 2.11 is deduced from Ampere law which implies time varying magnetic field produces electric field, meanwhile Equations 2.12 and 2.13 refer to Gauss law for electric field and magnetic field respectively.

Constitutive relation from (Yuffa & Scales, 2012), $\mathbf{D}(\mathbf{r},t)$ in time domain is expressed as

$$\mathbf{D}(\mathbf{r},t) = \int_{-\infty}^{\infty} \varepsilon(t-\tau)\mathbf{E}(\mathbf{r},\tau)\,d\tau + \mathbf{P}^{NL}(\mathbf{r},t) \tag{2.19}$$

where

$$\varepsilon(t-\tau) = \delta(t-\tau) + \chi^{(1)}(t-\tau)$$

for short memory linear response, $t-\tau \simeq 0$, therefore

$$\begin{aligned} \int_{-\infty}^{\infty} \varepsilon(t-\tau)\mathbf{E}(\mathbf{r},\tau)\,d\tau &= \mathbf{E}(\mathbf{r},t)\int_{-\infty}^{\infty} \varepsilon(t-\tau)\,d\tau \\ &= \varepsilon\mathbf{E}(\mathbf{r},t) \end{aligned}$$

where $\int_{-\infty}^{\infty} \varepsilon(t-\tau)\,d\tau = \varepsilon$, therefore 2.19 could be written as

$$\mathbf{D}(\mathbf{r},t) = \varepsilon\mathbf{E}(\mathbf{r},t) + \mathbf{P}^{NL}(\mathbf{r},t) \tag{2.20}$$

where $\mathbf{P}^{NL}(\mathbf{r},t)$ is nonlinear polarization and ε is permittivity of the medium. We also could write $\varepsilon = \varepsilon_0\varepsilon_{eff}$ where ε_{eff} is dimensionless relative permittivity.

Menawhile another constitutive relation $\mathbf{B}(\mathbf{r},t)$ is expressed as

$$\begin{aligned}
\mathbf{B}(\mathbf{r},t) &= \mu_0(\mathbf{H}(\mathbf{r},t) + \mathbf{M}(\mathbf{r},t)) \\
&= \mu_0(\mathbf{H}(\mathbf{r},t) + \chi^m\mathbf{H}(\mathbf{r},t)) \\
&= \mu_0(1+\chi^m)\mathbf{H}(\mathbf{r},t) \\
&= \mu_0\mu_{eff}\mathbf{H}(\mathbf{r},t) \\
&= \mu\mathbf{H}(\mathbf{r},t)
\end{aligned} \tag{2.21}$$

with induced magnetic polarization $\mathbf{M}(\mathbf{r},t) = \chi_m\mathbf{H}(\mathbf{r},t)$, χ_m is magnetic susceptibility and μ_{eff} is dimensionless relative permeability, μ is permeability of the medium. Take curl on Equation 2.10 and eliminate $\mathbf{B}(\mathbf{r},t)$, $\mathbf{D}(\mathbf{r},t)$ and $\mathbf{H}(\mathbf{r},t)$, we could obtain standard equation for electromagnetic wave propagation in nonlinear optical medium

$$\nabla^2\mathbf{E}(\mathbf{r},t) - \mu\varepsilon\frac{\partial^2\mathbf{E}(\mathbf{r},t)}{\partial t^2} = \mu\frac{\partial^2\mathbf{P}^{NL}(\mathbf{r},t)}{\partial t^2} \tag{2.22}$$

the detail of deriviation for Equation 2.22 is depicted in appendix. For medium where $\varepsilon_{eff} = 1$ and $\mu_{eff} = 1$, Equation 2.22 becomes

$$\nabla^2\mathbf{E}(\mathbf{r},t) - \frac{1}{c^2}\frac{\partial^2\mathbf{E}(\mathbf{r},t)}{\partial t^2} = \mu_0\frac{\partial^2\mathbf{P}^{NL}(\mathbf{r},t)}{\partial t^2} \tag{2.23}$$

From RHS of Equation 2.22, as long as $\frac{\partial^2\mathbf{P}^{NL}(\mathbf{r},t)}{\partial t^2}$ is non zero, charges would be accelerated and subsequently generate electromagnetic radiation obeying Larmor's theorem. For laser beam propagation in one dimensional nonlinear optical medium (z axis), We could reduce Equation 2.22 to

$$\nabla^2\mathbf{E}(z,t) - \mu\varepsilon\frac{\partial^2\mathbf{E}(z,t)}{\partial t^2} = \mu\frac{\partial^2\mathbf{P}^{NL}(z,t)}{\partial t^2} \tag{2.24}$$

For non zero $\frac{\partial^2\mathbf{P}^{NL}(z,t)}{\partial t^2}$, Equation 2.24 model the nonlinear optical process dependent on $\mathbf{P}^{NL}(z,t)$. For finding SH electric field induced by second order nonlinear polarization only, we could substitute $\mathbf{P}^{NL}(z,t)$ with $\mathbf{P}^{(2)}(z,t)$ into 2.24

$$\nabla^2\mathbf{E}(z,t) - \mu\varepsilon\frac{\partial^2\mathbf{E}(z,t)}{\partial t^2} = \mu\frac{\partial^2\mathbf{P}^{(2)}(z,t)}{\partial t^2} \tag{2.25}$$

and similarly for nonlinear third order process, we could substitute $\mathbf{P}^{NL}(z,t)$ with $\mathbf{P}^{(3)}(z,t)$

$$\nabla^2\mathbf{E}(z,t) - \mu\varepsilon\frac{\partial^2\mathbf{E}(z,t)}{\partial t^2} = \mu\frac{\partial^2\mathbf{P}^{(3)}(z,t)}{\partial t^2} \tag{2.26}$$

In the absence of nonlinear polarization, Equation 2.22 is reduced to homogeneous wave equation

$$\nabla^2\mathbf{E}(\mathbf{r},t) - \mu\varepsilon\frac{\partial^2\mathbf{E}(\mathbf{r},t)}{\partial t^2} = 0 \tag{2.27}$$

2.3 Nonlinear Optical Interaction

2.3.1 Overview of Parametric Process

Nonlinear optical interaction is a process of creation and varnish of frequency when laser beam pumped upon nonlinear optical medium. There are parametric and non parametric processes in nonlinear optical interaction. In parametric processes, energy and momentum conservation shall be satisfied among photons. Optical parametric processes have been explored by reseachers from all round the world, both fundamentally (D. Lee & Wong, 1993; Dou, Josse, & Zyss, 1993; Powers, Ellingson, Pelouch, & Tang, 1993) and experimentally (Spielmann et al., 1997; Hui & Mecozzi, 1992; Myers, Eckardt, Fejer, Byer, & Bosenberg, 1996). Optical medium is a catalyzer to accelarate energy exchange between photons during interaction but no energy is transfered to medium (H. Guo, 2007). In non parametric process, the energy conservation among photons is not necessary because energy could be transferred from or to optical medium. The interaction is contributed by nonlinear polarization in Equation 2.22. In general, there are two parts in nonlinear optical interaction which requires application of laser. Firstly, the intense beam would induce a nonlinear response in a medium and subsequently medium would react accordingly to modify the optical field in nonlinear manner as described by nonlinear polarization $\mathbf{P}^{NL}$. These processes lead to wave mixing and creation of wave(s) with new frequency which are explained in detail by Shen (Y. R. Shen, 1984). We present an overview of parametric processes such as second harmonic generation (SHG), sum frequency generation (SFG) and difference frequency generation (DFG) which are relevant and important in this thesis. These parametric processes are explained in detail in (Byod, 2003) and we briefly explain some of the essential points here.

Consider two laser beams with time varying electric field with two frequency components are pumped upon non zero $\chi^{(2)}$ medium

$$\mathbf{E}(z,t) = E_1 e^{-i\omega_1 t} + E_2 e^{-i\omega_2 t} + c.c. \tag{2.28}$$

therefore, the second order polarization induced is

$$\begin{aligned} \mathbf{P}^{(2)}(\omega) &= \chi^{(2)}\left[E_1 e^{-i\omega_1 t} + E_2 e^{-i\omega_2 t} + c.c.\right]^2 \\ &= \chi^{(2)} E_1^2 e^{-i2\omega_1 t} + \chi^{(2)} E_2^2 e^{-i2\omega_2 t} + 2\chi^{(2)} E_1 E_2 e^{-i(\omega_1+\omega_2)t} \\ &\quad + 2\chi^{(2)} E_1 E_2^* e^{-i(\omega_1 - i\omega_2)t} + c.c. + 2\chi^{(2)}\left[E_1 E_1^* + 2E_2 E_2^*\right] \end{aligned} \tag{2.29}$$

and rewrite

$$\mathbf{P}^{(2)}(2\omega_1) = \chi^{(2)} E_1^2 e^{-i2\omega_1 t} \tag{2.30}$$

$$\mathbf{P}^{(2)}(2\omega_2) = \chi^{(2)} E_2^2 e^{-i2\omega_2 t} \tag{2.31}$$

$$\mathbf{P}^{(2)}(\omega_1 + \omega_2) = 2\chi^{(2)} E_1 E_2 e^{-i(\omega_1+\omega_2)t} \tag{2.32}$$

$$\mathbf{P}^{(2)}(\omega_1 - \omega_2) = 2\chi^{(2)} E_1 E_2^* e^{-i(\omega_1 - i\omega_2)t} \tag{2.33}$$

$$\mathbf{P}^{(2)}(0) = 2\chi^{(2)}\left[E_1 E_1^* + 2E_2 E_2^*\right] \tag{2.34}$$

Equations 2.30 and 2.31 depict SHG polarization which is proportional to square of electric field, Equations 2.32 and 2.33 depict SFG and DFG polarizations and Equation 2.34 provides qualitative expression for optical rectification. The expression of polarization of conjugate component in Equation 2.29 is not necessary because it is just a polarization with negative frequency, i.e. $\mathbf{P}^{(2)}(-2\omega_1)$, $\mathbf{P}^{(2)}(-2\omega_2)$, $\mathbf{P}^{(2)}(-(\omega_1+\omega_2))$ and $\mathbf{P}^{(2)}(-(\omega_1-\omega_2))$.

2.3.2 Sum and Difference Frequency Generations

The principle of SFG is straight forward in which two laser beams at frequencies of ω_1 (wave vector k_1) and ω_2 (wave vector k_2) are interacting with nonlinear optical medium and induce nonlinear polarization $\mathbf{P}^{(2)}(\omega_3 = \omega_1 + \omega_2)$ and subsequently generate new wave at frequency $\omega_3 = \omega_1 + \omega_2$ (wave vector k_3). SFG was first discovered experimentally in triglycine sulfate (Bass, Franken, Hill, Peters, & Weinreich, 1962). Two ruby laser beams with wavelength different by 10Å apart from each other induce emission of two SH waves and also wave with sum frequency of the pump lasers in 3470Å region.

Incident fields at ω_1 and ω_2 interact with nonlinear optical medium and cause atoms inside optical medium to develop oscillating dipole moment at frequency which is summation of incident fields $\omega_1 + \omega_2$ and radiate the new frequency component $\omega_3 = \omega_1 + \omega_2$ with dipole pattern as shwon in Figure 2.2. This non zero polarization serves as a source for electromagnetic radiation with frequency ω_3. The schematic of SFG is shown in Figure 2.3.

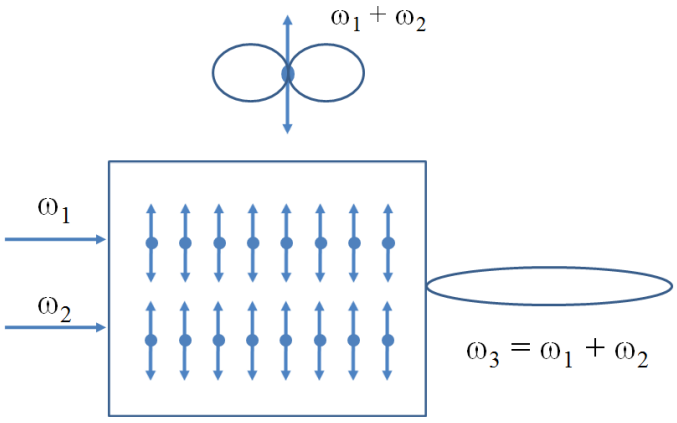

Figure 2.2: Atom in medium develops oscillating dipole moment at frequency $\omega_1 + \omega_2$ lead to radiation in the dipole pattern. Dipole radiations generated by bulk atoms in medium would generate new electromagnetic wave at new frequency $\omega_3 = \omega_1 + \omega_2$.

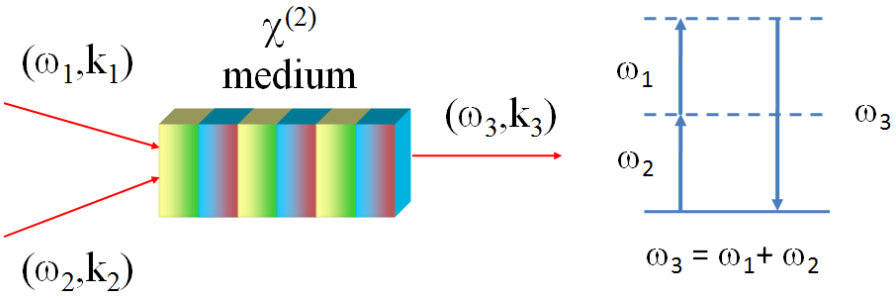

Figure 2.3: Two laser beams with of frequencies of ω_1 and ω_2 are pumped upon $\chi^{(2)}$ medium and induce polarization to generate new electromagnetic wave with frequency $\omega_3 = \omega_1 + \omega_2$.

The sum frequency relationship $\omega_3 = \omega_1 + \omega_2$ satisfies energy conservation principle derived from

$$\hbar\omega_{input} = \hbar\omega_{new} \tag{2.35}$$

where ω_{input} is photon energy of the input wave and ω_{new} is photon energy of newly generated wave caused by polarization. The energy is tranferred from ω_1 and ω_2 photons to ω_3 photon. Meanwhile, conservation of momentum would only be satisfied when perfect phase matching condition is achieved where wave vector mismatch is

$$\Delta k = k_1 + k_2 - k_3 \tag{2.36}$$

This is polarization described analytically in equation 2.32. Under phase matching condition, dipole patterns radiated by atoms in bulk would be strongly peak in certain direction and hence radiate new electromagnetic wave with frequency ω_3. The effect of phase matching in enhancing the intensity of newly generated electromagnetic wave by compensating dispersion is presented by Maker *et al* (Maker, Terhune, Nisenoff, & Savage, 1962).

DFG is another parametric process in which two fields ω_1 and ω_2 where $\omega_1 > \omega_2$ interact with $\chi^{(2)}$ optical medium to produce new wave with frequency $\omega_3 = \omega_1 - \omega_2$ as shown in Figure 2.4. The wave vector mismatch for DFG is

$$\Delta k = k_3 - k_1 - k_2 \tag{2.37}$$

which different from wave vector mismatch of SFG.

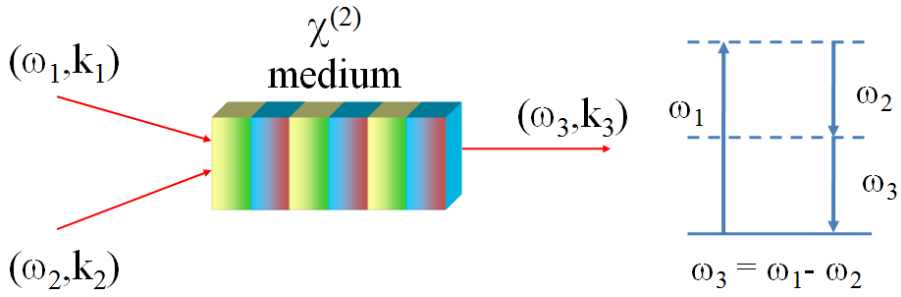

Figure 2.4: Two laser beams with of frequencies of ω_1 and ω_2 where $\omega_1 > \omega_2$ are pumped upon $\chi^{(2)}$ medium and induce polarization to generate new electromagnetic wave with frequency $\omega_3 = \omega_1 - \omega_2$.

2.3.3 Second Harmonic Generation

SHG is nonlinear optical interaction between one incident laser beam with medium. It is degenerate case of SFG where $k_1 = k_2$ and we could write $\omega_1 = \omega_2 = \omega$. From Equations 2.30 or 2.31, we could simplify polarization to be $\chi^{(2)}E^2e^{-2i\omega t}$, this polarization

leads to radiation of new electromagnetic wave with frequency of 2ω. The wave vector mismatch for SHG is

$$\Delta k = k_2 - 2k_1 \tag{2.38}$$

The schematic of SHG is shown in Figure 2.5. SHG is only feasible in non centrosymetry crystal (Y. R. Shen, 1989). The phase matching is important in ensuring efficient energy transfer between propagating and generated waves.

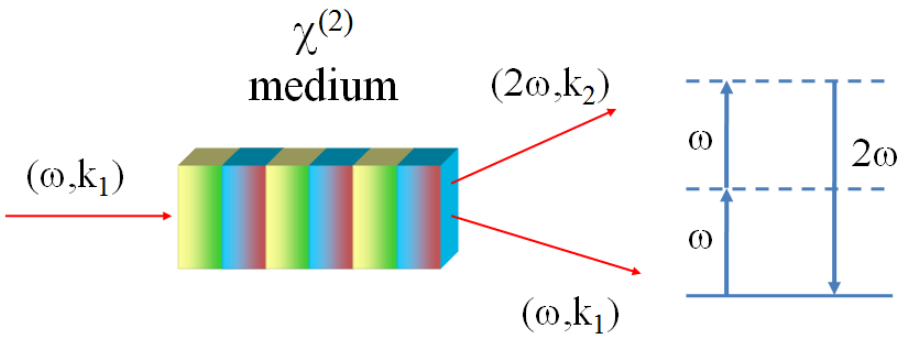

Figure 2.5: An incident laser with FF frequency ω is pumped upon $\chi^{(2)}$ medium and induce polarization to generate new electromagnetic wave with frequency 2ω. The FF output has the same frequency with FF input ω.

Energy coupling process of FF and SH waves is described by

$$\frac{\partial \tilde{A}_x}{\partial z} = \frac{i\omega^2 \mu \chi^{(2)}_{xxx}}{k^{(1)}} \tilde{B}_x \tilde{A}^*_x e^{i\Delta kz} \tag{2.39}$$

and

$$\frac{\partial \tilde{B}_x}{\partial z} = \frac{2i\omega^2 \mu \chi^{(2)}_{xxx}}{k^{(2)}} \tilde{A}^2_x e^{-i\Delta kz} \tag{2.40}$$

where $\tilde{A}_x$ and $\tilde{B}_x$ represent FF and SH electric field amplitudes, derivation of Equations 2.39 and 2.40 is illustrated in appendix. Nonlinear optical responses in layered composite material have been studied (Sipe & Boyd, 1992; Boyd & Sipe, 1994; Gehr, Fischer, Boyd, & Sipe, 1996). In this thesis, SHG is the nonlinear optical interaction to be explored. Propagation of laser beam in crystal and associated electro optics effects which enable nonlinear optical interaction such as SHG are explained in detail in Optical Waves in Crystal (Yariv & Yeh, 1984). The refractive index data is important for developing second harmonic generator, Chang *et al* collected useful data of refractive index and coresponding SHG efficiency (Chang, Wen, Wang, & Li, 1992). Many reseaches have been

carried out to enhance SHG. Using QPM material is the most common method. Lim *et al* proposed periodically poled planar lithium niobate waveguide to generate SH of green light at 532nm at room temperature (E. J. Lim, Fejer, & Byer, 1989). Ito *et al* used direct electron beam writing on $LiNbO_3$ to produce QPM structure with consistent periodicity in order to enhance SHG (Ito, Takyu, & Inaba, 1991). Ma *et al* proposed 1 dimensional periodic bilayer photonic crystal in which the first layer is $LiNbO_3$ and second layer is air film to enhance SHG at photonic band gap edge (Ma, Ren, Dou, & Li, 2010). Recently, Wang *et al* also investigated enhancement of SHG from metalic nanohole arrays (R. L. Wang et al., 2013).

Pulsed SHG in one dimensional photonic band gap material doped with $\chi^{(2)}$ medium has been demonstrated (Scalora et al., 1997). SHG in metal and antiferromagnetic thin film has also been studied (Rudnick & Stern, 1971; S. C. Lim, 2002). Zhou *et al* also investigated SHG from antiferromagnetic film embedded in 1 dimensional photonic crystal (S. Zhou, Li, Fu, & Wang, 2009). It is shown that strong SHG would occur near photonic band edge (D'Aguanno et al., 2001). In silicon photonic, second and third order susceptibilities are used to convert wavelengths in optical communication (Leuthold, Koos, & Freude, 2010). Other methods to enhance SHG are introducing defect or cavity quantum electrodynamic effect (H. Cao, Hall, Torkelson, & Cao, 2000; B. Shi, Jiang, & Wang, 2001), disorder structure (Faccio & Bragheri, 2005), pumping of slow light (Iliew, Etrich, Perstsch, & Lederer, 2008; Iliew, Etrich, Perstsch, Lederer, & Kivshar, 2010), controlling of pump beam intensity (Y. Kong, Chen, & Zhu, 2010) and introduction of Bragg reflector mirrors (Ren & Li, 2009) in which strong localization of fundamental field (FF) enhances coupling of waves in $\chi^{(2)}$ medium.

Nonlinear optical inteaction in crystal Potassium Titanil Phosphate $KTiOPO_4$ (KTP) has been studied experimentally (Berlein & Ahmed, 1987). Raman scattering and fluorescent spectra have been observed in KTP (L. Xu, Chang, Niu, & Jia, 1989). KTP is nonlinear crystal with large electro-optic coefficients and low dielectric constants makes it a good device for SHG by using diode pumped Nd:YAG laser at 1064nm to produce SH field at 532nm (Bierlein & Vanherzeele, 1989). Driscoll *et al* aslo demoenstrated KTP is efficient SHG generator with conversion efficiency more than 50% (Driscoll, Hoffman, Stone, & Perkins, 1986). The typical experimental set up of SHG from KTP by using

Nd:YAG laser is shown in Figure 2.6.

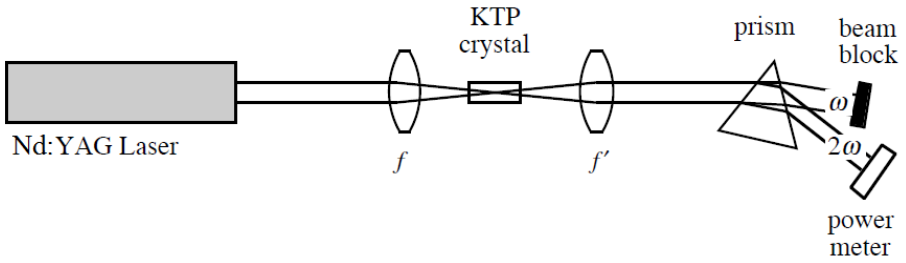

Figure 2.6: Typical experimental set up for SHG in KTP, laser beam with $\lambda = 1064$nm is pumped upon KTP crystal to generate SH wave with $\lambda = 532$nm.

Nd:YAG (neodymium-doped yttrium aluminum garnet; Nd:$Y_3Al_5O_{12}$) is a crystal that act as lasing medium to enable emission of laser beam (Geusic, Marcos, & Van Uitert, 1964) and being known as stable laser source (B. K. Zhou, Kane, Dixon, & Byer, 1985). Boulanger *et al* demonstrated that wavelength of Nd:YAG laser is typically 1064nm and converted to 532nm by using KTP crystal (Boulanger, Fejer, Blachman, & Bordui, 1994). Various researches have been conducted to study generation of Nd:YAG laser at 1064nm (Gong et al., 2008; Kang, Zhang, Yan, Wang, & Gong, 2008; Y. J. Yu et al., 2009) and 1319nm (H. Liu, Gong, Wushouer, & Gao, 2010; H. Zhu et al., 2007) and 946nm (Fan & Byer, 1987; Hanson, 1995) so that SH fields could be generated at 532nm (green), 660nm (red) and 473nm (blue) respectively by means of frequency doubling process. Recently, Shen *et al* also demonstrated frequency dobled Nd:YAG/KTP laser at 561nm from fundamental laser at 1123nm produced by the diode pumped laser at 808nm (H. B. Shen et al., 2013). Laser diode was developed in 1960's (Hall, Fenner, Kingsley, Soltys, & Carlson, 1962; Holonyak & Bevacqua, 1962), it is used as pump source for generating laser beam from crystal. Properties of laser pumped solid state lasers were investigated (Barnes, 1973; Saleh & Teich, 1991). Urata and Wada have also developed continuous wave Tm:$GdVO_4$ laser by using 808nm laser diode as pump source (Urata & Wada, 2005).

2.4 Phase Matching

Phase matching is condition where propagating and generated electromagnetic waves inside optical medium are propagating with the phase velocities in the same direction. Co-

herent sum of the dipole radiation from atoms in the medium would generate new wave and it needs to constructively interfere with input field so that both waves would propagate in the same phase and direction. In general, phase matching is conservation of photon momentum

$$\hbar k_{input} = \hbar k_{new} \tag{2.41}$$

Efficient parametric process could only be achieced with efficient conservation in energy and momentum. The importance of phase matching in frequency up conversion in nonlinear crystal has been evaluated (Voronin & Strizhevskii, 1979). The wave vector for phase matching is illustrated in Figure 2.7.

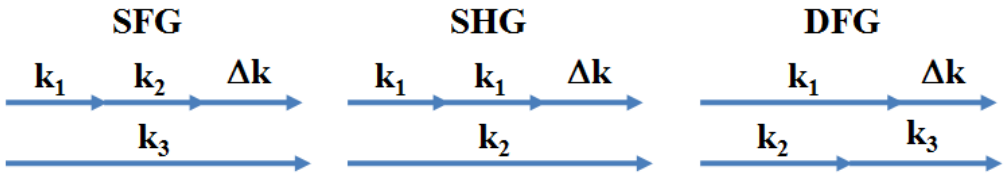

Figure 2.7: Phase matching for SFG, SHG and DFG.

Perfect phase matching is not practical in real parametric process due to dispersion of the medium. The waves would travel at different velocities. After a distance known as coherent length when generated wave is lagging by phase of π of propagated wave, destructive interference occurs and lead to change of power flow direction. Phase mismatch of electromagnetic waves is also expressed as wave vector mismatch Δk from Equation 2.41

$$\Delta k = k_{new} - k_{input} \tag{2.42}$$

The phase mismatch formulas of SHG, SFG and DFG are discussed in previous section. Recall Equation 2.36 for lossless medium, if $\Delta k = 0$ and $\omega_3 > \omega_2 > \omega_1$

$$\begin{aligned} k_3 &= k_1 + k_2 \\ \frac{\omega_3 n_3}{c} &= \frac{\omega_1 n_1}{c} + \frac{\omega_2 n_2}{c} \\ \omega_3 n_3 &= \omega_1 n_1 + \omega_2 n_2 \end{aligned} \tag{2.43}$$

Recall that $\omega_3 = \omega_1 + \omega_2$ for parametric process,

$$(\omega_1 + \omega_2) n_3 = \omega_1 n_1 + \omega_2 n_2 \tag{2.44}$$

Due to normal dispersion of the medium, refractive index would increase in the function of frequency which implies $n_3 \neq n_1 \neq n_2$, therefore Equation 2.44 has no solution. For SHG, $\Delta k = 0$ leads to

$$\begin{aligned} k_2 &= 2k_1 \\ n_2 &= 2n_1 \end{aligned} \tag{2.45}$$

It is clear that n_2 at frequency 2ω would be greater than $2n_1$ at frequency ω considering the refractive index increases monotonically with frequency when far away from absorption region due to normal dispersion. Phase mismatch between electrogmatic waves causes inefficient energy transfer between photons and further decay along the propagation path. One of the method to achieve phase matching is anomalous dispersion. Absorption region in certain frequency region would exhibit dispersion that counteract normal dispersion (Korobkin, 1995; Knight, 2000; J. Liu et al., 1995), this method has been applied to design wave guide (Kowalczyk, Singer, & Cahill, 1995).

We could use birefringence which is the property of certain crystal in which it exhibits two or more distinct refractive indices for propagation of light in specific direction and temperature range. A birefringent material is optically anisotropic. Birefringence has been investigated experimentally in infra red spectrum (Shields & Ellis, 1956). Birefringence in quartz and calcite has also been demonstrated in visible wave length (Smart & Steel, 1959). Haertle *et al* demonstrated improved phase matching for type 1 SHG by using $Sn_2P_2S_6$ crystal (Haertle, Jazbinsek, Montemezzani, & Gunter, 2005). Vacuum is also shown to exhibit birefringence in 1960s (J. J. Klein & Nigam, 1964). Natural birefrigent material could be used to control polarization state of light wave. However, it is not practical to design optical device with birefringent crystal because birefringence of crystal is not enough to compensate dispersion of over the interest frequency range besides other limitation such as light propagation direction and operating temperature range. Hence, quasi phase matching (QPM) concept has been proposed to overcome this limitation (Franken & Ward, 1963). Miller demonstrated SHG enhancement in ferroelectric $BaTiO_3$ in 1964 (Miller, 1964). Since then, ferroelectric material such as $LiNbO_3$ has been employed to implement periodic poling for enhancing SHG (Szilagyi, Hordvik, & Schlossberg, 1976; Okada, Takizawa, & Ieiri, 1976, 1985; E. J. Lim et al., 1989). In

QPM, the sign of nonlinear second order susceptibility $\chi^{(2)}$ is modulated throughout the nonlinear medium. The sign of $\chi^{(2)}$ is reversed after the phase slip between interacting waves accumulates 180° at coherence length. Modulation of $\chi^{(2)}$ is achieved by applying external electric field (Khanarian, Norwood, Haas, Feuer, & Karim, 1990; Yamada, Nada, Satoh, & Watanabe, 1993; Kim & Yoon, 2002; K. Liu & Chen, 2009).

$$l_c = \frac{\pi}{\Delta k} \tag{2.46}$$

In SHG, FF wave propagates at phase velocity $v = \frac{c}{n_1}$ interacts with $\chi^{(2)}$ of medium to induce radiation of SH wave which propagates at phase velocity $v = \frac{c}{n_2}$. They travel in the same direction. Normal dispersion of medium implies that $n_2 \neq n_1$, therefore their phase velocities would be different along the propagation path. When phase slip accumulates 180°, alternation of power flow direction would occur. This causes decay of SH intensity along the interaction path. The reversal of $\chi^{(2)}$ sign periodically would compensate the non zero Δk at every coherence length and therefore improve SHG efficiency (Fejer, Magel, Jundt, & Byer, 1992; Tunyagi, 2004) as shown in Figure 2.8.

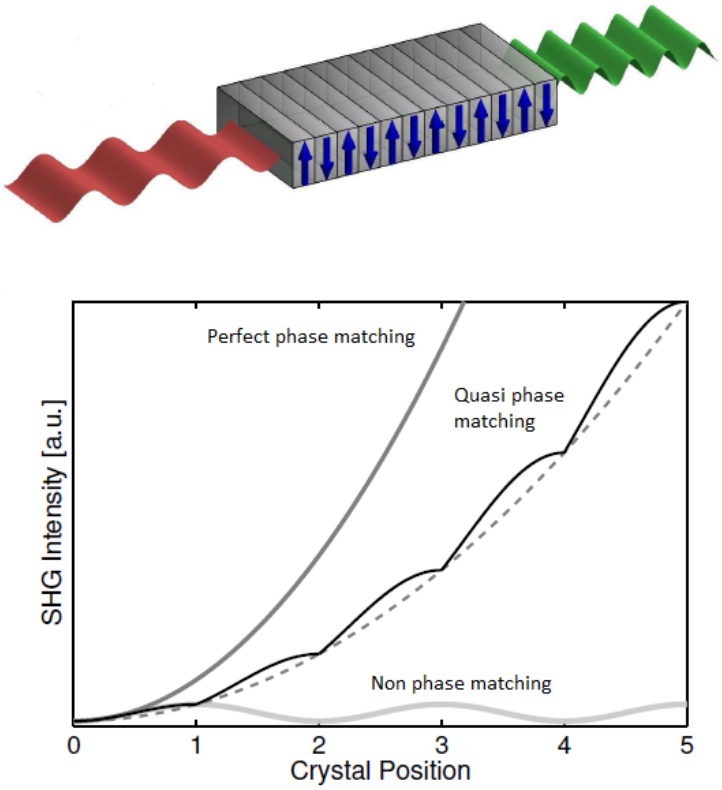

Figure 2.8: The incident wave pumped upon 1 dimensional quasi phase matched photonic crystal to generate SH wave.

Various QPM techniques are presented by Hum and Fejer (Hum & Fejer, 2007). QPM could be realized by means of electric poling in medium in which 2 different thickness and polarization layers are arranged in Fibbonacci sequence (S. Zhu, Zhu, & Ming, 1997; Clausen, Kivshar, Bang, & Christiansen, 1999). Enhancement of third harmonic generation is reported in QPM medium (Zhang et al., 2001). Bahabad *et al* predicted that QPM could also be achieved by using forward pump beam and also counterpropagating train pulse for SHG enhancement (Bahabad, Cohen, Murnane, & Kapteyn, 2008), however this method is common. Periodically poled lithium niobate (PPLN) in 2D photonic crystal could generate SH wave with significant intensity (Ni, Ma, Wang, Cheng, & Zhang, 2003; P. Xu et al., 2004). SHG in QPM PC has been extensively studied (Jeong & Lee, 1999; Torres et al., 2004; Y. Kong et al., 2010). Periodically poled QPM has been applied to enhance nonlinear plasmonic frequency conversion in surface-plasmon polariton (SPP) (Z. Wu et al., 2010). Xu *et al* also reported hexagonally poled 2 dimensional $LiTaO_3$ photonic crystal would enhance SHG significantly as well (P. Xu et al., 2004). The limitation of QPM is it only could be applied in ferroelectric materials.

2.5 Transfer Matrix for Wave Propagation in Periodic Optical Medium

In most of the analysis in nonlinear optics, there are few considerations to be taken into account such as band structure and refractive index to model propagation of electromagnetic wave inside optical medium from Equation 2.22. Periodic optical medium plays important role in nonlinear optics, In periodic optical medium with either finite, semi-infinite or finite period, matrix and translation operator are useful tools to analyze electromagnetic wave propagation in accurate manner (Yeh, Yariv, & Hong, 1977). Matrix developed is also being used to investigate other properties such as birefringence and dispersion of periodic stratified medium (Yariv & Yeh, 1977). In multilayer optical medium, there would be transmission and reflection at every interface that eventually lead to backward and forwrd propagating wave amplitudes inside the medium which could be described in accurate manner by using 2×2 transfer matrix (Makino, 1995). TMM has also been used to model polarization of TE and TM wave propagation in finite bilayer electric structure with different permittivities and investigate transmission, reflection and absorption for few applications such as distributed Bragg reflector, narrow band filter with

two Fabry-Parot resonantors and others (Oraizi & Asfahi, 2007).

Since then TMM has been widely used to model various optical system, such as dispersion in optical fiber (Shenoyu, Thyagarajan, & Ghatak, 1988; Mokhtar, 2005), optical harmonic generation in multilayer medium (Bethune, 1989), multilayer 1 dimensional PC (Eghlidi, Mehrany, & Rashidian, 2006; Z. Y. Li, 2005; Z. Y. Li & Lin, 2003; Katsidis & Siapkas, 2002; L. L. Lin, Li, & Ho, 2003) and non-slanted reflection grating (Frances, Neipp, Marquez, Belendez, & Pascual, 2011). TMM could be further developed for calculating the optical response of multilayer systems which is capable to handle coherent, partially coherent, and incoherent interference for accurate simulation via Fresnel coefficients in a 2x2 matrix configuration (Troparevsky, Sabau, Lupini, & Zhang, 2010). Owens demonstrated that transfer matrix could accurately model linear and nonlinear optical properties in metal-dielectric multilayer structure (Owens, 2010). On the other hand, transfer matrix is being used to model resonance in multilayer 1 dimensional photonic crystal (Maksimovic, 2008) and conducting interfaces (Khorasani & Rashidian, 2002). TMM also could be employed to investigate nonlinear frequency conversion in photonic crystal (J. J. Li, Li, & Zhang, 2008), multilayer medium with negative refractive index (P. F. Cao, Zhang, & Cheng, 2009) and photonic crystal with defect (Z. Y. Wang, Chen, He, & Fan, 2009). As a short summary, transfer matrix could handle change of refractive index and phase into account when modeling electromagnetic wave propagation from layer to layer in multilayer system from propagation equation. Hence, it is being used in this thesis to model both linear and nonlinear optical interactions of laser beam with 1 dimensional photonic structure.

2.6 Metamaterial

2.6.1 Negative Refractive Index

The idea of negative refractive index achieved by simultaneous negative permittivity ε and permeability μ without violating any physics law was proposed by Russian physicst Veselago in 1960s (V. G. Veselago, 1968). Vesalago *et al* and Ramakrishna have provided good overview of negative refraction metamaterial (Ramakhrishna, 2005; V. Veselago, Braginsky, Shklover, & Hafner, 2006). The negative refractive index caused by simultaneous negative permeability and permittivity has been explored theoretically (Smith,

Padilla, Vier, Nemat-Nasser, & Schultz, 2000) and demonstrated experimentally (Shelby, Smith, & Schultz, 2001; Shelby, Smith, Nemat-Nasser, & Schultz, 2001). Metamaterial with negative permittivity ε and permeability μ is not available in nature (Sihvola, 2007). The mathematical derivation for LHM has been studied (Moss, Grzegorczyk, Zhang, & Kong, 2002). Refractive index of medium is

$$n^2 = \varepsilon\mu \tag{2.47}$$

let us write $\mu = -1 = \exp(i\pi)$ and $\varepsilon = -1 = \exp(i\pi)$ and substitute back into Equation 2.47, we have

$$\begin{aligned} n &= \sqrt{\exp(i\pi)\exp(i\pi)} \\ &= \exp(i\pi) = -1 \end{aligned}$$

This mathematical result clearly shows that refractive index would be negative when both permeability and permittivity are negative. The wave vector k of ω frequency electromagnetic wave propagation inside medium is

$$k = n^2\frac{\omega^2}{c^2} = \varepsilon\mu\frac{\omega^2}{c^2} \tag{2.48}$$

Equation 2.48 shows that simultaneous negative ε and μ have no impact on the equation itself from mathematical point of view. Recall Equations 2.10, 2.11, 2.20 and 2.21 and consider monochromatic plane electromagnetic wave $\mathbf{E}$, we have

$$\mathbf{k}\times\mathbf{E} = \omega\mu\mathbf{H} \tag{2.49}$$

$$\mathbf{k}\times\mathbf{H} = -\omega\varepsilon\mathbf{E} \tag{2.50}$$

from Equations 2.49 and 2.50, when $\mu > 0$, $\varepsilon > 0$, the wave vector $\mathbf{k}$ is in $+z$ direction for conventional right handed material, meanwhile $\mu < 0$, $\varepsilon < 0$ would give wave vector in $-z$ direction and negative group velocity for LHM

$$v_g = \frac{d\omega}{dk} < 0 \tag{2.51}$$

and Poynting vector is expressed as

$$\begin{aligned} \mathbf{S} &= \mathbf{E}\times\mathbf{H} \\ &= \mathbf{E}\times\frac{\mathbf{B}}{\mu} \end{aligned} \tag{2.52}$$

for $\mu < 0$, the phase velocity (same direction with **k**) and group velocity (same direction with Poynting power) are in opposite direction, this means that power propagation of electromagnetic wave and wave vector are anti-parallel indicating a backward wave propagating (H. Chen, Wu, & Kong, 2006; Pendry, 2004) as shown in Figure 2.9.

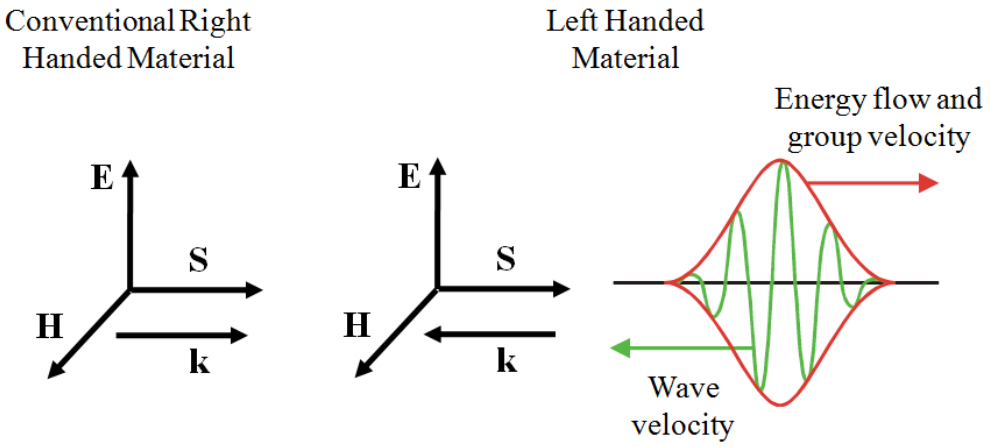

Figure 2.9: Relationship of **k**,**E** and **H** for right handed material $(\mu > 0, \varepsilon > 0)$ and left handed material $(\mu < 0, \varepsilon < 0)$. Wave velocity is opposite of energy flow and group velocity for wave envelope propagation in LHM.

2.6.2 Realization of Metamaterial

Pendry demonstrated that negative refractive medium would still obey Snell law but refract light to angle opposite of conventional lens with positive refractive index (Pendry, 2000). This is achieved by using both $\varepsilon = -1$ and $\mu = -1$. The wire array with lattice spacing that act as plasma with resonant frequency ω_{ep} would yield dielectric response over microwave region (Sievenpiper, Sickmiller, & Yablonovitch, 1996; Pendry, Holden, Stewart, & Youngs, 1996; Pendry, Holdent, Robbins, & Stewart, 1998) meanwhile SRR would induce magnetic response (Pendry, Holden, Robbins, & Stewart, 1999). Smith and Kroll presented analytical formula to obtain negative refractive index $n(\omega)$ from effective permittivity $\varepsilon_{eff}(\omega)$ and effective permeability $\mu_{eff}(\omega)$ (Smith & Kroll, 2000; J. A. Kong, 2002) where ω_{ep} is dielectric resonance, when $\omega_{ep}^2 > \omega^2$, $\varepsilon_{eff}(\omega)$ would have negative sign. The ring shape structure would induce magnetic response with magnetic resonant ω_{mp} , F is area fraction of SRR and Γ is dissipation factor.

$$n(\omega) = \varepsilon_{eff}(\omega)\,\mu_{eff}(\omega) \tag{2.53}$$

$$\varepsilon_{eff}(\omega) = 1 - \frac{\omega_{ep}^2}{\omega^2} \tag{2.54}$$

$$\mu_{eff}(\omega) = 1 - \frac{F\omega_{mp}^2}{\omega^2 - \omega_{mp}^2 - i\omega\Gamma} \tag{2.55}$$

When $\omega_{mp}^2 > \omega^2$, $\mu_{eff}(\omega)$ would have negative sign. In the region $\omega_{mp} < \omega < \omega_{ep}$, both $\mu_{eff}(\omega)$ and $\varepsilon_{eff}(\omega)$ are simultaneously negative. Hence, Real part of $n(\omega)$ is negative and propagation is feasible.

Ziolkowski writes permeability μ and permittivity ε as

$$\mu = |\mu| \exp i\phi_\mu \tag{2.56}$$

$$\varepsilon = |\varepsilon| \exp i\phi_\varepsilon \tag{2.57}$$

such that refractive index n is

$$n = |n| \exp \frac{1}{2} i\left(\phi_\varepsilon + \phi_\mu\right) \tag{2.58}$$

where $\frac{\pi}{2} < \frac{1}{2}\left(\phi_\varepsilon + \phi_\mu\right) < \pi$ in which Im n is always positive but Re n could be positive or negative (Ziolkowski & Heyman, 2001). Propagation of electromagnetic wave and SHF inside metamaterial has been investigated (M. W. McCall, Lakhtakia, & Weiglhofer, 2002; Popov & Shalaev, 2006). Various metamaterials have been designed to achieve negative refraction at (Engheta, 2002; Fu et al., 2002; Marques, Martel, Mesa, & Medina, 2002; Martin, Bonache, Falcone, Sorolla, & Marques, 2003; H. Chen et al., 2003, 2004; Gokkavas et al., 2006; Ooi & Ng, 2011; Tuong et al., 2012) GHz and (Ishikawa, Tanaka, & Kawata, 2005; Wongkasem & Akyurtlu, 2006) THz spectrums. Metamaterial at wavelength of 900nm has also been demeonstrated by Klein *et al* (M. W. Klein, Enkrich, Wegener, Soukoulis, & Linden, 2006). Recently, metamaterials from radio frequency to infrared (Padilla, Basov, & Smith, 2006) have been realized.

Wiltshire and Aryeh demonstrated the characteristics of electromagnetic wave propagation in medium with negative permittivity and permeability which lays good foundation for understanding of negative refraction (Wiltshire, 2001; Aryeh, 2005). Quadrant diagram of refraction studied by Wiltshire shown in Figure 2.9 clearly depicts electromagnetic wave propagation through interface between mediums with different ε and μ. The metamaterial with frequency dependent ε and μ is highly dispersive as refractive

index varies rapidly when the sign of ε and μ change from positive to negative or via versa. Investigation of electromagnetic wave propagation inside circular waveguide by Baqir and Choudhury also provides useful insight in modeling of chiral metamaterial (Baqir & Choudhury, 2012). Popov *et al* also demonstrated backward phase matching condition of SHG in metamaterial causes significant change in Manely-Rowe relations (Popov, Slabko, & Shalaev, 2006). Tang *et al* employed both theoretical calculation and experiments to study nonlinear responses in metamaterials (Tang et al., 2011).

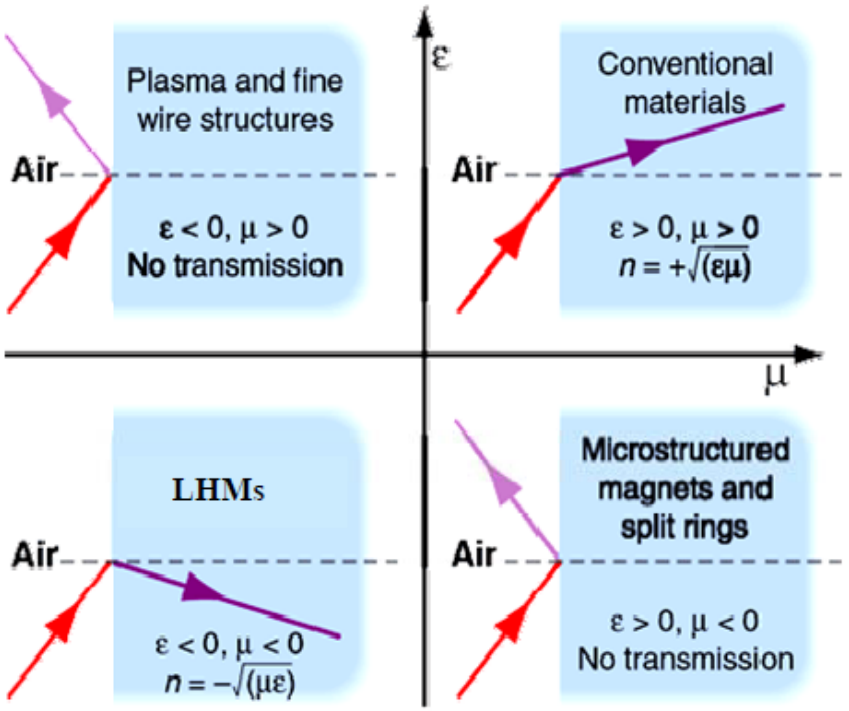

Figure 2.10: The first quadrant shows normal refraction when electromagnetic wave propagating from air to medium with positive μ and ε and the third quadrant shows negative refraction when electromagnetic wave propagating from air to medium with negative μ and ε.

2.7 Photonic Crystal

2.7.1 Overview

PC is an artificial periodic material that used to control propagation of light. PC could be designed and configured in 1, 2 and 3 dimensional periodic structure as shown in Figure 2.10 (Joannopoulos et al., 2008). Dielectric PC that exhibits bandgap at certain frequency range is interesting artificial material that has wide applications (Cowan &

Young, 2002) such as control the propagation of electromagnetic wave (Guida, Lustrac, & Priou, 2003) for developing various optical devices (Soukoulis, 1996). The multiple reflections of electromagnetic wave at the layer interface in one dimensional photonic crystal lead to forbidden (photonic bandgap) region where electromagnetic field is reflected and strongly damped (evanescent wave) within the structure (Quimby, 2006; Ribbing, Hogstrom, & Rung, 2006). PC composed of metalic-dielectric layers demonstrates enhancement of absorption for frequencies within photonic band gap (J. Yu et al., 2004). PC has been made of dielectric rod array (Ozbay, Abeyta, et al., 1994) and stacking of micromachined silicon wafers (Ozbay, Michel, Tuttle, Biswas, Sigalas, & Ho, 1994; Ozbay, Michel, Tuttle, Biswas, Ho, et al., 1994). It was demonstrated number of allowed bands of PC increases with the increase in difference between refractive indices of different layers, besides that, widths of the allowed and forbidden bands also increase with the increase in layer thickness (Ibrahim, Choudhury, & Alias, 2005). PC plays important role optoelectronics technology to develop various optical applications in the area of communication, data storage, imaging, computing and so on (Choudhury & Lakhtakia, 2008).

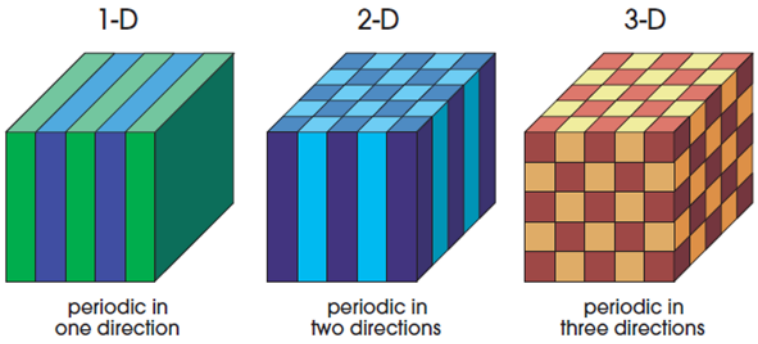

Figure 2.11: 1, 2 and 3 dimensional photonic crystal in which dielectric slabs with different refractive index are arranged in periodic order to reflect light propagation at certain frequency range.

2.7.2 Design and Fabrication of Photonic Crystal

PC has been realized in 1989 by Yablonovitch (Yablonovitch & Gmitter, 1989, 1990). Experiment demonstrated 3 dimensional periodic face centered cubic (FCC) Al_3O_3 dielectric structure could produce a band gap in which no light propagation is allowed in certain frequency band when refractive index contrast ratio between dielectric to empty

space inside structure is 3.5 where the dielctric structure consists of 86% empty space. Yablonovitch also designed diamond PC which could be fabricated by drilling three sets of holes with specified angle onto top surface of wafer slab (Yablonovitch, Gmitter, & Leung, 1991). This structure is known Yablonovite. The FCC and fabrication of diamond PC are illustrated in Figure 2.12.

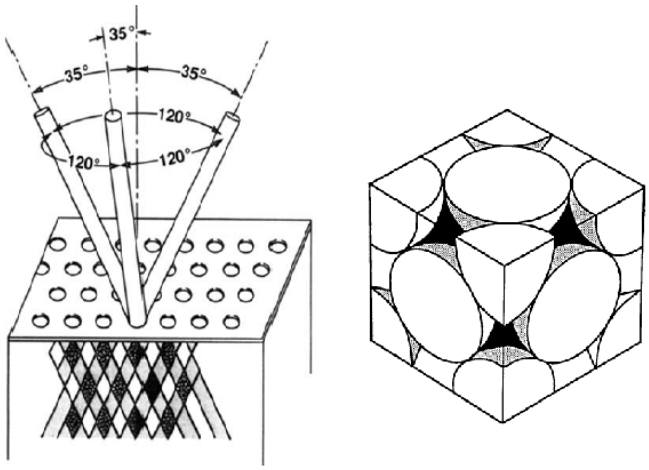

Figure 2.12: Fabrication of FCC by drilling three sets of holes onto top surface of wafer slab to form PC with band gap at micro wave region.

Ho *et al* employed plane wave expansion method to solve Maxwell equation for modeling light propagating as Bloch wave inside periodic dielectric lattice arranged in diamond structure and suggested a novel method to obtain optimum parameters such as refractive index contrast and filling ratio of dielectric with respect to empty space for PC (Ho, Chan, & Soukoulis, 1990). Yablonovitch *et al* introduced defect into FCC PC and observed donor and acceptor mode inside photonic bandgap which opens up possibility to design laser microresonator cavities (Yablonovitch, Gmitter, Meade, et al., 1991). Sajeev and Wang also analyzed quantum electrodynamic near a photonic band gap (John & Wang, 1990). 2 dimensional PCs with various design as shown in Figure 2.13 have been designed and fabricated to identify both transmission band and band gap (S. L. McCall, Platzman, Dalichaouch, Smith, & Schultz, 1991; Plihal & Maradudin, 1991; Plihal, Shambrook, Maradudin, & Sheng, 1991; Meade, Brommer, Rappe, & Joannopoulos, 1992; Villeneuve & Piche´, 1992; Pan, Zhuang, & Li, 2003; Kalra & Sinha, 2006; Lazar & Sterian, 2008).

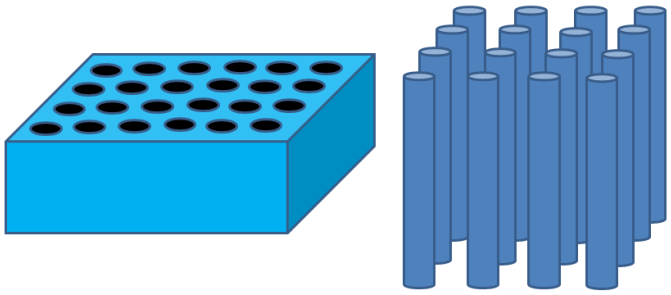

Figure 2.13: 2D PC design: periodic air hole array on dielectric and dielectric rods in air arranged in square lattice.

The 3 dimensional PC could be fabricated by doping metallodielectric on silicon substrates (McIntosh et al., 1997). The first 3 dimensional PC with infrared bandgap was realized with the wood pile structure in which silicon tiny rods piled layer by layer to form periodic configuration (S. Y. Lin, Fleming, et al., 1998; Noda, Tomoda, Yamamoto, & Chutinan, 2000) as shown in Figure 2.14. In 1999, 3 dimensional PC was constructed by stacking GaAs (or InP) stripes with a wafer-fusion technique to form an asymmetric face-centered-cubic structure to produce bandgap at infrared region and the band gap is observed independently of the incident angles of the pumped laser beam (Noda, Yamamoto, Kobayashi, Okano, & Tomoda, 1999).

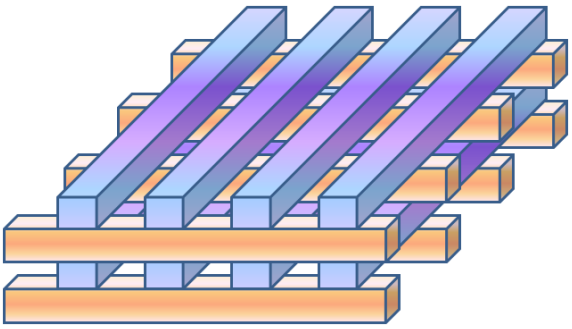

Figure 2.14: Stacking of crystaline semiconductor strip in wood pile structure.

It is reported that very high transmission efficiency of light would occur at certain frequency range in 1 dimensional PC. This would guide the light to propagate around a sharp corner (Mekis et al., 1996). Lin *et al* used 2 dimensional PC to construct waveguide to guide the light in straight and also steer light around a sharp corner at mircowave region as shown in Figure 2.15 (S. Y. Lin, Chow, Hietala, Villeneuve, & Joannopoulos, 1998).

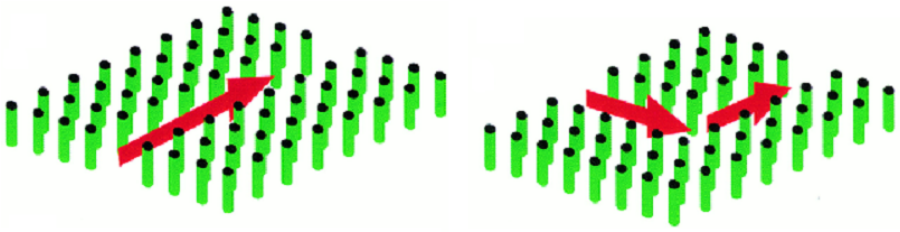

Figure 2.15: Photonic crystal waveguide confine the light and guide its propagation in straight direction and steers light propagation around the sharp corner.

PC could enhance nonlinear effect and therefore enable design of efficient optical signal processing device (Soljacic & Joannopoulos, 2004) which control group velocity of light (Soljacic et al., 2002). The 1 dimesnional PC has been used as refractometer to detect refrective index of material with high accuracy (Matias, Del Villar, Arregui, & Claus, 2003). Band gap structure of nonlinear 1 dimensional PC with Kerr effect has been investigated by Huttunen (Huttunen & Torma, 2002) for designing optical switching device. Further details of slow light control by PC and various applications are explained comprehensively by Notomi (Notomi, 2010). Light trapping is also feasible in PC (Mallick, Agrawal, & Peumans, 2010; D. Zhou & Biswas, 2008; Vardeny & Raikh, 2007).

PCs with metamaterial that show negative refraction have been extensively studied (Shvets, 2003; Luo, Johnson, Joannopoulos, & Pendry, 2003; Parimi et al., 2004; Popov, Shalaev, Slabko, Myslivets, & Nefedov, 2013). TMM has been employed to compute transmission, reflection, phase of reflection, and absorption in metamaterials (Markos & Soukoulis, 2001). Chen *et al* investigated photon tunnelling in 1 dimensional metamaterial photonic crystals by using transfer matrix (Y. Y. Chen, Huang, Wang, Li, & Shi, 2005). Du *et al* demonstrated significant SHG enhancement from periodic 1 dimensional PC with negative permittivity and permeability (Du, Ren, Kam, & Sun, 2009). Gynko *et al* studied near field coupling and SHG in SRR arrays (Grynko et al., 2012). SHG in metamaterial photonic structure has been studied (Biris & Panoiu, 2010). Klein *et al* also investigated SHG from photonic metamaterials experimentally by using 170fs pulse (M. W. Klein, Wegener, Feth, & Linden, 2007). Hao and Lei developed 4×4 transfer matrix to study electromagnetic wave scattering in metamaterials (J. Hao & Zhou, 2008). Coupling effects in photonic metamaterials have also been studied (H. Xu et al., 2011).

These interesting findings have motivated us to further investigate SHG from nonlinear PC with negative refraction by using TMM.

2.8 Utrashort Pulse

2.8.1 Overview

In 1966, DeMaria demonstrated ultrashort pulse laser in picosecond which has accelerated research in nonlinear optics (DeMaria, Ferrar, & Danielson, 1966). Ultrashort pulse is commonly known as electromagnetic pulse whose pulse duration falls in the range in picosecond (ps) where 1ps=10^{-12}s to femtosecond (fs) where 1fs=10^{-15}s. Generation of faster pulse in attosecond scale (10^{-18}s) become feasible in early 2000 (Corkum, 2000; Reid, 2001). In general, ultrashort pulse generation could be realized by means of additive pulse mode locking and Kerr lens mode locking. This has stimulated various novel methods to generate ultrashort pulse such as nonlinear external resonator (Mark, Liu, Hall, Haus, & Ippen, 1989), mode locking of Nd:glass laser (Krausz, Brabec, Wintner, & Schmidt, 1989; Spielmann, Krausz, Brabec, Wintner, & Schmidt, 1991) which has disadvantage of thermal instability , mode locking of neodymium-doped fiber laser (Wigley, French, & R., 1990; Sargsjan, Stamm, Unger, Zschocke, & Ledig, 1991), mode locking of erbium-doped fiber laser (Takada & Miyazawa, 1990; Davey, Langford, & Ferguson, 1991; Chow et al., 1996), mode locking of Pr^{3+}-doped silica fiber laser (Y. Shi, Poulsen, Sejka, & Poulsen, 1994) and mode locking of Nd^{3+}-doped mixed scandium garnets (Sorokin et al., 1993). Ultrashort pulse has very high peak power compared with longer pulses, hence it opens up possibility for efficient data transfer by ultilizing high carrier frequency and larger bandwidth. These unique features of ultrashort pulse make it superior to continuous laser beam in applications that require short interaction time and high peak power (Rusu, 2006). The nonlinear optical interaction is significantly enhanced by using ultrashort pulse (Diels & Rudolph, 1996). Nonlinear processes induced by ultrashort pulse in silicon-on-insulator waveguide such as self phase modulation, four wave mixing, stimulated Raman scattering etc are tabulated by Dekker *et al* (Dekker, Usechak, Forst, & Driessen, 2007). In general, electric field E of ultrashort pulse could be expressed in either time or frequency domain. Electric field in time domain is $E(t)$ and $\tilde{E}(\omega)$ in frequency (spectral) domain could be obtained by performing complex Fourier

transform

$$\begin{aligned}\tilde{E}(\omega) &= \mathscr{F}\{E(t)\} \\ &= \int_{-\infty}^{\infty} E(t)\, e^{-i\omega t} dt \\ &= \left|\tilde{E}(\omega)\right| e^{i\Phi(\omega)}\end{aligned} \tag{2.59}$$

where $\left|\tilde{E}(\omega)\right|$ is spectral amplitude and $\Phi(\omega)$ is spectral phase. $E(t)$ could be obtained by performing inverse Fourier transform

$$\begin{aligned}E(t) &= \mathscr{F}^{-1}\left\{\tilde{E}(\omega)\right\} \\ &= \frac{1}{2\pi}\int_{-\infty}^{\infty} \tilde{E}(\omega)\, e^{i\omega t} d\omega\end{aligned} \tag{2.60}$$

this relationship is important to investigate response of ultrashort pulse propagation in optical medium. The shape of ultrashort pulse is defined in spectral domain $\tilde{E}(\omega)$ where $\Phi(\omega)$ determines pulse duration and shape for any given$\left|\tilde{E}(\omega)\right|$. $E(t)$ is real quantity, hence

$$\tilde{E}(\omega) = \tilde{E}^{*}(\omega) \tag{2.61}$$

where $\tilde{E}^{*}(\omega)$ is complex conjugate of $\tilde{E}(\omega)$. When ultrashort pulse propagating through the dispersive medium, spectral content of pulse is modified by self phase modulation (SPM) process (Brewer, 1967; Shimizu, 1967; Cheung, Rank, Chiao, & Townes, 1968; Stolen & Lin, 1978). Ultrashort pulse will induce varying refractive index in the medium caused by Kerr effect. As a result, this varying refractive index would lead to phase shift in the pulse itself. For any optical pulse with electric field $\tilde{E}(z,t)$, carrier frequency ω_0 and amplitude $\tilde{A}(z,t)$

$$\tilde{E}(z,t) = \tilde{A}(z,t)\, e^{i(kz-\omega_0 t)} + c.c \tag{2.62}$$

in an optical medium with length of L and refractive index due to Kerr effect expressed as

$$n(t) = n_0 + n_2 I(t) \tag{2.63}$$

where n_0 and n_2 are linear and second order nonlinear refractive index respectively meanwhile

$$I(t) = \frac{n_0 c}{2\pi}\left|\tilde{A}(z,t)\right|^2 \tag{2.64}$$

assuming no pulse shaping and medium responds to pulse intensity in instantaneous manner, phase change of the transmitted pulse is

$$\phi_{NL}(t) = -\frac{n_2 I(t)\,\omega_0 L}{c} \tag{2.65}$$

where $I(t)$ is time varying intensity of the pulse, suppose pulse hyperbolic secant (sech) pulses, $I(t)$ is written

$$I(t) = I_0 \,\mathrm{sech}^2\left(\frac{t}{\tau_0}\right) \tag{2.66}$$

τ_0 is the pulse width. The instantaneous frequency of the pulse is

$$\omega(t) = \omega_0 + \delta\omega(t) \tag{2.67}$$

$$\begin{aligned} \delta\omega(t) &= \frac{d}{dt}\phi_{NL}(t) \\ &= \frac{2n_2\omega_0 L}{\tau_0 c} I_0^2 \,\mathrm{sech}\left(\frac{t}{\tau_0}\right)\tanh\left(\frac{t}{\tau_0}\right) \end{aligned} \tag{2.68}$$

therefore, Equation 2.67 becomes

$$\omega(t) = \omega_0 + \frac{2n_2\omega_0 L}{\tau_0 c} I_0^2 \,\mathrm{sech}\left(\frac{t}{\tau_0}\right)\tanh\left(\frac{t}{\tau_0}\right) \tag{2.69}$$

as we could observe Equation 2.69, spectral broadening occurs for $n_2 > 0$ as shown in Figure 2.16.

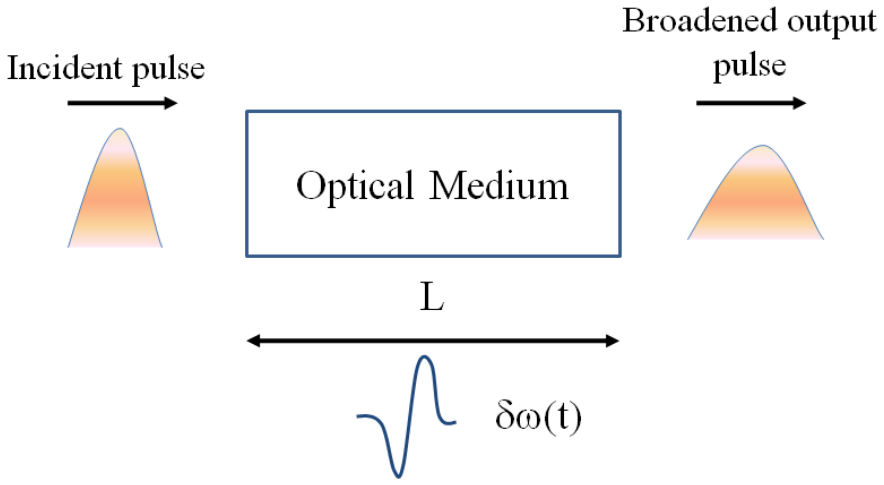

Figure 2.16: Incident pulse propagates through medium with length of L, change in instantaneous frequency of pulse $\delta\omega(t)$ causes broadening of output pulse.

SPM is important in generating broadened spectra in optical engineering . Parmigiani *et al* proposed superstructured fiber Bragg grating to generate SPM broadened spectra (Parmigiani et al., 2006; Okawachi, Sharping, Xu, & Gaeta, 2006). Optical pulse

propagation in photonic crystal has been studied (Bhat & Sipe, 2001). The propagation equation of ultrashort pulse could be described by Equation 2.22.

2.8.2 Application of Ultrashort Pulse Laser

The Ultrashort pulse laser has many applications due to its property compared with continuous beam as discussed in previous section (Keller, 2003). Ashikin tabulated applications of ultrashort pulse in light scattering, cloud physics, aerosol science, atomic physics, quantum optics, and high-resolution spectroscopy (Ashkin, 1980). Ashikin demonstrated application of continuous laser pulse to accelerate and trap particle (Ashkin, 1970). Ultrashort pulse with characteristics of short pulse duration, high peak power, wide spectral bandwidth, and low timing jitter has wide application in optically interconnected system such as time-division multiplexing, single-source wavelength-division multiplexing, and precise time-domain testing of circuits (Keeler et al., 2003). It has been demonstrated that femtosecond lasers could be used for optical tweezing and simultaneously utilized to induce nonlinear multi-photon processes such as two-photon excitation (Agate, Brown, Sibbett, & Dholakia, 2004; De, Roy, & Goswami, 2011). Ultrashort pulse has been applied to develop efficient resolution imaging system for biological system (Campagnola, Wei, Lewis, & Loew, 1999; Bordenave, Abraham, Jonusauskas, Oberle, & Rulliere, 2002). Other than imaging system, laser has also been employed in surgery (Loesel, Niemz, Bille, & Juhasz, 1996; Juhasz et al., 1999, 2000).

Femtosecond laser could be used to fabricate naostructure material (Korte et al., 2000, 2003). This is important for fabrication of photonic crystals and microoptical devices. Ultrashort laser is also widely applied in ablation and machining process (Nedialkov, Imamova, & Atanasov, 2004; Shah, Tawney, Richardson, & Richardson, 2004, 2005). Jaque demonstrated generation of red, green, and blue laser light by means of frequency doubling and self sum frequancy mixing where ultrashort pulse is pumped upon crystal (Jaque, Capmany, & Garcia Sole, 1999). Korn *et al* demosntrated a continuous, stable, ultrashort pulse hard x-ray point source by focusing 50fs laser pulse onto liquid-metal gallium jet (Korn et al., 2002). Ultrashort pulse is ideal pump source for strong nonlinear optical interaction which would lead to ultra broadband radiation. One of the example is supercontinuum generation in photonic crystal (Dudley, Genty, & Coen, 2006).

Kano and Hamaguchi demonstrated supercontiuum generation from photonic crystal fiber and suggested application for coherent Raman spectroscopy (Kano & Hamaguchi, 2003). Klarskov *et al* experimentally demonstrated generation of broadened spectral needed for coherent anti-Stokes Raman scattering microscopy by pumping femtosecond laser pulse onto photonic crystal fiber (Klarskov, Isomaki, Hansen, & Andersen, 2011). Supercontinuum generation from ultrahigh numerical aperture fiber by pumping Ti:sapphire laser could generate the single-mode, high-bandwidth light needed for developing coherence tomography system (Marks, Oldenburg, Reynolds, & Boppart, 2002).

CHAPTER 3

SHG IN NONLINEAR PC WITH NEGATIVE REFRACTIVE INDEX

3.1 Introduction

In this chapter, we investigate SHG in photonic crystal with negative refractive index. Recently, a novel phased matched structure was introduced to control SHG in metamaterial (Rose, Huang, & Smith, 2000; Shadrivov, Zharov, & Kivshar, 2006; Gentile et al., 2011). Their works motivate our theoretical study of SHG in photonic crystal with negative refractive index materials. We consider a 1D periodic photonic crystal driven by a laser field with frequency ω and directed along the z axis as shown in Figure 3.1.

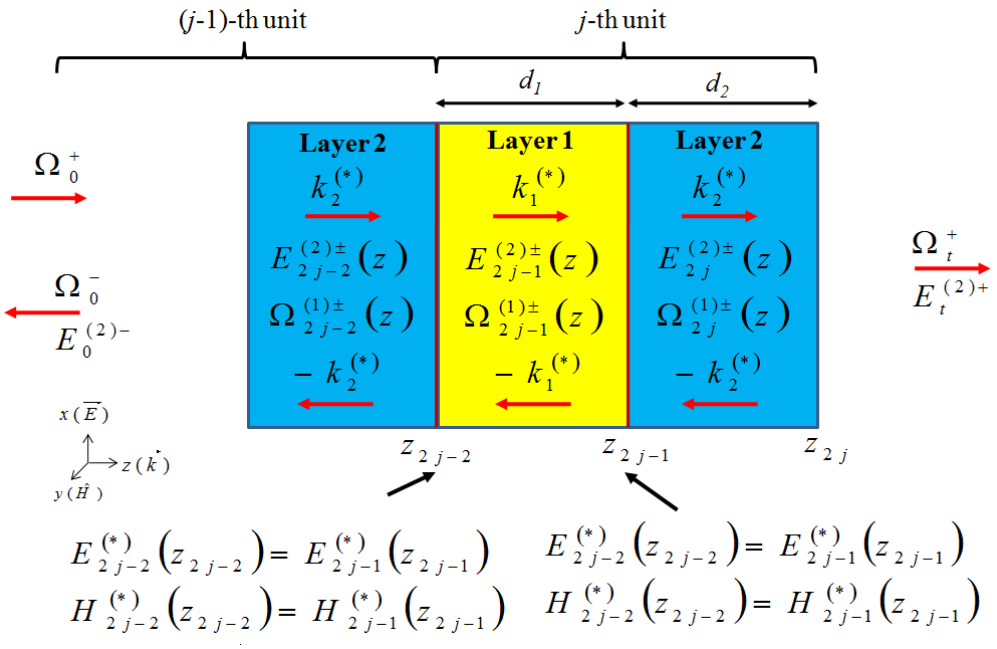

Figure 3.1: An incident field Ω_0^+ is pumped upon photonic crystal, Ω_0^- is the reflected FF field. $E_i^{(*)\pm}$, $H_i^{(*)\pm}$ and $k_i^{(*)}$ represent electric field, magnetic field and wave vector of FF and SH wave in the i-th layer respectively. Here, $* = 1$ and $* = 2$ represent FF and SH respectively, $+$ for forward and $-$ for backward, $i = 2j-2, 2j$ for layer 2 (even layer) and $i = 2j-1$ for layer 1 (odd layer). The $E_i^{(*)}$ and $H_i^{(*)}$ fields are continuous accross interface $z = 2j-2$, $z = 2j-1$ and $z = 2j$. The transmitted FF and SH fields are Ω_t^+ and $E_t^{(2)+}$ respectively.

The structure has N period, each unit is a bilayer consisting of two thin layers, called odd and even layers. Previous work (J. J. Li, Li, & Zhang, 2007) considered nonlinear photonic crystal with susceptibility $\chi_2^{(2)}$ at even layer that has a phase difference of π from the odd layer, i.e. $\chi_1^{(2)} = -\chi_2^{(2)}$ and also linear photonic crystal with negative refractive index (Z. Y. Wang, Chen, He, Fan, & Yan, 2008). Here, we consider a different scenario, nonlinear photonic crystal composed of generally complex ε_{eff} and μ_{eff} around resonant regions and real values for far away from any resonance, allowing for layers with simultaneous negative permittivity and negative permeability. We use TMM to compute the FF and SH field inside the nonlinear photonic crystal. Transmission and reflection spectra for both FF and SH fields are analyzed for different thickness of the layers. Interesting effects of the SHG are found when negative refractive index materials are incorporated into the nonlinear photonic crystal, although material dispersion is neglected. The results provide useful insights and open up possibilities for developing novel frequency conversion devices.

3.2 Linear Part: Fundamental Fields

The complex fundamental field (FF, superscript (1)) electric field inside the homogenous layer i with respect to time is

$$E_i^{(1)}(z,t) = [\Omega_i^+ e^{ik_i^{(1)}(z-z_{i-1})} + \Omega_i^- e^{-ik_i^{(1)}(z-z_{i-1})}]e^{-i\omega t} \tag{3.1}$$

where Ω_i^+ and Ω_i^- are transmission and reflection amplitudes, respectively, $k_i^{(1)} = n_i^{(1)} k_0^{(1)}$ is the wavevector, $z_i - z_{i-1} = d_i$ is the thickness of layer i. The wavevector for FF wave in vacuum is $k_0^{(1)} = \frac{\omega}{c}$. Here $n_i^{(1)}(\omega) = \pm\sqrt{\mu_{eff(i)}^{(1)}(\omega)\,\varepsilon_{eff(i)}^{(1)}(\omega)} = \frac{k_i^{(1)}}{k_0^{(1)}}$ where $\mu_{eff(i)}^{(1)}(\omega)$ is the dimensionless relative magnetic permeability of the medium. The Maxwell equation $\nabla \times \mathbf{E}_i^{(1)} = ik_0^{(1)} c\mu_0 \mu_{eff(i)}^{(1)}(\omega)\,\mathbf{H}_i^{(1)}$ gives magnetic field inside the homogenous layer i with respect to time

$$c\mu_0 H_i^{(1)}(z,t) = \frac{n_i^{(1)}}{\mu_{eff(i)}^{(1)}}[\Omega_i^+ e^{ik_i^{(1)}(z-z_{i-1})} - \Omega_i^- e^{-ik_i^{(1)}(z-z_{i-1})}]e^{-i\omega t} \tag{3.2}$$

Arrange $E_i^{(1)}(z,t)$ and $H_i^{(1)}(z,t)$ in the matrix,

$$\begin{bmatrix} E_i^{(1)}(z) \\ c\mu_0 H_i^{(1)}(z) \end{bmatrix} = \begin{bmatrix} 1 & 1 \\ \frac{n_i^{(1)}}{\mu_{eff(i)}^{(1)}} & -\frac{n_i^{(1)}}{\mu_{eff(i)}^{(1)}} \end{bmatrix} \begin{bmatrix} \Omega_i^+(z) \\ \Omega_i^-(z) \end{bmatrix} \tag{3.3}$$

This Equation 3.3 would be the baseline to develop transfer matrix in this chapter. We shall refer to Figure 3.1 when applying the continuity condition for E and H fields across interfaces to develop the entire transfer matrix for FF and SH electric fields. From Equation 3.1, we have the field $E^{(1)}_{2j-1}(z,t)$ across the odd $(i=2j-1)$ and $E^{(1)}_{2j}(z,t)$ across even layers $(i=2j)$ with $j=1,2,...N$ being the index for the j-th unit. Then $\Omega^{\pm}_{2j}$ and $\Omega^{\pm}_{2j-1}$ are the transmission (reflection) complex field amplitude of FF at the interface z_{2j-1} and z_{2j-2}, respectively. The general expressions of electric field in odd and even layers are

$$E^{(1)}_{2j-1}(z,t) = [\Omega^{+}_{2j-1}e^{ik^{(1)}_1(z-z_{2j-2})}+\Omega^{-}_{2j-1}e^{-ik^{(1)}_1(z-z_{2j-2})}]e^{-i\omega t} \quad (3.4)$$

$$E^{(1)}_{2j}(z,t) = [\Omega^{+}_{2j}e^{ik^{(1)}_2(z-z_{2j-1})}+\Omega^{-}_{2j}e^{-ik^{(1)}_1(z-z_{2j-1})}]e^{-i\omega t} \quad (3.5)$$

where $\Omega^{\pm}_{2j}$ and $\Omega^{\pm}_{2j-1}$ are the transmission (reflection) complex field amplitude of FF at the interface z_{2j-1} and z_{2j-2}, respectively.

3.2.1 Boundary Condition for Odd-Even (OE) Interface

At the back boundaries ($z=z_{2j-1}=z_{2j-2}+d_1$) of the even $2j$ layers,$j=1,2,3,...$, we consider $E^{(1)}_{2j-1}$ at interface $2j-2$ and $E^{(1)}_{2j}$ at interface $2j-1$

$$\begin{aligned} E^{(1)}_{2j-1}(z_{2j-2},t) &= [\Omega^{+}_{2j-1}e^{ik^{(1)}_1(z_{2j-2}-z_{2j-2})}+\Omega^{-}_{2j-1}e^{-ik^{(1)}_1(z_{2j-2}-z_{2j-2})}]e^{-i\omega t} \quad (3.6)\\ &= [\Omega^{+}_{2j-1}+\Omega^{-}_{2j-1}]e^{-i\omega t} \end{aligned}$$

and

$$\begin{aligned} E^{(1)}_{2j}(z_{2j-1},t) &= [\Omega^{+}_{2j}e^{ik^{(1)}_2(z_{2j-1}-z_{2j-1})}+\Omega^{-}_{2j}e^{-ik^{(1)}_1(z_{2j-1}-z_{2j-1})}]e^{-i\omega t} \quad (3.7)\\ &= [\Omega^{+}_{2j}+\Omega^{-}_{2j}]e^{-i\omega t} \end{aligned}$$

from Equations 3.6 and 3.7, we write the fields in matrix form

$$\begin{bmatrix} E^{(1)}_{2j-1}(z_{2j-2},t) \\ c\mu_0 H^{(1)}_{2j-1}(z_{2j-2},t) \end{bmatrix} = D_1 \begin{bmatrix} \Omega^{+}_{2j-1} \\ \Omega^{-}_{2j-1} \end{bmatrix} e^{-i\omega t} \quad (3.8)$$

$$\begin{bmatrix} E^{(1)}_{2j}(z_{2j-1},t) \\ c\mu_0 H^{(1)}_{2j}(z_{2j-1},t) \end{bmatrix} = D_2 \begin{bmatrix} \Omega^{+}_{2j} \\ \Omega^{-}_{2j} \end{bmatrix} e^{-i\omega t} \quad (3.9)$$

where $D_i = \begin{bmatrix} 1 & 1 \\ \frac{n_i^{(1)}}{\mu_{eff(i)}^{(1)}} & -\frac{n_i^{(1)}}{\mu_{eff(i)}^{(1)}} \end{bmatrix}$ with $i = 2j, 2j-1$.At the front boundaries ($z = z_{2j-1} = z_{2j-2} + d_1$) of $2j-1$(odd) layer, we consider $E_{2j-1}^{(1)}$ at interface $2j-1$ and $E_{2j}^{(1)}$ at interface z_{2j-1}

$$\begin{aligned} E_{2j-1}^{(1)}\left(z_{2j-1},t\right) &= [\Omega_{2j-1}^{+} e^{ik_1^{(1)}\left(z_{2j-1}-z_{2j-2}\right)} + \Omega_{2j-1}^{-} e^{-ik_1^{(1)}\left(z_{2j-1}-z_{2j-2}\right)}]e^{-i\omega t} \quad (3.10) \\ &= [\Omega_{2j-1}^{+} e^{ik_1^{(1)}d_1} + \Omega_{2j-1}^{-} e^{-ik_1^{(1)}d_1}]e^{-i\omega t} \end{aligned}$$

and

$$\begin{aligned} E_{2j}^{(1)}\left(z_{2j},t\right) &= [\Omega_{2j}^{+} e^{ik_2^{(1)}\left(z_{2j}-z_{2j-1}\right)} + \Omega_{2j}^{-} e^{-ik_1^{(1)}\left(z_{2j}-z_{2j-1}\right)}]e^{-i\omega t} \quad (3.11) \\ &= [\Omega_{2j}^{+} e^{ik_2^{(1)}d_2} + \Omega_{2j}^{-} e^{-ik_1^{(1)}d_2}]e^{-i\omega t} \end{aligned}$$

from Equations 3.10 and 3.11, the fields in matrix form are

$$\begin{bmatrix} E_{2j-1}^{(1)}\left(z_{2j-1},t\right) \\ c\mu_0 H_{2j-1}^{(1)}\left(z_{2j-1},t\right) \end{bmatrix} = D_1 \begin{bmatrix} \Omega_{2j-1}^{+} e^{ik_1^{(1)}d_1} \\ \Omega_{2j-1}^{-} e^{-ik_1^{(1)}d_1} \end{bmatrix} e^{-i\omega t} \quad (3.12)$$

$$\begin{bmatrix} E_{2j}^{(1)}\left(z_{2j},t\right) \\ c\mu_0 H_{2j}^{(1)}\left(z_{2j},t\right) \end{bmatrix} = D_2 \begin{bmatrix} \Omega_{2j}^{+} e^{ik_2^{(1)}d_2} \\ \Omega_{2j}^{-} e^{-ik_2^{(1)}d_2} \end{bmatrix} e^{-i\omega t} \quad (3.13)$$

since $z_{2j-1} - z_{2j-2} = d_1$ and $z_{2j} - z_{2j-1} = d_2$ are the thickness of the odd$(i=1)$ layer 1 and even $(i=2)$ layer 2. Considering the continuity of the tangential fields at boundary across z_{2j-1}, combining Equations 3.9 and 3.12, we could obtain Maxwell boundary condition equation

$$\begin{bmatrix} E_{2j-2}^{(1)}\left(z_{2j-2},t\right) \\ c\mu_0 H_{2j-2}^{(1)}\left(z_{2j-2},t\right) \end{bmatrix} = \begin{bmatrix} E_{2j-1}^{(1)}\left(z_{2j-2},t\right) \\ c\mu_0 H_{2j-1}^{(1)}\left(z_{2j-2},t\right) \end{bmatrix} \quad (3.14)$$

$$D_2 \begin{bmatrix} \Omega_{2j-2}^{+} e^{ik_2^{(1)}d_2} \\ \Omega_{2j-2}^{-} e^{-ik_2^{(1)}d_2} \end{bmatrix} = D_1 \begin{bmatrix} \Omega_{2j-1}^{+} \\ \Omega_{2j-1}^{-} \end{bmatrix} \quad (3.15)$$

and subsequently transfer matrix for odd-even interface

$$D_1 P_1 \begin{bmatrix} \Omega_{2j-1}^{+} \\ \Omega_{2j-1}^{-} \end{bmatrix} = D_2 \begin{bmatrix} \Omega_{2j}^{+} \\ \Omega_{2j}^{-} \end{bmatrix} \quad (3.16)$$

where $D_1 = D_{2j-1} = \begin{bmatrix} 1 & 1 \\ \frac{n_1^{(1)}}{\mu_{eff(1)}^{(1)}} & -\frac{n_1^{(1)}}{\mu_{eff(1)}^{(1)}} \end{bmatrix}$, $D_2 = D_{2j} = \begin{bmatrix} 1 & 1 \\ \frac{n_2^{(1)}}{\mu_{eff(2)}^{(1)}} & -\frac{n_2^{(1)}}{\mu_{eff(2)}^{(1)}} \end{bmatrix}$ and $P_1 = \begin{bmatrix} e^{ik_1^{(1)}d_1} & 0 \\ 0 & e^{-ik_1^{(1)}d_1} \end{bmatrix}$ describes phase changes in odd layers, $n_1^{(1)}$ and $n_2^{(1)}$ are refractive indices of the odd and even layers respectively.

3.2.2 Boundary Condition for Even-Odd (EO) Interface

Across the even ($i = 2j-2$) and odd ($i = 2j-1$) layers at $z = z_{2j-2} = z_{2j-3} + d_2$, with $j = 2,3,...$ we could find E at the back boundaries (z_{2j-3} and z_{2j-2}) of $2j-2$ and $2j-1$ layers by using 3.4 and 3.5 and corresponding equations in the matrix form by using Equation 3.3.

$$\begin{aligned} E_{2j-2}^{(1)}\left(z_{2j-3},t\right) &= [\Omega_{2j-2}^{+}e^{ik_2^{(1)}\left(z_{2j-3}-z_{2j-3}\right)} + \Omega_{2j-2}^{-}e^{-ik_1^{(1)}\left(z_{2j-3}-z_{2j-3}\right)}]e^{-i\omega t} \quad (3.17) \\ &= [\Omega_{2j-2}^{+} + \Omega_{2j-2}^{-}]e^{-i\omega t} \end{aligned}$$

and

$$\begin{aligned} E_{2j-1}^{(1)}\left(z_{2j-2},t\right) &= [\Omega_{2j-1}^{+}e^{ik_1^{(1)}\left(z_{2j-2}-z_{2j-2}\right)} + \Omega_{2j-1}^{-}e^{-ik_1^{(1)}\left(z_{2j-2}-z_{2j-2}\right)}]e^{-i\omega t} \quad (3.18) \\ &= [\Omega_{2j-1}^{+} + \Omega_{2j-1}^{-}]e^{-i\omega t} \end{aligned}$$

from Equations 3.17 and 3.18, the fields in matrix form could be obtained

$$\begin{bmatrix} E_{2j-2}^{(1)}\left(z_{2j-3},t\right) \\ c\mu_0 H_{2j-1}^{(1)}\left(z_{2j-2},t\right) \end{bmatrix} = D_2 \begin{bmatrix} \Omega_{2j-2}^{+} \\ \Omega_{2j-2}^{-} \end{bmatrix} \quad (3.19)$$

$$\begin{bmatrix} E_{2j-1}^{(1)}\left(z_{2j-2},t\right) \\ c\mu_0 H_{2j-1}^{(1)}\left(z_{2j-2},t\right) \end{bmatrix} = D_1 \begin{bmatrix} \Omega_{2j-1}^{+} \\ \Omega_{2j-1}^{-} \end{bmatrix} \quad (3.20)$$

At the front boundaries (z_{2j-2} and z_{2j-1}) of $2j-2$ and $2j-1$ layers, we consider $E_{2j-2}^{(1)}$ at interface $2j-2$ and $E_{2j-1}^{(1)}$ at interface $2j-1$

$$\begin{aligned} E_{2j-2}^{(1)}\left(z_{2j-2},t\right) &= [\Omega_{z_{2j-2}}^{+}e^{ik_2^{(1)}\left(z_{2j-2}-z_{2j-3}\right)} + \Omega_{z_{2j-2}}^{-}e^{-ik_1^{(1)}\left(z_{2j-2}-z_{2j-3}\right)}]e^{-i\omega t} \quad (3.21) \\ &= [\Omega_{z_{2j-2}}^{+}e^{ik_2^{(1)}d_2} + \Omega_{z_{2j-2}}^{-}e^{-ik_1^{(1)}d_2}]e^{-i\omega t} \end{aligned}$$

and

$$\begin{aligned} E_{2j-1}^{(1)}(2j-1,t) &= [\Omega_{2j-1}^{+}e^{ik_1^{(1)}\left(z_{2j-1}-z_{2j-2}\right)} + \Omega_{2j-1}^{-}e^{-ik_1^{(1)}\left(z_{2j-1}-z_{2j-2}\right)}]e^{-i\omega t} \quad (3.22) \\ &= [\Omega_{2j-1}^{+}e^{ik_1^{(1)}d_1} + \Omega_{2j-1}^{-}e^{-ik_1^{(1)}d_1}]e^{-i\omega t} \end{aligned}$$

from Equations 3.21 and 3.22, the fields in matrix form are

$$\begin{bmatrix} E^{(1)}_{2j-2}\left(z_{2j-2},t\right) \\ c\mu_0 H^{(1)}_{2j-2}\left(z_{2j-2},t\right) \end{bmatrix} = D_2 \begin{bmatrix} \Omega^{+}_{2j-2} e^{ik^{(1)}_2 d_2} \\ \Omega^{-}_{2j-2} e^{-ik^{(1)}_2 d_2} \end{bmatrix} \tag{3.23}$$

$$\begin{bmatrix} E^{(1)}_{2j-1}\left(z_{2j-1},t\right) \\ c\mu_0 H^{(1)}_{2j-1}\left(z_{2j-1},t\right) \end{bmatrix} = D_1 \begin{bmatrix} \Omega^{+}_{2j-1} e^{ik^{(1)}_1 d_1} \\ \Omega^{-}_{2j-1} e^{-ik^{(1)}_1 d_1} \end{bmatrix} \tag{3.24}$$

where $z_{2j-1} - z_{2j-2} = d_1$ and $z_{2j-2} - z_{2j-3} = d_2$, where $\Omega^{\pm}_{2j-2}$ and $\Omega^{\pm}_{2j-1}$ are the transmission (reflection) complex field amplitude of FF at the interface z_{2j-3} and z_{2j-2}, respectively. Considering the continuity at the boundary across z_{2j-2}, combining Equations 3.23 and 3.20 we have Maxwell boundary condition equation

$$\begin{bmatrix} E^{(1)}_{2j-2}\left(z_{2j-2},t\right) \\ c\mu_0 H^{(1)}_{2j-2}\left(z_{2j-2},t\right) \end{bmatrix} = \begin{bmatrix} E^{(1)}_{2j-1}\left(z_{2j-2},t\right) \\ c\mu_0 H^{(1)}_{2j-1}\left(z_{2j-2},t\right) \end{bmatrix} \tag{3.25}$$

and subsequently transfer matrix for even-odd interface

$$D_2 P_2 \begin{bmatrix} \Omega^{+}_{2j-2} \\ \Omega^{-}_{2j-2} \end{bmatrix} = D_1 \begin{bmatrix} \Omega^{+}_{2j-1} \\ \Omega^{-}_{2j-1} \end{bmatrix} \tag{3.26}$$

where $P_2 = \begin{bmatrix} e^{ik^{(1)}_2 d_2} & 0 \\ 0 & e^{-ik^{(1)}_2 d_2} \end{bmatrix}$ describes phase changes in the even layer. Combining Equations 3.16 and 3.26 to eliminate $\begin{bmatrix} \Omega^{+}_{2j-1} \\ \Omega^{-}_{2j-1} \end{bmatrix}$ we have

$$\begin{bmatrix} \Omega^{+}_{2j} \\ \Omega^{-}_{2j} \end{bmatrix} = D_2^{-1} D_1 P_1 D_1^{-1} D_2 P_2 \begin{bmatrix} \Omega^{+}_{2j-2} \\ \Omega^{-}_{2j-2} \end{bmatrix} \tag{3.27}$$

3.2.3 Boundary Condition At Input and Output

At the boundary between air (left) and layer 1, we have

$$\begin{bmatrix} \Omega^{+}_{1} \\ \Omega^{-}_{1} \end{bmatrix} = D_1^{-1} D_0 \begin{bmatrix} \Omega^{+}_{0} \\ \Omega^{-}_{0} \end{bmatrix} \tag{3.28}$$

where

$$D_0 = \begin{bmatrix} 1 & 1 \\ n_0 & -n_0 \end{bmatrix} \tag{3.29}$$

with n_0 being the reflective index for air, Ω_0^+ is the incident fundamental wave and Ω_0^- is the reflected fundamental wave. At the boundary between layer $2N$ (left) and air (right), the transmitted FF field Ω_t^+ is related by

$$D_0 \begin{bmatrix} \Omega_t^+ \\ 0 \end{bmatrix} = D_2 P_2 \begin{bmatrix} \Omega_{2N}^+ \\ \Omega_{2N}^- \end{bmatrix}. \tag{3.30}$$

Combining Equations 3.16,3.26,3.27,3.28 and 3.30, we obtain the transfer matrix equation for period N

$$\begin{bmatrix} \Omega_t^+ \\ 0 \end{bmatrix} = D_0^{-1} L^N D_0 \begin{bmatrix} \Omega_0^+ \\ \Omega_0^- \end{bmatrix} \tag{3.31}$$

where we define $L = \left[D_2 P_2 D_2^{-1} D_1 P_1 D_1^{-1}\right]$ is a transfer matrix for single period consists of layer 1 and layer 2. P_i is known as propagation matrix meanwhile D_i is known as dynamical matrix. From Equation 3.31, we obtain the transmission $T^{(1)} = |t_1^{(1)}|^2$ and the reflection $R^{(1)} = |r^{(1)}|^2$ spectra of the FF wave by using the transmission and reflection coefficients,

$$t^{(1)} = \frac{\Omega_t^+}{\Omega_0^+} = T_{11}^{(1)} - T_{12}^{(1)} \frac{T_{21}^{(1)}}{T_{22}^{(1)}} \tag{3.32}$$

$$r^{(1)} = \frac{\Omega_0^-}{\Omega_0^+} = -\frac{T_{21}^{(1)}}{T_{22}^{(1)}} \tag{3.33}$$

where $T^{(1)} = D_0^{-1} L^N D_0 = \begin{bmatrix} T_{11}^{(1)} & T_{12}^{(1)} \\ T_{21}^{(1)} & T_{22}^{(1)} \end{bmatrix}$. Using the recurrence relations and at the boundary, we have the fundamental fields at any odd layer

$$\begin{bmatrix} \Omega_{2j-1}^+ \\ \Omega_{2j-1}^- \end{bmatrix} = D_1^{-1} L^{j-1} D_0 \begin{bmatrix} \Omega_0^+ \\ \Omega_0^- \end{bmatrix} \tag{3.34}$$

and any even layer

$$\begin{bmatrix} \Omega_{2j}^+ \\ \Omega_{2j}^- \end{bmatrix} = D_2^{-1} D_1 P_1 D_1^{-1} L^{j-1} D_0 \begin{bmatrix} \Omega_0^+ \\ \Omega_0^- \end{bmatrix}. \tag{3.35}$$

3.3 Nonlinear Part: Polarization and SH Fields

For nonlinear optical medium, the interaction of the fundamental wave with medium inside each layer would induce second order nonlinear polarization.

$$\begin{aligned} P_i^{NL}(z,t) &= \varepsilon_0 \chi_i^{(2)} \left(E_i^{(1)}(z,t)\right)^2 e^{-i2\omega t} \\ &= \varepsilon_0 \chi_i^{(2)} \begin{pmatrix} \left(\Omega_i^+\right)^2 e^{i2k_i^{(1)}(z-z_{i-1})} + \left(\Omega_i^-\right)^2 e^{-i2k_i^{(1)}(z-z_{i-1})} \\ +2\Omega_i^+\Omega_i^- \end{pmatrix} e^{-i2\omega t} \end{aligned} \tag{3.36}$$

The nonlinear polarization induced inside the photonic crystal will produce the SH field with frequency 2ω *propagating* along the z axis. The propagation equation of SH wave in i-th layer is

$$\left(\frac{\partial^2}{\partial z^2} + k_i^{(2)2}\right) E_i^{(2)}(z,t) = \mu_i^{(2)} \frac{\partial^2 P_i^{NL}(z,t)}{\partial t^2} \tag{3.37}$$

where $E_i^{(2)}$ is electric field of SH wave, $k_i^{(2)}$ is the SH wavevector inside i-th layer and $\mu_i^{(2)} = \mu_0 \mu_{eff(i)}^{(2)}(\omega)$. Equation 3.37 is derived from Equation 2.22 as shown in appendix. We assume a slowly varying envelope such that the space and time can be separated as $E_i^{(2)}(z,t) = E_i^{(2)}(z)\, e^{-i2\omega t} + c.c.$ Expanding Equation 3.37, we have the equation for the envelope

$$0 = \left(\frac{\partial^2}{\partial z^2} + k_i^{(2)2}\right) E_i^{(2)}(z) + \left(\frac{2\omega}{c}\right)^2 \mu_{eff(i)}^{(2)} \chi_i^{(2)} \begin{Bmatrix} \left(\Omega_i^+\right)^2 e^{i2k_i^{(1)}(z-z_{i-1})} \\ + \left(\Omega_i^-\right)^2 e^{-i2k_i^{(1)}(z-z_{i-1})} \\ +2\Omega_i^+\Omega_i^- \end{Bmatrix} \tag{3.38}$$

because $\frac{\partial^2 e^{(\pm i2\omega t)}}{\partial t^2} = (\pm i2\omega)^2 e^{(\pm i2\omega t)}$ and $c = \frac{1}{\sqrt{\mu_0 \varepsilon_0}}$. Using Laplace transform to solve Equation 3.37, we have the general solution of the SH field as

$$\begin{aligned} E_i^{(2)}(z) &= E_i^{(2)+} e^{ik_i^{(2)}(z-z_{i-1})} + E_i^{(2)-} e^{-ik_i^{(2)}(z-z_{i-1})} \\ &\quad + A_i \left(\Omega_i^+\right)^2 e^{i2k_i^{(1)}(z-z_{i-1})} + A_i \left(\Omega_i^-\right)^2 e^{-i2k_i^{(1)}(z-z_{i-1})} \\ &\quad + C_i 2\Omega_i^+\Omega_i^- \end{aligned} \tag{3.39}$$

where

$$A_i(\omega) = -\left(\frac{2\omega}{c}\right)^2 \frac{\mu_{eff(i)}^{(2)} \chi_i^{(2)}}{k_i^{(2)2} - 4k_i^{(1)2}}, \tag{3.40}$$

$$C_i(\omega) = -\left(\frac{2\omega}{c}\right)^2 \frac{\mu_{eff(i)}^{(2)} \chi_i^{(2)}}{k_i^{(2)2}}. \tag{3.41}$$

where $i = 1,2$ for odd and even layer respectively. Here, we note from Equations 3.40 and 3.41 (coefficients) that, instead of using periodical poling of the nonlinear media in the bilayers, one can achieve the QPM by an alternative method, namely by using negative permeability $\mu_{eff(i)}^{(2)}$ in place of negative $\chi_i^{(2)}$. The SH magnetic field as obtained from the Maxwell equation $\mathbf{H}_i^{(2)}(z) = \frac{1}{ik_0^{(2)} c\mu_i^{(2)}} \left(\nabla \times \mathbf{E}_i^{(2)}(z)\right)$ where

$$\begin{aligned} c\mu_0 H_i^{(2)}(z) &= \frac{n_i^{(2)}}{\mu_{eff(i)}^{(2)}} \left(E_i^{(2)+} e^{ik_i^{(2)}(z-z_{i-1})} - E_i^{(2)-} e^{-ik_i^{(2)}(z-z_{i-1})} \right) \\ &\quad + \frac{n_i^{(1)}}{\mu_{eff(i)}^{(2)}} A_i \left(\left(\Omega_i^+\right)^2 e^{i2k_i^{(1)}(z-z_{i-1})} - \left(\Omega_i^-\right)^2 e^{-i2k_i^{(1)}(z-z_{i-1})} \right) \end{aligned} \tag{3.42}$$

arrange $E_i^{(2)}(z)$ and $H_i^{(2)}(z)$ fields in the matrix form, we have

$$\begin{bmatrix} E_i^{(2)}(z) \\ c\mu_0 H_i^{(2)}(z) \end{bmatrix} = G_i \begin{bmatrix} E_i^{(2)+}(z) \\ E_i^{(2)-}(z) \end{bmatrix} + B_i \begin{bmatrix} A_i \left(\Omega_i^+(z)\right)^2 \\ A_i \left(\Omega_i^-(z)\right)^2 \end{bmatrix} + 2C_i \begin{bmatrix} 1 \\ 0 \end{bmatrix} \Omega_i^+(z)\,\Omega_i^-(z) \tag{3.43}$$

Consider even layers $i = 2(j-1)$

$$\begin{aligned} \begin{bmatrix} E_{2(j-1)}^{(2)}(z) \\ c\mu_0 H_{2(j-1)}^{(2)}(z) \end{bmatrix} &= G_2 \begin{bmatrix} E_{2(j-1)}^{(2)+}(z) \\ E_{2(j-1)}^{(2)-}(z) \end{bmatrix} + B_2 \begin{bmatrix} A_2 \left(\Omega_{2(j-1)}^+(z)\right)^2 \\ A_2 \left(\Omega_{2(j-1)}^-(z)\right)^2 \end{bmatrix} \\ &\quad + 2C_2 \begin{bmatrix} 1 \\ 0 \end{bmatrix} \Omega_{2(j-1)}^+(z)\,\Omega_{2(j-1)}^-(z) \end{aligned} \tag{3.44}$$

odd layers $i = 2j-1$

$$\begin{aligned} \begin{bmatrix} E_{2j-1}^{(2)}(z) \\ c\mu_0 H_{2j-1}^{(2)}(z) \end{bmatrix} &= G_1 \begin{bmatrix} E_{2j-1}^{(2)+}(z) \\ E_{2j-1}^{(2)-}(z) \end{bmatrix} + B_1 \begin{bmatrix} A_1 \left(\Omega_{2j-1}^+(z)\right)^2 \\ A_1 \left(\Omega_{2j-1}^-(z)\right)^2 \end{bmatrix} \\ &\quad + 2C_1 \begin{bmatrix} 1 \\ 0 \end{bmatrix} \Omega_{2j-1}^+(z)\,\Omega_{2j-1}^-(z) \end{aligned} \tag{3.45}$$

and even layers $i = 2j$

$$\begin{aligned} \begin{bmatrix} E_{2j}^{(2)}(z) \\ c\mu_0 H_{2j}^{(2)}(z) \end{bmatrix} &= G_2 \begin{bmatrix} E_{2j}^{(2)+}(z) \\ E_{2j}^{(2)-}(z) \end{bmatrix} + B_2 \begin{bmatrix} A_2 \left(\Omega_{2j}^+(z)\right)^2 \\ A_2 \left(\Omega_{2j}^-(z)\right)^2 \end{bmatrix} \\ &\quad + 2C_2 \begin{bmatrix} 1 \\ 0 \end{bmatrix} \Omega_{2j}^+(z)\,\Omega_{2j}^-(z) \end{aligned} \tag{3.46}$$

where we define

$$G_0 = \begin{bmatrix} 1 & 1 \\ n_{20} & -n_{20} \end{bmatrix} \tag{3.47}$$

$$G_i = \begin{bmatrix} 1 & 1 \\ \frac{n_i^{(2)}}{\mu_{eff(i)}^{(2)}} & -\frac{n_i^{(2)}}{\mu_{eff(i)}^{(2)}} \end{bmatrix} \tag{3.48}$$

$$B_i = \begin{bmatrix} 1 & 1 \\ \frac{2k_0^{(1)} n_i^{(1)}}{k_0^{(2)} \mu_{eff(i)}^{(2)}} & -\frac{2k_0^{(1)} n_i^{(1)}}{k_0^{(2)} \mu_{eff(i)}^{(2)}} \end{bmatrix} = \begin{bmatrix} 1 & 1 \\ \frac{n_i^{(1)}}{\mu_{eff(i)}^{(2)}} & -\frac{n_i^{(1)}}{\mu_{eff(i)}^{(2)}} \end{bmatrix} \tag{3.49}$$

3.3.1 Boundary Condition for Odd-Even Interface

Here, we consider the continuity of electric $E(z)$ and magnetic $H(z)$ fields at $z = z_{2j-1}$ the interface between $2j-1$ (odd) and $2j$ (even) layers ($j > 0$) where left is odd layer and right is even layer, thereforewe could obtain Maxwell boundary equation for odd-even interface

$$\begin{bmatrix} E_{2j-1}^{(2)}(z_{2j-1}) \\ c\mu_0 H_{2j-1}^{(2)}(z_{2j-1}) \end{bmatrix} = \begin{bmatrix} E_{2j}^{(2)}(z_{2j-1}) \\ c\mu_0 H_{2j}^{(2)}(z_{2j-1}) \end{bmatrix} \tag{3.50}$$

by using Equations 3.45 and 3.46, transfer matrix that relates $E_{2j-1}^{(2)\pm}$ and $E_{2j}^{(2)\pm}$ is developed

$$\begin{aligned} \begin{bmatrix} E_{2j-1}^{(2)+} \\ E_{2j-1}^{(2)-} \end{bmatrix} &= (G_1Q_1)^{-1}G_2 \begin{bmatrix} E_{2j}^{(2)+} \\ E_{2j}^{(2)-} \end{bmatrix} + (G_1Q_1)^{-1}B_2 \begin{bmatrix} A_2\left(\Omega_{2j}^{+}\right)^2 \\ A_2\left(\Omega_{2j}^{-}\right)^2 \end{bmatrix} \\ &\quad -(G_1Q_1)^{-1}B_1F_1 \begin{bmatrix} A_1\left(\Omega_{2j-1}^{+}\right)^2 \\ A_1\left(\Omega_{2j-1}^{-}\right)^2 \end{bmatrix} + (G_1Q_1)^{-1}2C_2 \begin{bmatrix} 1 \\ 0 \end{bmatrix} \Omega_{2j}^{+}\Omega_{2j}^{-} \\ &\quad -(G_1Q_1)^{-1}2C_1 \begin{bmatrix} 1 \\ 0 \end{bmatrix} \Omega_{2j-1}^{+}\Omega_{2j-1}^{-} \end{aligned} \tag{3.51}$$

where

$$Q_i = \begin{bmatrix} e^{ik_i^{(2)}d_i} & 0 \\ 0 & e^{-ik_i^{(2)}d_i} \end{bmatrix} \tag{3.52}$$

and

$$F_i = P_i^2 = \begin{bmatrix} e^{i2k_i^{(1)}d_i} & 0 \\ 0 & e^{-i2k_i^{(1)}d_i} \end{bmatrix} \tag{3.53}$$

3.3.2 Boundary Condition for Even-Odd Interface

At the interface $z = z_{2(j-1)}$, where left is even layer and right is odd layer, $j > 0$

$$\begin{bmatrix} E^{(2)}_{2(j-1)}\left(z_{2(j-1)}\right) \\ c\mu_0 H^{(2)}_{2(j-1)}\left(z_{2(j-1)}\right) \end{bmatrix} = \begin{bmatrix} E^{(2)}_{2j-1}\left(z_{2(j-1)}\right) \\ c\mu_0 H^{(2)}_{2j-1}\left(z_{2(j-1)}\right) \end{bmatrix} \tag{3.54}$$

by using Equations 3.44 and 3.45, it is straight forward to obtain transfer matrix that relates $E^{(2)\pm}_{2j-1}$ and $E^{(2)\pm}_{2(j-1)}$

$$\begin{aligned} \begin{bmatrix} E^{(2)+}_{2j-1} \\ E^{(2)-}_{2j-1} \end{bmatrix} &= G_1^{-1}G_2Q_2 \begin{bmatrix} E^{(2)+}_{2(j-1)} \\ E^{(2)-}_{2(j-1)} \end{bmatrix} - G_1^{-1}B_1 \begin{bmatrix} A_1\left(\Omega^+_{2j-1}\right)^2 \\ A_1\left(\Omega^-_{2j-1}\right)^2 \end{bmatrix} \\ &+G_1^{-1}B_2F_2 \begin{bmatrix} A_2\left(\Omega^+_{2(j-1)}\right)^2 \\ A_2\left(\Omega^-_{2(j-1)}\right)^2 \end{bmatrix} + G_1^{-1}2C_2 \begin{bmatrix} 1 \\ 0 \end{bmatrix} \Omega^+_{2(j-1)}\Omega^-_{2(j-1)} \\ &-G_1^{-1}2C_1 \begin{bmatrix} 1 \\ 0 \end{bmatrix} \Omega^+_{2j-1}\Omega^-_{2j-1} \end{aligned} \tag{3.55}$$

3.3.3 Boundary Condition at Input and Output

At the (input) interface between air (at left) and layer 1 (at right),

$$G_1 \begin{bmatrix} E^{(2)+}_1 \\ E^{(2)-}_1 \end{bmatrix} = G_0 \begin{bmatrix} 0 \\ E^{(2)-}_0 \end{bmatrix} - B_1 \begin{bmatrix} A_1\left(\Omega^+_1\right)^2 \\ A_1\left(\Omega^-_1\right)^2 \end{bmatrix} - 2C_1 \begin{bmatrix} 1 \\ 0 \end{bmatrix} \Omega^+_1\Omega^-_1 \tag{3.56}$$

At the (output) interface between layer $2N$ (left) and air (right) (setting $j = N+1$),

$$G_0 \begin{bmatrix} E^{(2)+}_t \\ 0 \end{bmatrix} = G_2Q_2 \begin{bmatrix} E^{(2)+}_{2N} \\ E^{(2)-}_{2N} \end{bmatrix} + B_2F_2 \begin{bmatrix} A_2\left(\Omega^+_{2N}\right)^2 \\ A_2\left(\Omega^-_{2N}\right)^2 \end{bmatrix} + 2C_2 \begin{bmatrix} 1 \\ 0 \end{bmatrix} \Omega^+_{2N}\Omega^-_{2N} \tag{3.57}$$

connect $\begin{bmatrix} E^{(2)+}_1 \\ E^{(2)-}_1 \end{bmatrix}$ and $\begin{bmatrix} E^{(2)+}_2 \\ E^{(2)-}_2 \end{bmatrix}$, the fields in the first and second layers by setting $j = 1$, we have

$$\begin{aligned} \begin{bmatrix} E^{(2)+}_2 \\ E^{(2)-}_2 \end{bmatrix} &= G_2^{-1}G_1Q_1 \begin{bmatrix} E^{(2)+}_1 \\ E^{(2)-}_1 \end{bmatrix} - G_2^{-1}B_2 \begin{bmatrix} A_2\left(\Omega^+_2\right)^2 \\ A_2\left(\Omega^-_2\right)^2 \end{bmatrix} \\ &+G_2^{-1}B_1F_1 \begin{bmatrix} A_1\left(\Omega^+_1\right)^2 \\ A_1\left(\Omega^-_1\right)^2 \end{bmatrix} - G_2^{-1}2C_2 \begin{bmatrix} 1 \\ 0 \end{bmatrix} \Omega^+_2\Omega^-_2 \\ &+G_2^{-1}2C_1 \begin{bmatrix} 1 \\ 0 \end{bmatrix} \Omega^+_1\Omega^-_1 \end{aligned} \tag{3.58}$$

in Equation 3.51. Eliminating $\begin{bmatrix} E_1^{(2)+} \\ E_1^{(2)-} \end{bmatrix}$, we relate the input $E_0^{(2)+}$ and reflected $E_0^{(2)-}$ fields with the fields in the second layer $\begin{bmatrix} E_2^{(2)+} \\ E_2^{(2)-} \end{bmatrix}$. Combine Equations 3.58 and 3.56, we eliminate $\begin{bmatrix} E_1^{(2)+} \\ E_1^{(2)-} \end{bmatrix}$, we relate the input and reflected fields $\begin{bmatrix} E_0^{(2)+} \\ E_0^{(2)-} \end{bmatrix}$ with the fields in the second layer $\begin{bmatrix} E_2^{(2)+} \\ E_2^{(2)-} \end{bmatrix}$

$$\begin{aligned} \begin{bmatrix} E_2^{(2)+} \\ E_2^{(2)-} \end{bmatrix} &= G_2^{-1} N_1 G_0 \begin{bmatrix} E_0^{(2)+} \\ E_0^{(2)-} \end{bmatrix} + G_2^{-1} \left[B_1 F_1 - N_1 B_1 \right] \begin{bmatrix} A_1 \left(\Omega_1^+\right)^2 \\ A_1 \left(\Omega_1^-\right)^2 \end{bmatrix} \\ &\quad - G_2^{-1} B_2 \begin{bmatrix} A_2 \left(\Omega_2^+\right)^2 \\ A_2 \left(\Omega_2^-\right)^2 \end{bmatrix} - G_2^{-1} 2C_2 \begin{bmatrix} 1 \\ 0 \end{bmatrix} \Omega_2^+ \Omega_2^- \\ &\quad + G_2^{-1} [I - N_1] 2C_1 \begin{bmatrix} 1 \\ 0 \end{bmatrix} \Omega_1^+ \Omega_1^- \end{aligned} \tag{3.59}$$

3.4 Recursion Relation

The fields in the second layer is related to the fields in the fourth layer and hence to any even layers through a recursion relation. By combining Equations 3.55 and 3.51, the SH fields between adjacent even layers, $z = 2(j-1)$ and $2j$, could be related by eliminating $\begin{bmatrix} E_{2j-1}^{(2)+} \\ E_{2j-1}^{(2)-} \end{bmatrix}$ giving the recursion relation that relates $\begin{bmatrix} E_{2j}^{(2)+} \\ E_{2j}^{(2)-} \end{bmatrix}$ and $\begin{bmatrix} E_{2(j-1)}^{(2)+} \\ E_{2(j-1)}^{(2)-} \end{bmatrix}$.The fields in the second layer is related to the fields in the fourth layer and hence to any even layers through a recursion relation. By combining Equations 3.55 and 3.51, the SH fields between adjacent even layers, $z = 2(j-1)$ and $2j$, could be related by eliminating $E_{2j-1}^{(2)}$ giving the recursion relation that relates $E_{2j}^{(2)}$ and $E_{2j-2}^{(2)}$. It is helpful to write the recursion relation equation concisely as

$$\begin{bmatrix} E_{2j}^{(2)+} \\ E_{2j}^{(2)-} \end{bmatrix} = Z \begin{bmatrix} E_{2(j-1)}^{(2)+} \\ E_{2(j-1)}^{(2)-} \end{bmatrix} + Y_{2j} \tag{3.60}$$

where

$$Z = G_2^{-1} N_1 G_2 Q_2 \tag{3.61}$$

$$N_i = G_i Q_i G_i^{-1}, (i = 1,2) \tag{3.62}$$

$$Y_{2j} = G_2{}^{-1} \left(X_{2j-2} + O_{2j-1} - W_{2j} \right) \tag{3.63}$$

where

$$X_{2j-2} = N_1 \left\{ A_2 B_2 F_2 \begin{bmatrix} \left(\Omega_{2j-2}^{+}\right)^2 \\ \left(\Omega_{2j-2}^{-}\right)^2 \end{bmatrix} + 2C_2 \begin{bmatrix} 1 \\ 0 \end{bmatrix} \Omega_{2j-2}^{+} \Omega_{2j-2}^{-} \right\} \tag{3.64}$$

$$O_{2j-1} = \left\{ \begin{array}{l} A_1 (B_1 F_1 - N_1 B_1) \begin{bmatrix} \left(\Omega_{2j-1}^{+}\right)^2 \\ \left(\Omega_{2j-1}^{-}\right)^2 \end{bmatrix} \\ \\ +2C_1 (I - N_1) \begin{bmatrix} 1 \\ 0 \end{bmatrix} \Omega_{2j-1}^{+} \Omega_{2j-1}^{-} \end{array} \right\} \tag{3.65}$$

$$W_{2j} = A_2 B_2 \begin{bmatrix} \left(\Omega_{2j}^{+}\right)^2 \\ \left(\Omega_{2j}^{-}\right)^2 \end{bmatrix} + 2C_2 \begin{bmatrix} 1 \\ 0 \end{bmatrix} \Omega_{2j}^{+} \Omega_{2j}^{-} \tag{3.66}$$

for complicated mathematical derivation.

By induction, for $j = N$, we could derive SH recursion for N period as shown in appendix

$$\begin{aligned} \begin{bmatrix} E_{2N}^{(2)+} \\ E_{2N}^{(2)-} \end{bmatrix} &= Z \begin{bmatrix} E_{2(N-1)}^{(2)+} \\ E_{2(N-1)}^{(2)-} \end{bmatrix} + Y_{2N} \\ &= Z^{N-1} \begin{bmatrix} E_2^{(2)+} \\ E_2^{(2)-} \end{bmatrix} + \sum_{j=2}^{N} Z^{N-j} Y_{2j} \end{aligned} \tag{3.67}$$

By induction, we relate $\begin{bmatrix} E_{2N}^{(2)+} \\ E_{2N}^{(2)-} \end{bmatrix}$ to $\begin{bmatrix} E_2^{(2)+} \\ E_2^{(2)-} \end{bmatrix}$. Combining with Equations 3.57 and 3.56, after some straightforward algebras, we derive the final equation for SH output with forward electric field $E_t^{(2)+}$and backward electric field $E_0^{(2)-}$ for $j = N > 0$

$$\begin{bmatrix} E_t^{(2)+} \\ 0 \end{bmatrix} = G_0^{-1} S^N G_0 \begin{bmatrix} 0 \\ E_0^{(2)-} \end{bmatrix} \tag{3.68}$$

$$+G_0^{-1} \sum_{j=1}^{N} S^{N-j} \begin{Bmatrix} N_2 M_1 \begin{bmatrix} \left(\Omega_{2j-1}^{+}\right)^2 \\ \left(\Omega_{2j-1}^{-}\right)^2 \end{bmatrix} \\ +M_2 \begin{bmatrix} \left(\Omega_{2j}^{+}\right)^2 \\ \left(\Omega_{2j}^{-}\right)^2 \end{bmatrix} \\ +N_2 \vec{J}_1 \Omega_{2j-1}^{+} \Omega_{2j-1}^{-} + \vec{J}_2 \Omega_{2j}^{+} \Omega_{2j}^{-} \end{Bmatrix}$$

where $S = N_2 N_1$, $N_i = G_i Q_i G_i^{-1}$, $M_i = A_i(B_i F_i - N_i B_i)$ and $\vec{J}_i = 2C_i [I - N_i] \begin{bmatrix} 1 \\ 0 \end{bmatrix}$ $(i = 1,2)$. The linear amplitudes $\Omega_{2j-1}^{\pm}$ and $\Omega_{2j}^{\pm}$ are given by Equations 3.34 and 3.35. We note that the analytical result Equation 3.68 is slightly different from that of reference (J. J. Li et al., 2007) in the factor 2 in $2C_i$. They employ the air-gap layers in their calculations which is not being used in our work. Our result is also more general as it applies to arbitrary dispersive magnetic materials, making it possible to study nonlinear optical responses with metamaterials.

For convenience, we define

$$D_m = G_0^{-1} S^N G_0 = \begin{bmatrix} D_{11}^{(2)} & D_{12}^{(2)} \\ D_{21}^{(2)} & D_{22}^{(2)} \end{bmatrix} \tag{3.69}$$

and the second term on RHS of Equation 3.68 as

$$T_m = \begin{bmatrix} T_1^{(2)} \\ T_2^{(2)} \end{bmatrix} \tag{3.70}$$

hence, Equation 3.68 becomes

$$\begin{bmatrix} E_t^{(2)+} \\ 0 \end{bmatrix} = \begin{bmatrix} D_{12}^{(2)} E_0^{(2)-} + T_1^{(2)} \\ D_{22}^{(2)} E_0^{(2)-} + T_2^{(2)} \end{bmatrix} \tag{3.71}$$

which gives the reflected and the transmitted SH field, respectively

$$E_0^{(2)-} = -\frac{T_2^{(2)}}{D_{22}^{(2)}} \tag{3.72}$$

$$E_t^{(2)+} = -T_2^{(2)} \frac{D_{12}^{(2)}}{D_{22}^{(2)}} + T_1^{(2)} \tag{3.73}$$

Finally, the transmission $T^{(2)} = |t_2|^2$and reflection $R^{(2)} = |r_2|^2$ spectra for SH electric fields can be computed from corresponding coefficients

$$t_2 = \frac{E_t^{(2)+}}{\Omega_0^+} = \frac{D_{12}^{(2)} E_0^{(2)-} + T_1^{(2)}}{\Omega_0^+} \tag{3.74}$$

$$r_2 = \frac{E_0^{(2)-}}{\Omega_0^+} = -\frac{T_2^{(2)}}{\Omega_0^+ D_{22}^{(2)}} \tag{3.75}$$

We use matlab to put our model into computational program for numerical simulation. We verify accuracy and correctness of our model by reproducing results from other literature. Consider quasi-phase matched 1 dimensional PC made of stronium barium niobate (J. J. Li et al., 2007), refractive index is given by

$$n^2 = a + \frac{b}{\lambda^2 - c} + d\lambda \tag{3.76}$$

where $a = 4.78 + 0.38x$, $b = 1.02 \times 10^5 + 1.48 \times 10^4 x$, $c = 4.72 \times 10^4 + 2.67 \times 10^4 x$, $d = -2.14 \times 10^{-5} x$, λ is wavelenght in nm and $x = 0.75$. Here, $\mu_{eff(i)}^{(1)} = \mu_{eff(i)}^{(2)} = 1$, sign of $\chi^{(2)}$ in odd layer and even layer are positive and negative respectively due to periodic poling. The simulation results agree with findings of literature in which FF with wavelength of 848nm at bandedge would induce SH field at 424nm, transmission and reflection spectra of FF are shown in Figure 3.2.

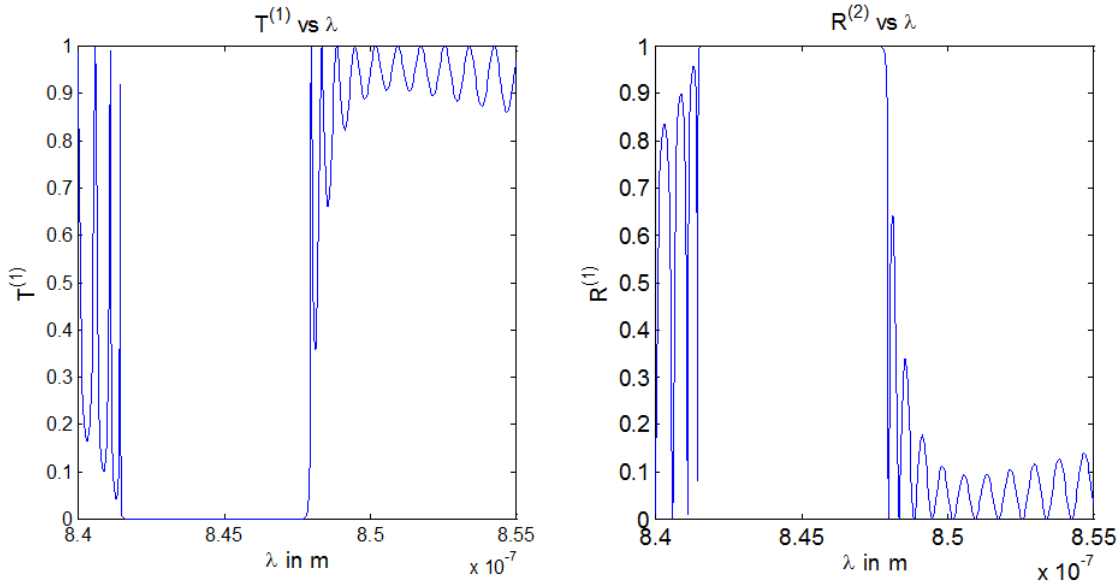

Figure 3.2: Plots of $T^{(1)}$ and $R^{(1)}$ for quasi-phase matched SBN photonic crystal.

3.5 Development of Transfer Matrix with Alternative Approach

Apart from transfer matrix derived in previous sections, we also develop transfer matrix from alternative approach. Here, we define the electric field in each layer shown in Figure 3.3 in which the transmited electric fields propagate from left to right whilst reflected electric fields propagate from right to left. The numerical simulations for both transfer matrice completely agree to each other. The derivation of the transfer matrix with alternative approach is illustrated in Appendix.

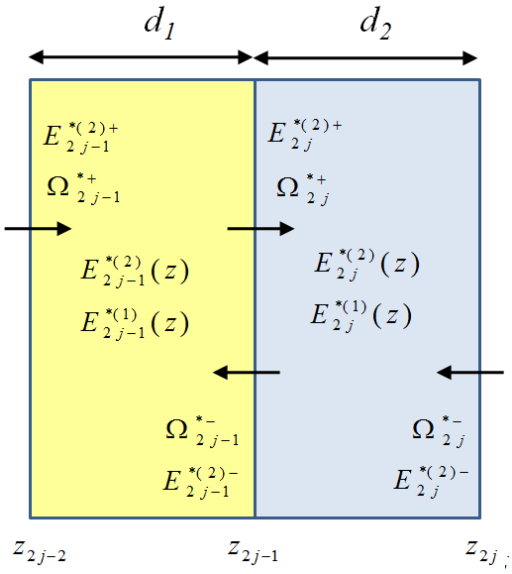

Figure 3.3: Reflected electric fields $E_i^{(j)-}$ propagate from right to left accross interface in bilayer structure for developing transfer matrix by alternative method.

3.6 Refractive Index Characteristics for Metamaterial

The $\mu_{eff(i)}$ is effective relative magnetic permeability and $\varepsilon_{eff(i)}$ is relative dielectric permittivity for negative index metamaterial is dependent on frequency ω. General form of $\mu^{(1)}_{eff(i)}$ for FF (superscipt 1) wave for i-th layer is

$$\mu^{(1)}_{eff(i)}(\omega) = 1 - \frac{F_i\omega^2}{\omega^2 - \omega_{mi}^2 + i\omega\Gamma_i} = A_i e^{i\alpha_i} \tag{3.77}$$

where F_i is area fraction of the nonmagnetic metallic resonator, Γ_i is the dissipation factor, ω_{mi} is the resonance frequency of the structure. The second relation gives the polar form of a complex number.

Similarly, effective relative electric permittivity for FF wave for i-th layer is

$$\varepsilon_{eff(i)}^{(1)}(\omega) = \varepsilon_{\infty i} + \frac{\widetilde{\omega}_i^2}{\omega_{ei}^2 - \omega^2 - i\omega\gamma_i} = B_i e^{i\phi_i} \tag{3.78}$$

where $\widetilde{\omega}_i = \omega_{ei}\sqrt{\varepsilon_{0i} - \varepsilon_{\infty i}}$ is the photon-photon coupling strength, γ_i is the damping coefficient, ω_{ei} is the transverse optical phonon without coupling. The sign of real $\varepsilon_{eff(i)}^{(j)}$ and $\mu_{eff(i)}^{(j)}$ would change from positive to negative or vice versa across the resonance frequencies.

For SH wave, the effective permeability and permittivity become $\mu_{eff}^{(2)}$ and $\varepsilon_{eff}^{(2)}$ where ω in Equations 3.77 and 3.78 are replaced by 2ω for i-th layer which is $\mu_{eff(i)}^{(2)}(\omega) = \mu_{eff(i)}^{(1)}(2\omega)$ and $\varepsilon_{eff(i)}^{(2)}(\omega) = \varepsilon_{eff(i)}^{(1)}(2\omega)$

$$\mu_{eff(i)}^{(2)}(2\omega) = 1 - \frac{F(2\omega)^2}{(2\omega)^2 - \omega_{mi}^2 + i(2\omega)\Gamma_i} \tag{3.79}$$

and

$$\varepsilon_{eff(i)}^{(2)}(2\omega) = \varepsilon_{\infty i} + \frac{\widetilde{\omega}_i^2}{\omega_{ei}^2 - (2\omega)^2 - i\gamma_i(2\omega)} \tag{3.80}$$

The refractive index is defined as

$$n_i^{(j)} = \pm\sqrt{\mu_{eff(i)}^{(j)}\varepsilon_{eff(i)}^{(j)}} \tag{3.81}$$

for both odd and even mediums $(i = 1,2)$ and FF and SH waves $(j = 1,2)$. In the polar form

$$n_i^{(j)} = \sqrt{A_i B_i}\, e^{i(\alpha_i + \phi_i)/2} \tag{3.82}$$

The sign of $\mathrm{Re}n_i^{(j)}$ shall be negative when $0 < (\theta_\varepsilon + \theta_\mu)/2 < \pi/2$ or $3\pi/2 < (\theta_\varepsilon + \theta_\mu)/2 < 2\pi$, particilarly when both $\mu_{eff(i)}^{(j)}$ and $\varepsilon_{eff(i)}^{(j)}$ are negative. The complex $n_i^{(j)}$ would be used to determine wave vector $k_i^{(j)} = jn_i^{(j)}\omega/c$ for both fundamental and second harmonic waves.

In addition to the constant values, we also explore realistic scenario of frequency dependent $\mu_{eff(i)}^{(j)}$ and $\varepsilon_{eff(i)}^{(j)}$, specifically at around resonance region where the parameters are complex. This situation has not been explored so far. The challenge is that at the resonance, the imaginary part of the wavevectors increase significanty. If $\mathrm{Im}k_i^{(j)}$ or $\mathrm{Im}n_i^{(j)}$ is too large, cascaded matrix multiplication in S^N, S^{N-j} and L^N tends to diverge as the term $\exp(\mathrm{Im}k_i^{(j)}d_i)$ in P, Q and F matrices would ramp up rapidly due to instantaneous change of sign in $\mu_{eff(i)}^{(j)}$ and $\varepsilon_{eff(i)}^{(j)}$, this exceeds the numerical capability of the simulations and

eventually causes numerical catastrophe. To overcome this problem, we apply matrix in (Born & Wolf, 1999) to find N-th power of any unimodular M matrix to compute S^N, S^{N-j} and L^N

$$M^N = \begin{bmatrix} m_{11}U_{N-1}(a) - U_{N-2}(a) & m_{12}U_{N-1}(a) \\ m_{21}U_{N-1}(a) & m_{22}U_{N-1}(a) - U_{N-2}(a) \end{bmatrix} \tag{3.83}$$

where $U_N(x) = \frac{\sin\left[(N+1)\cos^{-1}a\right]}{\sqrt{1-a^2}}$ and $a = \frac{1}{2}(m_{11}+m_{22})$.Due to the finite damping it is only possible to use d and N that are smaller than the case of real refractive index to obtain finite output signal. Thus, we use $N = 5$ and $d = 0.1\mu m$ for dispersive material, where we explore the cases of: a) same resonant frequency in both layers and in both $\mu^{(j)}_{eff(i)}$ and $\varepsilon^{(j)}_{eff(i)}$, b) same resonant frequency in both layers but different resonant frequencies in $\mu^{(j)}_{eff(i)}$ and $\varepsilon^{(j)}_{eff(i)}$, c) different resonant frequencies in the layers but same resonant frequency in $\mu^{(j)}_{eff(i)}$ and $\varepsilon^{(j)}_{eff(i)}$, d) different resonant frequencies in both layers and in both $\mu^{(j)}_{eff(i)}$ and $\varepsilon^{(j)}_{eff(i)}$.

3.7 Phase Matching Consideration

Phase matching is important to conserve momentum between FF and SH waves to enable efficient energy transfer from FF photon to SH photon. There are various technique to overcome phase mismatch in nonlinear metamaterial (Rose & Smith, 2011). Recall Equation 2.38 for phase mismatch in SHG, phase mismatch in layer i is written as

$$\Delta k_i = k_i^{(2)} - 2k_i^{(1)} \tag{3.84}$$

this term appears due to the combination of the matrices $Q_i = \begin{bmatrix} e^{ik_i^{(2)}d_i} & 0 \\ 0 & e^{-ik_i^{(2)}d_i} \end{bmatrix}$ and $F_i = \begin{bmatrix} e^{i2k_i^{(1)}d_i} & 0 \\ 0 & e^{-i2k_i^{(1)}d_i} \end{bmatrix}$ in Equations 3.51 and 3.55. The effect of phase mismatch can be reduced for thinner layers. From Equation 3.84, $k_i^{(2)} = \frac{2\omega}{c}n_i^{(2)}$ and $k_i^{(1)} = \frac{\omega}{c}n_i^{(1)}$ we have

$$\begin{aligned} \Delta k_i &= \frac{2\omega}{c}n_i^{(2)} - 2\frac{\omega}{c}n_i^{(1)} \\ &= \frac{2\omega}{c}\left(n_i^{(2)} - n_i^{(1)}\right) \end{aligned} \tag{3.85}$$

for perfect phase matching, $n_i^{(1)} = n_i^{(2)}$ has to be satisfied such as in vacuum, where both FF and SH waves are propagating in the same direction with same phase velocities. However, this is not possible in practice due to dispersion of the medium. Therefore both $\mu_{eff(i)}^{(j)}$ and $\varepsilon_{eff(i)}^{(j)}$ could be carefully chosen in such a way that $\sqrt{\mu_{eff(i)}^{(2)}\varepsilon_{eff(i)}^{(2)}} \simeq 2\sqrt{\mu_{eff(i)}^{(1)}\varepsilon_{eff(i)}^{(1)}}$ to improve phase matching. QPM is a better option to improve phase matching due to inherent constraints of the first two methods.

We use transcendental equation (Ooi & Au Yeung, 1999) to relate Bloch wave vector K_B with frequency ω

$$\cos(K_B d) = \cos\left(k_1^{(1)} d_1\right)\cos\left(k_2^{(1)} d_2\right) - \frac{1}{2}\left(\frac{p}{q} + \frac{q}{p}\right)\sin\left(k_1^{(1)} d_1\right)\sin\left(k_2^{(1)} d_2\right) \quad (3.86)$$

for our case, we use E-polarized electric field in which

$$\frac{p}{q} = \frac{k_2^{(1)}}{k_1^{(1)}} \quad (3.87)$$

hence, Equation 3.86 becomes

$$K_B = \frac{1}{d}\cos^{-1}\left(\cos\left(k_1^{(1)} d_1\right)\cos\left(k_2^{(1)} d_2\right) - \frac{1}{2}\left(\frac{k_2^{(1)}}{k_1^{(1)}} + \frac{k_1^{(1)}}{k_2^{(1)}}\right)\sin\left(k_1^{(1)} d_1\right)\sin\left(k_2^{(1)} d_2\right)\right)$$

we could evaluate photonic band gap structure by studying relationship of K_B and ω in Brillioun zone.

3.8 Results and Discussions

3.8.1 Nondispersive Material

Firstly, we consider two nondispersive layers in which $\mu_{eff(i)}^{(j)}$ and $\varepsilon_{eff(i)}^{(j)}$ are constant and real (postive and negative) such that negative $n_i^{(j)}$ could be obtained. This is feasible because it is a good approximation for frequency far away from resonant region where the values are almost costant over a wide range of frequency range. We consider 1 dimensional periodic bilayer photonic crystal is made of strontium barium niobate (SBN) which has high second order susceptibility $\chi_1^{(2)} = 27.2$ pm/V with period of N. Contrast of refractive index between odd and even layer could be controlled by selecting values of $\mu_{eff(i)}^{(j)}$ and $\varepsilon_{eff(i)}^{(j)}$. The characteristics of both transmission and reflection spectra at FF and SH frequency in relation to N, $\mu_{eff(i)}^{(j)}$ and $\varepsilon_{eff(i)}^{(j)}$ are investigated. This regime is also desirable for practical applications since a small absorption in the medium will cause

significant loss of transmission and reflection over several layers. Secondly, the use of constant values yield results that contain clear and interesting qualitative features as the results of different possibile signs (positive and negative) and magnitudes in the $\mu_{eff(i)}^{(j)}$ and $\varepsilon_{eff(i)}^{(j)}$ compared with their counterparts which are frequency dependent and complex $\mu_{eff(i)}^{(j)}(\omega)$ and $\varepsilon_{eff(i)}^{(j)}(\omega)$. As we could see from Equation 3.40, the denominator is

$$\begin{aligned} k_i^{(2)2} - 4k_i^{(1)2} &= \left[\left(\frac{2\omega}{c}\right)^2 n_i^{(2)2} - 4\left(\frac{\omega}{c}\right)^2 n_i^{(1)2}\right] \\ &= \left(\frac{2\omega}{c}\right)^2 \left[n_i^{(2)2} - n_i^{(1)2}\right] \\ &= \left(\frac{2\omega}{c}\right)^2 \left[\mu_{eff(i)}^{(2)}\varepsilon_{eff(i)}^{(2)} - \mu_{eff(i)}^{(1)}\varepsilon_{eff(i)}^{(1)}\right] \end{aligned} \tag{3.88}$$

therefore, for any real $\mu_{eff(i)}^{(j)}$ and $\varepsilon_{eff(i)}^{(j)}$ which are independent of frequency ω, this would result $\left[\mu_{eff(i)}^{(2)}\varepsilon_{eff(i)}^{(2)} - \mu_{eff(i)}^{(1)}\varepsilon_{eff(i)}^{(1)}\right] = 0$ and therefore numerical error in simulation. Therefore, we introduce $\Delta\mu_{eff(i)}^{(2)} = 0.1$ and $\Delta\varepsilon_{eff(i)}^{(2)} = 0.1$ in such a way that

$$k_i^{(2)2} - 4k_i^{(1)2} = \left[\left(\mu_{eff(i)}^{(2)} + \Delta\mu_{eff(i)}^{(2)}\right)\left(\varepsilon_{eff(i)}^{(2)} + \Delta\varepsilon_{eff(i)}^{(2)}\right) - \mu_{eff(i)}^{(1)}\varepsilon_{eff(i)}^{(1)}\right] \neq 0 \tag{3.89}$$

this approach is valid because it is reasonable to introduce slight difference between refractive index at SH and refractive index at FF for numerical simulation.

Now we evaluate the first scenario where $\mu_{eff(i)}^{(j)}$ and $\varepsilon_{eff(i)}^{(j)}$ for any layer are of same sign and magnitude but same sign and different magnitude between layers

$$S^{(j)} = \left[\pm\mu_{eff(1)}^{(j)}, \pm\varepsilon_{eff(1)}^{(j)}, \pm\mu_{eff(2)}^{(j)}, \pm\varepsilon_{eff(2)}^{(j)}\right]$$

where $\left|\mu_{eff(1)}^{(j)}\right| = \left|\varepsilon_{eff(1)}^{(j)}\right|$ and $\left|\mu_{eff(2)}^{(j)}\right| = \left|\varepsilon_{eff(2)}^{(j)}\right|$, we choose parameters

$$S^{(1)} = (\pm 1, \pm 1, \pm 5, \pm 5), S^{(2)} = (\pm 1.1, \pm 1.1, \pm 5.1, \pm 5.1)$$

Refractive index contrast between two layers at FF ($j = 1$) and SH ($j = 2$) is

$$\Delta n^{(j)} = \sqrt{\left(\pm\mu_{eff(2)}^{(j)}\right)\left(\pm\varepsilon_{eff(2)}^{(j)}\right)} - \sqrt{\left(\pm\mu_{eff(1)}^{(j)}\right)\left(\pm\varepsilon_{eff(1)}^{(j)}\right)}$$

the refractive indices of two layers are same in signs. We use $d = 1\mu$m and $\Omega_0^+ = 8 \times 10^7$ V/m for simulation.

We observe zero reflection $R^{(1)} = 0$ and absolute transmission $T^{(1)} = 1$ in the FF for all values of ω and $\frac{d_1}{d}$ even though there is a significant contrast between the refractive

indices of the two medium. The pump wave intensity is strong enough in such a way that FF propagates through PC without any reflection. In Figure 3.4, we choose $N = 10$ reflected SH signal $R^{(2)}$ shows regular harmonics that depend on ω and $\frac{d_1}{d}$ in the order of 10^{-5}. Transmitted SH signal $T^{(2)}$ is independent of $\frac{d_1}{d}$ and has a maximum around $\omega = 5 \times 10^{14}\text{rads}^{-1}$. $R^{(2)}$ is only ten times smaller than $T^{(2)}$.

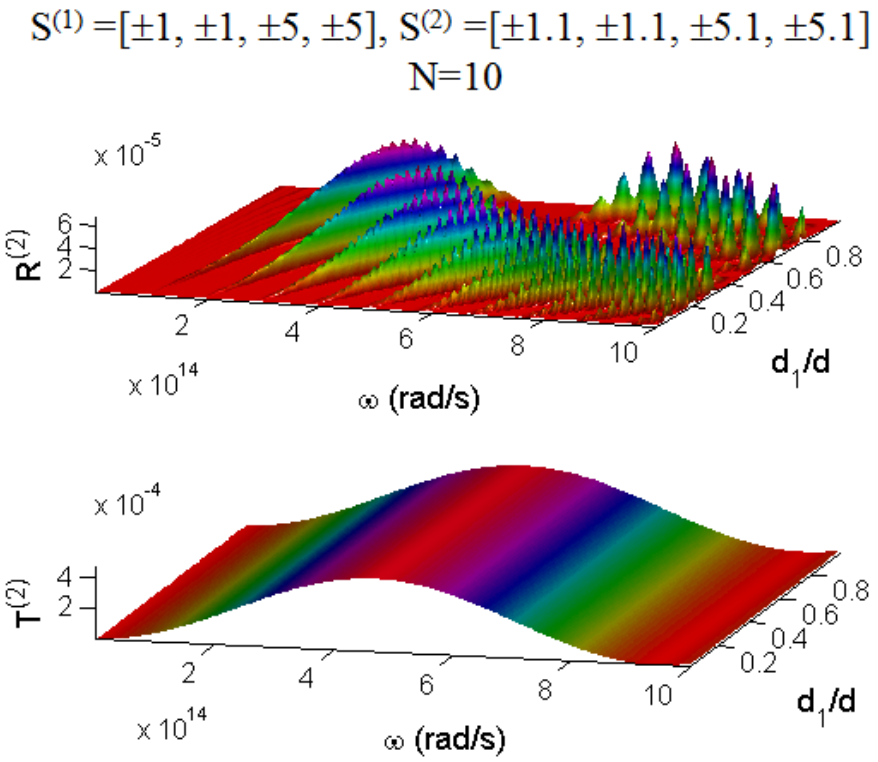

Figure 3.4: 3D plots of $R^{(1)}$,$T^{(1)}$, $R^{(2)}$ and $T^{(2)}$ vs ω and $\frac{d_1}{d}$ for $S^{(1)} = (\pm1, \pm1, \pm5, \pm5)$, $S^{(2)} = (\pm1.1, \pm1.1, \pm5.1, \pm5.1)$ where $N = 10$.

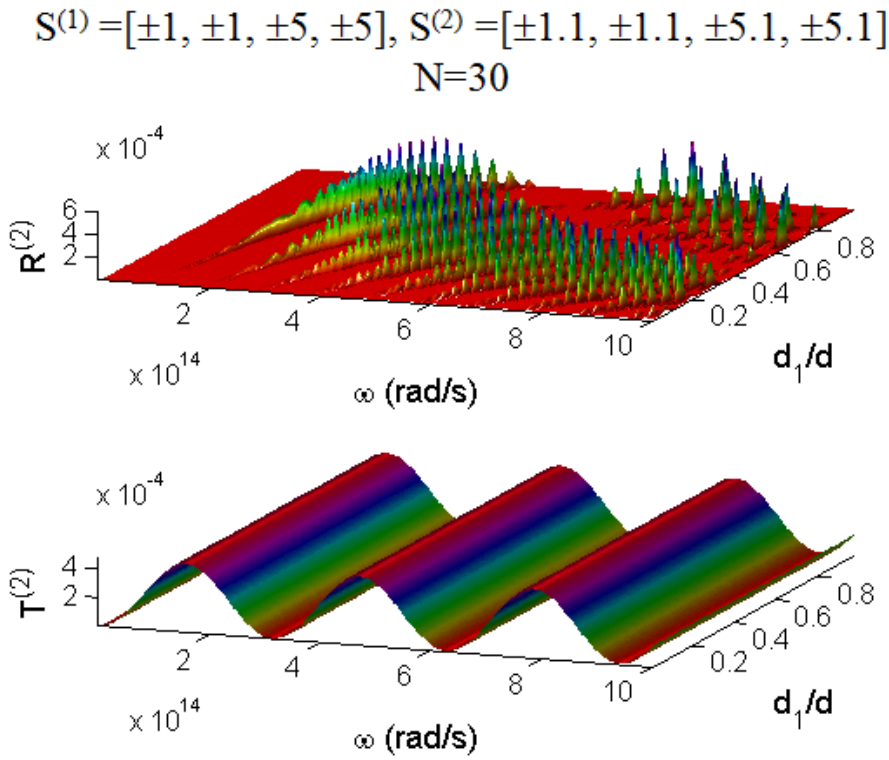

Figure 3.5: 3D plots of $R^{(1)}$,$T^{(1)}$, $R^{(2)}$ and $T^{(2)}$ vs ω and $\frac{d_1}{d}$ for $S^{(1)} = (\pm 1, \pm 5, \pm 1, \pm 5)$, $S^{(2)} = (\pm 1.1, \pm 5.1, \pm 1.1, \pm 5.1)$ where $N = 30$.

When $N = 30$, we again observe reflected SH signal $R^{(2)}$ shows regular harmonics that depend on ω and $\frac{d_1}{d}$ in $R^{(2)}$ in the order of 10^{-4} which is higher than $R^{(2)}$ for $N = 10$ as shown in Figure 3.5. Transmitted SH signal $T^{(2)}$ is independent of $\frac{d_1}{d}$ and shows sinusoidal profile with respect to ω in the order of 10^{-2}. $T^{(2)}$ is still greater than $R^{(2)}$ when N increases. The SH field is induced by FF which propagates through the PC. When N increases, more peaks are observed in $R^{(2)}$ due to more multiple reflections between layers. The patterns of $T^{(2)}$ and $R^{(2)}$ are influenced by refractive index contrast and also period number.

We evaluate the second scenario where $\mu^{(j)}_{eff(i)}$ and $\varepsilon^{(j)}_{eff(i)}$ for any layer are of same sign and magnitude but different sign and magnitude between layers

$$S^{(j)} = \left[\mp\mu^{(j)}_{eff(1)}, \mp\varepsilon^{(j)}_{eff(1)}, \pm\mu^{(j)}_{eff(2)}, \pm\varepsilon^{(j)}_{eff(2)}\right]$$

where $\left|\mu^{(j)}_{eff(1)}\right| = \left|\varepsilon^{(j)}_{eff(1)}\right|$ and $\left|\mu^{(j)}_{eff(2)}\right| = \left|\varepsilon^{(j)}_{eff(2)}\right|$, we choose parameters

$$S^{(1)} = (\mp 1, \mp 1, \pm 5, \pm 5), S^{(2)} = (\mp 1.1, \mp 1.1, \pm 5.1, \pm 5.1)$$

Refractive index contrast between two layers at FF ($j=1$) and SH ($j=2$) is

$$\Delta n^{(j)} = \sqrt{\left(\pm\mu^{(j)}_{eff(2)}\right)\left(\pm\varepsilon^{(j)}_{eff(2)}\right)} - \sqrt{\left(\mp\mu^{(j)}_{eff(1)}\right)\left(\mp\varepsilon^{(j)}_{eff(1)}\right)}$$

the refractive indices of two layers are opposite in signs.

We observe zero reflection $R^{(1)}=0$ and absolute transmission $T^{(1)}=1$ in the FF for all values of ω and $\frac{d_1}{d}$ even though there is a significant contrast between the opposite sign refractive indices of the two medium. For $N=10$ regular harmonics that change with respect to ω and $\frac{d_1}{d}$ are observed in $R^{(2)}$ as shown in Figure 3.6. $T^{(2)}$ increases gradually with respect to ω and has the largest value in the order of 10^{-3} around $\frac{d_1}{d}=0.5$. $T^{(2)}$ is larger than $R^{(2)}$ by order of 10^2. The broad $R^{(2)}$ spectrum in the frequency range of $1\times10^{14}-9\times10^{14}\text{rads}^{-1}$ is observed at $\frac{d_1}{d}=0.85$. It has maximum 4×10^{-5} around $5\times10^{14}\text{rads}^{-1}$ whereby other harmonics exhibit curved profile and also ripples.

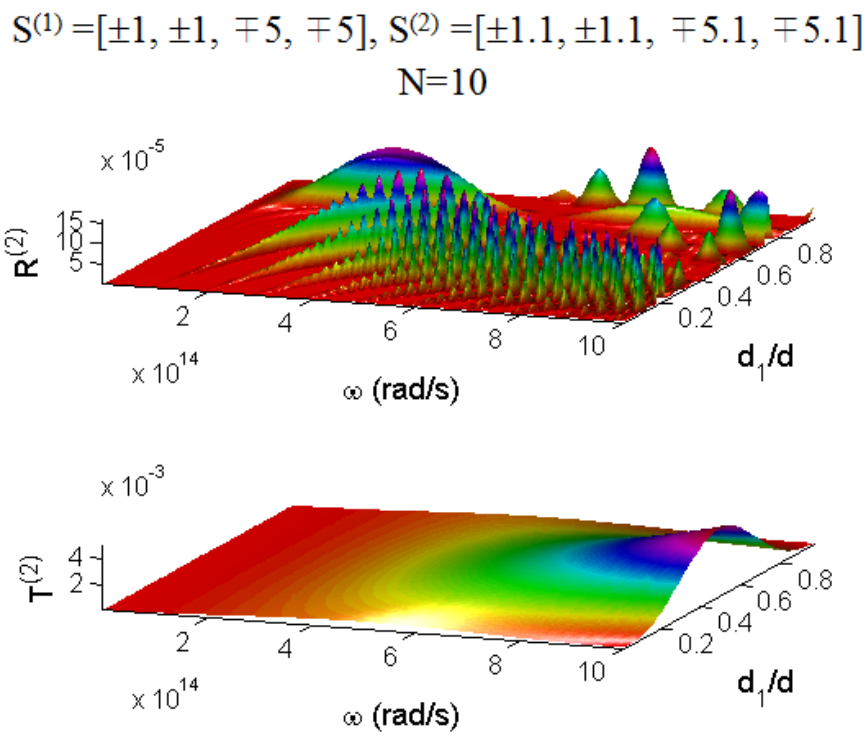

Figure 3.6: 3D plots of $R^{(1)}$,$T^{(1)}$, $R^{(2)}$ and $T^{(2)}$ vs ω and $\frac{d_1}{d}$ for $S^{(1)}=(\pm1,\pm1,\mp5,\mp5)$, $S^{(2)}=(\pm1.1,\pm1.1,\mp5.1,\mp5.1)$ where $N=10$.

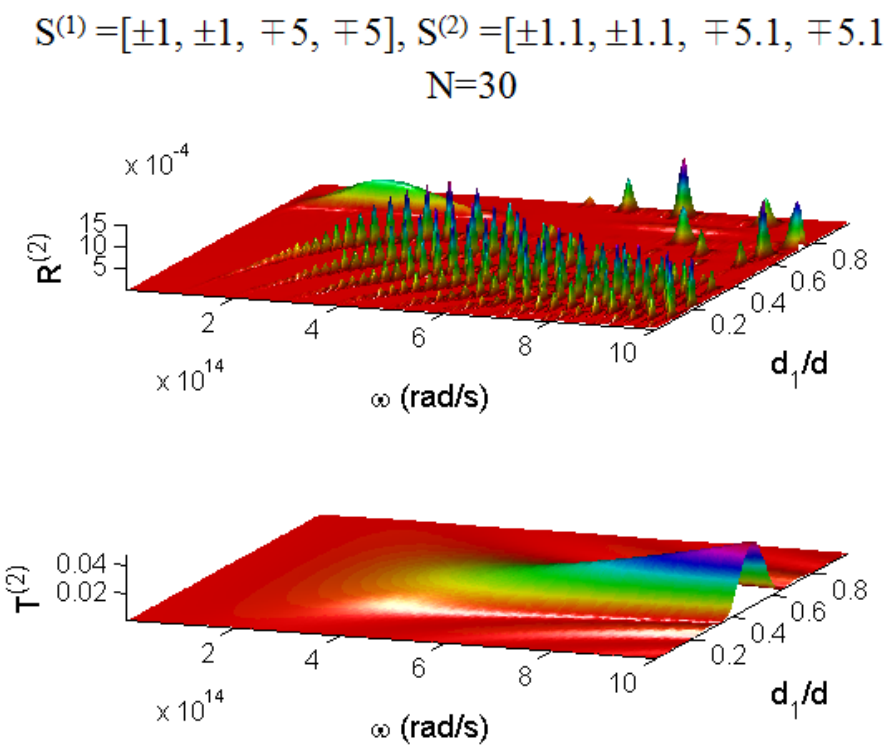

Figure 3.7: 3D plots of $R^{(1)}$,$T^{(1)}$, $R^{(2)}$ and $T^{(2)}$ vs ω and $\frac{d_1}{d}$ for $S^{(1)} = (\pm1, \pm1, \mp5, \mp5)$, $S^{(2)} = (\pm1.1, \pm1.1, \mp5.1, \mp5.1)$ where $N = 30$.

When N is increased to 30, similar harmonic patterns also being observed in $R^{(2)}$ in the order of 10^{-4} as shown in Figure 3.7. When N increases, reflected SH signal also becomes stronger. $T^{(2)}$ increases gradually with respect to ω and also has symmetry curving profile and has a maximum 0.04 at $\frac{d_1}{d} = 0.5$. Similar to $N = 10$, $T^{(2)}$ is larger than $R^{(2)}$ by order of 10^2. When $\frac{d_1}{d} = 0.5$, the interaction length in the odd layer is the same as interaction length in even layer. When one of the medium has negative refractive index $S^{(1)} = (\mp1, \mp1, \pm5, \pm5)$ correponds to $[n_1^{(1)}, n_2^{(1)}] = (\mp1, \pm5)$, reflected SH signal becomes stronger compared with $R^{(2)}$ for $S^{(1)} = (\pm1, \pm1, \pm5, \pm5)$ corresponds to $[n_1^{(1)}, n_2^{(1)}] = (\pm1, \pm5)$ as a result of improved phase matching in backward propagation. Zero reflection $R^{(1)} = 0$ and absolute transmission $T^{(1)} = 1$ in the FF for all values of ω and $\frac{d_1}{d}$ for $S^{(1)} = (\mp1, \mp1, \pm5, \pm5)$ and $S^{(1)} = (\pm1, \pm1, \pm5, \pm5)$ are interesting effects of using magnetic material $\mu_{eff(2)}^{(1)} \neq 1$. We find that the reflection $R^{(1)}$ is not zero when $\mu_{eff(2)}^{(1)}$ is different from $\varepsilon_{eff(2)}^{(1)}$, for example, $\mu_{eff(2)}^{(1)} = 1$ and $\varepsilon_{eff(2)}^{(1)} = 5$. The harmonic patterns in $R^{(2)}$ are caused by periodicity and multiple reflections inside nonlinear PC. When N increases, there are more interactions between FF and $\chi^{(2)}$ occur leading to

higher conversion energy efficiency. We also find that photonic band structures for $S^{(1)} = (\mp 1, \mp 1, \pm 5, \pm 5)$ and $S^{(1)} = (\pm 1, \pm 1, \pm 5, \pm 5)$ are the same as shown in Figure 3.8. This means that change of sign of refractive index in one layer would not affect photonic band structure but only have effect on $T^{(2)}$ and $R^{(2)}$.

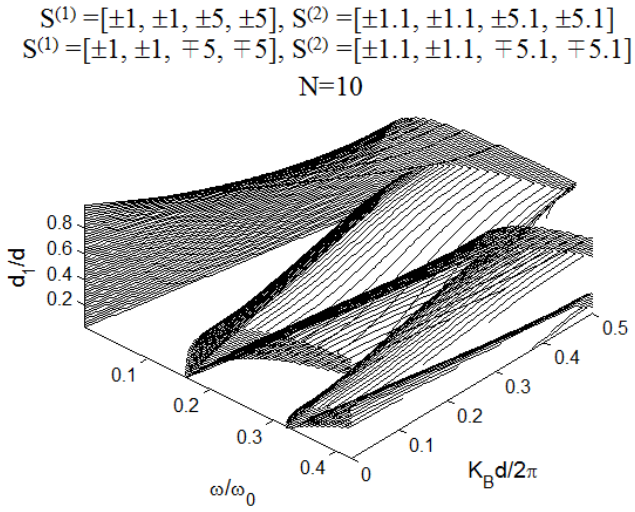

Figure 3.8: Band gap structure K_B vs $\frac{\omega}{\omega_0}$ for different $\frac{d_1}{d}$ where $d = 1000$nm and $N = 10$. (a) $S^{(1)} = (\pm 1, \pm 1, \mp 5, \mp 5)$, $S^{(2)} = (\pm 1.1, \pm 1.1, \mp 5.1, \mp 5.1)$ (b) $S^{(1)} = (\pm 1, \pm 1, \pm 5, \pm 5)$, $S^{(2)} = (\pm 1.1, \pm 1.1, \pm 5.1, \pm 5.1)$.

Now we evaluate the third scenario where $\mu^{(j)}_{eff(i)}$ and $\varepsilon^{(j)}_{eff(i)}$ of any layer are same sign and different magnitude, refractive index between two layers are equal in magnitude but have opposite sign

$$S^{(j)} = \left[\pm\mu^{(j)}_{eff(1)}, \pm\varepsilon^{(j)}_{eff(1)}, \mp\mu^{(j)}_{eff(2)}, \mp\varepsilon^{(j)}_{eff(2)}\right]$$

where $\left|\mu^{(j)}_{eff(1)}\right| = \left|\mu^{(j)}_{eff(2)}\right|$ and $\left|\varepsilon^{(j)}_{eff(1)}\right| = \left|\varepsilon^{(j)}_{eff(2)}\right|$, we choose parameters

$$S^{(1)} = (\pm 1, \pm 5, \mp 1, \mp 5), S^{(2)} = (\pm 1.1, \pm 5.1, \mp 1.1, \mp 5.1)$$

corresponds to $[n_1^{(1)}, n_2^{(1)}] = (\pm 5, \mp 5)$. The interesting results are observed in $T^{(1)}$, $R^{(1)}$, $T^{(2)}$ and $R^{(2)}$ compared previous scenarios. The sign is responsible for finite reflectance $R^{(1)}$ compared with Figures 3.4 to 3.7 and dependency on ω and $\frac{d_1}{d}$. Finite $T^{(1)}$ and $R^{(1)}$ that change respect to ω and $\frac{d_1}{d}$with symmetry at $\frac{d_1}{d} = 0.5$ are observed. The results are shown in Figure 3.9 for $N = 10$ and Figure 3.10 for $N = 30$.

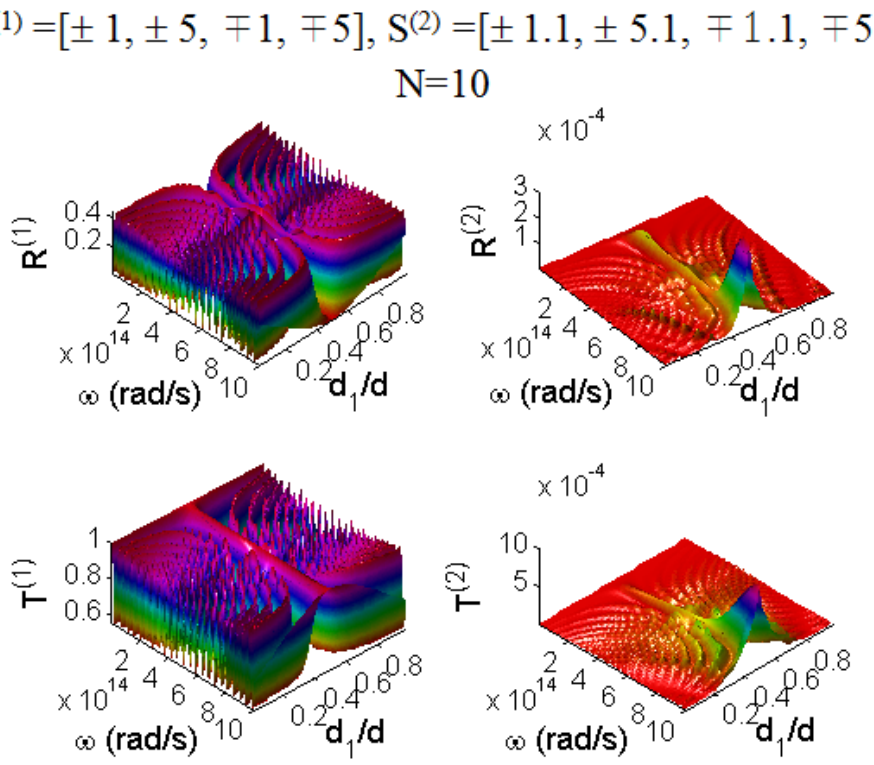

Figure 3.9: 3D plots of $R^{(1)}$,$T^{(1)}$, $R^{(2)}$ and $T^{(2)}$ vs ω and $\frac{d_1}{d}$ for $S^{(1)} = (\pm 1, \pm 5, \mp 1, \mp 5)$, $S^{(2)} = (\pm 1.1, \pm 5.1, \mp 1.1, \mp 5.1)$ where $N = 10$.

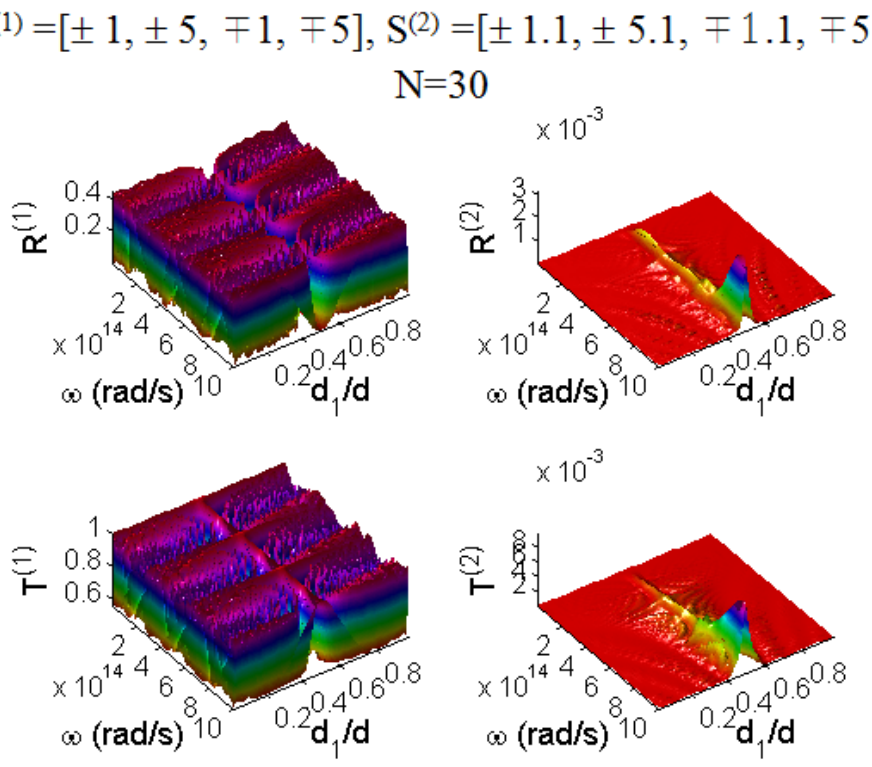

Figure 3.10: 3D plots of $R^{(1)}$,$T^{(1)}$, $R^{(2)}$ and $T^{(2)}$ vs ω and $\frac{d_1}{d}$ for $S^{(1)} = (\pm 1, \pm 5, \mp 1, \mp 5)$, $S^{(2)} = (\pm 1.1, \pm 5.1, \mp 1.1, \mp 5.1)$ where $N = 30$.

The spectra of both $R^{(2)}$ and $T^{(2)}$ quite similar. It is also noted that value of $R^{(2)}$ is quite close to $T^{(2)}$ where $T^{(2)}$ is about four times larger than $R^{(2)}$. There are more partitions observed in $T^{(1)}$ when N increases, this is caused by increased reflections with respect to increased period. At $\frac{d_1}{d} = 0.5$, $T^{(2)}$ and $R^{(2)}$ are finite for almost the entire range of pumping frequency. $R^{(2)}$ exhibits significant "backbone" feature compared with $T^{(2)}$. This is important for SH signal for generation of broadband frequency converted light that may be an alternative to supercontinuum laser.

Finally we evaluate the scenario where refractive index between two layers are unequal in magnitude and have opposite sign by using the parameters

$$S^{(1)} = (\pm 1, \pm 5, \mp 1, \mp 7), S^{(2)} = (\pm 1.1, \pm 5.1, \mp 1.1, \mp 7.1)$$

corresponds $[n_1^{(1)}, n_2^{(1)}] = (\pm 5, \mp 7)$. Simulation results in Figure 3.11 show spectra of $R^{(2)}$ and $T^{(2)}$ are no longer similar and symmetry at $\frac{d_1}{d} = 0.5$ is lost when parameters have no symmetry.

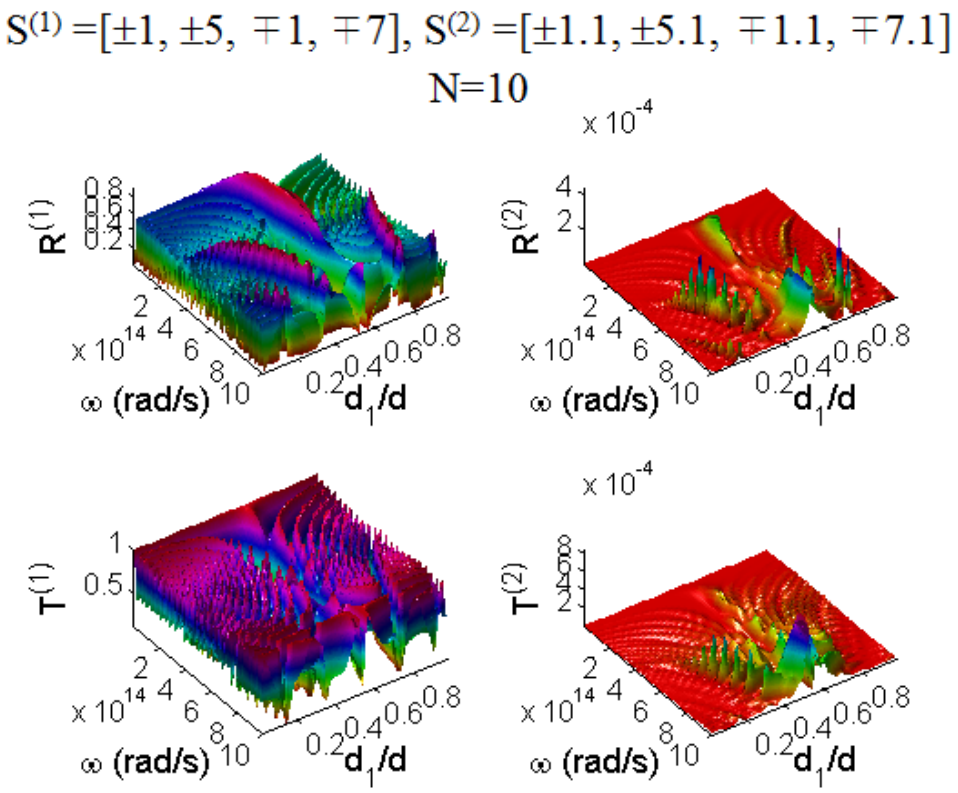

Figure 3.11: 3D plots of $R^{(1)}$,$T^{(1)}$, $R^{(2)}$ and $T^{(2)}$ vs ω and $\frac{d_1}{d}$ for $S^{(1)} = (\pm 1, \pm 5, \mp 1, \mp 7)$, $S^{(2)} = (\pm 1.1, \pm 5.1, \mp 1.1, \mp 7.1)$ where $N = 10$.

We also observe localized harmonics in $R^{(2)}$ and $T^{(2)}$ which are corresponding to harmonics in $R^{(1)}$ and $T^{(1)}$. The "backbone" feature is shifted to $\frac{d_1}{d} \sim 0.6$, change with respect to ω and $\frac{d_1}{d}$ and also become less evenly distributed. Besides that, the reflected SH field for this scenario is stronger than previous scenarios as $R^{(2)}$ and $T^{(2)}$ are in the same order. This is due to improved phase maching in backward propagation. The broken symmtery in $R^{(2)}$ and $T^{(2)}$ and strong backward SH wave propagation would be useful for designing efficient frequency steering device.

3.8.2 Dispersive Material

We discuss the effect of frequency dependent $\mu^{(j)}_{eff(i)}$ and $\varepsilon^{(j)}_{eff(i)}$ around resonance described in dispersive materials by Equations 3.77 and 3.78. The main feature resulting from resonances of the refractive indices $n^{(1)}_i$ is the low transmission $T^{(1)}$ and reflection $R^{(1)}$ signals due to absorption. The FF reflected field $R^{(1)}$ peaks correspond to the absorption peaks while the FF transmitted field $T^{(1)}$ peaks correspond to absorption valley. The presence of negative refraction in same single resonance (Figure 3.12) and different single resonance (Figure 3.16) scenarios reduce $R^{(1)}$ peaks in the resonant region compared with same double resonance (Figure 3.20) and different double resonance (Figure 3.24). We use $N = 5$, $d = 0.1\mu$m, $\omega_0 = \frac{2\pi c}{800\times 10^{-9}}$ rads^{-1} and $\Omega_0^+ = 8\times 10^7$ V/m for numerical simulation. Parameters used in $\varepsilon^{(j)}_{eff(i)}$ and $\mu^{(j)}_{eff(i)}$are

$$\begin{aligned}(\omega_{e1},\gamma_1,\varepsilon_{01},\varepsilon_{\infty 1}) &= \left(\omega_0,\frac{0.25}{\omega_0},1.5,3\right),(\omega_{e1},\gamma_2,\varepsilon_{02},\varepsilon_{\infty 2}) = \left(\omega_0,\frac{0.25}{\omega_0},1.1,1.8\right)\\ (\omega_{m1,}\Gamma_1,F_1) &= \left(\omega_0,\frac{0.25}{\omega_0},0.55\right),(\omega_{m2,}\Gamma_2,F_2) = \left(\omega_0,\frac{0.25}{\omega_0},0.4\right)\end{aligned}$$

respectively. Firstly, we evaluate the first scenario same single resonance where resonant frequency of $\mu^{(j)}_{eff(i)}$ and $\varepsilon^{(j)}_{eff(i)}$ are identical

$$\omega_{m1} = \omega_{e1}, \omega_{m2} = \omega_{e2}, \omega_{mi} = \omega_{ei}$$

In Figure 3.12, there is very small $R^{(1)}$ and zero $T^{(1)}$ around resonance. $R^{(2)}$ and $T^{(2)}$ are negligible around resonance and increase gradually with respect to ω. Negative refractive index is observed at FF where $n^{(1)}_1$ and $n^{(1)}_2$ are negative around resonance as shown in Figure 3.13. Plots of $R^{(1)}$, $T^{(1)}$, $R^{(2)}$ and $T^{(2)}$ for $\frac{d_1}{d} = 1$ are illustrated in Figure 3.14.The dispersion of photonic band structure in Figure 3.15 shows good correlation with $T^{(1)}$.

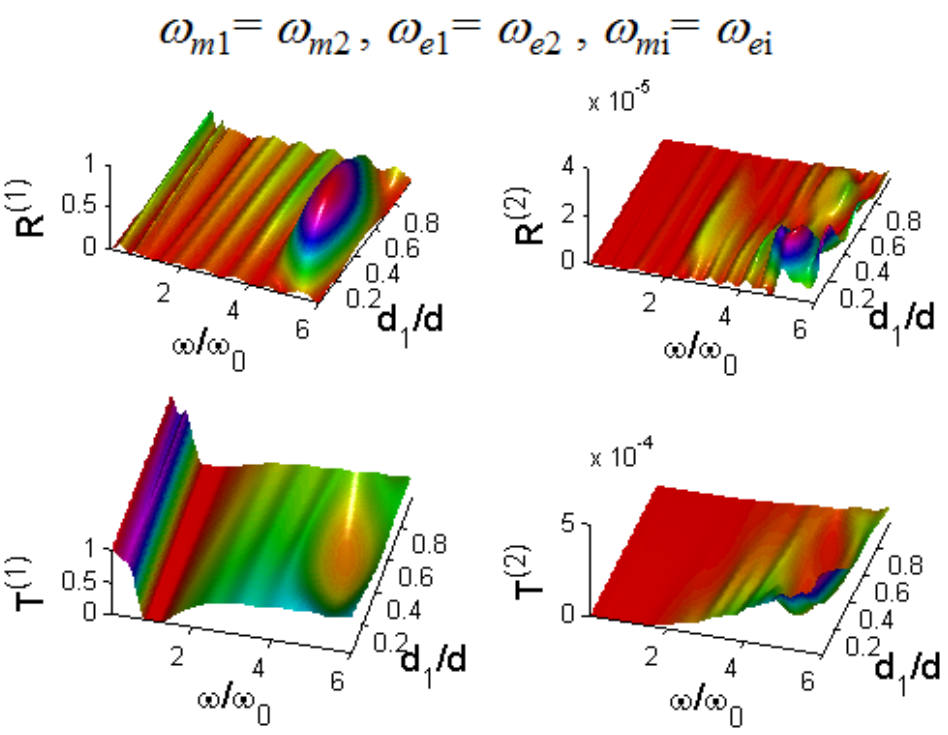

Figure 3.12: 3D plots of $R^{(1)}$, $T^{(1)}$, $R^{(2)}$ and $T^{(2)}$ vs ω/ω_0 and $\frac{d_1}{d}$ for $\omega_{m1} = \omega_{e1}, \omega_{m2} = \omega_{e2}, \omega_{mi} = \omega_{ei}$.

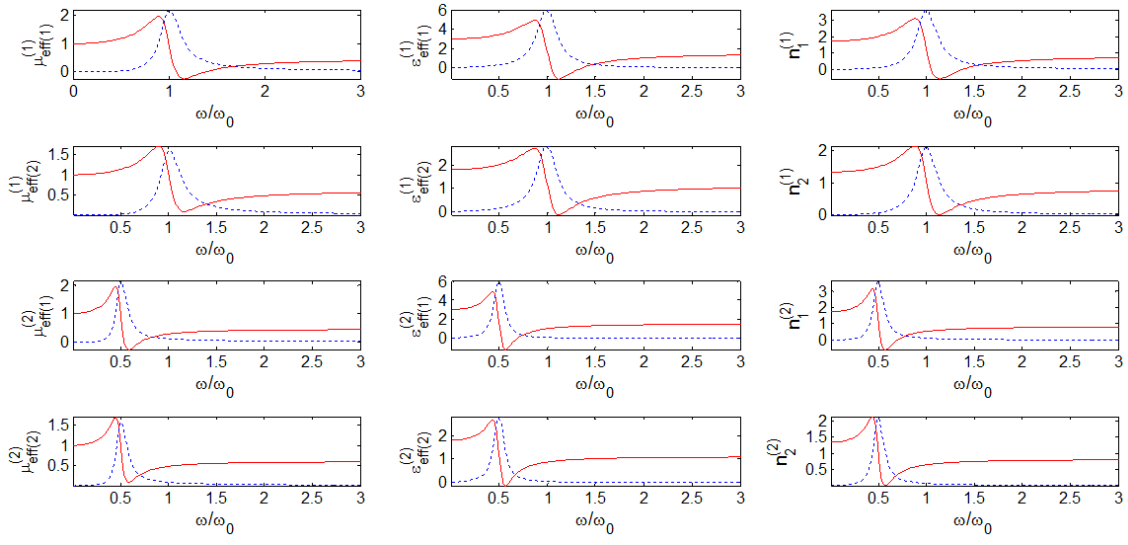

Figure 3.13: $\mu^{(1)}_{eff(1)}$,$\varepsilon^{(1)}_{eff(1)}$,$\mu^{(2)}_{eff(1)}$,$\varepsilon^{(2)}_{eff(2)}$,$n^{(1)}_1$,$n^{(1)}_2$,$n^{(2)}_1$,$n^{(2)}_2$ (red solid line - real part and blue dashed line - imaginary part) vs $\frac{\omega}{\omega_0}$ for $\omega_{m2} = \omega_{m1}, \omega_{e2} = \omega_{e1}, \omega_{mi} = \omega_{ei}$ when $\frac{d_1}{d} = 1$.

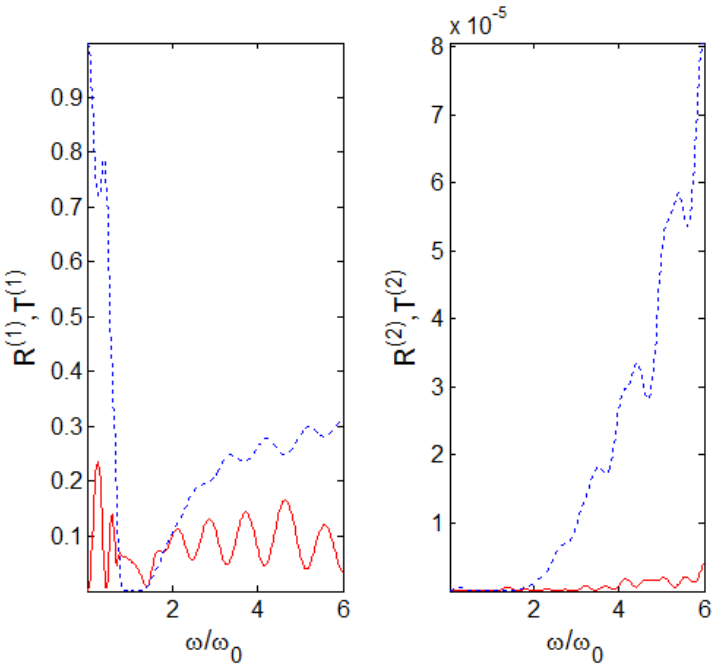

Figure 3.14: 2D plots of $R^{(1)}$, $R^{(2)}$ (red solid line), $T^{(1)}$ and $T^{(2)}$ (blue dashed line) vs ω/ω_0 for $\omega_{m2} = \omega_{m1}, \omega_{e2} = \omega_{e1}, \omega_{mi} = \omega_{ei}$ when $\frac{d_1}{d} = 1$.

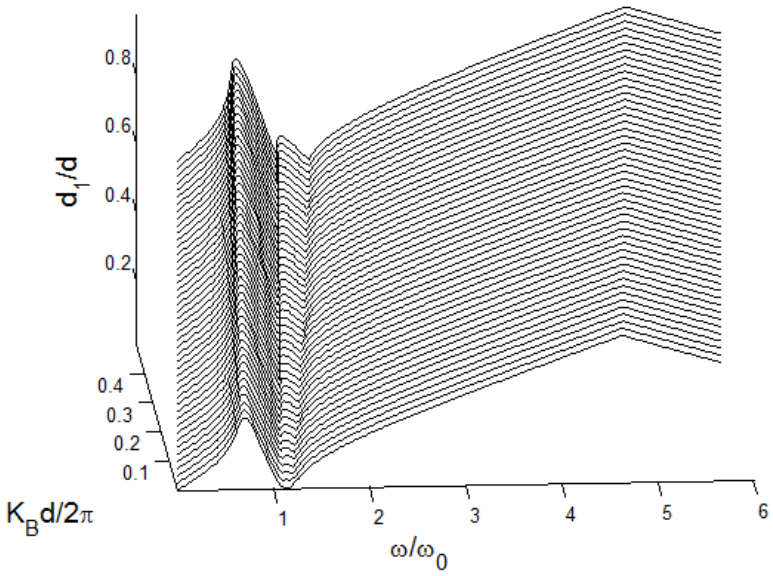

Figure 3.15: Photonic band structure for $\omega_{m1} = \omega_{e1}, \omega_{m2} = \omega_{e2}, \omega_{mi} = \omega_{ei}$.

Now we evaluate the second scenario different single resonance where $\mu^{(j)}_{eff(2)}$ resonant is double of $\mu^{(j)}_{eff(1)}$ resonant, $\varepsilon^{(j)}_{eff(2)}$ resonant is double of $\varepsilon^{(j)}_{eff(1)}$ resonant and $\mu^{(j)}_{eff(i)}$ resonant is identical to $\varepsilon^{(j)}_{eff(i)}$ resonant, this is expressed as

$$\omega_{m2} = 2\omega_{m1}, \omega_{e2} = 2\omega_{e1}, \omega_{mi} = \omega_{ei}$$

the negative refractive indice $n_1^{(1)}$, $n_2^{(1)}$, $n_1^{(2)}$ and $n_2^{(2)}$ are observed and they are not coincide. The absorption peaks which correspond to peaks of $n_1^{(1)}$ and $n_2^{(1)}$ are found in $R^{(1)}$ as shown in Figure 3.16. As there is a change of sign of $n_1^{(1)}$ and $n_2^{(1)}$ rapidly around resonance as shown in Figure 3.17, absorption valley corresponding to region between absorption peaks in $n_1^{(1)}$ and $n_2^{(1)}$ is found in $T^{(1)}$. The valley region between those resonance gives a finite and tunable narrow transmission $T^{(1)}$ ridge whose position varies with $\frac{d_1}{d}$ between absorption peaks between two layers. It is notice that $T^{(2)}$ is negligible around resonance. The very small $R^{(2)}$ peak is observed around resonant region for small $\frac{d_1}{d}$. This is the effect of negative refractive index on SHG. Here, the resonant frequencies in the layers are different eventhough there is the same resonant frequency in $\mu_{eff(i)}^{(j)}$ and $\varepsilon_{eff(i)}^{(j)}$. Bandgap in $T^{(1)}$ and small $R^{(1)}$, $R^{(2)}$ and $T^{(2)}$ are illutrated for $\frac{d_1}{d} = 1$ are shown in Figure 3.18. The photonic band structure which agrees with FF transmission spectra $T^{(1)}$ around resonance is illustrated in Figure 3.19.

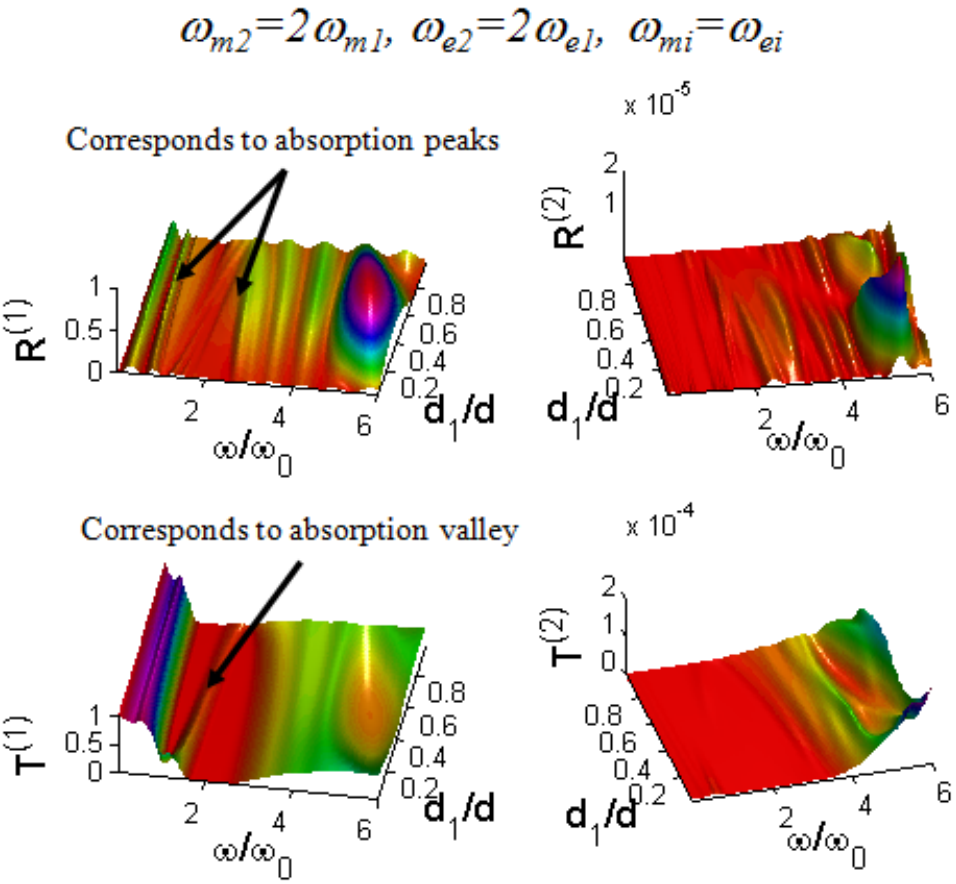

Figure 3.16: 3D plots of $R^{(1)}$, $T^{(1)}$, $R^{(2)}$ and $T^{(2)}$ vs ω/ω_0 and $\frac{d_1}{d}$ for $\omega_{m2} = 2\omega_{m1}, \omega_{e2} = 2\omega_{e1}, \omega_{mi} = \omega_{ei}$.

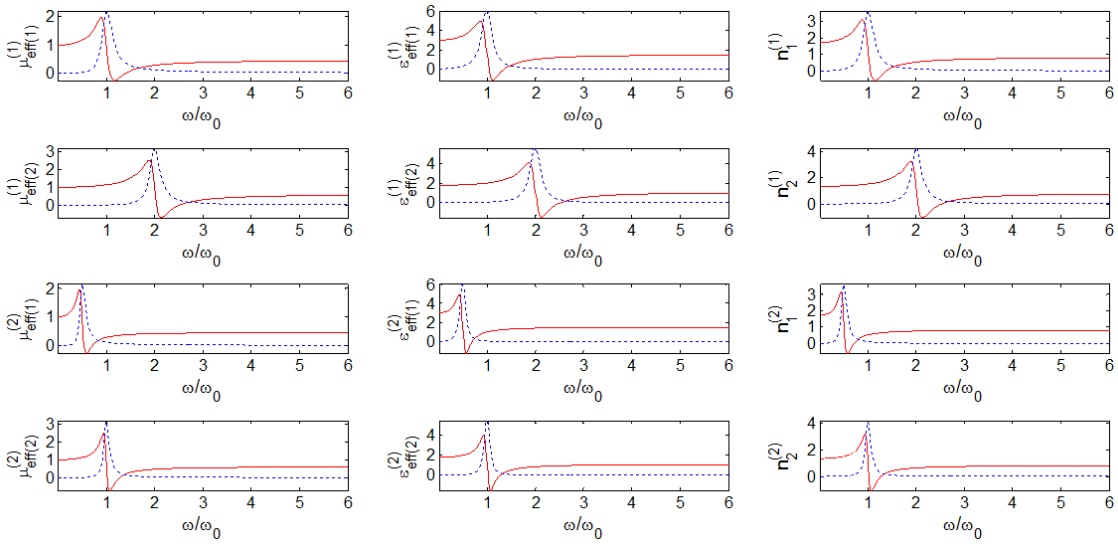

Figure 3.17: $\mu^{(1)}_{eff(1)}$,$\varepsilon^{(1)}_{eff(1)}$,$\mu^{(2)}_{eff(1)}$,$\varepsilon^{(2)}_{eff(2)}$,$n^{(1)}_1$,$n^{(1)}_2$,$n^{(2)}_1$,$n^{(2)}_2$ (red solid line - real part and blue dashed line - imaginary part) vs $\frac{\omega}{\omega_0}$ for for $\omega_{m2} = 2\omega_{m1}, \omega_{e2} = 2\omega_{e1}, \omega_{mi} = \omega_{ei}$ when $\frac{d_1}{d} = 1$.

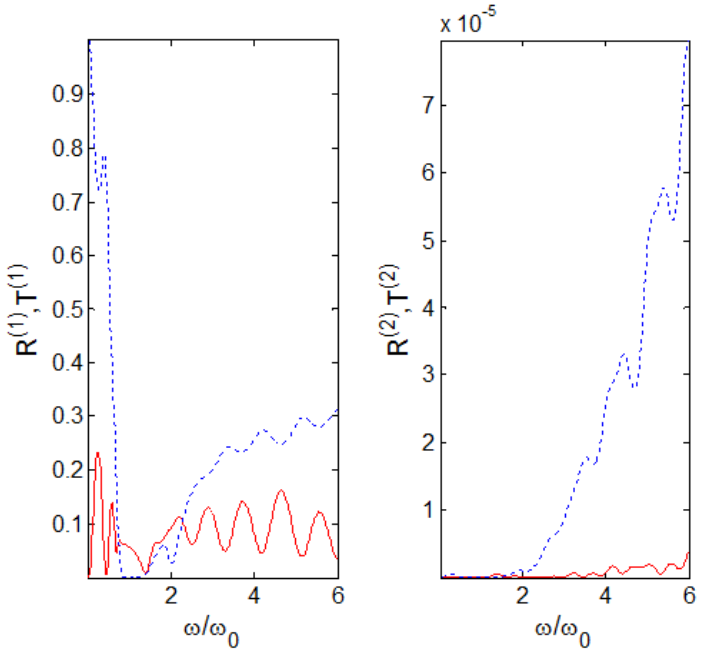

Figure 3.18: 2D plots of $R^{(1)}$, $R^{(2)}$ (red solid line), $T^{(1)}$ and $T^{(2)}$ (blue dashed line) vs ω/ω_0 for $\omega_{m2} = 2\omega_{m1}, \omega_{e2} = 2\omega_{e1}, \omega_{mi} = \omega_{ei}$ when $\frac{d_1}{d} = 1$.

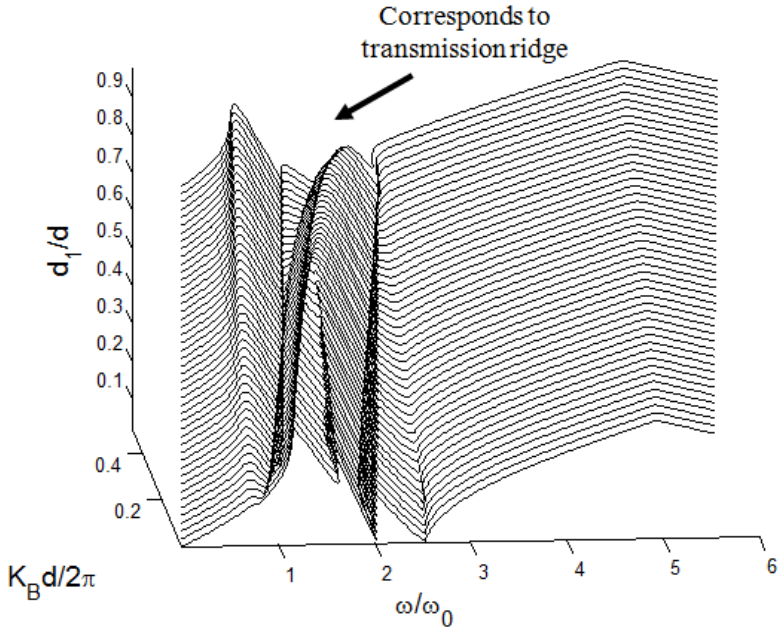

Figure 3.19: Photonic band structure for $\omega_{m1} = 2\omega_{e1}, \omega_{m2} = 2\omega_{e2}, \omega_{mi} = \omega_{ei}$.

We evaluate the third scenario same double resonance where $\mu^{(j)}_{eff(i)}$ resonant and $\varepsilon^{(j)}_{eff(i)}$ resonant are identical for both odd and even layer, $\mu^{(j)}_{eff(i)}$ resonant is double of $\varepsilon^{(j)}_{eff(i)}$ resonant,

$$\omega_{m2} = \omega_{m1}, \omega_{e2} = \omega_{e1}, \omega_{mi} = 2\omega_{ei}$$

there is no negative refractive index being observed. Interestingly, we observe a constant narrow transmission $T^{(1)}$ ridge in absorption valley as shown in Figure 3.20 as a result of of different resonant frequencies in $\mu^{(j)}_{eff(i)}$ and $\varepsilon^{(j)}_{eff(i)}$ but the same resonant frequency in both layers. $R^{(2)}$ and $T^{(2)}$ remain small around resonant region. Refractive indices $n^{(1)}_1/n^{(2)}_1$ coincide with $n^{(1)}_2/n^{(2)}_2$ to form absorption peaks and valley which are corresponding to peaks of $n^{(1)}_1/n^{(2)}_1$ and $n^{(1)}_2/n^{(2)}_2$ as shown in Figure 3.21. The absorption valley for this identical double resonance is also wider than absorption valley in previous different single resonance scenario. This is caused by $\omega_{mi} = 2\omega_{ei}$ which yields two absorption peaks. We could cleary observe the constant ridge in bandgap around resonance in 2D plots for $T^{(1)}$ where $\frac{d_1}{d} = 1$ as shown in Figure 3.22. Here, $R^{(1)}$ is approximately 0.45 around resonance, this is larger than $R^{(1)}$ with negative refractive index. The finite transmission ridges correspond to larger Bloch wave vector K_B around absorption valley as shown in Figure 3.23.

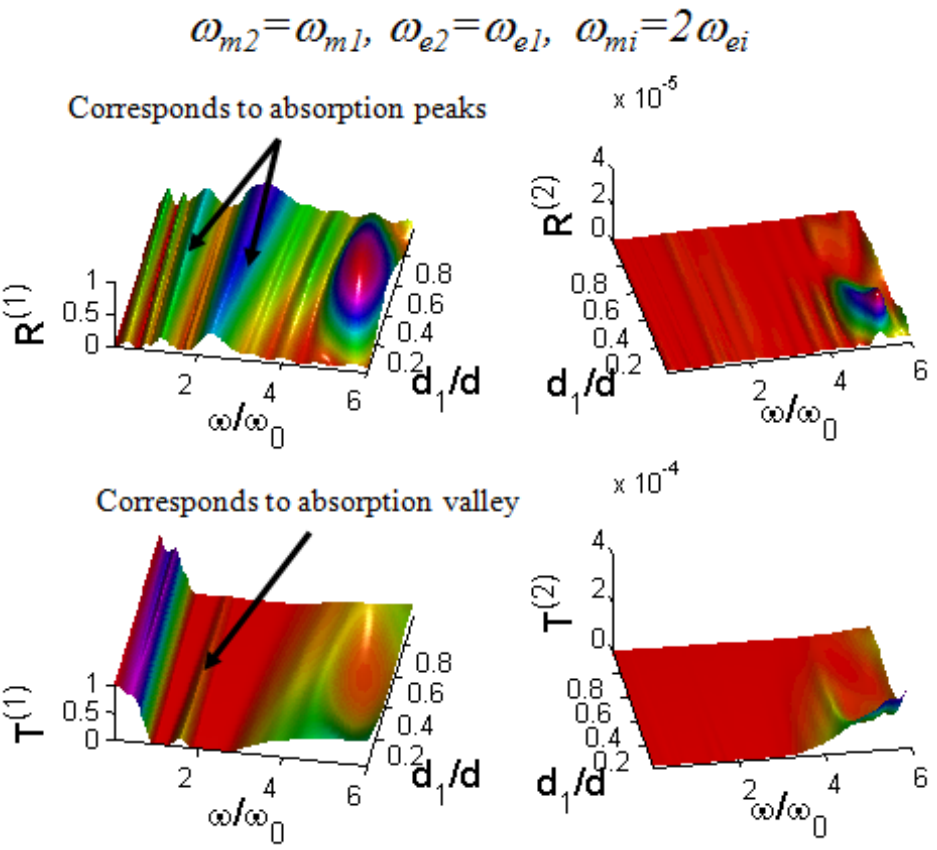

Figure 3.20: 3D plots of $R^{(1)}$, $T^{(1)}$, $R^{(2)}$ and $T^{(2)}$ vs ω/ω_0 and $\frac{d_1}{d}$ for $\omega_{m2}=\omega_{m1}, \omega_{e2}=\omega_{e1}, \omega_{mi}=2\omega_{ei}$.

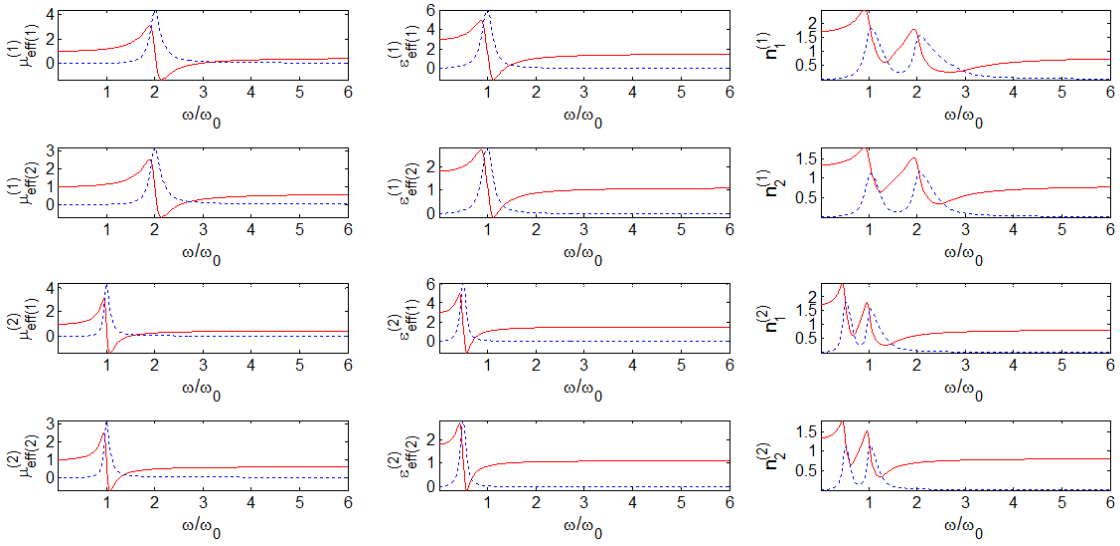

Figure 3.21: $\mu^{(1)}_{eff(1)}$,$\varepsilon^{(1)}_{eff(1)}$,$\mu^{(2)}_{eff(1)}$,$\varepsilon^{(2)}_{eff(2)}$,$n^{(1)}_1$,$n^{(1)}_2$,$n^{(2)}_1$,$n^{(2)}_2$ (red solid line - real part and blue dashed line - imaginary part) vs $\frac{\omega}{\omega_0}$ for for $\omega_{m2}=\omega_{m1}, \omega_{e2}=\omega_{e1}, \omega_{mi}=2\omega_{ei}$ when $\frac{d_1}{d}=1$.

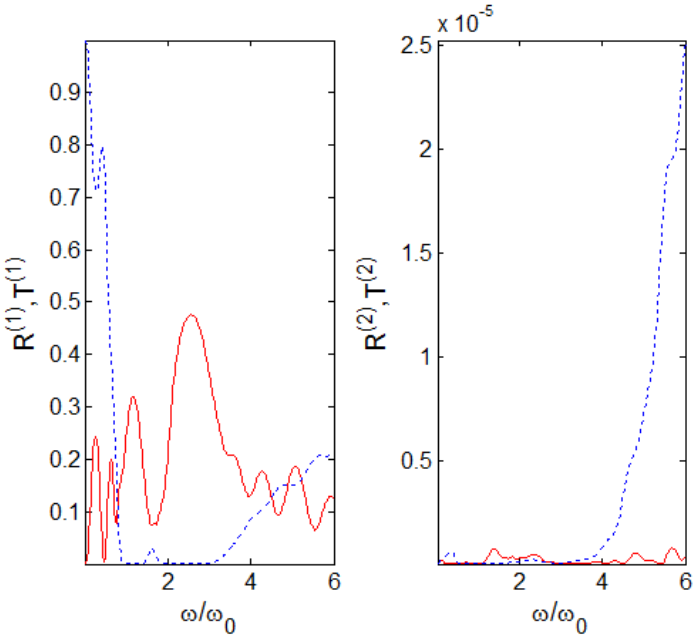

Figure 3.22: 2D plots of $R^{(1)}$, $R^{(2)}$ (red solid line), $T^{(1)}$ and $T^{(2)}$ (blue dashed line) vs ω/ω_0 for $\omega_{m2} = \omega_{m1}, \omega_{e2} = \omega_{e1}, \omega_{mi} = 2\omega_{ei}$ when $\frac{d_1}{d} = 1$.

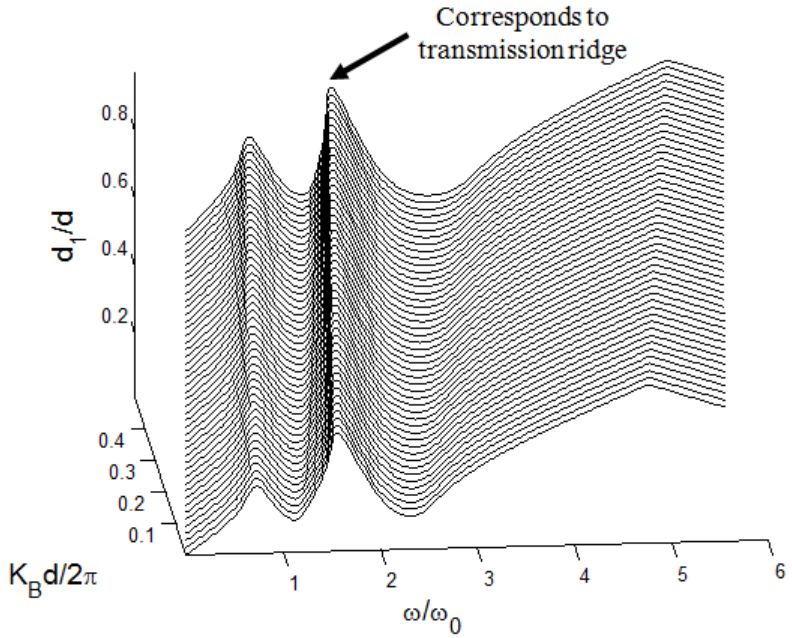

Figure 3.23: Photonic band structure for $\omega_{m1} = \omega_{e1}, \omega_{m2} = \omega_{e2}, \omega_{mi} = 2\omega_{ei}$.

We evaluate the fourth scenario different double resonance where $\mu^{(j)}_{eff(2)}$ resonant is double of $\mu^{(j)}_{eff(1)}$ resonant, $\varepsilon^{(j)}_{eff(2)}$ resonant is double of $\varepsilon^{(j)}_{eff(1)}$ resonant and $\mu^{(j)}_{eff(i)}$ is double of $\varepsilon^{(j)}_{eff(i)}$ resonance.

$$\omega_{m2} = 2\omega_{m1}, \omega_{e2} = 2\omega_{e1}, \omega_{mi} = 2\omega_{ei}$$

the refractive indices $n_1^{(1)}$, $n_1^{(2)}$, $n_2^{(1)}$ and $n_2^{(2)}$ demonstrate two absorption peaks and also form a absorption valley around resonance as shown in Figure 3.24. Two transmission $T^{(1)}$ ridges are observed within resonant region. One ridge observed around $\frac{\omega}{\omega_0} = 2$ is tunable that varies with respect to ω and $\frac{d_1}{d}$ meanwhile the other does not. The wider absorption region is a result of different resonant frequencies of $\mu_{eff(i)}^{(j)}$ and $\varepsilon_{eff(i)}^{(j)}$ in the two layers. This feature provides tunability of the transmission frequency as function of layer thickness ratio $\frac{d_1}{d}$. $T^{(2)}$ and $R^{(2)}$ when remain small around resonant region but is obviosuly higher than previous scenarios. Small curved transmission spectra is observed in $T^{(2)}$, the curved spectra is corresponding to curved ridge in $T^{(1)}$. The refractive indices are shown in Figure 3.25 in which we observe wider valley in $n_2^{(1)}$. The two ridges could be clearly seen in $T^{(1)}$ vs $\frac{\omega}{\omega_0}$ as shown in Figure 3.26 positive refractive index also gives larger $R^{(1)}$ compared with the first and second scenarios.

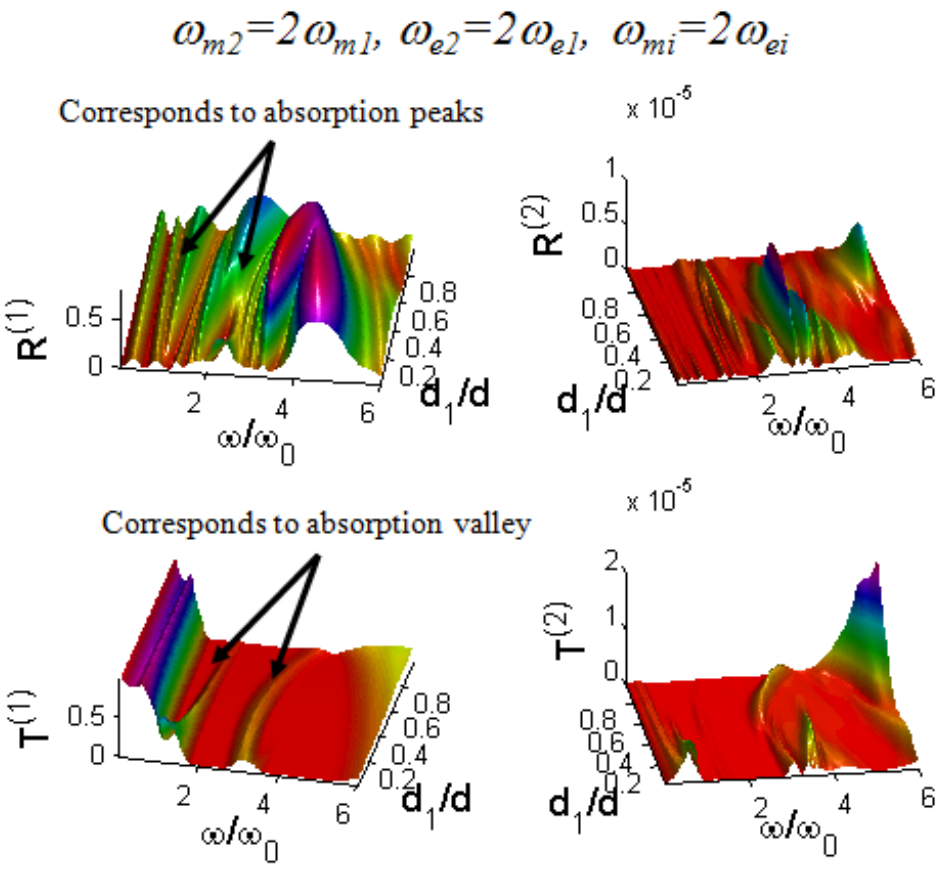

Figure 3.24: 3D plots of $R^{(1)}$, $T^{(1)}$, $R^{(2)}$ and $T^{(2)}$ vs ω/ω_0 and $\frac{d_1}{d}$ for $\omega_{m2} = 2\omega_{m1}, \omega_{e2} = 2\omega_{e1}, \omega_{mi} = 2\omega_{ei}$.

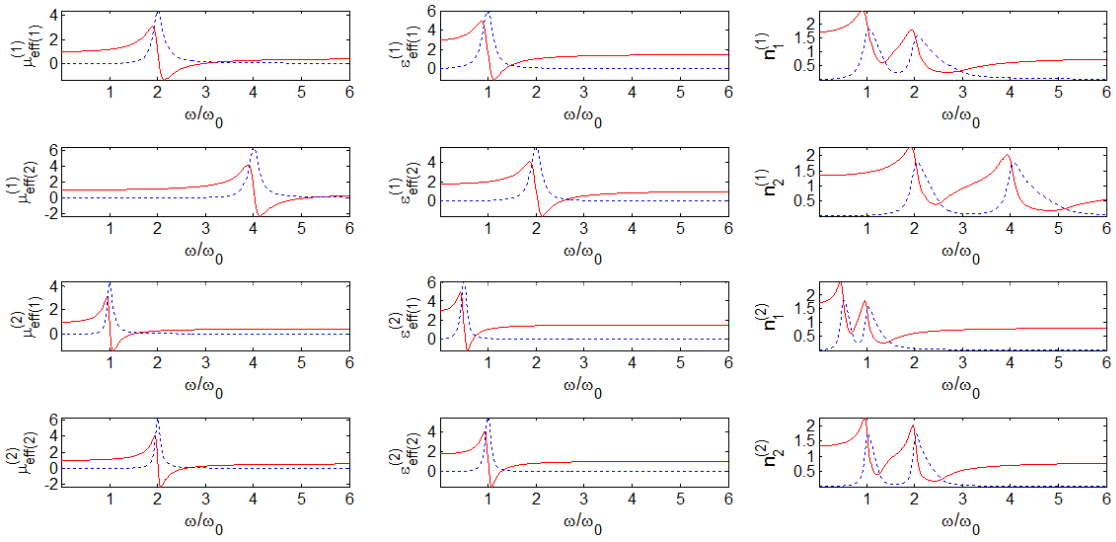

Figure 3.25: $\mu^{(1)}_{eff(1)}$,$\varepsilon^{(1)}_{eff(1)}$,$\mu^{(2)}_{eff(1)}$,$\varepsilon^{(2)}_{eff(2)}$,$n^{(1)}_1$,$n^{(1)}_2$,$n^{(2)}_1$,$n^{(2)}_2$ (red solid line - real part and blue dashed line - imaginary part) vs $\frac{\omega}{\omega_0}$ for for $\omega_{m2} = 2\omega_{m1}, \omega_{e2} = 2\omega_{e1}, \omega_{mi} = 2\omega_{ei}$ when $\frac{d_1}{d} = 1$.

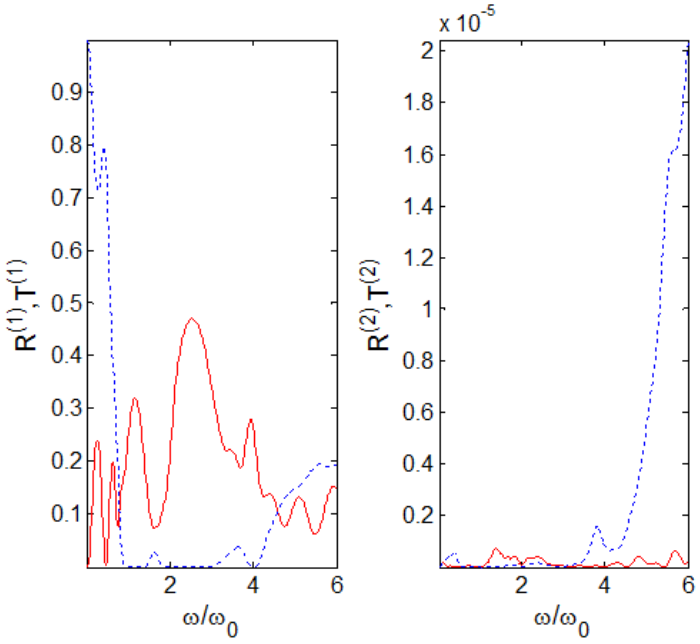

Figure 3.26: 2D plots of $R^{(1)}$, $R^{(2)}$ (red solid line), $T^{(1)}$ and $T^{(2)}$ (blue dashed line) vs ω/ω_0 for $\omega_{m2} = 2\omega_{m1}, \omega_{e2} = 2\omega_{e1}, \omega_{mi} = 2\omega_{ei}$ when $\frac{d_1}{d} = 1$.

The finite transmission ridges correspond to larger Bloch wave vector K_B closer to the Brillouin zone edge around absorption valley as shown in Figure 3.27. From Figures

3.15 and 3.19, the negative refractive index at slightly higher frequency than the resonance ω_0 tends to give larger K_B causing the shift of the dispersion with $\frac{d_1}{d}$.

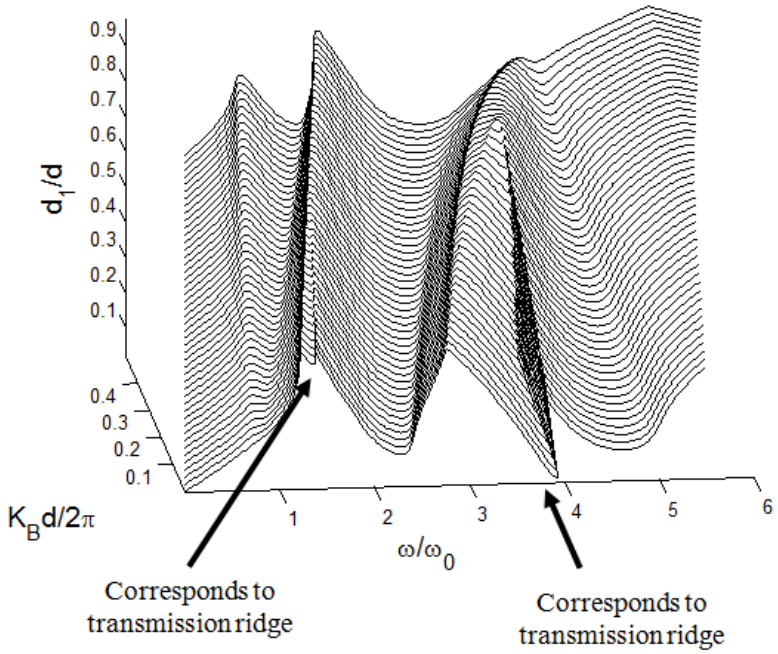

Figure 3.27: Photonic band structure for $\omega_{m2} = 2\omega_{m1}, \omega_{e2} = 2\omega_{e1}, \omega_{mi} = 2\omega_{ei}$.

In general, $T^{(1)}$ and $R^{(1)}$ are small around resonant region with due to absorption. SH fields are negligibly small in the low frequency and around resonance regions. There are small peaks in $R^{(2)}$ when $\frac{d_1}{d}$ is small and negative refraction occurs. This is effect of negative refractive index on nonlinear processes, particulary in SHG. The transmitted SH signal is larger than reflected signal $\left(T^{(2)} > R^{(2)}\right)$ outside the resonant region as shown in Figures 3.13, 3.17, 3.21 and 3.25. Transmission ridge exists in $T^{(1)}$ except the case where resonant of $\mu^{(j)}_{eff(i)}$ is identical to $\varepsilon^{(j)}_{eff(i)}$. This is caused by strong dispersion due to contrast of resonant in both layers. In practice, negative $\mu^{(j)}_{eff(i)}$ can be realized around the visible frequency range by using SRR structure (Ishikawa et al., 2005) such as array of U-shaped metallic SRR (Enkrich et al., 2005). Negative $\varepsilon^{(j)}_{eff(i)}$ could be realized with plasma or metals at high frequency and with thin wires structures at lower frequencies (Pendry et al., 1996) like infrared, terahertz and microwave regions. Lastly, we evaluate the scenario for $\frac{\omega}{\omega_0}$ far away from resonance as shown in Figure 3.28. As we could see, $T^{(2)}$ and $R^{(2)}$ away from resonance are significantly higher compared with $T^{(2)}$ and $R^{(2)}$ around resonance. $T^{(2)}$ and $R^{(2)}$ contain peaks at regular ω and $\frac{d_1}{d}$ corresponding to

constructive interference of the multiple waves through the phase change $\exp\left(\frac{n_i^{(2)}\omega d_i}{c}\right)$. $T^{(2)}$ is one order higher than $R^{(2)}$.

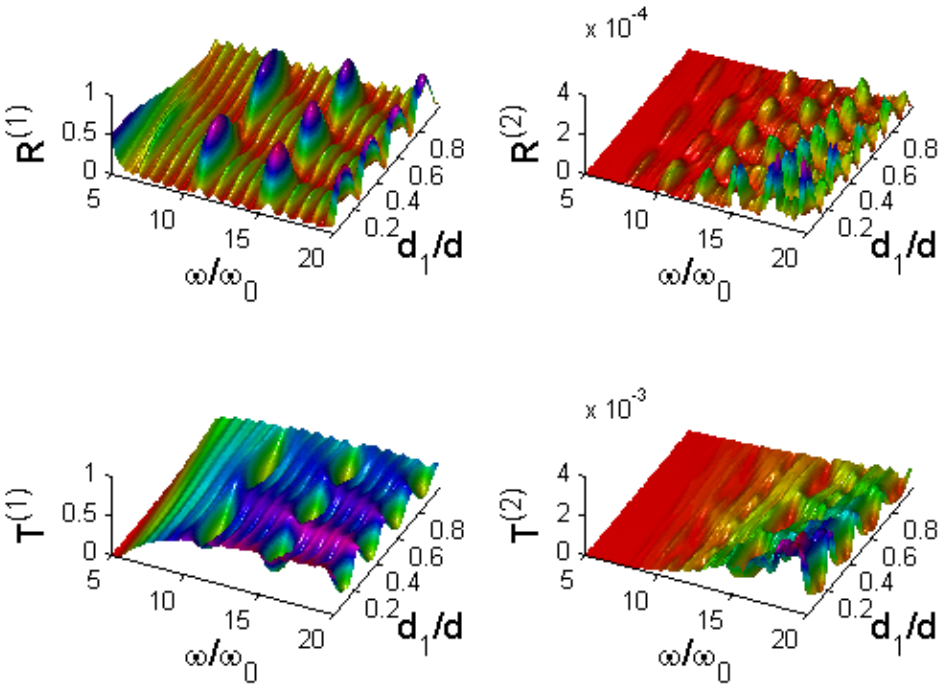

Figure 3.28: 3D plots of $R^{(1)}$, $T^{(1)}$, $R^{(2)}$ and $T^{(2)}$ vs ω/ω_0 ($\omega_0 = 2\pi c/800$nm) and $\frac{d_1}{d}$ far away from resonance.

3.9 Conclusions

We have studied the second harmonic field reflected and transmitted from a nonlinear photonic crystal with N periods of bilayers with dielectric and magnetic permeability functions using the transfer matrix theory. Constant negative permeability and permittivity are used to model nondispersive material meanwhile frequency dependent permeability and permittivity are used to model dispersive material. Simulation results with simultaneous negative permeability μ_{eff} and negative permittivity ε_{eff} (negative refractive index) show interesting features in the transmitted and reflected SH fields for both nondispersive and dispersive materials. The negative refractive indices cause the change of sign of SH wavevectors, providing improved phase matching and give rise to strong SH backward electric field in nondispersive material. Parameters such as thickness ratio $\frac{d_1}{d}$ and frequency ω are important to obtain optimum reflected SH wave particulary localized harmonic when permittivity and permeability are opposite of sign and not equal for both layers. The results show that asymmetric parameters with constant negative permit-

tivity and permeability (realizable beyond any resonance or absorption) offers interesting features such as broadband signal and improved nonlinear signal. The results provide insights on how the signs of dielectric and magnetic materials affect the linear and nonlinear responses of multilayer structures. For dispersive materials, absorption peaks and valley are formed around resonant region due to rapid change of refractive index sign from positive to negative. It is interesting to observe $\frac{d_1}{d}$ dependent transmission ridge inside absorption valley for some resonant configurations. We also observe that negative refractive index reduces reflected SH signal in resonant region. The results provide a qualitative analysis of how negative permittivity and permeability affect both linear and nonlinear response in 1 dimensional periodic bilayer photonic crystal. This may stimulate further experiments with nonlinear metamaterials in both lossless as well as around resonant regimes of infrared and optical frequencies, leading to design of efficient frequency converter.

CHAPTER 4

ULTRASHORT PULSE PROPAGATION IN NONLINEAR SUPERCONDUCTOR MAGNETIC PC

4.1 Introduction

In this chapter, we investigate interaction between ultrashort pulse with PC composed of dielectric and superconductor layer. Ultrashort pulse plays important role in development of optical engineering and physics. Ultrashort pulse possess high peak intensity and also short interaction duration with optical medium.

Normally semiconductor or dielectric materials are used to construct PC. Integration of superconductor in nonlinear PC is still a new field to be explored. The presence of bandgap at low frequency region and its tunability with temperature make superconductor an attractive material for engineering optothermal devices for pulses in the far infrared (FIR) region. The two fluid model (Bardeen, 1958; Linden, Orlando, & Lyons, 1994) provides a convenient description for investigation of band structure in superconducting PC (C. J. Wu, Liu, & Yang, 2011). Recently, optical properties of superconductor-ferromagnetic bilayer structure (C. J. Wu & Chen, 2011) have been studied using the two fluid model. Lee and Wu also used two fluid model to investigate transmission spectra in 1 dimensional superconductor dielectric PC (H. M. Lee & Wu, 2010).

Nonlinear PC introduces strong dispersion for spectral broadening and strong nonlinearity which enables pulse shaping and light-control-light functionality. Recently work shows SHG in periodically poled lithium niobate waveguide driven by femtosecond laser pulses (Huang et al., 2010). Besides, generation of ultrashort pulse in organic crystal has been demonstrated in the range of 10-30 THz (Kuroda et al., 2010). SRR (Pendry et al., 1999) and thin wire array (Pendry et al., 1996) can be used to yield frequency dependent magnetic permeability and permittivity. The feasibility of SHG in metamaterials has been demonstrated (M. W. Klein, Enkrich, Wegener, & Linden, 2006; Rose et al., 2000).

In this thesis, we explore pulsed SHG in bilayer photonic crystal composed of superconductor combined with magnetic resonance to form negative refractive index re-

gion (V. G. Veselago, 1968; Padilla et al., 2006). Article by Anlage regarding physics and application of superconducting metamaterials motivate us to explore nonlinear optical interaction between ultrashort laser pulse with superconducting photonic crystal with metamaterial feature (Anlage, 2011). The input pump pulse propagates through the nonlinear photonic crystal (NPC) while generating/producing a SH pulse through nonlinear frequency conversion process as shown in Figure 4.1.

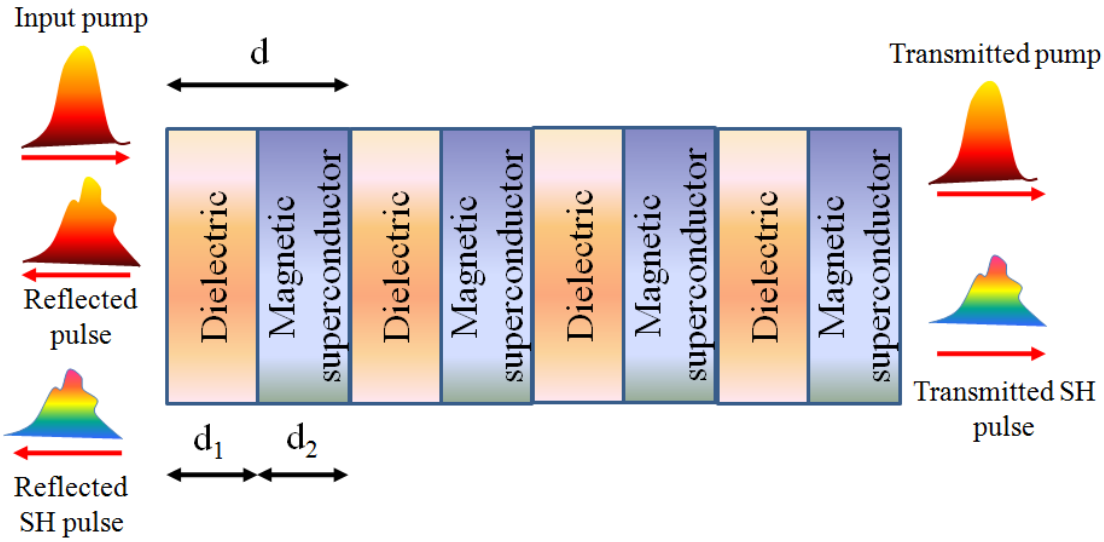

Figure 4.1: Pump laser pulse Ω_0^+ propagates through 1 dimensional bilayer periodic photonic crystal composed of dielectric (thickness d_1) and magnetic superconductor (thickness d_2) layers and interact with mediums to induce radiation of transmitted $E_t^{(2)+}$ and reflected $E_0^{(2)-}$ second harmonic pulses and at frequency 2ω. Pulse transfers some of its energy to generate SH pulse. The transmitted and reflected pulses are Ω_t^+ and Ω_0^- respectively.

The harmonic generation in nonlinear optical medium by using ultrashort pulse has been demonstrated (Ganeev et al., 2012). The nonlinear photonic crystal converts a small fraction of energy in the pump laser pulse into SH signal by frequency doubling, even in the absence of seed second harmonic. Pump pulse interact with nonlinear photonic crystal to induce polarization which leads to radiation of SH pulse in both forward and backward directions. The energy of the SH pulse is supplied by the input pump pulse which is assumed to be suficiently strong such that the effects of depletion/distortion on

the SH process are negligible so that the pump pulse inside the NPC can be assumed to be the input pulse. Also, the SHG can be assumed to be negligible so that the effects of nonlinear process (the SH signal) on the propagation of the pump pulse can be neglected. The SH pulse exists only when the pump pulse is present. Therefore the process involves propagation of the pump pulse and production of the SH signal through frequency conversion. We analyze transmission and reflection spectra of the FF and SH fields with respect to temperature and the output SH pulse in frequency and time domains and show that the dispersive magnetic-superconductor photonic crystal provides a method for generating short pulse in the infrared (IR) region.

4.2 Model and Method

We use transfer matrix method (TMM) to model electromagnetic wave propagation (Yeh et al., 1977), harmonic generation for arbitrary wavevector directions (Bethune, 1989) of SHG (J. J. Li et al., 2007; Faccio, Bragheri, & Cherchi, 2004) in the nonlinear photonic crystal driven by a pump laser or a fundamental field (FF). We develop transfer matrix in frequency domain. For arbitrarily short pulse, SVEA which has been used for continuous wave is not valid (Milonni & Eberly, 2010). In order to obtain solutions where dispersion is fully incorporated, we use the formal solution in frequency domain that satisfies the homogeneous wave equation $\{\frac{\partial^2}{\partial z^2} + \frac{n_i^2(\omega)\omega^2}{c^2}\}\Omega_i(z,\omega) \simeq 0$ for propagation through the i-th layer in the photonic crystal. This is good approximation for propagation in which nonlinear effect on FF wave is negligible. Electric field of FF is

$$E_i^{(1)}(z,\omega) = \Omega_i^+(\omega)\, e^{ik_i(\omega)(z-z_{i-1})} + \Omega_i^-(\omega)\, e^{-ik_i(\omega)(z-z_{i-1})} \tag{4.1}$$

subjected to initial input pulse

$$\Omega_0^+(\omega) = \Omega_0^+ \exp[-\left(\frac{\omega-\omega_L}{\sigma_L}\right)^2] \tag{4.2}$$

with carrier frequency ω_L and bandwidth σ_L. The linear propagation of layer i-th is governed by the refractive index

$$n_i^{(1)}(\omega) = \sqrt{\mu_{eff(i)}^{(1)}(\omega)\,\varepsilon_{eff(i)}^{(1)}(\omega)} \tag{4.3}$$

where $\mu_{eff(i)}^{(1)}$ and $\varepsilon_{eff(i)}^{(1)}$ are frequency dependent (dimensionless) relative permeability and permittivity of the medium induced by magnetic response and electric response. By

using Maxwell equation

$$\nabla \times \mathbf{E}_i^{(1)}(z,\omega) = i\omega\mu_0\mu_{eff(i)}^{(1)}(\omega)\,\mathbf{H}_i^{(1)}(z,\omega) \tag{4.4}$$

we have the magnetic field (along x-axis)

$$H_i^{(1)}(z,\omega) = \frac{\xi_j(\omega)}{c\mu_0}[\Omega_i^+(\omega)\,e^{ik_i(\omega)(z-z_{i-1})} - \Omega_i^-(\omega)\,e^{-ik_i(\omega)(z-z_{i-1})}] \tag{4.5}$$

where $\xi_i^{(1)}(\omega) = \frac{n_i^{(1)}(\omega)}{\mu_{eff(i)}^{(1)}(\omega)}$.

We arrange Equations 4.1 and 4.5 in matrix form

$$\begin{bmatrix} E_i^{(1)}(z,\omega) \\ c\mu_0 H_i^{(1)}(z,\omega) \end{bmatrix} = D_i \begin{bmatrix} \Omega_i^+(z,\omega) \\ \Omega_i^-(z,\omega) \end{bmatrix} \tag{4.6}$$

where

$$D_i = \begin{bmatrix} 1 & 1 \\ \xi_i^{(1)}(\omega) & -\xi_i^{(1)}(\omega) \end{bmatrix} \tag{4.7}$$

is the matrix that describes the refractive index of individual layer.

Consider continuity of $E_i^{(1)}(z,\omega)$ and $H_i^{(1)}(z,\omega)$ and Maxwell boundary condition at interface of odd and even layers and input and output interface (air left and right of photonic crystal) in which we have worked out in Chapter 3, we could obtain transfer matrix of FF wave propagation for N period

$$\begin{bmatrix} \Omega_t^+ \\ 0 \end{bmatrix} = \mathscr{T}^{(1)} \begin{bmatrix} \Omega_0^+ \\ \Omega_0^- \end{bmatrix} \tag{4.8}$$

where

$$\mathscr{T}^{(1)} = D_0^{-1} L^N D_0 = \begin{bmatrix} T_{11}^{(1)} & T_{12}^{(1)} \\ T_{21}^{(1)} & T_{22}^{(1)} \end{bmatrix} \tag{4.9}$$

is the final transfer matrix,

$$D_0 = \begin{bmatrix} 1 & 1 \\ n_0(\omega) & -n_0(\omega) \end{bmatrix} \tag{4.10}$$

$n_0(\omega)$ is the refractive index of the air. The transfer matrix of single period is

$$L = D_2 P_2 D_2^{-1} D_1 P_1 D_1^{-1} \tag{4.11}$$

where propagation matrix that model the phase change is

$$P_i = \begin{bmatrix} e^{ik_i(\omega)d_i} & 0 \\ 0 & e^{-ik_i(\omega)d_i} \end{bmatrix} \tag{4.12}$$

with the layer thickness $z_i - z_{i-1} = d_i$.

$$D_i P_i D_i^{-1} = \begin{bmatrix} \cos\theta_i & i\frac{\sin\theta_i}{\xi_i^{(1)}(\omega)} \\ i\xi_i^{(1)}(\omega)\sin\theta_i & \cos\theta_i \end{bmatrix} \tag{4.13}$$

where $\theta_i = k_i^{(1)}(\omega)d_i$, so that an analytical matrix for L could be obtained.

The fields in the odd layers $(i = 2j-1)$ are

$$\begin{bmatrix} \Omega_{2j-1}^{+} \\ \Omega_{2j-1}^{-} \end{bmatrix} = D_1^{-1} L^{j-1} D_0 \begin{bmatrix} \Omega_0^{+} \\ \Omega_0^{-} \end{bmatrix} \tag{4.14}$$

and in the even layers $(i = 2j)$

$$\begin{bmatrix} \Omega_{2j}^{+} \\ \Omega_{2j}^{-} \end{bmatrix} = D_2^{-1} D_1 P_1 D_1^{-1} L^{j-1} D_0 \begin{bmatrix} \Omega_0^{+} \\ \Omega_0^{-} \end{bmatrix}. \tag{4.15}$$

Equations 4.14 and 4.15 are used to compute the propagation of SH fields generated in layer $i = 2j-1$ and layer $i = 2j$ respectively. The transmission $t^{(1)}$ and reflection $r^{(1)}$ coefficients are

$$t^{(1)} = \frac{\Omega_t^{+}}{\Omega_0^{+}} = \mathscr{T}_{11}^{(1)} - \mathscr{T}_{12}^{(1)} \frac{\mathscr{T}_{21}^{(1)}}{\mathscr{T}_{22}^{(1)}} \tag{4.16}$$

$$r^{(1)} = \frac{\Omega_0^{-}}{\Omega_0^{+}} = -\frac{\mathscr{T}_{21}^{(1)}}{\mathscr{T}_{22}^{(1)}} \tag{4.17}$$

where $\Omega_r^{(1)} = \Omega_0^{-}$ and $\Omega_t^{(1)} = \Omega_{2N}^{+}$. Hence, we could determine the transmission $T^{(1)} = |t^{(1)}|^2$ and the reflection $R^{(1)} = |r^{(1)}|^2$ spectra.

Assuming a nonlinearly generated field in the i-th layer is a plane wave which has no radial dependence, the vector wave equation

$$(\nabla^2 + \varepsilon_i \mu_i \frac{\omega^2}{c^2}) E_i = -\mu_o \mu_i \omega^2 P_i^{NL} \tag{4.18}$$

in Fourier frequency domain ω becomes

$$(\frac{\partial^2}{\partial z^2} + k_i^{(2)2}(\omega')) E_i^{(2)}(z,\omega') = -\mu_0 \mu_{eff(i)}^{(2)}(\omega')\, \omega'^2 P_i^{NL}(z,\omega') \tag{4.19}$$

where $\omega' = 2\omega$, $k_i^{(j)}(\omega') = n_i^{(j)}(\omega')\frac{\omega'}{c}$ is the SH wavevector in the i-th layer. The nonlinear polarization induced in the i-th layer is

$$\begin{aligned} P_i^{NL}(z,\omega') &= \varepsilon_0 \chi_i^{(2)}(\omega') E_i^{(1)}(z,\omega)^2 \\ &= \varepsilon_0 \chi_i^{(2)}(\omega') \begin{bmatrix} \left(\Omega_i^+(\omega)\right)^2 e^{i2k_i^{(1)}(z-z_{i-1})} \\ +\left(\Omega_i^-(\omega)\right)^2 e^{-i2k_i^{(1)}(z-z_{i-1})} + 2\Omega_i^+(\omega)\Omega_i^-(\omega) \end{bmatrix} \end{aligned} \tag{4.20}$$

Using Laplace transform to solve Eq. 4.19, we have the general solution of SH electric field $E_i^{(2)}$ in the i-th layer as

$$\begin{aligned} E_i^{(2)}(z,\omega') &= E_i^{(2)+}(\omega) e^{ik_i(\omega')(z-z_{i-1})} + E_i^{(2)-}(\omega) e^{-ik_i(\omega')(z-z_{i-1})} \\ &+A_i \left(\Omega_i^+(\omega)\right)^2 e^{i2k_i^{(1)}(\omega)(z-z_{i-1})} \\ &+A_i \left(\Omega_i^-(\omega)\right)^2 e^{-i2k_i^{(1)}(\omega)(z-z_{i-1})} \\ &+C_i 2\Omega_i^+(\omega)\Omega_i^-(\omega) \end{aligned} \tag{4.21}$$

where

$$A_i(\omega) = -\left(\frac{\omega'}{c}\right)^2 \frac{\mu_i^{(2)}(\omega')\chi_i^{(2)}(\omega')}{k_i^{(2)2}(\omega') - 4k_i^{(1)2}(\omega)}, \tag{4.22}$$

$$C_i(\omega) = -\left(\frac{\omega'}{c}\right)^2 \frac{\mu_i^{(2)}(\omega')\chi_i^{(2)}(\omega')}{k_i^{(2)2}(\omega')}. \tag{4.23}$$

The SH magnetic field $H_i^{(2)}(z,\omega')$ in the i-th layer could be obtained from Maxwell equation

$$\nabla \times \mathbf{E}_i^{(2)}(z,\omega') = i\omega\mu_0\mu_i^{(2)}(\omega')\mathbf{H}_i^{(2)}(z,\omega') \tag{4.24}$$

which is

$$\begin{aligned} c\mu_0 H_i^{(2)}(z,\omega') &= \frac{n_{eff(i)}^{(2)}(\omega')}{\mu_{eff(i)}^{(2)}(\omega')} \begin{pmatrix} E_j^{(2)+}(\omega') e^{ik_i^{(2)}(z-z_{i-1})} \\ -E_i^{(2)-}(\omega') e^{-ik_i^{(2)}(z-z_{i-1})} \end{pmatrix} \\ &+\frac{n_i^{(1)}(\omega)}{\mu_{eff(i)}^{(2)}(\omega')} A_i \begin{pmatrix} \left(\Omega_i^+(\omega)\right)^2 e^{i2k_i(\omega)(z-z_{i-1})} \\ -\left(\Omega_i^-(\omega)\right)^2 e^{-i2k_i(\omega)(z-z_{i-1})} \end{pmatrix} \end{aligned} \tag{4.25}$$

we arrange $E_i^{(2)}(z,\omega')$ and $H_i^{(2)}(z,\omega')$ fields in the matrix form

$$\begin{aligned} \begin{bmatrix} E_i^{(2)}(z,\omega') \\ c\mu_0 H_i^{(2)}(z,\omega') \end{bmatrix} &= G_i \begin{bmatrix} E_i^{(2)+}(z,\omega') \\ E_i^{(2)-}(z,\omega') \end{bmatrix} + B_i \begin{bmatrix} A_i \left(\Omega_i^+(z,\omega)\right)^2 \\ A_i \left(\Omega_i^-(z,\omega)\right)^2 \end{bmatrix} \\ &+2C_i \begin{bmatrix} 1 \\ 0 \end{bmatrix} \Omega_i^+(z,\omega)\Omega_i^-(z,\omega) \end{aligned} \tag{4.26}$$

where

$$G_i = \begin{bmatrix} 1 & 1 \\ \xi_i^{(2)}(\omega') & -\xi_i^{(2)}(\omega') \end{bmatrix} \tag{4.27}$$

$$B_i = \begin{bmatrix} 1 & 1 \\ \frac{n_i^{(1)}(\omega)}{\mu_{eff(i)}^{(2)}(\omega')} & -\frac{n_i^{(1)}(\omega)}{\mu_{eff(i)}^{(2)}(\omega')} \end{bmatrix} \tag{4.28}$$

and $\xi_i^{(2)}(\omega') = \frac{n_i^{(2)}(\omega')}{\mu_i^{(2)}(\omega')}$. For simplification, we define

$$\begin{aligned} E_i^{(2)\pm}(z,\omega') &= E_i^{(2)\pm}(\omega')\, e^{\pm ik_i^{(2)}(z-z_{i-1})} \\ \Omega_i^{\pm}(z,\omega) &= \Omega_i^{\pm}(\omega)\, e^{\pm ik_i(z-z_{i-1})} \end{aligned} \tag{4.29}$$

Again, consider continuity of $E_i^{(2)}(z,\omega')$ and $H_i^{(2)}(z,\omega')$ by referring to Maxwell boundary condition at interface of odd and even layers and input and output interface (air left and right of photonic crystal), we obtain transfer matrix of SH wave propagation for N period to compute SH forward $E_t^{(2)+}$ and backward $E_0^{(2)-}$ outputs for $j = N > 0$

$$\begin{aligned} G_0 \begin{bmatrix} E_t^{(2)+}(\omega') \\ 0 \end{bmatrix} &= S^N G_0 \begin{bmatrix} E_0^{(2)+}(\omega') \\ E_0^{(2)-}(\omega') \end{bmatrix} \\ &\quad + \sum_{j=1}^{N} S^{N-j} \begin{Bmatrix} N_2 M_1 \vec{I}_{2j-1}(z) + M_2 \vec{I}_{2j}(z) \\ +N_2 \vec{J}_1 \Omega_{2j-1}^{+}(\omega)\, \Omega_{2j-1}^{-}(\omega) \\ +\vec{J}_2 \Omega_{2j}^{+}(\omega)\, \Omega_{2j}^{-}(\omega) \end{Bmatrix} \end{aligned} \tag{4.30}$$

where $S = N_2 N_1$, $N_i = G_i Q_i G_i^{-1}\,(i = 1,2)$, $M_i = A_i(B_i F_i - N_i B_i)$, $\vec{J} = \begin{bmatrix} 1 \\ 0 \end{bmatrix}$ and $\vec{J}_i = 2C_i[I - N_i]\vec{J}$. Here, the matrice for phase change are

$$Q_i = \begin{bmatrix} e^{ik_i^{(2)}d_i} & 0 \\ 0 & e^{-ik_i^{(2)}d_i} \end{bmatrix} \tag{4.31}$$

and

$$F_i = P_i^2 = \begin{bmatrix} e^{i2k_i^{(1)}d_i} & 0 \\ 0 & e^{-i2k_i^{(1)}d_i} \end{bmatrix} \tag{4.32}$$

The approach that we use to derive Equations 4.21, 4.25, 4.26 and 4.30 is the same we have used in Chapter 3 which is not reiterated in this chapter. To prevent accumulated

numerical errors, we use the matrix relation below (Born & Wolf, 1999) to find N-th power of any unimodular M matrix to compute S^N, S^{N-j} and L^N

$$M^N = \begin{bmatrix} m_{11}U_{N-1} - U_{N-2} & m_{12}U_{N-1} \\ m_{21}U_{N-1} & m_{22}U_{N-1} - U_{N-2} \end{bmatrix} \tag{4.33}$$

where $U_N(a) = \frac{\sin\left[(N+1)\cos^{-1}a\right]}{\sqrt{1-a^2}}$ and $a = \frac{1}{2}(m_{11}+m_{22})$. For convenience, we define $D_m = G_0^{-1}S^N G_0 = \begin{bmatrix} D_{11}^{(2)} & D_{12}^{(2)} \\ D_{21}^{(2)} & D_{22}^{(2)} \end{bmatrix}$ and the second term on RHS of Equation 4.30 as $T_m = \begin{bmatrix} T_1^{(2)} \\ T_2^{(2)} \end{bmatrix}$. Hence, Equation 4.30 becomes

$$\begin{bmatrix} E_t^{(2)+} \\ 0 \end{bmatrix} = \begin{bmatrix} D_{11}^{(2)}E_0^{(2)+} + D_{12}^{(2)}E_0^{(2)-} + T_1^{(2)} \\ D_{21}^{(2)}E_0^{(2)+} + D_{22}^{(2)}E_0^{(2)-} + T_2^{(2)} \end{bmatrix} \tag{4.34}$$

which gives the reflected and the transmitted SH field, respectively

$$E_0^{(2)-}(2\omega) = -\frac{D_{21}^{(2)}E_0^{(2)+} + T_2^{(2)}}{D_{22}^{(2)}} \tag{4.35}$$

$$E_t^{(2)+}(2\omega) = (\frac{\det D^{(2)}}{D_{22}^{(2)}})E_0^{(2)+} - \frac{D_{12}^{(2)}T_2^{(2)}}{D_{22}^{(2)}} + T_1^{(2)} \tag{4.36}$$

where $E_0^{(2)+}(2\omega)$ is the input second harmonic (seed) field. It is important to realize that, while the linear reflectivity and transmitivity $r^{(1)}$ and $t^{(1)}$ depend on ω they do not depend on the spectral content of the pump pulse. However, the nonlinear reflected $E_0^{(2)-}(2\omega)$ and transmitted $E_t^{(2)+}(2\omega)$ fields can depend on the spectral content of the pump pulse through $\Omega_0^+(\omega) = \Omega_0^+ \exp[-\left(\frac{\omega-\omega_L}{\sigma_L}\right)^2]$. To obtain the transmission $T^{(2)} = |t_2|^2$and reflection $R^{(2)} = |r_2|^2$ spectra for SH electric fields, we divide the fields by the $\Omega_0^+(\omega) = \Omega_0^+$ amplitude of the pump field, i.e.$r_2 = \frac{E_0^{(2)-}}{\Omega_0^+}$ and $t_2 = \frac{E_t^{(2)+}}{\Omega_0^+}$. The reflected (superscript '$-$') and transmitted (superscript '$+$') fields in time domain are obtained by FT, $E_j^{(2)\pm}(z,t) = \mathscr{F}\{E_j^{(2)\pm}(z,\omega')\}$ and $\Omega_j^{(1)\pm}(z,t) = \mathscr{F}\{\Omega_j^{(1)\pm}(z,\omega)\}$.

4.3 Superconductor with temperature dependence

Now we apply two fluid model to describe electromagnetic propagation in the superconducting layer at nonzero temperature (Ooi, Au Yeung, Kam, & Lim, 2000; Ooi &

Au Yeung, 1999). The electrical conductivity of a superconductor is

$$\sigma = \sigma_n + \sigma_s \tag{4.37}$$

where σ_n is conductivity of the unpaired normal electron with density of n_n and σ_s is conductivity of paired superelectrons with density of n_s. The total electron number density is

$$n = n_n + n_s$$

The frequency dependent conductivity at nonzero frequency is given in (Ooi & Kam, 2010)

$$\sigma(\omega) = \frac{n\tau e^2}{m}\left[\frac{f_n}{1+(\omega\tau)^2} + i\left(\frac{f_n\omega\tau}{1+(\omega\tau)^2} + \frac{f_s}{\omega\tau}\right)\right] \tag{4.38}$$

where $f_n = \frac{n_n}{n}$ and $f_s = \frac{n_s}{n}$ are fluid fractions and τ is electron mean relaxation time, m and e are mass and charge of electron respectively.

For excitations involving fields with higher frequencies that may exceed the superconducting bandgap $2\Delta(T)$ which depends on temperature T, we must introduce the notch functions (Rauh & Genenko, 2008)

$$f_\pm = \frac{1}{e^{\pm u}+1}, u = \frac{\omega - 2\Delta}{k_B T}, \Delta(T) = \Delta_0(1-x^3)^4 \tag{4.39}$$

into the conductivity

$$\sigma(\omega, T) = f_-\sigma^<(\omega) + f_+\sigma^>(\omega) \tag{4.40}$$

where the conductivity for $\omega < 2\Delta$ is rewritten as

$$\sigma^<(\omega) = (1-x^4)i\frac{ne^2}{m\omega} + x^4\left(\frac{\sigma_{tot}}{1-i\omega\tau}\right) \tag{4.41}$$

where $\frac{n_n(T)}{n} = x^4$, while the conductivity above the bandgap is essentially normal conductor

$$\sigma^>(\omega) = \frac{\sigma_{tot}}{1-i\omega\tau} \tag{4.42}$$

where $\sigma_{tot} = \frac{ne^2\tau}{m}$ and $n = \frac{m}{\mu_0 e^2 \lambda_d^2(0)}$ with $\lambda_d(0)$ as the penetration depth at absolute zero. Since $\frac{1}{\lambda_d^2(T)} = \frac{n_s(T)\mu_0 e^2}{m}$ we have $\frac{\lambda_d^2(0)}{\lambda_d^2(T)} = \frac{n_s(T)}{n} = 1 - x^4 < 1$. For superconductor photonic crystal, Ooi and Gong demonstrated that it is possible to obtain large field transmission through a periodic structure at frequencies where the field is lossy in a finite temperature superconductor (Ooi & Gong, 2011). Hence, we would investigate the effect of temperature on transmission and reflection spectra in this thesis as well.

The dielectric function of superconductor is related to $\sigma(\omega,T)$ by

$$\varepsilon_s(\omega) = \varepsilon_b + i\frac{\sigma(\omega)}{\varepsilon_0\omega} \tag{4.43}$$

expanding 4.43,

$$\begin{aligned}
\varepsilon_s(\omega) &= \varepsilon_b + i\frac{1}{\varepsilon_0\omega}\frac{n\tau e^2}{m}\left[\frac{f_n}{1+(\omega\tau)^2} + i\left(\frac{f_n\omega\tau}{1+(\omega\tau)^2} + \frac{f_s}{\omega\tau}\right)\right] \\
&= \varepsilon_b + \left[i\frac{1}{\varepsilon_0\omega}\frac{n\tau e^2}{m}\frac{f_n}{1+(\omega\tau)^2} - \frac{1}{\varepsilon_0\omega}\frac{n\tau e^2}{m}\left(\frac{f_n\omega\tau}{1+(\omega\tau)^2} + \frac{f_s}{\omega\tau}\right)\right] \\
&= \varepsilon_b - \frac{1}{\varepsilon_0\omega}\frac{n\tau e^2}{m}\left(\frac{f_n\omega\tau}{1+(\omega\tau)^2} + \frac{f_s}{\omega\tau}\right) + i\frac{1}{\varepsilon_0\omega}\frac{n\tau e^2}{m}\frac{f_n}{1+(\omega\tau)^2}
\end{aligned} \tag{4.44}$$

for layer i, frequency dependent permittivities at pump and SH frequencies are $\varepsilon^{(1)}_{eff(i)}(\omega)$ and $\varepsilon^{(2)}_{eff(i)}(\omega)$

$$\varepsilon^{(1)}_{eff(i)}(\omega) = \varepsilon_b - \frac{1}{\varepsilon_0\omega}\frac{n\tau e^2}{m}\left(\frac{f_n\omega\tau}{1+(\omega\tau)^2} + \frac{f_s}{\omega\tau}\right) + i\frac{1}{\varepsilon_0\omega}\frac{n\tau e^2}{m}\frac{f_n}{1+(\omega\tau)^2} \tag{4.45}$$

$$\varepsilon^{(2)}_{eff(i)}(\omega) = \varepsilon_b - \frac{1}{\varepsilon_0(2\omega)}\frac{n\tau e^2}{m}\left(\frac{f_n(2\omega)\tau}{1+(2\omega\tau)^2} + \frac{f_s}{(2\omega)\tau}\right) + i\frac{1}{\varepsilon_0(2\omega)}\frac{n\tau e^2}{m}\frac{f_n}{1+(2\omega\tau)^2} \tag{4.46}$$

The frequency ω_f where $\mathrm{Re}\varepsilon_s$ flips from negative to positive can be estimated from

$$\frac{ne^2\tau^2}{\varepsilon_0 m}[f_-(1-\frac{x^4}{1+(\omega_f\tau)^2}) + f_+\frac{(\omega_f\tau)^2}{1+(\omega_f\tau)^2}] = (\omega_f\tau)^2 \tag{4.47}$$

For magnetic response, SRR is integrated into photonic crystal in such a way that frequency dependent permeabilities (Pendry et al., 1999; Smith et al., 2000) are induced at pump and SH frequencies as

$$\mu^{(1)}_{eff(i)}(\omega) = 1 - \frac{F}{\omega^2+\omega_{mi}^2+i\omega\Gamma} \tag{4.48}$$

$$\mu^{(2)}_{eff(i)}(\omega) = 1 - \frac{F}{(2\omega)^2+\omega_{mi}^2+i(2\omega)\Gamma} \tag{4.49}$$

here F is fraction factor of SRR in the photonic crystal, Γ is the dissipation factor and ω_{mi} is the resonant frequency of SRR in i-th layer.

4.4 Results and Discussion

4.4.1 Magnetic Superconductor Photonic Crystal

We investigate characteristics of transmission and reflection spectra when ultrashort pulse propagating through PC composed of dielectric layer and magnetic superconductor layer without second harmonic seed $E_0^{(2)+}$. Odd layer is dielctric medium with cosntant permittivity $\varepsilon_{eff(1)}^{(j)} = 3$ and permeability $\mu_{eff(1)}^{(j)} = 1$, therefore odd layer is nonabsorptive and nondispersive. Even layer is superconductor medium with SRR that would induce magnetic response. The parameters used to compute dielectric function $\varepsilon_{eff(2)}^{(j)}$ for superconductor medium are $\varepsilon_b = 15,\ \lambda_d = 0.2d,\ d_1 = 0.5d,\ \tau = 10^{-13}$s, $T_c = 300$K, $\hbar\Delta_0 = 0.01$eV whilst parameters used to compute permeability $\mu_{eff(2)}^{(j)}$ for magnetic material are $\omega_{m2} = 2\Delta_0, \Gamma_2 = 2\times 10^{12}s^{-1}, F_2 = 0.55$. The parameters used are feasible for fabrication of superconducting layer and enable us to investigate optical properties at room temperature. The PC substrate is strontium barium niobate (SBN) with second order susceptibility $\chi^{(2)} = 27.2$ pm/V. The incident ultrashort laser pulse has carrier frequency $\omega_L = 2\Delta_0$, bandwidth σ_L and period thickness $d = 10\mu$m and odd layer thickness d_1.

We evaluate the case $N = 5$ and $\sigma_L = \Delta_0$, several interesting features are found in the pulse propagation in the nonlinear periodic medium. Multiple passbands are observed in $R^{(1)}$, $T^{(1)}$, $R^{(2)}$ and $T^{(2)}$ in Figure 4.2. In superconductor medium, the frequency ω_f where ε_s in Equation 4.47 is zero turns out to be in the far infrared region $\sim 3\times 10^{13}s^{-1}$ domain, which is quite close to the superconducting gap, $2\Delta_0 \simeq 3\times 10^{13}s^{-1}$. Reflection SH spectra $R^{(2)}$ is higher than SH transmission spectra $T^{(2)}$ by one order of magnitude. Around resonance ω_{m2}, negative refractive index is formed due to change of sign of $\mu_{eff(2)}^{(j)}$ from positive to negative. This creates a narrow region of negative refractive index for medium 2 but it has little effect on the output of broadband pulse since it covers only a narrow resonance region of the magnetic permeability. medium 1 has constant $\mu_{eff(1)}^{(j)}$ and $\varepsilon_{eff(1)}^{(j)}$, it is non-absorptive and non-dispersive.

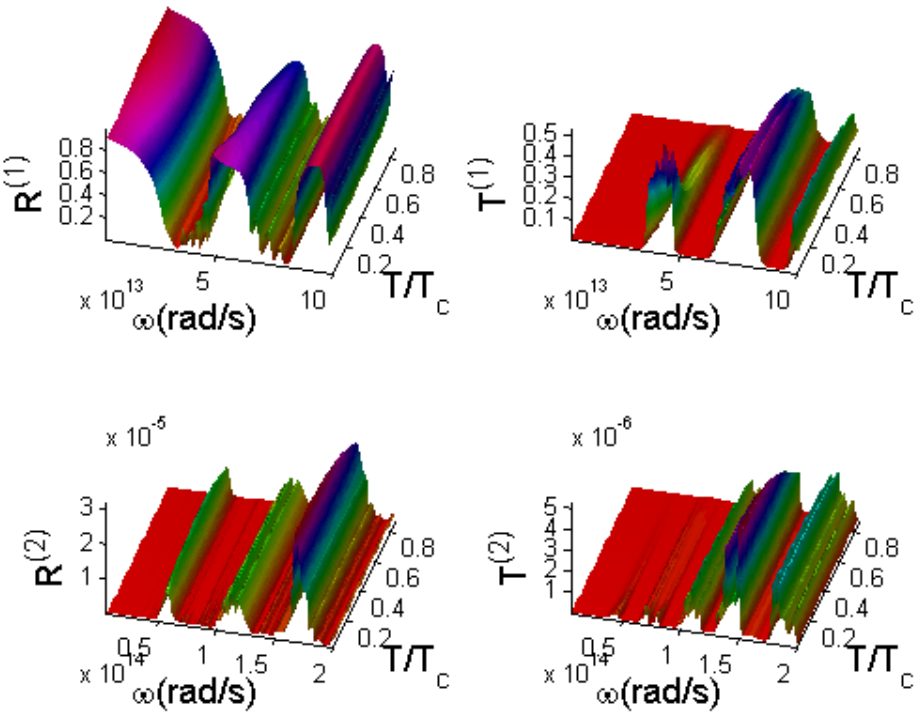

Figure 4.2: 3D plots of $R^{(1)}$, $T^{(1)}$, $R^{(2)}$ and $T^{(2)}$ vs ω and $\frac{T}{T_c}$, $N = 5$, $d = 10\mu$m, $d_1 = 0.5d$, $\mu^{(1)}_{eff(1)} = 1$, $\varepsilon^{(1)}_{eff(1)} = 3$, $F_2 = 0.4$, $\Gamma = 2 \times 10^{12}\text{s}^{-1}$, $\tau = 1 \times 10^{-13}$s, $\lambda_d(0) = 0.2d$, $\varepsilon_b = 15, \sigma_L = \Delta_0$.

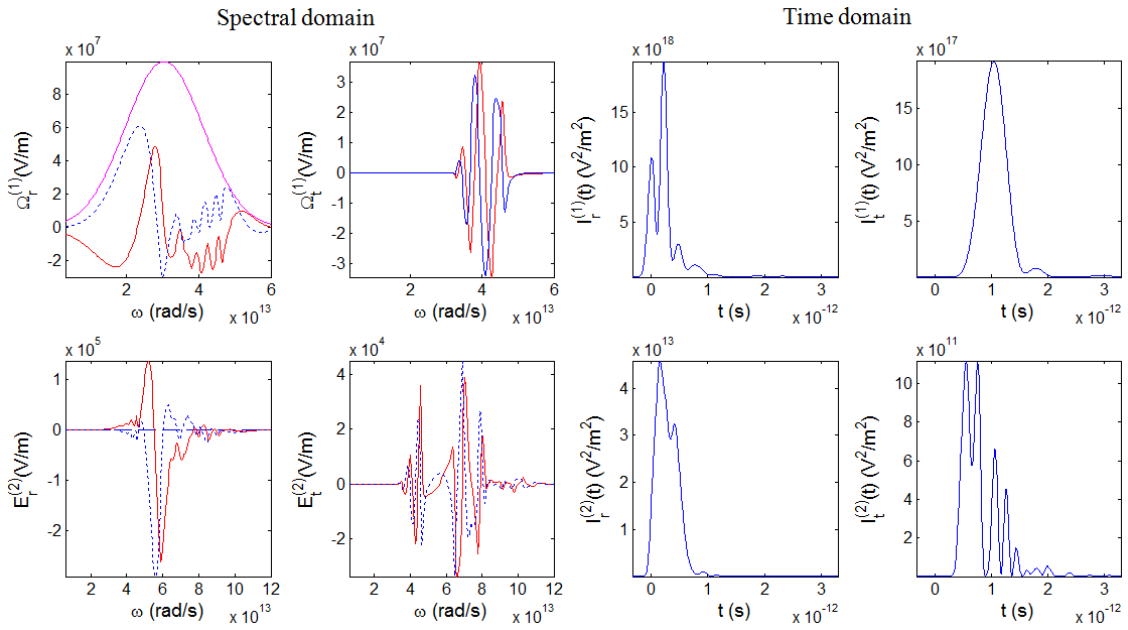

Figure 4.3: Input electric and output electric fields $\Omega^{(1)}_0(\omega)$ (magneta line), $\Omega^{(1)}_{r,t}(\omega)$ / $E^{(2)}_{r,t}(\omega)$ vs ω and $\Omega^{+}_0(\omega)$ (magneta line), $\Omega^{(1)}_{r,t}(t)$ / $E^{(2)}_{r,t}(t)$ vs t (red line - real part, blue dashed line - imaginary part) for Figure 4.2.

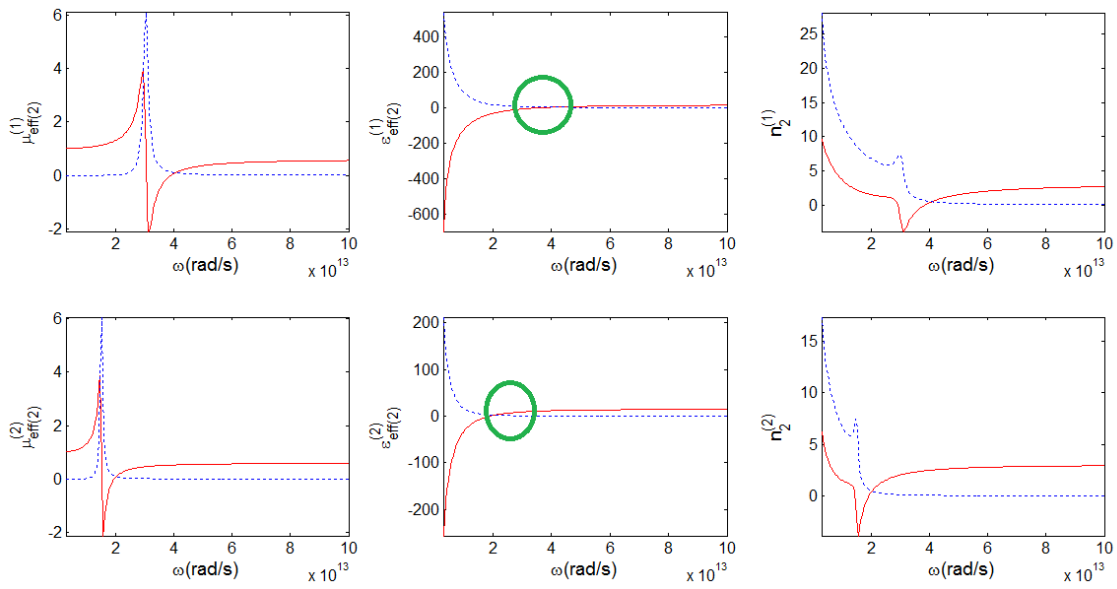

Figure 4.4: $\mu_{eff(i)}^{(j)}$, $\varepsilon_{eff(i)}^{(j)}$ and $n_i^{(j)}$ vs ω for Figure 4.2, green circle shows ω_f where $\mathrm{Re}(\varepsilon_s)$ becomes zero (red line - real part, blue dashed line - imaginary part).

The pulse shapes of $I_{r,t}^{(1)} = \left|\Omega_{r,t}^{(1)}\right|^2$, $I_{r,t}^{(2)} = \left|E_{r,t}^{(2)}\right|^2$, $\Omega_{r,t}^{(1)}$ and $E_{r,t}^{(2)}$ in frequency and time domains when $T = 0.09T_c$ are illustrated in Figure 4.3. The presence of multiple passbands in $R^{(1)}$, $T^{(1)}$, $R^{(2)}$ and $T^{(2)}$ translates into modulated pulse with short sub-pulses in the time domain. As seen in Figure 4.3, the SH pulse exists only when the pump pulse is present, the points where the output pump intensity is zero give no SH signal at output. It is also observed that reflected SH spectra $R^{(2)}$ is higher than transmitted SH spectra $T^{(2)}$ by one order of magnitude. The time delayed effect of the output pump and SH pulses is observed in plots $I_{r,t}^{(1)}$, $I_{r,t}^{(2)}$ versus t. The slow light effect is more significant on the transmitted pulse propagating in the forward direction. It is not uniquely due to the nonlinear effect, but a result of multiple reflections and strong dispersion around the resonance region. Also, the reflected pump and SH pulses are stronger than transmitted pulses because strong reflection is the result of the absorptive nature of the materials. Figure 4.4 shows $\varepsilon_{eff(i)}^{(j)}$, $\mu_{eff(i)}^{(j)}$ and $n_i^{(j)}$ in frequency domain, negative refractive index index for pulse is clearly illustrated around resonance ω_{m2}.

Now we evaluate scenario where $N = 10$, $d_1 = 0.5d$ and $\sigma_L = \Delta_0$ while other parameters remain the same. It is found that more passbands being observed in Figure 4.5 compared with Figure 4.2 for previous scenario where $N = 5$. The reflected SH signal

$R^{(2)}$ is also larger than transmitted SH signal $T^{(2)}$ by one order. We observe that spectral domain of The effect of delayed SH pulses $I_{r,t}^{(1)}$ and $I_{r,t}^{(2)}$ in Figure 4.6 is also more significant compared with Figure 4.3. Comparing $\Omega_t^{(1)}$ and $E_t^{(2)}$ in spectral domain for $N = 5$ and $N = 10$, $\Omega_t^{(1)}$ and $E_t^{(2)}$ oscilate at faster rate when $N = 10$. This is due to increasing number of period N which has led to more multiple reflection at the interfaces. Meanwhile, the characteristics of $\mu_{eff(i)}^{(j)}$, $\varepsilon_{eff(i)}^{(j)}$ and $n_i^{(j)}$as shown in Figure 4.7 are quite similar to those in Figure 4.4 as the parameters used in $\mu_{eff(i)}^{(j)}$ and $\varepsilon_{eff(i)}^{(j)}$ are the same.

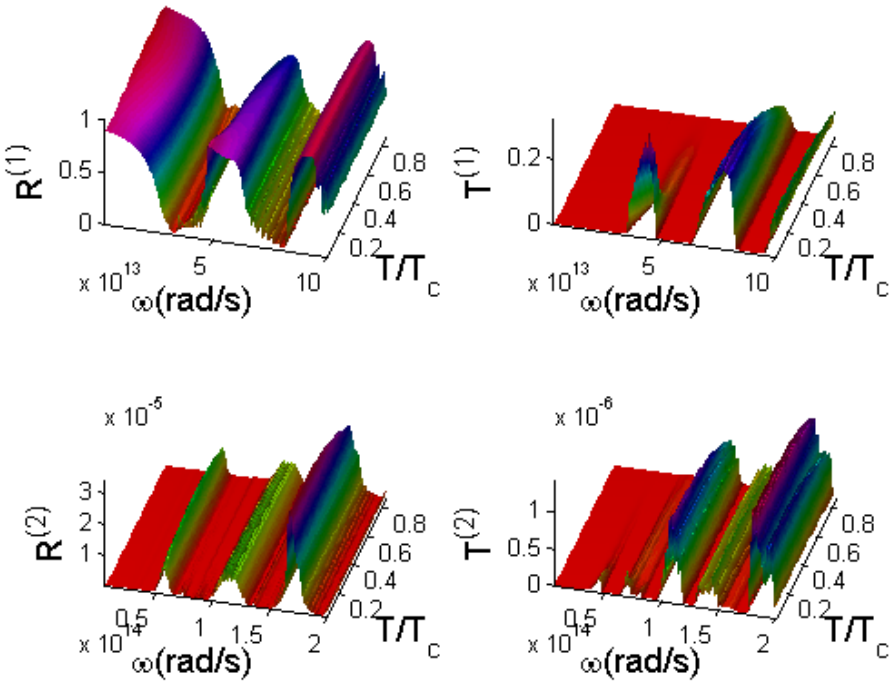

Figure 4.5: 3D plots of $R^{(1)}$, $T^{(1)}$, $R^{(2)}$ and $T^{(2)}$ vs ω/ω_0 and $\frac{T}{T_c}$, $N = 10$, $d = 10\mu$m, $d_1 = 0.5d$, $\mu_{eff(1)}^{(1)} = 1$, $\varepsilon_{eff(1)}^{(1)} = 3$, $F_2 = 0.4$, $\Gamma = 2 \times 10^{12}$, $\tau = 1 \times 10^{-13}$, $\lambda_d(0) = 0.2d$, $\varepsilon_b = 15, \sigma_L = \Delta_0$.

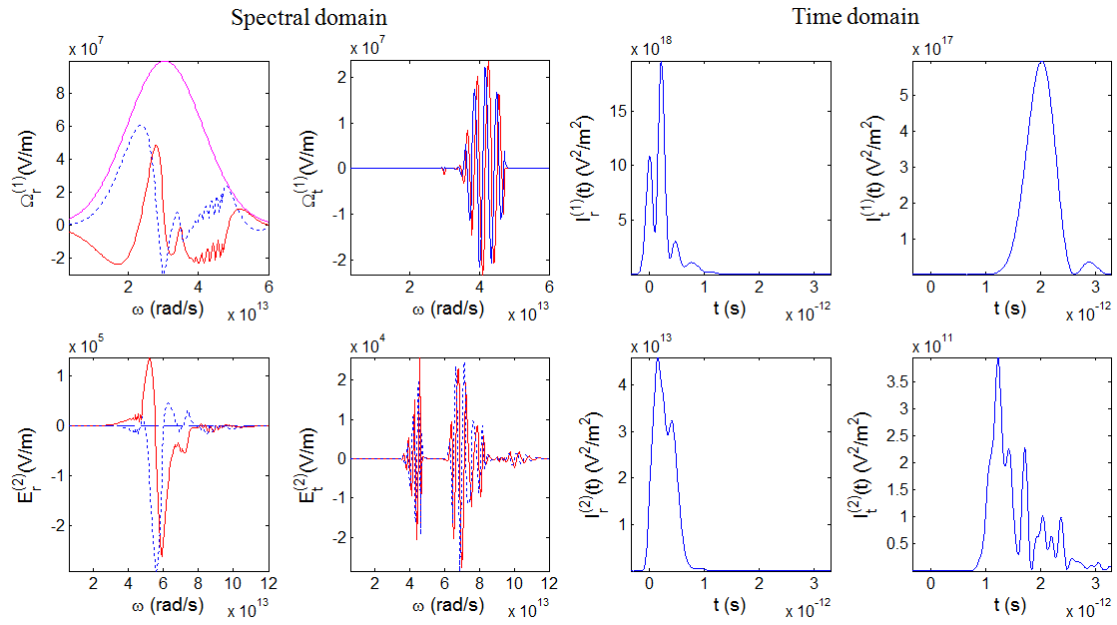

Figure 4.6: Input electric and output electric fields $\Omega_0^{(1)}(\omega)$ (magneta line), $\Omega_{r,t}^{(1)}(\omega)$ / $E_{r,t}^{(2)}(\omega)$ vs ω and $\Omega_0^{+}(\omega)$ (magneta line), $\Omega_{r,t}^{(1)}(t)$ / $E_{r,t}^{(2)}(t)$ vs t (red line - real part, blue dashed line - imaginary part) for Figure 4.5.

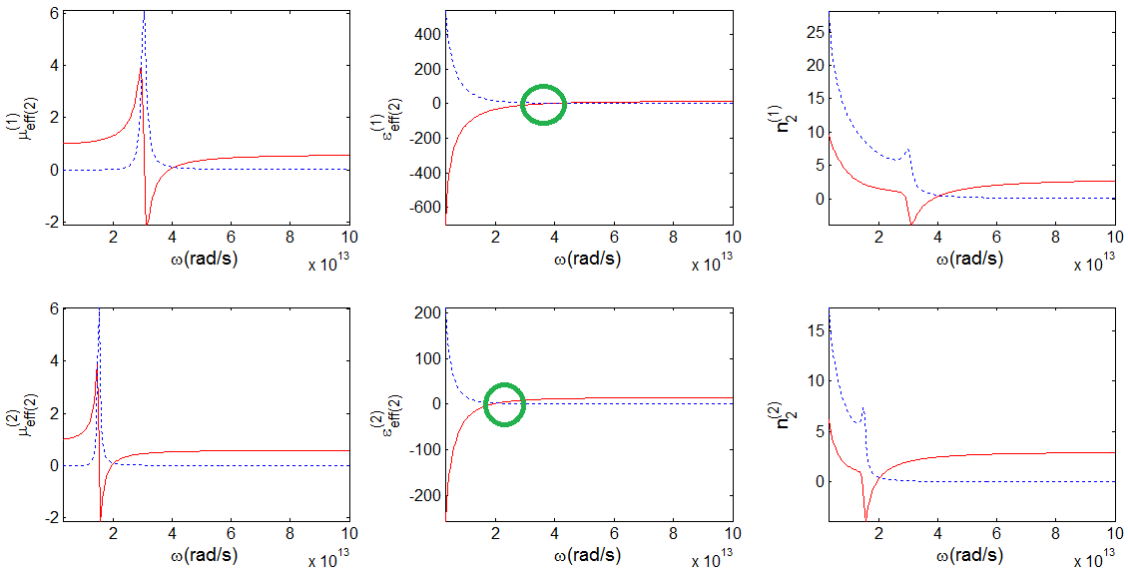

Figure 4.7: $\mu_{eff(i)}^{(j)}$, $\varepsilon_{eff(i)}^{(j)}$ and $n_i^{(j)}$ vs ω for Figure 4.5, green circle shows ω_f where $\mathrm{Re}(\varepsilon_s)$ becomes zero (red line - real part, blue dashed line - imaginary part).

We then double bandwidth of input pulse $\sigma_L = 2\Delta_0$, more passbands are observed in transmission and reflection spectra as shown in Figure 4.8. There are more subpulses

being observed in $E_t^{(2)}$ in Figure 4.9 compared with $E_t^{(2)}$ for $\sigma_L = \Delta_0$ in Figure 4.6. This could be a new mechanism for generating efficient SH reflected short sub-pulses by modulating or breaking up a pulse. It is also observed that reflected SH spectra $R^{(2)}$ is higher than transmitted SH spectra $T^{(2)}$ by one order of magnitude. One common feature in Figures 4.2, 4.5 and 4.8 is higher reflected SH signal being observed in resonant region, this is due to enhancement of SH wave vector at backward propagation due to presence of negative refractive index.

The temperature dependence in the reflection and transmission spectra is not prominent except close to the zero point frequency ω_f region which shows stronger temperature dependence due to high sensitivity of superconducting dielectric function in this region. At around and below ω_f there is essentially no transmitted SH signal except at low temperature.

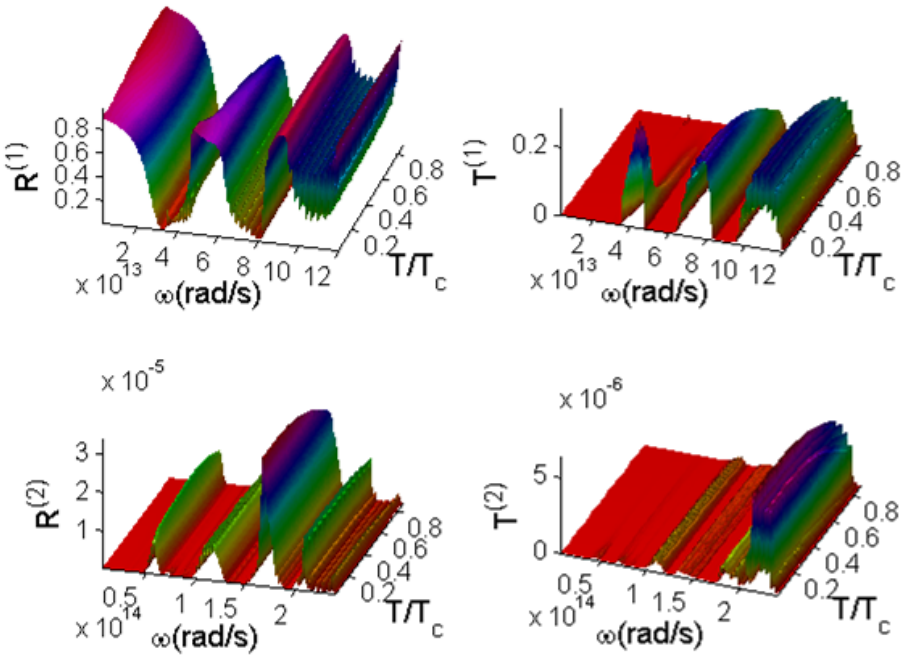

Figure 4.8: 3D plots of $R^{(1)}$, $T^{(1)}$, $R^{(2)}$ and $T^{(2)}$ vs ω/ω_0 and $\frac{T}{T_c}$, $N = 10$, $d = 10\mu$m, $d_1 = 0.5d$, $\mu^{(1)}_{eff(1)} = 1$, $\varepsilon^{(1)}_{eff(1)} = 3$, $F_2 = 0.4$, $\Gamma = 2\times10^{12}$, $\tau = 1\times10^{-13}$, $\lambda_d(0) = 0.2d$, $\varepsilon_b = 15, \sigma_L = 2\Delta_0$.

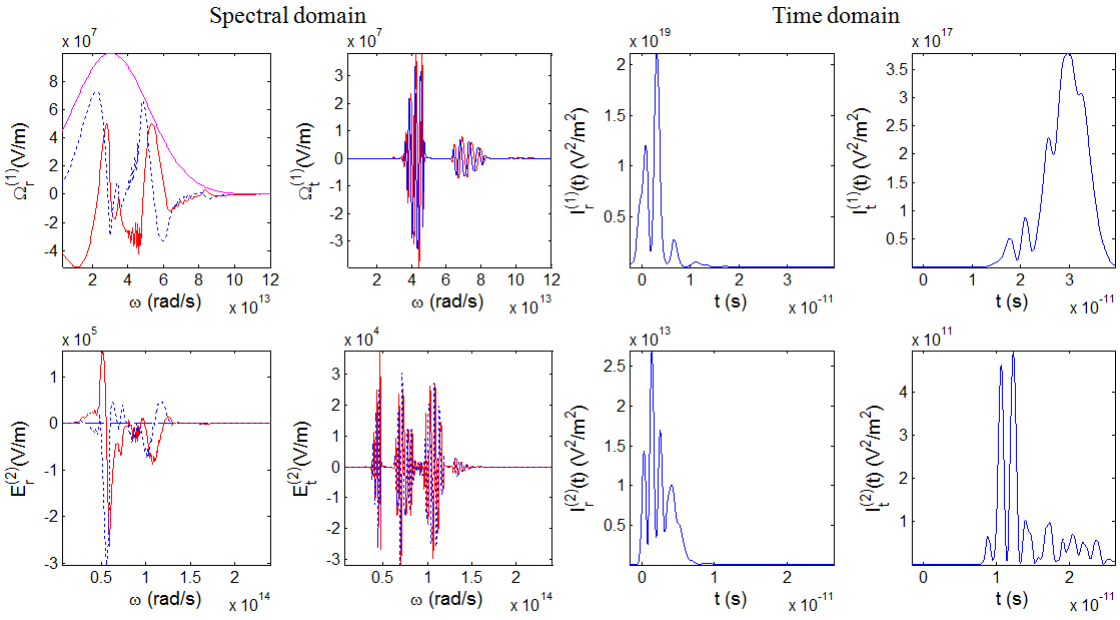

Figure 4.9: Input electric and output electric fields $\Omega_0^{(1)}(\omega)$ (magneta line), $\Omega_{r,t}^{(1)}(\omega)$ / $E_{r,t}^{(2)}(\omega)$ vs ω and $\Omega_0^{+}(\omega)$ (magneta line), $\Omega_{r,t}^{(1)}(t)$ / $E_{r,t}^{(2)}(t)$ vs t (red line - real part, blue dashed line - imaginary part) for Figure 4.8.

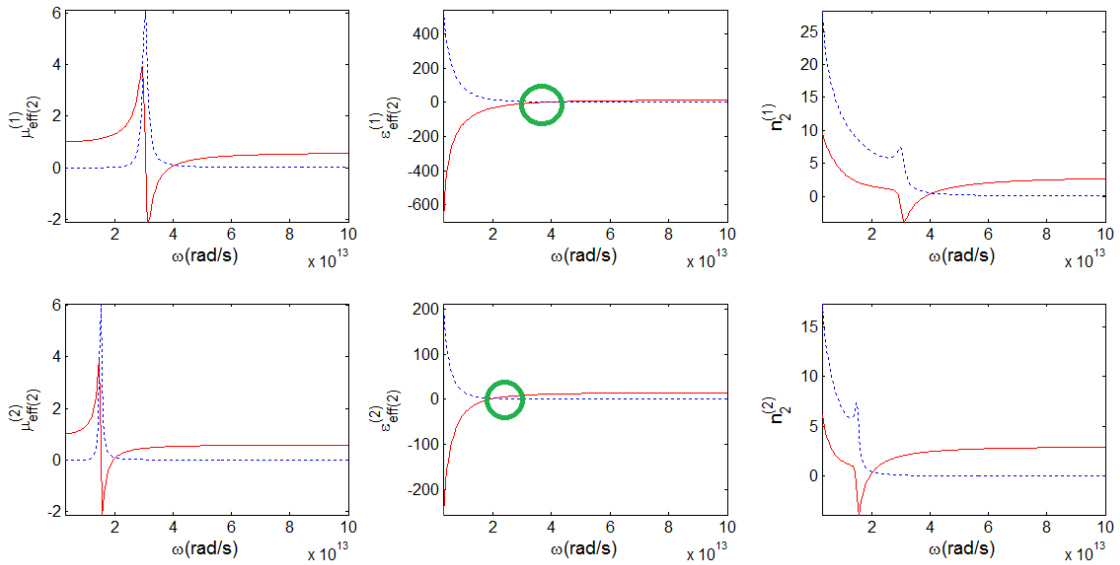

Figure 4.10: $\mu_{eff(i)}^{(j)}$, $\varepsilon_{eff(i)}^{(j)}$ and $n_i^{(j)}$ vs ω for Figure 4.8, green circle shows ω_f where $\mathrm{Re}(\varepsilon_s)$ becomes zero (red line - real part, blue dashed line - imaginary part).

4.4.2 Composite Magnetic and Superconductor Photonic Crystal

When medium 1 is magnetic and medium 2 is superconductor. We find that the temperature dependence can be seen more clearly in Figure 4.11 compared with dielectric-magnetic superconductor PC in Figure 4.2 with the same period $N = 5$ and parameters in $\mu_{eff(i)}^{(j)}$ and $\varepsilon_{eff(i)}^{(j)}$. The FF reflected signal $R^{(1)}$ is modulated into multiple sub-pulses with bigger amplitude but not temperature dependence for entire frequency range compared with dielectric-magnetic superconductor PC. The reflected SH signal $R^{(2)}$ shows interesting feature, a long pulse containing many sub-pulses, almost periodically spaced, extending over larger times (see $I_r^{(2)}$) as shown in Figure 4.12. It is also one higher than SH transmitted signal $T^{(2)}$. The slow light effect becomes more significant in forward propagation direction as illustrated by delayed $I_t^{(1)}$ and $I_t^{(2)}$. This could be due to the strong dispersion and resonance in both medium 1 and 2, not only in medium 2 as in case of Figure 4.2. This creates group velocity delay also in medium 1 and not just medium 2.

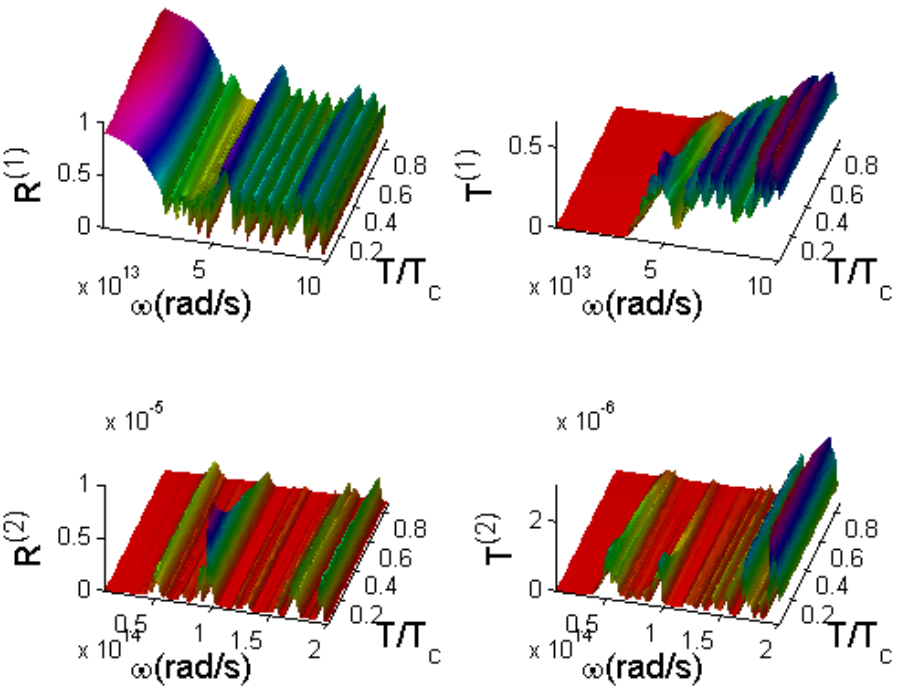

Figure 4.11: 3D plots of $R^{(1)}$, $T^{(1)}$, $R^{(2)}$ and $T^{(2)}$ vs ω and $\frac{T}{T_c}$, $N = 5$, $d = 10\mu$m, $d_1 = 0.5d$, $\mu_{eff(1)}^{(2)} = 1$, $\varepsilon_{eff(1)}^{(1)} = 3$, $F_1 = 0.55$, $\Gamma = 2 \times 10^{12}\text{s}^{-1}$, $\tau = 1 \times 10^{-13}$s, $\lambda_d(0) = 0.2d$, $\varepsilon_b = 15, \sigma_L = \Delta_0$.

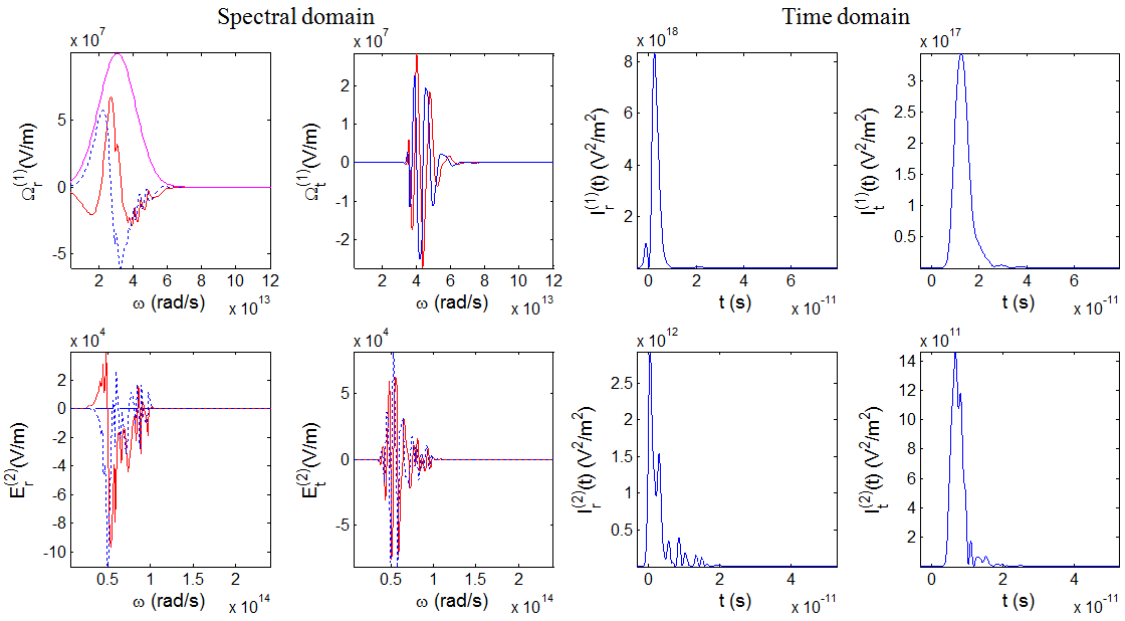

Figure 4.12: Input electric and output electric fields $\Omega_0^{(1)}(\omega)$ (magneta line), $\Omega_{r,t}^{(1)}(\omega)$ / $E_{r,t}^{(2)}(\omega)$ vs ω and $\Omega_0^{+}(\omega)$ (magneta line), $\Omega_{r,t}^{(1)}(t)$ / $E_{r,t}^{(2)}(t)$ vs t (red line - real part, blue dashed line - imaginary part) for Figure 4.11.

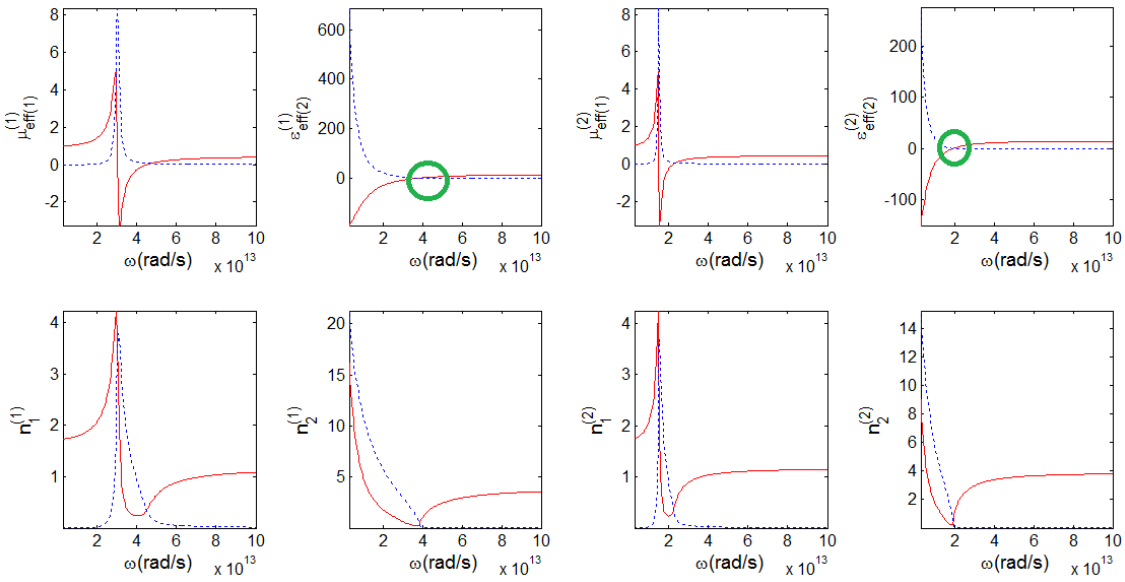

Figure 4.13: $\mu_{eff(i)}^{(j)}$, $\varepsilon_{eff(i)}^{(j)}$ and $n_i^{(j)}$ vs ω for Figure 4.11, green circle shows ω_f where $\mathrm{Re}(\varepsilon_s)$ becomes zero (red line - real part, blue dashed line - imaginary part).

We double the bandwidth $\sigma_L = 2\Delta_0$ and observe that reflected SH signal $R^{(2)}$ is the

same order with transmitted SH signal $T^{(2)}$ in Figure 4.14 unlike the dielectric magnetic superconductor PC in which $R^{(2)}$ is one order higher than $T^{(2)}$. There is no negative refractive index being created as magnetic resonance in medium 1 is not overlap with dielectric resonance in layer 2. Therefore, phase mismatch in backward propagation is not adequately compensated in the case of PC with negative refraction. Reflected SH signal $R^{(2)}$ and transmitted SH signal $T^{(2)}$ are stronger at the lower temperature. It is also interesting to observe that both transmitted and reflected SH signals are modulated into more sub-pulses as shown in $I_t^{(2)}$ and $I_r^{(2)}$ (Figure 4.15). The feature of delayed $I_t^{(1)}$ and $I_t^{(2)}$ when $\sigma_L = 2\Delta_0$ is similar to the case when $\sigma_L = \Delta_0$. The patterns of $R^{(1)}$ and $T^{(1)}$ in this case do not demonstrating significant difference compared with $R^{(1)}$ and $T^{(1)}$ for $\sigma_L = \Delta_0$. This is also could be observed in $I_t^{(1)}$ and $I_r^{(1)}$ as illustrated in Figure 4.15. There is no significant difference of $\mu_{eff(i)}^{(j)}$, $\varepsilon_{eff(i)}^{(j)}$ and $n_i^{(j)}$ between the scenarios $\sigma_L = 2\Delta_0$ (Figure 4.15) and $\sigma_L = \Delta_0$ (Figure 4.13) as the parameters remain unchanged.

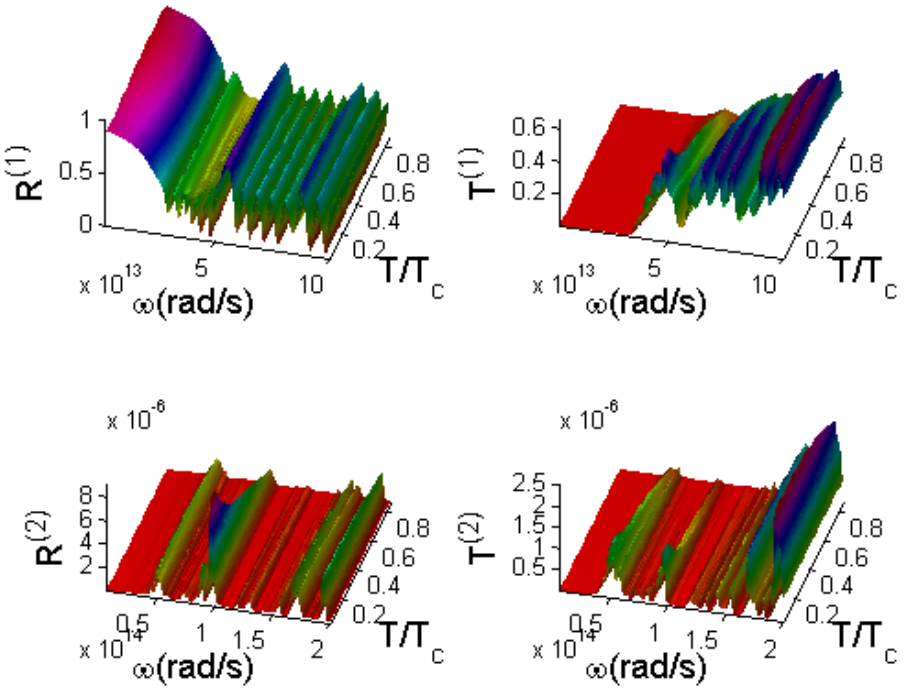

Figure 4.14: 3D plots of $R^{(1)}$, $T^{(1)}$, $R^{(2)}$ and $T^{(2)}$ vs ω and $\frac{T}{T_c}$, $N = 5$, $d = 10\mu$m, $d_1 = 0.5d$, $\mu_{eff(1)}^{(2)} = 1$, $\varepsilon_{eff(1)}^{(1)} = 3$, $F_1 = 0.55$, $\Gamma = 2 \times 10^{12}\text{s}^{-1}$, $\tau = 1 \times 10^{-13}$s, $\lambda_d(0) = 0.2d$, $\varepsilon_b = 15, \sigma_L = 2\Delta_0$.

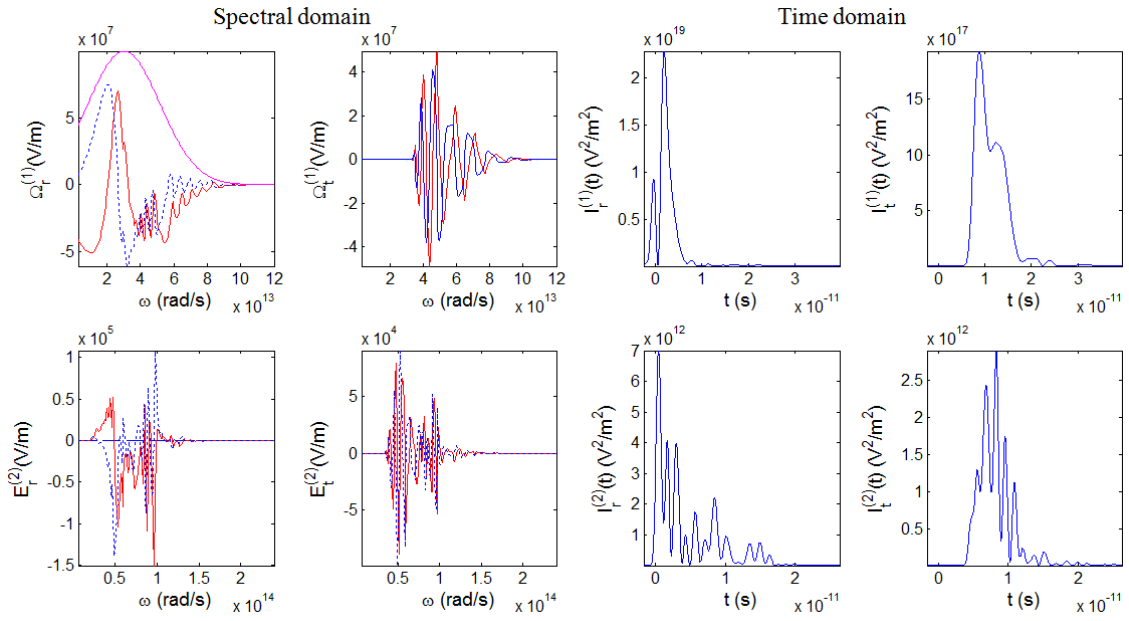

Figure 4.15: Input electric and output electric fields $\Omega_0^{(1)}(\omega)$ (magneta line), $\Omega_{r,t}^{(1)}(\omega)$ / $E_{r,t}^{(2)}(\omega)$ vs ω and $\Omega_0^{+}(\omega)$ (magneta line), $\Omega_{r,t}^{(1)}(t)$ / $E_{r,t}^{(2)}(t)$ vs t (red line - real part, blue dashed line - imaginary part) for Figure 4.14.

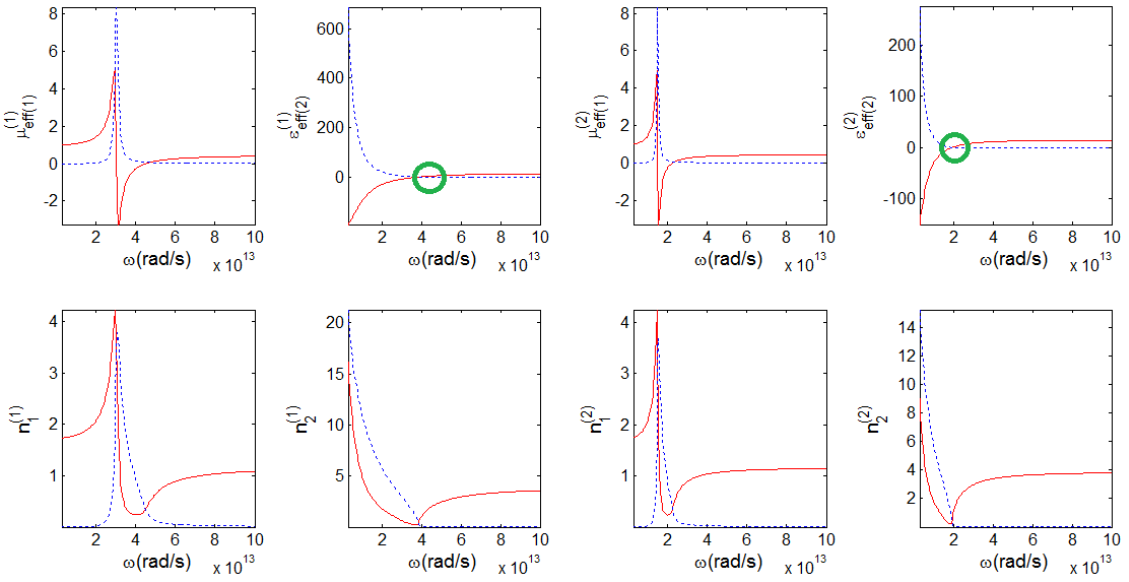

Figure 4.16: $\mu_{eff(i)}^{(j)}$, $\varepsilon_{eff(i)}^{(j)}$ and $n_i^{(j)}$ vs ω for Figure 4.14, green circle shows ω_f where $\mathrm{Re}(\varepsilon_s)$ becomes zero (red line - real part, blue dashed line - imaginary part).

Slow light effect is also more obvious when N is doubled ($N = 10$), we see that

delay of both SH reflected and transmitted signals are illustrated in $I_t^{(1)}$ and $I_r^{(1)}$ versus t plots in Figure 4.18, the delay effect is more significant than $I_t^{(1)}$ and $I_r^{(1)}$ for $N = 5$ and $\sigma_L = \Delta_0, 2\Delta_0$. This phenomeno is due to more multiple reflections due to increased period number. No significant difference being observed for $\mu_{eff(i)}^{(j)}$, $\varepsilon_{eff(i)}^{(j)}$ and $n_i^{(j)}$ when $N = 10$ and $\sigma_L = \Delta_0$ compared with previous cases which is expected because parameters in $\mu_{eff(i)}^{(j)}$ and $\varepsilon_{eff(i)}^{(j)}$ remain unchanged. When we increase bandwidth $\sigma_L = 2\Delta_0$ while maintaining $N = 10$, Figure 4.20 shows that FF reflection spectra $R^{(1)}$ has more passbands compared with all previous cases. In Figure 4.21, we see more significant slow light effect in pump pulse compared with transmitted SH pulse. This is due to more multiple reflections and transmission processes caused by increased period number. It is observed that both reflected and transmitted SH pulses are modulated into more sub-pulses as shown in plots $I_t^{(2)}$ and $I_r^{(2)}$ in time domain, this is the effect caused by increased bandwidth $\sigma_L = 2\Delta_0$. Again, the effect of increasing bandwidth has no influence on $\mu_{eff(i)}^{(j)}$, $\varepsilon_{eff(i)}^{(j)}$ and $n_i^{(j)}$ as shown in Figure 4.22.

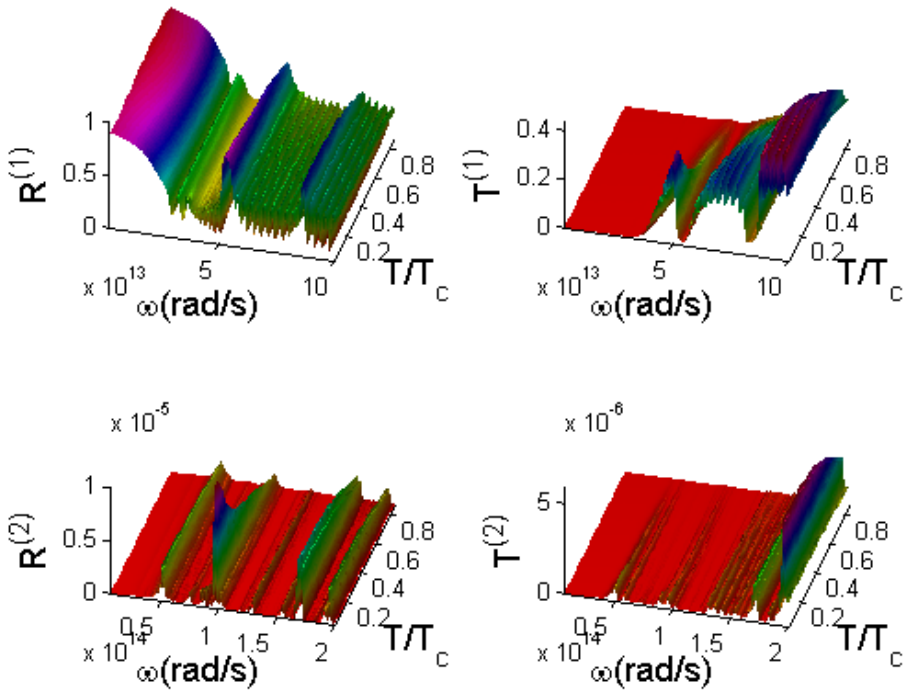

Figure 4.17: 3D plots of $R^{(1)}$, $T^{(1)}$, $R^{(2)}$ and $T^{(2)}$ vs ω and $\frac{T}{T_c}$, $N = 10$, $d = 10\mu$m, $d_1 = 0.5d$, $\mu_{eff(1)}^{(2)} = 1$, $\varepsilon_{eff(1)}^{(1)} = 3$, $F_1 = 0.55$, $\Gamma = 2 \times 10^{12}\text{s}^{-1}$, $\tau = 1 \times 10^{-13}$s, $\lambda_d(0) = 0.2d$, $\varepsilon_b = 15, \sigma_L = \Delta_0$.

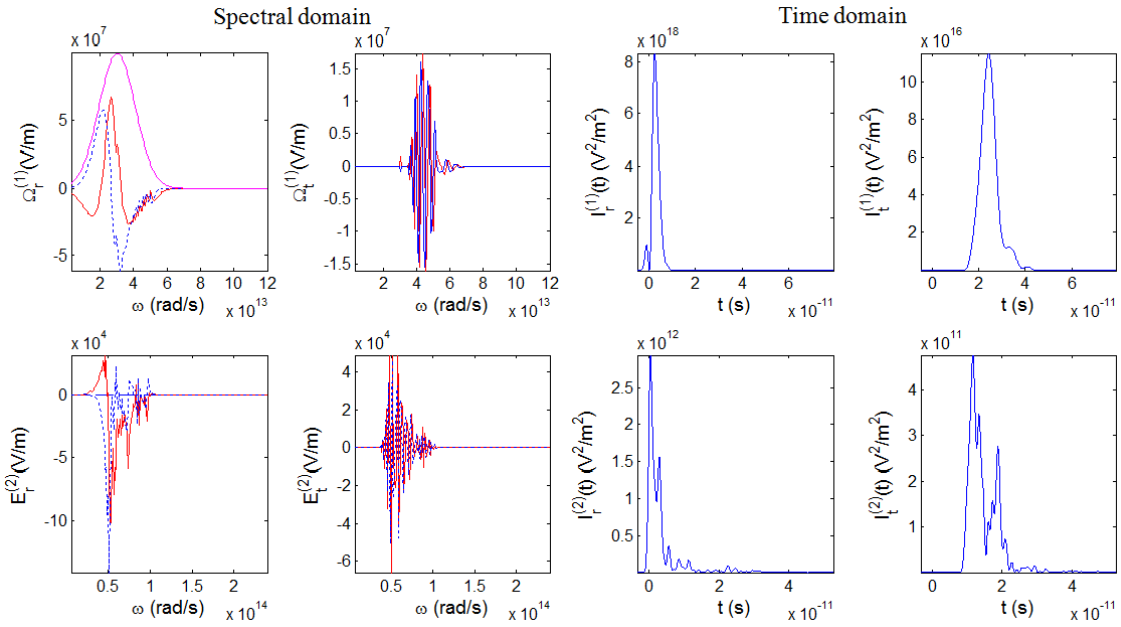

Figure 4.18: Input electric and output electric fields $\Omega_0^{(1)}(\omega)$ (magneta line), $\Omega_{r,t}^{(1)}(\omega)$ / $E_{r,t}^{(2)}(\omega)$ vs ω and $\Omega_0^{+}(\omega)$ (magneta line), $\Omega_{r,t}^{(1)}(t)$ / $E_{r,t}^{(2)}(t)$ vs t (red line - real part, blue dashed line - imaginary part) for Figure 4.17.

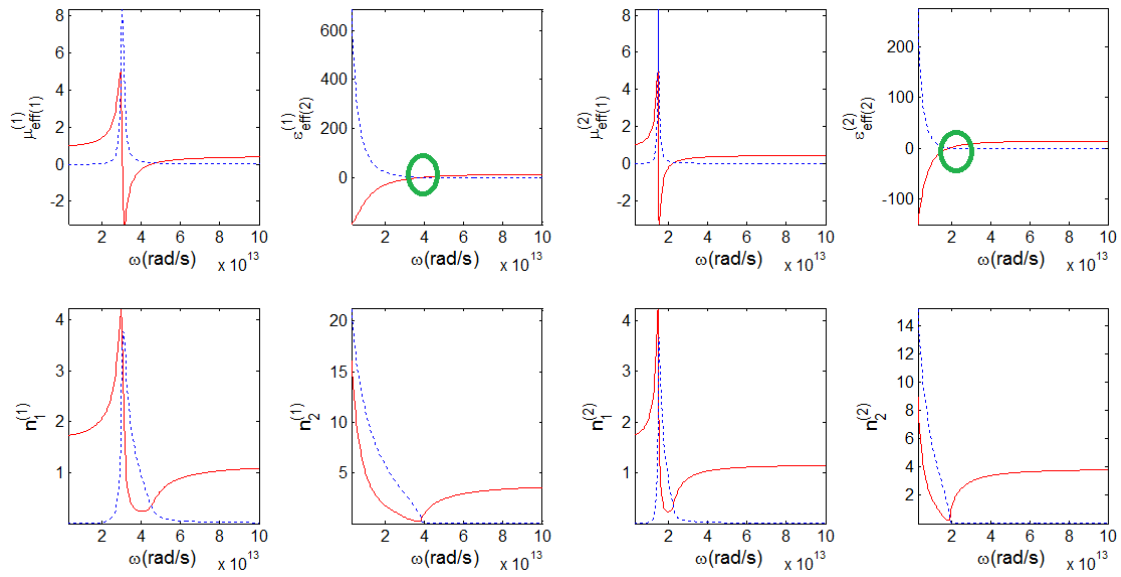

Figure 4.19: $\mu_{eff(i)}^{(j)}$, $\varepsilon_{eff(i)}^{(j)}$ and $n_i^{(j)}$ vs ω for Figure 4.17, green circle shows ω_f where $\mathrm{Re}(\varepsilon_s)$ becomes zero (red line - real part, blue dashed line - imaginary part).

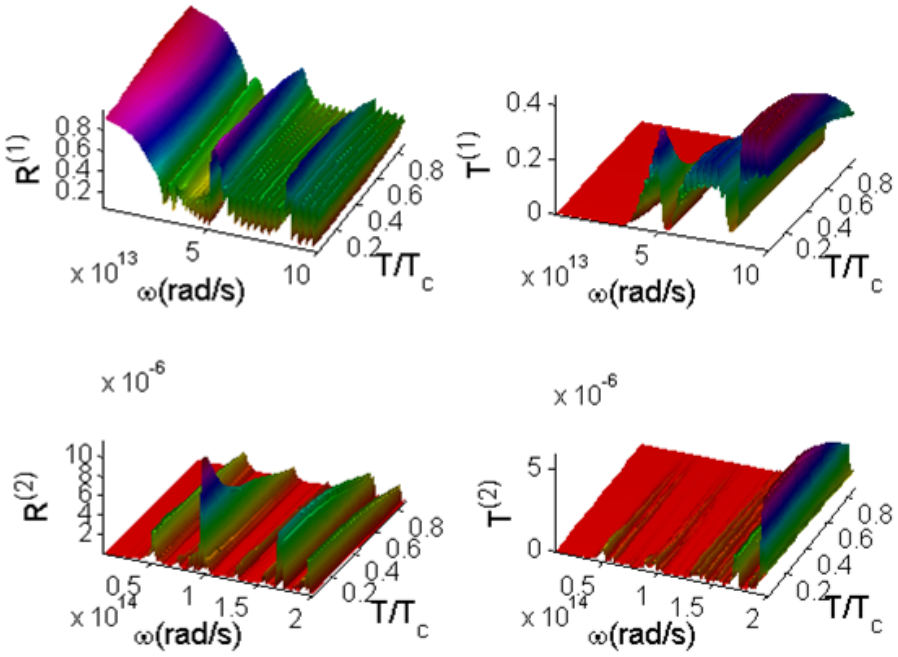

Figure 4.20: 3D plots of $R^{(1)}$, $T^{(1)}$, $R^{(2)}$ and $T^{(2)}$ vs ω and $\frac{T}{T_c}$, $N = 10$, $d = 10\mu$m, $d_1 = 0.5d$, $\mu^{(2)}_{eff(1)} = 1$, $\varepsilon^{(1)}_{eff(1)} = 3$, $F_1 = 0.55$, $\Gamma = 2\times10^{12}\text{s}^{-1}$, $\tau = 1\times10^{-13}$s, $\lambda_d(0) = 0.2d$, $\varepsilon_b = 15, \sigma_L = 2\Delta_0$.

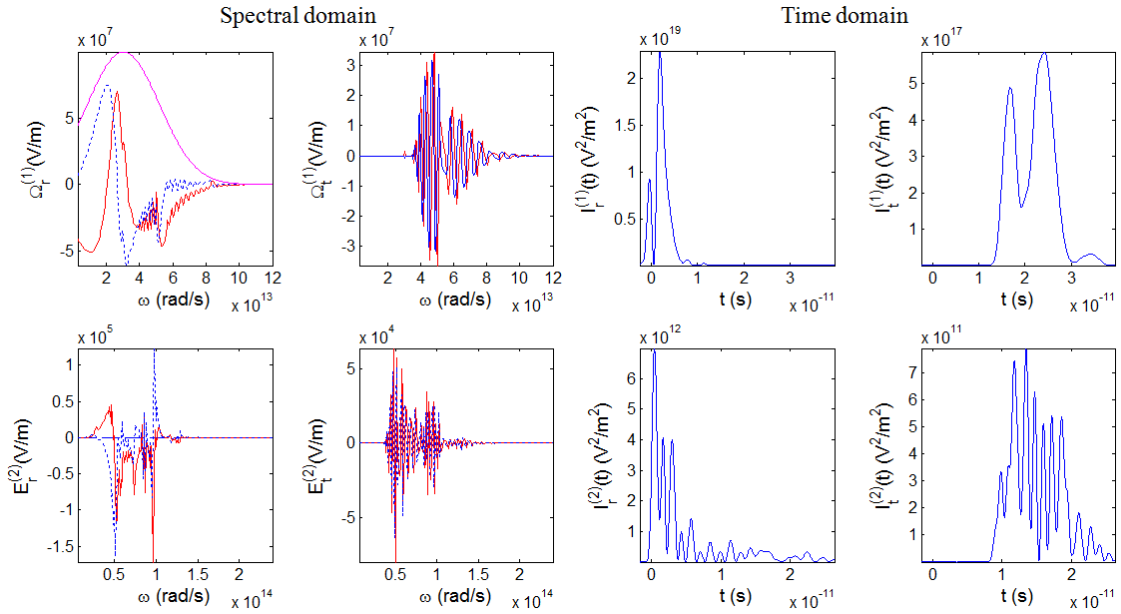

Figure 4.21: Input electric and output electric fields $\Omega^{(1)}_0(\omega)$ (magneta line), $\Omega^{(1)}_{r,t}(\omega)$ / $E^{(2)}_{r,t}(\omega)$ vs ω and $\Omega^{+}_0(\omega)$ (magneta line), $\Omega^{(1)}_{r,t}(t)$ / $E^{(2)}_{r,t}(t)$ vs t (red line - real part, blue dashed line - imaginary part) for Figure 4.20.

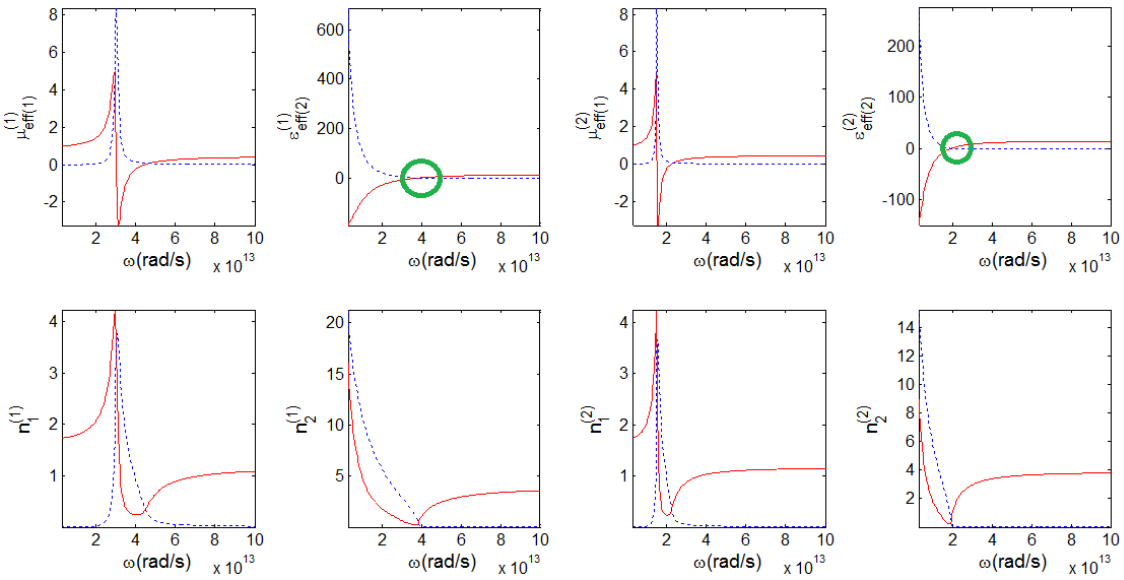

Figure 4.22: $\mu^{(j)}_{eff(i)}$, $\varepsilon^{(j)}_{eff(i)}$ and $n^{(j)}_i$ vs ω for Figure 4.20, green circle shows ω_f where $\mathrm{Re}(\varepsilon_s)$ becomes zero (red line - real part, blue dashed line - imaginary part).

From the above evaluation, it is clearly seen that increasing period number N would cause delay in output pump pulse propagation and increasing bandwidth σ_L would induce stronger SH pulse modulation. Therefore, it opens up possibility for designing pulse converter device by adjusting N and also σ_L.

We note that the resulting pump pulse shown in all figures is entirely due to linear process of multiple scattering in the multilayers while the SH pulse produced is due to nonlinear (second harmonic) process. Significant distortion in the fundamental input pump pulse Ω_0^+ (with Gaussian spectrum) can be seen in Figures 4.2, 4.5 and 4.8 by comparing it with the fundamental output pulse $\Omega_r^{(1)}, \Omega_t^{(1)}$. It is the result of multiple scattering (reflections and transmissions) and nonlinearity has no effect here. Thus, the pulse reshaping is entirely due to linear scattering process. Now, if we compare the second harmonic fields $E_r^{(2)}, E_t^{(2)}$ with the fundamental fields $\Omega_r^{(1)}, \Omega_t^{(1)}$ in spectral domains, we see that both are significantly different. They are different because the SH fields are due to the nonlinear process, in addition to the linear process of multiple scattering. Recall coupled equation 2.39 $\frac{\partial \tilde{A}_x}{\partial z} = \frac{i\omega^2 \mu \chi^{(2)}_{xxx}}{k^{(1)}} \tilde{B}_x \tilde{A}_x^* e^{i\Delta k z}$, for small SH magnitude of $\tilde{B}_x$ is much less than magnitude of $\tilde{A}_x$ $\left(\tilde{B}_x \ll \tilde{A}_x\right)$, thefore the RHS Equation 2.39 is ngegligible, which becomes homogeneous differential equation and the propagation of FF is entirely due to

linear process which agrees with our results here.

We emphasize that SH output shall not be considered as pulses as it simply appears to have been a fraction of energy from the pump pulse that has been produced by nonlinear frequency conversion and strongly modulated by linear process of multiple scattering into sub-pulses. The multiple peaks of the field amplitude in the spectral domain does not guarantee that there are also similar peaks in the time domain due to the fact that the phase, i.e. the imaginary part, also plays a role when Fourier transforming to the time domain. The output pulse may seem chaotic but there is no statistical nor random process involved. Instead, several underlying physical processes are molding the resulting modulated pulse. The output pulse may be useful that it contains some information about the mixture of optical processes; namely multiple scattering, propagation and second harmonic generation in the nonlinear photonic crystal. The results help to better understand the underlying optical processes such as dispersion, phase matching and slow light that lead to intensity modulation or breakup of the pump pulse and production of a strongly modulated SH pulse. Thus, this work forms a foundation for future works aimed at optimizing pulse modulation for applications such as in spectroscopy.

4.5 Conclusions

We have shown that photonic crystal with superconducting layer and second order nonlinearity can be used to generate mid- or far-infrared (MIR-FIR) pulse using a nonlinear material through second harmonic generation process. An input (Gaussian) pump pulse is dramatically distorted and becomes shorter by strong dispersion and absoprtion around the resonant region of the magnetic material and the superconducting bandgap, as well as by multiple scattering. It provides an alternative method to free electron laser (Knippels, Mols, Meer, Oepts, & Amersfoort, 1995) and specialized crystals (Dantzig, Planken, & Bakker, 1998) for reshaping and converting infrared (IR) pulse to higher harmonics by incorporating the resonances of magnetic and superconducting materials. We emphasize that there is no amplification nor lasing process involved as in the FEL. The mechanism here is nonlinear frequency conversion that produces second harmonic pulse in the IR wavelength. At low temperature, the superconducting layer provides higher SHG conversion efficiency. The magnetic and superconducting nonlinear photonic crys-

tal provides a new mechanism for reshaping and converting short pulse by combining resonant multiple scattering and nonlinear optical process for photonic spectral engineering.

CHAPTER 5

CONCLUSION

We wrap up the conclusion for our findings in chapters 3 and 4 in the following sections. The recommendation for future works are also being addressed.

5.1 SHG in Metamaterial Photonic Crystal by Continuous Wave Laser Beam

We model SHG in 1 dimensional dielctric PC with metamaterial by using TMM. We then demonstrate that transmission and reflection spectra of FF and SH fields exhibit interesting harmonic patterns when undepleted CW laser beam is pumped upon 1 dimensional nondispersive PC with constant and real negative effective permeability and permittivity. The period thickness is 1μm. The values and signs of effective permeability and permittivity are choosen to determine refractive index contrast between odd and even layers. The important parameters for studying characteristics of FF and SH transmission and reflection are thickness ratio of odd layer with respect to period thickness and also frequency spectrum of pump beam. When refractive index contrast between layers are significant and same sign, there is zero reflection and absolute transmission for FF. Regular harmonics depend on thickness ratio and frequency are observed in SH reflection spectra. The SH transmission spectra is independent of thickness ratio but have symmetry at the center of frequency spectrum. SH reflected field is only ten times smaller than transmitted SH field. When refractive index contrast is significant but with opposite sign, which means only one layer has negative refractive index, localized broad spectrum is observed around thickness ratio 0.85 in SH reflection spectra. The transmitted SH field strength increases with respect to frequency and symmetry at thickness ratio around 0.5. This finding is valid when N is increased from 10 to 30.

When insignificant refractive index contrast is achieved by using same magnitude permeabilities, permittivities and refractive index in both layers but with opposite sign, transmission and reflection spectra of FF and SH are almost similar and having symmetry at thickness ratio of 0.5. They are finite over entire range of frequency spectrum. Board

spectrum is observed for entire frequency spectrum in SH reflection spectra, this feature may open up possibility for supercontiuum laser generation. When magnitude and sign of permeability and permittivity are not the same in odd and even layers, the symmetry and similarity of reflection and transmission spectra of FF and SH are no longer being observed. Instead, localized harmonics are observed in SH reflection and transmission spectra. This broken symmetry is useful for developing more efficient frequency conversion devices. The negative refractive indices cause the change in the sign of SH wavevectors, providing improved phase matching and strong SH backward electric field compared with conventional PC.

For dispersive PC, permeability and permittivity are frequency dependent and negative refractive index would be observed when magnetic resonant and dielectric resonant are overlapping to each other. This leads to formation of absorption peaks in FF reflection spectra and absorption valley in FF transmission spectra. The parameters used for simulation are $N = 5$ and $d = 0.1\mu$m. For both layers with single resonances, narrow bandgap around resonance is observed in FF transmission spectra, meanwhile reflection is small around resonance. When both magnetic and electric resonants in one layer are double of another layer, the finite and tunable narrow transmission ridge is observed in FF transmission spectra, the reflected SH field remains small. For layers with double identical resonances, finite and cosntant narrow transmission ridge is also being observed in FF transmission spectra. This time, more significant absorption peaks are observed in FF reflection spectra. For layers with different double resonances, wider absorption region is formed and two tunable transmission ridges are observed in FF transmission spectra. In general, SH fields are negligible around resonance for dispersive PC.

5.2 SHG in Superconducting Magnetic Photonic Crystal by Ultrashort Pulse Laser Beam

We model propagation of strong ultrashort pulse through nonlinear magnetic PC with superconducting layer by using frequency domain TMM. Two fluid model is used to describe temperature conductivity and permittivity of the superconducting layer. We consider input pulse is strong enough such that effect on SH process is negligible, therefore the characteristic of pulse propagating inside the PC could be assumed to be the

same as input pulse. There is no second harmonic seed applied in this study as it is intended to evaluate effect solely caused by ultrashort pulse propagation in this nonlinear PC. In bilayer dielectric magnetic superconducting PC, reflected SH signal is stronger than transmitted SH signal due to presence of negative refractive index around resonant region which has improved phase matching in SH backward propagation. Meanwhile, in bilayer PC where odd layer is magnetic material and even layer is superconductor, SH reflection spectra $R^{(2)}$ is in the same order with transmission spectra $T^{(2)}$ as there is no negative refraction occurs due to no overlapping of magnetic resonance and dielectric resonance to produce negative refractive index.

Slow light effect is observed for output pulse and also SH transmitted pulse in both dielectric-magnetic superconductor PC and also magnetic-superconductor PC. Propagation of output pulse is subjected to linear multiple scattering at the interface inside PC, propagation delay effect is more significant when number of period is increased. We also observe that increasing bandwidth of pump pulse would cause stronger modulation of SH pulse. SH pulse is produced from small fraction energy of pump pulse by mean of frequency conversion caused by nonlinearity and then strongly modulated by linear multiple scattering into sub-pulses. The conversion efficiency of SH is in the order of 10^{-5} and 10^{-6} in this model because strong pump pulse is propagating through PC in such a way that it is approximated to propagation in homogenoues medium and has small effect in nonlinear interaction with $\chi^{(2)}$ of the PC. This study enable us to understand the basis of SH generation and pulse reshaping/modulation when ultrashort is pumped upon superconducting PC with magnetic response by using straight forward TMM. We also obtain the characteristics of output pulse and SH pulse in relation to number of period and also bandwidth of pump pulse, this is useful information in optical engineering which opens up approach to design efficient frequency converter device.

5.3 Future Works

TMM developed in this thesis is capable to handle numerical simulation with small period number as it would diverge around resonance to create negative refractive index, hence improvement is needed so that it could be used to study SHG with larger period number. Besides that, we assume that FF or pump pulse is undepleted and nonlinear SHG

has negligible effect on the FF and pump pulse, this is good approximation in the PC with small period only, propagation equation that takes depletion shall be applied for more accurate numerical simulation when number of period increases. It is also meaningful to include Kerr effect in magnetic superconducting PC to further investigate interaction between ultrashort pulse and PC as it is known that high intense ultrashort pulse would strongly modify optical properties of medium with Kerr effect. Our model in this thesis could be extended to model SHG in 2D and 3D nonlinear PC. Other than that, it is also possible to use TMM in this thesis as baseline to develop new transfer matrix to model SFG and four wave mixing in PC integrated with metamaterial and also superconducting medium.

Appendices

APPENDIX A

DERIVATION OF MATHEMATICAL FORMULA

A.1 Wave Propagation Equation

From Equation 2.10, we take curl at RHS and LHS

$$\nabla \times \nabla \times \mathbf{E}(\mathbf{r},t) = \nabla \times \left(-\frac{\partial \mathbf{B}(\mathbf{r},t)}{\partial t} \right) \tag{A.1}$$

use vector calculus, we evaluate RHS of A.1

$$\begin{aligned} \nabla \times \nabla \times \mathbf{E}(\mathbf{r},t) &= \nabla(\nabla \cdot \mathbf{E}(\mathbf{r},t)) - \nabla^2 \mathbf{E}(\mathbf{r},t) \\ &= \frac{\varepsilon}{\varepsilon} \nabla(\nabla \cdot \mathbf{E}(\mathbf{r},t)) - \nabla^2 \mathbf{E}(\mathbf{r},t) \\ &= \frac{1}{\varepsilon} \nabla(\nabla \cdot \varepsilon \mathbf{E}(\mathbf{r},t)) - \nabla^2 \mathbf{E}(\mathbf{r},t) \\ &= \frac{1}{\varepsilon} \nabla(\nabla \cdot \mathbf{D}(\mathbf{r},t)) - \nabla^2 \mathbf{E}(\mathbf{r},t) \end{aligned} \tag{A.2}$$

where effect of $\mathbf{P}^{NL}(\mathbf{r},t)$ is negligible in $\nabla \cdot \mathbf{D}(\mathbf{r},t)$, from Equation 2.17, we have

$$\begin{aligned} \nabla \times \nabla \times \mathbf{E}(\mathbf{r},t) &= \frac{1}{\varepsilon} \nabla(0) - \nabla^2 \mathbf{E}(\mathbf{r},t) \\ &= -\nabla^2 \mathbf{E}(\mathbf{r},t) \end{aligned}$$

We also evaluate LHS of A.1,

$$\begin{aligned} \nabla \times \left(-\frac{\partial \mathbf{B}(\mathbf{r},t)}{\partial t} \right) &= -\frac{\partial}{\partial t} (\nabla \times \mu \mathbf{H}(\mathbf{r},t)) \\ &= -\frac{\partial}{\partial t} (\nabla \times \mu \mathbf{H}(\mathbf{r},t)) \\ &= -\mu \frac{\partial}{\partial t} (\nabla \times \mathbf{H}(\mathbf{r},t)) \\ &= -\mu \frac{\partial}{\partial t} \left(\frac{\partial \mathbf{D}(\mathbf{r},t)}{\partial t} \right) \\ &= -\mu \frac{\partial}{\partial t} \frac{\partial}{\partial t} \left(\varepsilon \mathbf{E}(\mathbf{r},t) + \mathbf{P}^{NL}(\mathbf{r},t) \right) \\ &= -\mu \frac{\partial^2}{\partial t^2} \left(\varepsilon \mathbf{E}(\mathbf{r},t) + \mathbf{P}^{NL}(\mathbf{r},t) \right) \\ &= -\mu \frac{\partial^2}{\partial t^2} \varepsilon \mathbf{E}(\mathbf{r},t) - \mu \frac{\partial^2 \mathbf{P}^{NL}(\mathbf{r},t)}{\partial t^2} \end{aligned} \tag{A.3}$$

Therefore, we have

$$\nabla^2 \mathbf{E}(\mathbf{r},t) - \mu\varepsilon \frac{\partial^2 \mathbf{E}(\mathbf{r},t)}{\partial t^2} = \mu \frac{\partial^2 \mathbf{P}^{NL}(\mathbf{r},t)}{\partial t^2} \tag{A.4}$$

Now we evaluate wave propagation equation for SHG, from Equation 2.9, we could write electric field for SH wave propagating with angular frequency of 2ω, $\mathbf{A}^{(2)}(\mathbf{r},t)$ is complex field amplitude

$$\mathbf{E}^{(2)}(\mathbf{r},t) = \mathbf{A}^{(2)}(\mathbf{r},t)\, e^{-i2\omega t} \tag{A.5}$$

therefore, $\frac{\partial^2 \mathbf{E}^{(2)}(\mathbf{r},t)}{\partial t^2}$ is

$$\begin{aligned} \frac{\partial^2 \mathbf{E}^{(2)}(\mathbf{r},t)}{\partial t^2} &= \mathbf{A}^{(2)}(\mathbf{r},t)\frac{\partial^2}{\partial t^2} e^{-i2\omega t} \\ &= (-i2\omega)^2 \mathbf{A}^{(2)}(\mathbf{r},t)\, e^{-i2\omega t} \\ &= -4\omega^2 \mathbf{E}^{(2)}(\mathbf{r},t) \end{aligned} \tag{A.6}$$

now we substitute Equation A.6 into LHS of Equation A.4

$$\begin{aligned} \nabla^2 \mathbf{E}^{(2)}(\mathbf{r},t) + 4\omega^2 \mu\varepsilon \mathbf{E}^{(2)}(\mathbf{r},t) &= \nabla^2 \mathbf{E}^{(2)}(\mathbf{r},t) + 4\omega^2 \frac{1}{v^2} \mathbf{E}^{(2)}(\mathbf{r},t) \\ &= \nabla^2 \mathbf{E}^{(2)}(\mathbf{r},t) + 4\omega^2 \frac{n^2}{c^2} \mathbf{E}^{(2)}(\mathbf{r},t) \\ &= \nabla^2 \mathbf{E}^{(2)}(\mathbf{r},t) + \left(4\omega^2 \frac{n^2}{c^2}\right) \mathbf{E}^{(2)}(\mathbf{r},t) \\ &= \nabla^2 \mathbf{E}^{(2)}(\mathbf{r},t) + k^{(2)2} \mathbf{E}^{(2)}(\mathbf{r},t) \\ &= \left(\nabla^2 + k^{(2)2}\right) \mathbf{E}^{(2)}(\mathbf{r},t) \end{aligned} \tag{A.7}$$

therefore, we could derive useful SH wave propagation equation

$$\left(\nabla^2 + k^{(2)2}\right) \mathbf{E}^{(2)}(\mathbf{r},t) = \mu \frac{\partial^2 \mathbf{P}^{(2)}(\mathbf{r},t)}{\partial t^2} \tag{A.8}$$

where SH wave vector $k^{(2)}$ is

$$k^{(2)} = n^{(2)} \frac{2\omega}{c} \tag{A.9}$$

where $n^{(2)}$ is refractive index at SH frequency defined as

$$n^{(2)} = \mu\varepsilon \tag{A.10}$$

and speed of SH wave in the medium v is

$$v = \frac{c}{n} \tag{A.11}$$

Now, we evaluate the laser beam propagation in direction z only, hence propagation equation of SH wave from Equation A.8 could be reduced to

$$\left(\frac{\partial^2}{\partial z^2} + k^{(2)2}\right) \mathbf{E}^{(2)}(z,t) = \mu \frac{\partial^2 \mathbf{P}^{(2)}(z,t)}{\partial t^2} \tag{A.12}$$

In multi-layer photonic crystal, the scalar propagation equation for i-th layer could be represented with subscript i. This is the equation we use in chapter 3.

$$\left(\frac{\partial^2}{\partial z^2}+k_i^{(2)2}\right)E_i^{(2)}(z,t)=\mu\frac{\partial^2 P_i^{(2)}(z,t)}{\partial t^2} \tag{A.13}$$

Taking Fourier transform for Equation A.12, wave propagation equation in frequency domain could be written as

$$\left(\frac{\partial^2}{\partial z^2}+k_i^{(2)2}\right)E_i^{(2)}=-\mu\omega^2 P_i^{(2)} \tag{A.14}$$

because Forurier transform $\frac{\partial^2}{\partial t^2}\rightarrow(i\omega)^2$. This Equation A.14 is used in chapter 4.

A.2 Derivation of Coupled Equation

Consider laser beam with slowly varying field amplitude of total field

$$\tilde{E}_i(z,t)=\tilde{A}_i(z)\,e^{i\left(k^{(1)}z-\omega t\right)}+\tilde{B}_i(z)\,e^{i\left(k^{(2)}z-2\omega t\right)}+c.c.$$

where $\tilde{A}_i$ and $\tilde{B}_i$ are complex amplitudes of FF and SH waves respectively, we also write wave vector of FF $k^{(1)}$ and SH $k^{(2)}$ as

$$\begin{aligned}k^{(1)} &= n^{(1)}(\omega)\frac{\omega}{c}\\ k^{(2)} &= n^{(2)}(2\omega)\frac{2\omega}{c}\end{aligned}$$

now we substitute $\tilde{E}_i$ into wave propagation equation

$$\nabla^2\tilde{E}_i-\mu\varepsilon\frac{\partial^2\tilde{E}_i}{\partial t^2}=\mu\frac{\partial^2\tilde{P}^{(2)}}{\partial t^2} \tag{A.15}$$

and write nonlinear polarization

$$\begin{aligned}\tilde{P}^{(2)} &= \sum_{j,k=x,y,z}\chi_{ijk}^{(2)}\tilde{E}_j\tilde{E}_k \qquad\qquad (A.16)\\ &= \chi_{ixx}^{(2)}\tilde{E}_x\tilde{E}_x+\chi_{ixy}^{(2)}\tilde{E}_x\tilde{E}_y+\chi_{ixz}^{(2)}\tilde{E}_xE_z\\ &\quad+\chi_{iyy}^{(2)}\tilde{E}_y\tilde{E}_y+\chi_{iyx}^{(2)}\tilde{E}_y\tilde{E}_x+\chi_{iyz}^{(2)}\tilde{E}_y\tilde{E}_z\\ &\quad+\chi_{izz}^{(2)}\tilde{E}_z\tilde{E}_z+\chi_{izx}^{(2)}\tilde{E}_z\tilde{E}_x+\chi_{izy}^{(2)}\tilde{E}_z\tilde{E}_y\end{aligned}$$

also

$$E_x = \tilde{A}_xe^{i\left(k^{(1)}z-\omega t\right)}+\tilde{B}_xe^{i\left(k^{(2)}z-2\omega t\right)}+cc \tag{A.17}$$

$$E_y = \tilde{A}_ye^{i\left(k^{(1)}z-\omega t\right)}+\tilde{B}_ye^{i\left(k^{(2)}z-2\omega t\right)}+cc \tag{A.18}$$

$$E_z = \tilde{A}_ze^{i\left(k^{(1)}z-\omega t\right)}+\tilde{B}_ze^{i\left(k^{(2)}z-2\omega t\right)}+cc \tag{A.19}$$

Now we evaluate

$$\chi^{(2)}_{ixx}\tilde{E}_x\tilde{E}_x = \chi^{(2)}_{ixx}\left\{\begin{array}{c}\left(\tilde{A}_x e^{i\left(k^{(1)}z-\omega t\right)}+\tilde{B}_x e^{i\left(k^{(2)}z-2\omega t\right)}\right)\\ +\left(\tilde{A}^*_x e^{-i\left(k^{(1)}z-\omega t\right)}+\tilde{B}^*_x e^{-i\left(k^{(2)}z-2\omega t\right)}\right)\end{array}\right\}^2 \tag{A.20}$$

$$= \chi^{(2)}_{ixx}\left\{\begin{array}{c}\tilde{A}^2_x e^{2ik^{(1)}z-2i\omega t}+\tilde{A}^{*2}_x e^{-i2k^{(1)}z+2i\omega t}\\ +2\tilde{A}_x\tilde{B}^*_x e^{i\left(k^{(1)}-k^{(2)}\right)z+i\omega t}+2\tilde{B}_x\tilde{A}^*_x e^{i\left(k^{(2)}-k^{(1)}\right)z-i\omega t}\\ +2\tilde{A}_x\tilde{B}_x e^{i\left(k^{(1)}+k^{(2)}\right)z-3i\omega t}+2\tilde{A}^*_x\tilde{B}^*_x e^{-i\left(k^{(1)}+k^{(2)}\right)+3i\omega t}\\ +\tilde{B}^2_x e^{2ik^{(2)}z-4i\omega t}+\tilde{B}^{*2}_x e^{-i2k^{(2)}z+4i\omega t}\\ +2\tilde{A}_x\tilde{A}^*_x+2\tilde{B}_x\tilde{B}^*_x\end{array}\right\}$$

hence, we could write

$$\chi^{(2)}_{iyy}\tilde{E}_y\tilde{E}_y = \chi^{(2)}_{iyy}\left\{\begin{array}{c}\tilde{A}^2_y e^{2ik^{(1)}z-2i\omega t}+\tilde{A}^{*2}_y e^{-i2k^{(1)}z+2i\omega t}\\ +2\tilde{A}_y\tilde{B}^*_y e^{i\left(k^{(1)}-k^{(2)}\right)z+i\omega t}+2\tilde{B}_y\tilde{A}^*_y e^{i\left(k^{(2)}-k^{(1)}\right)z-i\omega t}\\ +2\tilde{A}_y\tilde{B}_y e^{i\left(k^{(1)}+k^{(2)}\right)z-3i\omega t}+2\tilde{A}^*_y\tilde{B}^*_y e^{-i\left(k^{(1)}+k^{(2)}\right)+3i\omega t}\\ +\tilde{B}^2_y e^{2ik^{(2)}z-4i\omega t}+\tilde{B}^{*2}_y e^{-i2k^{(2)}z+4i\omega t}\\ +2\tilde{A}_y\tilde{A}^*_y+2\tilde{B}_y\tilde{B}^*_y\end{array}\right\} \tag{A.21}$$

$$\chi^{(2)}_{izz}\tilde{E}_z\tilde{E}_z = \chi^{(2)}_{izz}\left\{\begin{array}{c}\tilde{A}^2_z e^{2ik^{(1)}z-2i\omega t}+\tilde{A}^{*2}_z e^{-i2k^{(1)}z+2i\omega t}\\ +2\tilde{A}_z\tilde{B}^*_z e^{i\left(k^{(1)}-k^{(2)}\right)z+i\omega t}+2\tilde{B}_z\tilde{A}^*_z e^{i\left(k^{(2)}-k^{(1)}\right)z-i\omega t}\\ +2\tilde{A}_z\tilde{B}_z e^{i\left(k^{(1)}+k^{(2)}\right)z-3i\omega t}+2\tilde{A}^*_z\tilde{B}^*_z e^{-i\left(k^{(1)}+k^{(2)}\right)+3i\omega t}\\ +\tilde{B}^2_z e^{2ik^{(2)}z-4i\omega t}+\tilde{B}^{*2}_z e^{-i2k^{(2)}z+4i\omega t}\\ +2\tilde{A}_z\tilde{A}^*_z+2\tilde{B}_z\tilde{B}^*_z\end{array}\right\} \tag{A.22}$$

$$\chi^{(2)}_{ixy}\tilde{E}_x\tilde{E}_y = \chi^{(2)}_{ixy}\left\{\begin{array}{c}\tilde{A}_x\tilde{A}_y e^{i2k^{(1)}z-i2\omega t}+\tilde{A}^*_x\tilde{A}^*_y e^{-i2k^{(1)}z+2i\omega t}\\ +\left(\tilde{A}_x\tilde{B}_y+\tilde{B}_x\tilde{A}_y\right)e^{i\left(k^{(2)}+k^{(1)}\right)z-3i\omega t}\\ +\left(\tilde{A}^*_x\tilde{B}^*_y+\tilde{B}^*_x\tilde{A}^*_y\right)e^{-i\left(k^{(2)}+k^{(1)}\right)z+3i\omega t}\\ +\tilde{A}_x\tilde{B}^*_y e^{i\left(k^{(1)}-k^{(2)}\right)z+i\omega t}\\ +\left(\tilde{A}^*_x\tilde{B}_y+\tilde{B}_x\tilde{A}^*_y\right)e^{i\left(k^{(2)}-k^{(1)}\right)z-i\omega t}\\ +\tilde{B}_x\tilde{B}_y e^{i2k^{(2)}z-4i\omega t}+\tilde{B}^*_x\tilde{B}^*_y e^{-i2k^{(2)}z+4i\omega t}\\ +\tilde{A}_x\tilde{A}^*_y+\tilde{A}^*_x\tilde{A}_y+\tilde{B}^*_x\tilde{B}_y e^{i\left(k^{(2)}z-k^{(2)}\right)z}+\tilde{B}^*_x\tilde{B}_y+\tilde{B}_x\tilde{B}^*_y\end{array}\right\} \tag{A.23}$$

$$\chi^{(2)}_{ixz}\tilde{E}_x\tilde{E}_z = \chi^{(2)}_{ixz}\left\{\begin{array}{c}\tilde{A}_x\tilde{A}_z e^{i2k^{(1)}z-i2\omega t}+\tilde{A}^*_x\tilde{A}^*_z e^{-i2k^{(1)}z+2i\omega t}\\ +\left(\tilde{A}_x\tilde{B}_z+\tilde{B}_x\tilde{A}_z\right)e^{i\left(k^{(2)}+k^{(1)}\right)z-3i\omega t}\\ +\left(\tilde{A}^*_x\tilde{B}^*_z+\tilde{B}^*_x\tilde{A}^*_z\right)e^{-i\left(k^{(2)}+k^{(1)}\right)z+3i\omega t}\\ +\tilde{A}_x\tilde{B}^*_z e^{i\left(k^{(1)}-k^{(2)}\right)z+i\omega t}\\ +\left(\tilde{A}^*_x\tilde{B}_z+\tilde{B}_x\tilde{A}^*_z\right)e^{i\left(k^{(2)}-k^{(1)}\right)z-i\omega t}\\ +\tilde{B}_x\tilde{B}_z e^{i2k^{(2)}z-4i\omega t}+\tilde{B}^*_x\tilde{B}^*_z e^{-i2k^{(2)}z+4i\omega t}\\ +\tilde{A}_x\tilde{A}^*_z+\tilde{A}^*_x\tilde{A}_z+\tilde{B}^*_x\tilde{B}_z e^{ik^{(2)}z-ik^{(2)}z}+\tilde{B}^*_x\tilde{B}_z+\tilde{B}_x\tilde{B}^*_z\end{array}\right\} \tag{A.24}$$

$$\chi^{(2)}_{iyx}\tilde{E}_y\tilde{E}_x = \chi^{(2)}_{iyx}\left\{\begin{array}{c}\tilde{A}_y\tilde{A}_x e^{i2k^{(1)}z-i2\omega t}+\tilde{A}^*_y\tilde{A}^*_x e^{-i2k^{(1)}z+2i\omega t}\\ +\left(\tilde{A}_y\tilde{B}_x+\tilde{B}_y\tilde{A}_x\right)e^{i\left(k^{(2)}+k^{(1)}\right)z-3i\omega t}\\ +\left(\tilde{A}^*_y\tilde{B}^*_x+\tilde{B}^*_y\tilde{A}^*_x\right)e^{-i\left(k^{(2)}+k^{(1)}\right)z+3i\omega t}\\ +\tilde{A}_y\tilde{B}^*_x e^{i\left(k^{(1)}-k^{(2)}\right)z+i\omega t}\\ +\left(\tilde{A}^*_y\tilde{B}_x+\tilde{B}_y\tilde{A}^*_x\right)e^{i\left(k^{(2)}-k^{(1)}\right)z-i\omega t}\\ +\tilde{B}_y\tilde{B}_x e^{i2k^{(2)}z-4i\omega t}+\tilde{B}^*_y\tilde{B}^*_x e^{-i2k^{(2)}z+4i\omega t}\\ +\tilde{A}_y\tilde{A}^*_x+\tilde{A}^*_y\tilde{A}_x+\tilde{B}^*_y\tilde{B}_x e^{ik^{(2)}z-ik^{(2)}z}+\tilde{B}^*_y\tilde{B}_x+\tilde{B}_y\tilde{B}^*_x\end{array}\right\} \tag{A.25}$$

$$\chi^{(2)}_{iyz}\tilde{E}_y\tilde{E}_z = \chi^{(2)}_{iyz}\left\{\begin{array}{c}\tilde{A}_y\tilde{A}_z e^{i2k^{(1)}z-i2\omega t}+\tilde{A}^*_y\tilde{A}^*_z e^{-i2k^{(1)}z+2i\omega t}\\ +\left(\tilde{A}_y\tilde{B}_z+\tilde{B}_y\tilde{A}_z\right)e^{i\left(k^{(2)}+k^{(1)}\right)z-3i\omega t}\\ +\left(\tilde{A}^*_y\tilde{B}^*_z+\tilde{B}^*_y\tilde{A}^*_z\right)e^{-i\left(k^{(2)}+k^{(1)}\right)z+3i\omega t}\\ +\tilde{A}_y\tilde{B}^*_z e^{i\left(k^{(1)}-k^{(2)}\right)z+i\omega t}\\ +\left(\tilde{A}^*_y\tilde{B}_z+\tilde{B}_y\tilde{A}^*_z\right)e^{i\left(k^{(2)}-k^{(1)}\right)z-i\omega t}\\ +\tilde{B}_y\tilde{B}_z e^{i2k^{(2)}z-4i\omega t}+\tilde{B}^*_y\tilde{B}^*_z e^{-i2k^{(2)}z+4i\omega t}\\ +\tilde{A}_y\tilde{A}^*_z+\tilde{A}^*_y\tilde{A}_z+\tilde{B}^*_y\tilde{B}_z e^{ik^{(2)}z-ik^{(2)}z}+\tilde{B}^*_y\tilde{B}_z+\tilde{B}_y\tilde{B}^*_z\end{array}\right\} \tag{A.26}$$

$$\chi^{(2)}_{izx}\tilde{E}_z\tilde{E}_x = \chi^{(2)}_{izx}\left\{\begin{array}{c}\tilde{A}_z\tilde{A}_x e^{i2k^{(1)}z-i2\omega t}+\tilde{A}^*_z\tilde{A}^*_x e^{-i2k^{(1)}z+2i\omega t}\\ +\left(\tilde{A}_z\tilde{B}_x+\tilde{B}_z\tilde{A}_x\right)e^{i\left(k^{(2)}+k^{(1)}\right)z-3i\omega t}\\ +\left(\tilde{A}^*_z\tilde{B}^*_x+\tilde{B}^*_z\tilde{A}^*_x\right)e^{-i\left(k^{(2)}+k^{(1)}\right)z+3i\omega t}\\ +\tilde{A}_z\tilde{B}^*_x e^{i\left(k^{(1)}-k^{(2)}\right)z+i\omega t}\\ +\left(\tilde{A}^*_z\tilde{B}_x+\tilde{B}_z\tilde{A}^*_x\right)e^{i\left(k^{(2)}-k^{(1)}\right)z-i\omega t}\\ +\tilde{B}_z\tilde{B}_x e^{i2k^{(2)}z-4i\omega t}+\tilde{B}^*_z\tilde{B}^*_x e^{-i2k^{(2)}z+4i\omega t}\\ +\tilde{A}_z\tilde{A}^*_x+\tilde{A}^*_z\tilde{A}_x+\tilde{B}^*_z\tilde{B}_x e^{ik^{(2)}z-ik^{(2)}z}+\tilde{B}^*_z\tilde{B}_x+\tilde{B}_z\tilde{B}^*_x\end{array}\right\} \tag{A.27}$$

$$\chi^{(2)}_{izy}\tilde{E}_z\tilde{E}_y = \chi^{(2)}_{izy}\left\{\begin{array}{c} \tilde{A}_z\tilde{A}_y e^{i2k^{(1)}z-i2\omega t} + \tilde{A}^*_z\tilde{A}^*_y e^{-i2k^{(1)}z+2i\omega t} \\ +\left(\tilde{A}_z\tilde{B}_y + \tilde{B}_z\tilde{A}_y\right)e^{i\left(k^{(2)}+k^{(1)}\right)z-3i\omega t} \\ +\left(\tilde{A}^*_z\tilde{B}^*_y + \tilde{B}^*_z\tilde{A}^*_y\right)e^{-i\left(k^{(2)}+k^{(1)}\right)z+3i\omega t} \\ +\tilde{A}_z\tilde{B}^*_y e^{i\left(k^{(1)}-k^{(2)}\right)z+i\omega t} \\ +\left(\tilde{A}^*_z\tilde{B}_y + \tilde{B}_z\tilde{A}^*_y\right)e^{i\left(k^{(2)}-k^{(1)}\right)z-i\omega t} \\ +\tilde{B}_z\tilde{B}_y e^{i2k^{(2)}z-4i\omega t} + \tilde{B}^*_z\tilde{B}^*_y e^{-i2k^{(2)}z+4i\omega t} \\ +\tilde{A}_z\tilde{A}^*_y + \tilde{A}^*_z\tilde{A}_y + \tilde{B}^*_z\tilde{B}_y e^{ik^{(2)}z-ik^{(2)}z} + \tilde{B}^*_z\tilde{B}_y + \tilde{B}_z\tilde{B}^*_y \end{array}\right\} \tag{A.28}$$

Hence,

$$\frac{\partial^2\tilde{P}^{(2)}}{\partial t^2} = \frac{\partial^2}{\partial t^2}\left\{\begin{array}{c} \chi^{(2)}_{ixx}\tilde{E}_x\tilde{E}_x + \chi^{(2)}_{ixy}\tilde{E}_x\tilde{E}_y \\ +\chi^{(2)}_{ixz}\tilde{E}_xE_z + \chi^{(2)}_{iyy}\tilde{E}_y\tilde{E}_y \\ +\chi^{(2)}_{iyx}\tilde{E}_y\tilde{E}_x + \chi^{(2)}_{iyz}\tilde{E}_y\tilde{E}_z \\ +\chi^{(2)}_{izz}\tilde{E}_z\tilde{E}_z + \chi^{(2)}_{izx}\tilde{E}_z\tilde{E}_x \\ +\chi^{(2)}_{izy}\tilde{E}_z\tilde{E}_y \end{array}\right\} \tag{A.29}$$

now we need to find

$$\frac{\partial^2}{\partial t^2}\chi^{(2)}_{ixx}\tilde{E}_x\tilde{E}_x = \chi^{(2)}_{ixx}\frac{\partial^2}{\partial t^2}\left\{\begin{array}{c} \tilde{A}^2_x e^{2ik^{(1)}z-2i\omega t} + \tilde{A}^{*2}_x e^{-i2k^{(1)}z+2i\omega t} \\ +2\tilde{A}_x\tilde{B}^*_x e^{i\left(k^{(1)}-k^{(2)}\right)z+i\omega t} \\ +2\tilde{B}_x\tilde{A}^*_x e^{i\left(k^{(2)}-k^{(1)}\right)z-i\omega t} \\ +2\tilde{A}_x\tilde{B}_x e^{i\left(k^{(1)}+k^{(2)}\right)z-3i\omega t} \\ +2\tilde{A}^*_x\tilde{B}^*_x e^{-i\left(k^{(1)}+k^{(2)}\right)+3i\omega t} \\ +\tilde{B}^2_x e^{2ik^{(2)}z-4i\omega t} + \tilde{B}^{*2}_x e^{-i2k^{(2)}z+4i\omega t} \\ +2\tilde{A}_x\tilde{A}^*_x + 2\tilde{B}_x\tilde{B}^*_x \end{array}\right\} \tag{A.30}$$

firstly, find

$$\begin{aligned} \frac{\partial^2}{\partial t^2}\tilde{A}^2_x e^{2ik^{(1)}z-2i\omega t} &= \tilde{A}^2_x e^{2ik^{(1)}z}\frac{\partial^2}{\partial t^2}e^{-2i\omega t} \\ &= -4\omega^2\tilde{A}^2_x e^{2ik^{(1)}z}e^{-2i\omega t} \end{aligned} \tag{A.31}$$

therefore,

$$\frac{\partial^2}{\partial t^2}\tilde{A}^{*2}_x e^{-i2k^{(1)}z+2i\omega t} = -4\omega^2\tilde{A}^{*2}_x e^{-i2k^{(1)}z}e^{2i\omega t} \tag{A.32}$$

$$\frac{\partial^2}{\partial t^2}2\tilde{A}_x\tilde{B}^*_x e^{i\left(k^{(1)}-k^{(2)}\right)z+i\omega t} = -2\omega^2\tilde{A}_x\tilde{B}^*_x e^{i\left(k^{(1)}-k^{(2)}\right)z}e^{i\omega t} \tag{A.33}$$

$$\frac{\partial^2}{\partial t^2} 2\tilde{B}_x \tilde{A}_x^* e^{i\left(k^{(2)}-k^{(1)}\right)z-i\omega t} = -2\omega^2 \tilde{B}_x \tilde{A}_x^* e^{i\left(k^{(2)}-k^{(1)}\right)z} e^{-i\omega t} \tag{A.34}$$

$$\frac{\partial^2}{\partial t^2} 2\tilde{A}_x \tilde{B}_x e^{i\left(k^{(1)}+k^{(2)}\right)z-3i\omega t} = -18\omega^2 \tilde{A}_x \tilde{B}_x e^{i\left(k^{(1)}+k^{(2)}\right)z} e^{-3i\omega t} \tag{A.35}$$

$$\frac{\partial^2}{\partial t^2} 2\tilde{A}_x^* \tilde{B}_x^* e^{-i\left(k^{(1)}+k^{(2)}\right)+3i\omega t} = -18\omega^2 \tilde{A}_x^* \tilde{B}_x^* e^{-i\left(k^{(1)}+k^{(2)}\right)} e^{3i\omega t} \tag{A.36}$$

$$\frac{\partial^2}{\partial t^2} \tilde{B}_x^2 e^{2ik^{(2)}z-4i\omega t} = -16\omega^2 \tilde{B}_x^2 e^{2ik^{(2)}z} e^{-4i\omega t} \tag{A.37}$$

$$\frac{\partial^2}{\partial t^2} \tilde{B}_x^{*2} e^{-i2k^{(2)}z+4i\omega t} = -16\omega^2 \tilde{B}_x^{*2} e^{-i2k^{(2)}z} e^{4i\omega t} \tag{A.38}$$

hence, substitute Equations A.31 to A.38 into Equation A.30, we have

$$\frac{\partial^2}{\partial t^2} \chi_{ixx}^{(2)} \tilde{E}_x \tilde{E}_x = \chi_{ixx}^{(2)} \left\{ \begin{array}{c} -4\omega^2 \left(\tilde{A}_x^2 e^{2ik^{(1)}z} e^{-2i\omega t} + \tilde{A}_x^{*2} e^{-i2k^{(1)}z} e^{2i\omega t} \right) \\ -2\omega^2 \left(\begin{array}{c} \tilde{A}_x \tilde{B}_x^* e^{i\left(k^{(1)}-k^{(2)}\right)z} e^{i\omega t} \\ +\tilde{B}_x \tilde{A}_x^* e^{i\left(k^{(2)}-k^{(1)}\right)z} e^{-i\omega t} \end{array} \right) \\ -18\omega^2 \left(\begin{array}{c} \tilde{A}_x \tilde{B}_x e^{i\left(k^{(1)}+k^{(2)}\right)z} e^{-3i\omega t} \\ +\tilde{A}_x^* \tilde{B}_x^* e^{-i\left(k^{(1)}+k^{(2)}\right)} e^{3i\omega t} \end{array} \right) \\ -16\omega^2 \left(\tilde{B}_x^2 e^{2ik^{(2)}z} e^{-4i\omega t} + \tilde{B}_x^{*2} e^{-i2k^{(2)}z} e^{4i\omega t} \right) \end{array} \right\} \tag{A.39}$$

subsequently, we can write

$$\frac{\partial^2}{\partial t^2} \chi_{iyy}^{(2)} \tilde{E}_y \tilde{E}_y = \chi_{iyy}^{(2)} \left\{ \begin{array}{c} -4\omega^2 \left(\tilde{A}_y^2 e^{2ik^{(1)}z} e^{-2i\omega t} + \tilde{A}_y^{*2} e^{-i2k^{(1)}z} e^{2i\omega t} \right) \\ -2\omega^2 \left(\begin{array}{c} \tilde{A}_y \tilde{B}_y^* e^{i\left(k^{(1)}-k^{(2)}\right)z} e^{i\omega t} \\ +\tilde{B}_y \tilde{A}_y^* e^{i\left(k^{(2)}-k^{(1)}\right)z} e^{-i\omega t} \end{array} \right) \\ -18\omega^2 \left(\begin{array}{c} \tilde{A}_y \tilde{B}_y e^{i\left(k^{(1)}+k^{(2)}\right)z} e^{-3i\omega t} \\ +\tilde{A}_y^* \tilde{B}_y^* e^{-i\left(k^{(1)}+k^{(2)}\right)} e^{3i\omega t} \end{array} \right) \\ -16\omega^2 \left(\tilde{B}_y^2 e^{2ik^{(2)}z} e^{-4i\omega t} + \tilde{B}_y^{*2} e^{-i2k^{(2)}z} e^{4i\omega t} \right) \end{array} \right\} \tag{A.40}$$

$$\frac{\partial^2}{\partial t^2}\chi^{(2)}_{izz}\tilde{E}_z\tilde{E}_z = \chi^{(2)}_{izz}\left\{\begin{array}{c} -4\omega^2\left(\tilde{A}_z^2 e^{2ik^{(1)}z}e^{-2i\omega t} + \tilde{A}_z^{*2}e^{-i2k^{(1)}z}e^{2i\omega t}\right) \\ -2\omega^2\left(\begin{array}{c}\tilde{A}_z\tilde{B}_z^* e^{i\left(k^{(1)}-k^{(2)}\right)z}e^{i\omega t} \\ +\tilde{B}_z\tilde{A}_z^* e^{i\left(k^{(2)}-k^{(1)}\right)z}e^{-i\omega t}\end{array}\right) \\ -18\omega^2\left(\begin{array}{c}\tilde{A}_z\tilde{B}_z e^{i\left(k^{(1)}+k^{(2)}\right)z}e^{-3i\omega t} \\ +\tilde{A}_z^*\tilde{B}_z^* e^{-i\left(k^{(1)}+k^{(2)}\right)}e^{3i\omega t}\end{array}\right) \\ -16\omega^2\left(\tilde{B}_z^2 e^{2ik^{(2)}z}e^{-4i\omega t} + \tilde{B}_z^{*2}e^{-i2k^{(2)}z}e^{4i\omega t}\right)\end{array}\right\} \tag{A.41}$$

$$\frac{\partial^2}{\partial t^2}\chi^{(2)}_{ixz}\tilde{E}_x\tilde{E}_z = \chi^{(2)}_{ixz}\left\{\begin{array}{c} -4\omega^2\left(\tilde{A}_x\tilde{A}_z e^{i2k^{(1)}z}e^{-i2\omega t} + \tilde{A}_x^*\tilde{A}_z^* e^{-i2k^{(1)}z}e^{2i\omega t}\right) \\ -9\omega^2\left(\begin{array}{c}\left(\tilde{A}_x\tilde{B}_z + \tilde{B}_x\tilde{A}_z\right)e^{i\left(k^{(2)}+k^{(1)}\right)z}e^{-i3\omega t} \\ +\left(\tilde{A}_x^*\tilde{B}_z^* + \tilde{B}_x^*\tilde{A}_z^*\right)e^{-i\left(k^{(2)}+k^{(1)}\right)z}e^{3i\omega t}\end{array}\right) \\ -\omega^2\left(\begin{array}{c}\tilde{A}_x\tilde{B}_z^* e^{i\left(k^{(1)}-k^{(2)}\right)z}e^{i\omega t} \\ +\left(\tilde{A}_x^*\tilde{B}_z + \tilde{B}_x\tilde{A}_z^*\right)e^{i\left(k^{(2)}-k^{(1)}\right)z}e^{-i\omega t}\end{array}\right) \\ -16\omega^2\left(\tilde{B}_x\tilde{B}_z e^{i2k^{(2)}z}e^{-4i\omega t} + \tilde{B}_x^*\tilde{B}_z^* e^{-i2k^{(2)}z}e^{4i\omega t}\right)\end{array}\right\} \tag{A.42}$$

$$\frac{\partial^2}{\partial t^2}\chi^{(2)}_{ixy}\tilde{E}_x\tilde{E}_y = \chi^{(2)}_{ixy}\left\{\begin{array}{c} -4\omega^2\left(\tilde{A}_x\tilde{A}_y e^{i2k^{(1)}z}e^{-i2\omega t} + \tilde{A}_x^*\tilde{A}_y^* e^{-i2k^{(1)}z}e^{2i\omega t}\right) \\ -9\omega^2\left(\begin{array}{c}\left(\tilde{A}_x\tilde{B}_y + \tilde{B}_x\tilde{A}_y\right)e^{i\left(k^{(2)}+k^{(1)}\right)z}e^{-i3\omega t} \\ +\left(\tilde{A}_x^*\tilde{B}_y^* + \tilde{B}_x\tilde{A}_y\right)e^{-i\left(k^{(2)}+k^{(1)}\right)z}e^{3i\omega t}\end{array}\right) \\ -\omega^2\left(\begin{array}{c}\tilde{A}_x\tilde{B}_y^* e^{i\left(k^{(1)}-k^{(2)}\right)z}e^{i\omega t} \\ +\left(\tilde{A}_x^*\tilde{B}_y + \tilde{B}_x\tilde{A}_y^*\right)e^{i\left(k^{(2)}-k^{(1)}\right)z}e^{-i\omega t}\end{array}\right) \\ -16\omega^2\left(\tilde{B}_x\tilde{B}_y e^{i2k^{(2)}z}e^{-4i\omega t} + \tilde{B}_x^*\tilde{B}_y^* e^{-i2k^{(2)}z}e^{4i\omega t}\right)\end{array}\right\} \tag{A.43}$$

$$\frac{\partial^2}{\partial t^2}\chi^{(2)}_{iyz}\tilde{E}_y\tilde{E}_z = \chi^{(2)}_{iyz}\left\{\begin{array}{c} -4\omega^2\left(\tilde{A}_y\tilde{A}_z e^{i2k^{(1)}z}e^{-i2\omega t} + \tilde{A}_y^*\tilde{A}_z^* e^{-i2k^{(1)}z}e^{2i\omega t}\right) \\ -9\omega^2\left(\begin{array}{c}\left(\tilde{A}_y\tilde{B}_z + \tilde{B}_y\tilde{A}_z\right)e^{i\left(k^{(2)}+k^{(1)}\right)z}e^{-i3\omega t} \\ +\left(\tilde{A}_y^*\tilde{B}_z^* + \tilde{B}_y^*\tilde{A}_z^*\right)e^{-i\left(k^{(2)}+k^{(1)}\right)z}e^{3i\omega t}\end{array}\right) \\ -\omega^2\left(\begin{array}{c}\tilde{A}_y\tilde{B}_z^* e^{i\left(k^{(1)}-k^{(2)}\right)z}e^{i\omega t} \\ +\left(\tilde{A}_y^*\tilde{B}_z + \tilde{B}_y\tilde{A}_z^*\right)e^{i\left(k^{(2)}-k^{(1)}\right)z}e^{-i\omega t}\end{array}\right) \\ -16\omega^2\left(\tilde{B}_y\tilde{B}_z e^{i2k^{(2)}z}e^{-4i\omega t} + \tilde{B}_y^*\tilde{B}_z^* e^{-i2k^{(2)}z}e^{4i\omega t}\right)\end{array}\right\} \tag{A.44}$$

$$\frac{\partial^2}{\partial t^2}\chi^{(2)}_{iyx}\tilde{E}_y\tilde{E}_x = \chi^{(2)}_{iyx}\left\{\begin{array}{c} -4\omega^2\left(\tilde{A}_y\tilde{A}_x e^{i2k^{(1)}z}e^{-i2\omega t}+\tilde{A}^*_y\tilde{A}^*_x e^{-i2k^{(1)}z}e^{2i\omega t}\right) \\ -9\omega^2\left(\begin{array}{c}\left(\tilde{A}_y\tilde{B}_x+\tilde{B}_y\tilde{A}_x\right)e^{i\left(k^{(2)}+k^{(1)}\right)z}e^{-i3\omega t} \\ +\left(\tilde{A}^*_y\tilde{B}^*_x+\tilde{B}^*_y\tilde{A}^*_x\right)e^{-i\left(k^{(2)}+k^{(1)}\right)z}e^{3i\omega t}\end{array}\right) \\ -\omega^2\left(\begin{array}{c}\tilde{A}_y\tilde{B}^*_x e^{i\left(k^{(1)}-k^{(2)}\right)z}e^{i\omega t} \\ +\left(\tilde{A}^*_y\tilde{B}_x+\tilde{B}_y\tilde{A}^*_x\right)e^{i\left(k^{(2)}-k^{(1)}\right)z}e^{-i\omega t}\end{array}\right) \\ -16\omega^2\left(\tilde{B}_y\tilde{B}_x e^{i2k^{(2)}z}e^{-4i\omega t}+\tilde{B}^*_y\tilde{B}^*_x e^{-i2k^{(2)}z}e^{4i\omega t}\right)\end{array}\right\} \tag{A.45}$$

$$\frac{\partial^2}{\partial t^2}\chi^{(2)}_{izx}\tilde{E}_z\tilde{E}_x = \chi^{(2)}_{izx}\left\{\begin{array}{c} -4\omega^2\left(\tilde{A}_z\tilde{A}_x e^{i2k^{(1)}z}e^{-i2\omega t}+\tilde{A}^*_z\tilde{A}^*_x e^{-i2k^{(1)}z}e^{2i\omega t}\right) \\ -9\omega^2\left(\begin{array}{c}\left(\tilde{A}_z\tilde{B}_x+\tilde{B}_y\tilde{A}_x\right)e^{i\left(k^{(2)}+k^{(1)}\right)z}e^{-i3\omega t} \\ +\left(\tilde{A}^*_z\tilde{B}^*_x+\tilde{B}^*_z\tilde{A}^*_x\right)e^{-i\left(k^{(2)}+k^{(1)}\right)z}e^{3i\omega t}\end{array}\right) \\ -\omega^2\left(\begin{array}{c}\tilde{A}_z\tilde{B}^*_x e^{i\left(k^{(1)}-k^{(2)}\right)z}e^{i\omega t} \\ +\left(\tilde{A}^*_z\tilde{B}_x+\tilde{B}_z\tilde{A}^*_x\right)e^{i\left(k^{(2)}-k^{(1)}\right)z}e^{-i\omega t}\end{array}\right) \\ -16\omega^2\left(\tilde{B}_z\tilde{B}_x e^{i2k^{(2)}z}e^{-4i\omega t}+\tilde{B}^*_z\tilde{B}^*_x e^{-i2k^{(2)}z}e^{4i\omega t}\right)\end{array}\right\} \tag{A.46}$$

$$\frac{\partial^2}{\partial t^2}\chi^{(2)}_{izy}\tilde{E}_z\tilde{E}_y = \chi^{(2)}_{izy}\left\{\begin{array}{c} -4\omega^2\left(\tilde{A}_z\tilde{A}_y e^{i2k^{(1)}z}e^{-i2\omega t}+\tilde{A}^*_z\tilde{A}^*_y e^{-i2k^{(1)}z}e^{2i\omega t}\right) \\ -9\omega^2\left(\begin{array}{c}\left(\tilde{A}_z\tilde{B}_y+\tilde{B}_y\tilde{A}_y\right)e^{i\left(k^{(2)}+k^{(1)}\right)z}e^{-i3\omega t} \\ +\left(\tilde{A}^*_z\tilde{B}^*_y+\tilde{B}^*_z\tilde{A}^*_y\right)e^{-i\left(k^{(2)}+k^{(1)}\right)z}e^{3i\omega t}\end{array}\right) \\ -\omega^2\left(\begin{array}{c}\tilde{A}_z\tilde{B}^*_y e^{i\left(k^{(1)}-k^{(2)}\right)z}e^{i\omega t} \\ +\left(\tilde{A}^*_z\tilde{B}_y+\tilde{B}_z\tilde{A}^*_y\right)e^{i\left(k^{(2)}-k^{(1)}\right)z}e^{-i\omega t}\end{array}\right) \\ -16\omega^2\left(\tilde{B}_z\tilde{B}_y e^{i2k^{(2)}z}e^{-4i\omega t}+\tilde{B}^*_z\tilde{B}^*_y e^{-i2k^{(2)}z}e^{4i\omega t}\right)\end{array}\right\} \tag{A.47}$$

therefore, we have complete expansion of Equation A.29. now we have LHS of Equation A.15 as

$$
\begin{aligned}
\mu\frac{\partial^2\tilde{P}^{(2)}}{\partial t^2} \;=\;
&-4\omega^2\mu\left\{\begin{array}{c}
\chi^{(2)}_{ixx}\tilde{A}_x^2+\chi^{(2)}_{iyy}\tilde{A}_y^2+\chi^{(2)}_{izz}\tilde{A}_z^2\\
+\chi^{(2)}_{ixz}\tilde{A}_x\tilde{A}_z+\chi^{(2)}_{ixy}\tilde{A}_x\tilde{A}_y+\chi^{(2)}_{iyz}\tilde{A}_y\tilde{A}_z\\
+\chi^{(2)}_{iyx}\tilde{A}_y\tilde{A}_x+\chi^{(2)}_{izx}\tilde{A}_z\tilde{A}_x+\chi^{(2)}_{izy}\tilde{A}_z\tilde{A}_y
\end{array}\right\}e^{i2k^{(1)}z}e^{-i2\omega t} \qquad \text{(A.48)}\\
&-4\omega^2\mu\left\{\begin{array}{c}
\chi^{(2)}_{ixx}\tilde{A}_x^{*2}+\chi^{(2)}_{iyy}\tilde{A}_y^{*2}+\chi^{(2)}_{izz}\tilde{A}_z^{*2}\\
+\chi^{(2)}_{ixz}\tilde{A}_x^*\tilde{A}_z^*+\chi^{(2)}_{ixy}\tilde{A}_x^*\tilde{A}_y^*+\chi^{(2)}_{iyz}\tilde{A}_y^*\tilde{A}_z^*\\
+\chi^{(2)}_{iyx}\tilde{A}_y^*\tilde{A}_x^*+\chi^{(2)}_{izx}\tilde{A}_z^*\tilde{A}_x^*+\chi^{(2)}_{izy}\tilde{A}_z^*\tilde{A}_y^*
\end{array}\right\}e^{-i2k^{(1)}z}e^{2i\omega t}\\
&-\omega^2\mu\left\{\begin{array}{c}
2\chi^{(2)}_{ixx}\tilde{A}_x\tilde{B}_x^*+2\chi^{(2)}_{iyy}\tilde{A}_y\tilde{B}_y^*+2\chi^{(2)}_{izz}\tilde{A}_z\tilde{B}_z^*\\
+\chi^{(2)}_{ixz}\tilde{A}_x\tilde{B}_z^*+\chi^{(2)}_{ixy}\tilde{A}_x\tilde{B}_y^*+\chi^{(2)}_{iyz}\tilde{A}_y\tilde{B}_z^*\\
+\chi^{(2)}_{iyx}\tilde{A}_y\tilde{B}_x^*+\chi^{(2)}_{izx}\tilde{A}_z\tilde{B}_x^*+\chi^{(2)}_{izy}\tilde{A}_z\tilde{B}_y^*
\end{array}\right\}e^{i\left(k^{(1)}-k^{(2)}\right)z}e^{i\omega t}\\
&-\omega^2\mu\left\{\begin{array}{c}
2\chi^{(2)}_{ixx}\tilde{B}_x\tilde{A}_x^*+2\chi^{(2)}_{iyy}\tilde{B}_y\tilde{A}_y^*+2\chi^{(2)}_{izz}\tilde{B}_z\tilde{A}_z^*\\
+\chi^{(2)}_{ixz}\left(\tilde{A}_x^*\tilde{B}_z+\tilde{B}_x\tilde{A}_z^*\right)+\chi^{(2)}_{ixy}\left(\tilde{A}_x^*\tilde{B}_y+\tilde{B}_x\tilde{A}_y^*\right)\\
+\chi^{(2)}_{iyz}\left(\tilde{A}_y\tilde{B}_z+\tilde{B}_y\tilde{A}_z\right)+\chi^{(2)}_{iyx}\left(\tilde{A}_y^*\tilde{B}_x+\tilde{B}_y\tilde{A}_x^*\right)\\
+\chi^{(2)}_{izx}\left(\tilde{A}_z^*\tilde{B}_x+\tilde{B}_z\tilde{A}_x^*\right)+\chi^{(2)}_{izy}\left(\tilde{A}_z^*\tilde{B}_y+\tilde{B}_z\tilde{A}_y^*\right)
\end{array}\right\}e^{i\left(k^{(2)}-k^{(1)}\right)z}e^{-i\omega t}\\
&-9\omega^2\mu\left\{\begin{array}{c}
2\chi^{(2)}_{ixx}\tilde{A}_x\tilde{B}_x+2\tilde{A}\chi^{(2)}_{iyyy}\tilde{B}_y+2\chi^{(2)}_{izz}\tilde{A}_z\tilde{B}_z\\
+\chi^{(2)}_{ixz}\left(\tilde{A}_x\tilde{B}_z+\tilde{B}_x\tilde{A}_z\right)+\chi^{(2)}_{ixy}\left(\tilde{A}_x\tilde{B}_y+\tilde{B}_x\tilde{A}_y\right)\\
+\chi^{(2)}_{iyz}\left(\tilde{A}_y\tilde{B}_z+\tilde{B}_y\tilde{A}_z\right)+\chi^{(2)}_{iyx}\left(\tilde{A}_y\tilde{B}_x+\tilde{B}_y\tilde{A}_x\right)\\
+\chi^{(2)}_{izx}\left(\tilde{A}_z\tilde{B}_x+\tilde{B}_y\tilde{A}_x\right)+\chi^{(2)}_{izy}\left(\tilde{A}_z\tilde{B}_y+\tilde{B}_y\tilde{A}_y\right)
\end{array}\right\}e^{i\left(k^{(1)}+k^{(2)}\right)z}e^{-3i\omega t}\\
&-9\omega^2\mu\left\{\begin{array}{c}
2\chi^{(2)}_{ixx}\tilde{A}_x^*\tilde{B}_x^*+2\chi^{(2)}_{iyy}\tilde{A}_y^*\tilde{B}_y^*+2\chi^{(2)}_{izz}\tilde{A}_z^*\tilde{B}_z^*\\
+\chi^{(2)}_{ixz}\left(\tilde{A}_x^*\tilde{B}_z^*+\tilde{B}_x^*\tilde{A}_z^*\right)+\chi^{(2)}_{ixy}\left(\tilde{A}_x^*\tilde{B}_y^*+\tilde{B}_x^*\tilde{A}_y^*\right)\\
+\chi^{(2)}_{iyz}\left(\tilde{A}_y^*\tilde{B}_z^*+\tilde{B}_y^*\tilde{A}_z^*\right)+\chi^{(2)}_{iyx}\left(\tilde{A}_y^*\tilde{B}_x^*+\tilde{B}_y^*\tilde{A}_x^*\right)\\
+\chi^{(2)}_{izx}\left(\tilde{A}_z^*\tilde{B}_x^*+\tilde{B}_y^*\tilde{A}_x^*\right)+\chi^{(2)}_{izy}\left(\tilde{A}_z^*\tilde{B}_y^*+\tilde{B}_y^*\tilde{A}_y^*\right)
\end{array}\right\}e^{-i\left(k^{(1)}+k^{(2)}\right)}e^{3i\omega t}\\
&-16\omega^2\mu\left\{\begin{array}{c}
\chi^{(2)}_{ixx}\tilde{B}_x^2+\chi^{(2)}_{iyy}\tilde{B}_y^2+\chi^{(2)}_{izz}\tilde{B}_z^2\\
+\chi^{(2)}_{ixz}\tilde{B}_x\tilde{B}_z+\chi^{(2)}_{ixy}\tilde{B}_x\tilde{B}_y+\chi^{(2)}_{iyz}\tilde{B}_y\tilde{B}_z\\
+\chi^{(2)}_{iyx}\tilde{B}_y\tilde{B}_x+\chi^{(2)}_{izx}\tilde{B}_z\tilde{B}_x+\chi^{(2)}_{izy}\tilde{B}_z\tilde{B}_y
\end{array}\right\}e^{2ik^{(2)}z}e^{-4i\omega t}\\
&-16\omega^2\mu\left\{\begin{array}{c}
\chi^{(2)}_{ixx}\tilde{B}_x^{*2}+\chi^{(2)}_{iyy}\tilde{B}_y^{*2}+\chi^{(2)}_{izz}\tilde{B}_z^{*2}\\
+\chi^{(2)}_{ixz}\tilde{B}_x^*\tilde{B}_z^*+\chi^{(2)}_{ixy}\tilde{B}_x^*\tilde{B}_y^*+\chi^{(2)}_{iyz}\tilde{B}_y^*\tilde{B}_z^*\\
+\chi^{(2)}_{iyx}\tilde{B}_y^*\tilde{B}_x^*+\chi^{(2)}_{izx}\tilde{B}_z^*\tilde{B}_x^*+\chi^{(2)}_{izy}\tilde{B}_z^*\tilde{B}_y^*
\end{array}\right\}e^{-i2k^{(2)}z}e^{4i\omega t}
\end{aligned}
$$

Now we evaluate $\nabla^2\tilde{E}_i - \mu\varepsilon\frac{\partial^2\tilde{E}_i}{\partial t^2}$, here we consider the electromagnetic wave propagate only in direction z only, therefore $\nabla^2\tilde{E}_i$ is reduced to $\frac{\partial^2}{\partial z^2}\tilde{E}_i$

$$\frac{\partial^2}{\partial z^2}\tilde{E}_i = \frac{\partial^2}{\partial z^2}\begin{pmatrix} \tilde{A}_i e^{i\left(k^{(1)}z-\omega t\right)} + \tilde{A}_i^* e^{-i\left(k^{(1)}z-\omega t\right)} \\ +\tilde{B}_i e^{i\left(k^{(2)}z-2\omega t\right)} + \tilde{B}_i^* e^{-i\left(k^{(2)}z-2\omega t\right)} \end{pmatrix} \tag{A.49}$$

evaluate $\frac{\partial^2}{\partial z^2}\tilde{A}_i e^{i\left(k^{(1)}z-\omega t\right)}$,

$$\begin{aligned} \frac{\partial^2}{\partial z^2}\tilde{A}_i e^{i\left(k^{(1)}z-\omega t\right)} &= \frac{\partial^2}{\partial z^2}\tilde{A}_i e^{ik^{(1)}z}e^{-i\omega t} \\ &= e^{-i\omega t}\frac{\partial^2}{\partial z^2}\tilde{A}_i e^{ik^{(1)}z} \\ &= e^{-i\omega t}\frac{\partial}{\partial z}\frac{\partial}{\partial z}\tilde{A}_i e^{ik^{(1)}z} \\ &= e^{-i\omega t}\frac{\partial}{\partial z}\left(e^{ik^{(1)}z}\frac{\partial}{\partial z}\tilde{A}_i + \tilde{A}_i ik^{(1)}e^{ik^{(1)}z}\right) \\ &= e^{-i\omega t}\left(e^{ik^{(1)}z}\frac{\partial^2}{\partial z^2}\tilde{A}_i + 2ik^{(1)}e^{ik^{(1)}z}\frac{\partial}{\partial z}\tilde{A}_i - k^{(1)2}\tilde{A}_i e^{ik^{(1)}z}\right) \end{aligned} \tag{A.50}$$

using the same method, we have

$$\frac{\partial^2}{\partial z^2}\tilde{B}_i e^{i\left(k^{(2)}z-2\omega t\right)} = e^{-i2\omega t}\left(e^{ik^{(2)}z}\frac{\partial^2}{\partial z^2}\tilde{B}_i + 2ik^{(2)}e^{ik^{(2)}z}\frac{\partial}{\partial z}\tilde{B}_i - k^{(2)2}\tilde{B}_i e^{ik^{(2)}z}\right) \tag{A.51}$$

$$\frac{\partial^2}{\partial z^2}\tilde{A}_i^* e^{-i\left(k^{(1)}z-\omega t\right)} = e^{i\omega t}\left(e^{ik^{(1)}z}\frac{\partial^2}{\partial z^2}\tilde{A}_i^* + 2ik^{(1)}e^{ik^{(1)}z}\frac{\partial}{\partial z}\tilde{A}_i^* - \tilde{A}_i^* k^{(1)2}e^{ik^{(1)}z}\right) \tag{A.52}$$

$$\frac{\partial^2}{\partial z^2}\tilde{B}_i^* e^{-i\left(k^{(2)}z-2\omega t\right)} = e^{i2\omega t}\left(e^{ik^{(2)}z}\frac{\partial^2}{\partial z^2}\tilde{B}_i^* + 2ik^{(2)}e^{ik^{(2)}z}\frac{\partial}{\partial z}\tilde{B}_i^* - \tilde{B}_i^* k^{(2)2}e^{ik^{(2)}z}\right) \tag{A.53}$$

Hence, substitute Equations A.50 to A.53 into Equation A.49,

$$\begin{aligned} \frac{\partial^2}{\partial z^2}\tilde{E}_i &= e^{-i\omega t}\left(e^{ik^{(1)}z}\frac{\partial^2}{\partial z^2}\tilde{A}_i + 2ik^{(1)}e^{ik^{(1)}z}\frac{\partial}{\partial z}\tilde{A}_i - k^{(1)2}\tilde{A}_i e^{ik^{(1)}z}\right) \\ &\quad + e^{i\omega t}\left(e^{ik^{(1)}z}\frac{\partial^2}{\partial z^2}\tilde{A}_i^* + 2ik^{(1)}e^{ik^{(1)}z}\frac{\partial}{\partial z}\tilde{A}_i^* - \tilde{A}_i^* k^{(1)2}e^{ik^{(1)}z}\right) \\ &\quad + e^{-i2\omega t}\left(e^{ik^{(2)}z}\frac{\partial^2}{\partial z^2}\tilde{B}_i + 2ik^{(2)}e^{ik^{(2)}z}\frac{\partial}{\partial z}\tilde{B}_i - k^{(2)2}\tilde{B}_i e^{ik^{(2)}z}\right) \\ &\quad + e^{i2\omega t}\left(e^{ik^{(2)}z}\frac{\partial^2}{\partial z^2}\tilde{B}_i^* + 2ik^{(2)}e^{ik^{(2)}z}\frac{\partial}{\partial z}\tilde{B}_i^* - \tilde{B}_i^* k^{(2)2}e^{ik^{(2)}z}\right) \end{aligned} \tag{A.54}$$

now, we evaluate $\frac{\partial^2 \tilde{E}_i}{\partial t^2}$

$$\begin{aligned}
\frac{\partial^2 \tilde{E}_i}{\partial t^2} &= \frac{\partial^2}{\partial t^2}\begin{pmatrix} \tilde{A}_i e^{i\left(k^{(1)}z-\omega t\right)} + \tilde{A}_i^* e^{-i\left(k^{(1)}z-\omega t\right)} \\ +\tilde{B}_i e^{i\left(k^{(2)}z-2\omega t\right)} + \tilde{B}_i^* e^{-i\left(k^{(2)}z-2\omega t\right)} \end{pmatrix} \\
&= \tilde{A}_i e^{ik^{(1)}z}\frac{\partial^2}{\partial t^2}e^{-i\omega t} + \tilde{A}_i^* e^{-ik^{(1)}z}\frac{\partial^2}{\partial t^2}e^{i\omega t} \\
&\quad +\tilde{B}_i e^{ik^{(2)}z}\frac{\partial^2}{\partial t^2}e^{-2i\omega t} + \tilde{B}_i^* e^{-ik^{(2)}z}\frac{\partial^2}{\partial t^2}e^{2i\omega t} \\
&= -\omega^2\tilde{A}_i e^{ik^{(1)}z}e^{-i\omega t} - \omega^2\tilde{A}_i^* e^{-ik^{(1)}z}e^{i\omega t} \\
&\quad -4\omega^2\tilde{B}_i e^{ik^{(2)}z}e^{-2i\omega t} - 4\omega^2\tilde{B}_i^* e^{-ik^{(2)}z}e^{2i\omega t}
\end{aligned} \tag{A.55}$$

and $\mu\varepsilon\frac{\partial^2 \tilde{E}_i}{\partial t^2}$ becomes

$$\begin{aligned}
\mu\varepsilon\frac{\partial^2 \tilde{E}_i}{\partial t^2} &= -k^{(1)2}\tilde{A}_i e^{ik^{(1)}z}e^{-i\omega t} - k^{(1)2}\tilde{A}_i^* e^{-ik^{(1)}z}e^{i\omega t} \\
&\quad -k^{(2)2}\tilde{B}_i e^{ik^{(2)}z}e^{-2i\omega t} - k^{(2)2}\tilde{B}_i^* e^{-ik^{(2)}z}e^{2i\omega t}
\end{aligned} \tag{A.56}$$

where $k^{(1)}$ and $k^{(2)}$ are FF and SH wave vector

$$\mu\varepsilon\omega^2 = \frac{n^{(1)2}\omega^2}{c^2} = k^{(1)2} \tag{A.57}$$

$$\mu\varepsilon 4\omega^2 = \frac{n^{(2)2}4\omega^2}{c^2} = k^{(2)2} \tag{A.58}$$

finally, substitute Equations A.56 and A.55 into RHS of Equation A.15, we have

$$\begin{aligned}
\frac{\partial^2}{\partial z^2}\tilde{E}_i - \mu\varepsilon\frac{\partial^2 \tilde{E}_i}{\partial t^2} &= e^{-i\omega t}e^{ik^{(1)}z}\left(\frac{\partial^2}{\partial z^2}\tilde{A}_i + 2ik^{(1)}\frac{\partial}{\partial z}\tilde{A}_i - k^{(1)2}\tilde{A}_i\right) \\
&\quad +e^{i\omega t}e^{ik^{(1)}z}\left(\frac{\partial^2}{\partial z^2}\tilde{A}_i^* + 2ik^{(1)}\frac{\partial}{\partial z}\tilde{A}_i^* - \tilde{A}_i^* k^{(1)2}\right) \\
&\quad +e^{-i2\omega t}e^{ik^{(2)}z}\left(\frac{\partial^2}{\partial z^2}\tilde{B}_i + 2ik^{(2)}\frac{\partial}{\partial z}\tilde{B}_i - k^{(2)2}\tilde{B}_i\right) \\
&\quad +e^{i2\omega t}e^{ik^{(2)}z}\left(\frac{\partial^2}{\partial z^2}\tilde{B}_i^* + 2ik^{(2)}\frac{\partial}{\partial z}\tilde{B}_i^* - \tilde{B}_i^* k^{(2)2}\right) \\
&\quad +k^{(1)2}\tilde{A}_i e^{ik^{(1)}z}e^{-i\omega t} + k^{(1)2}\tilde{A}_i^* e^{-ik^{(1)}z}e^{i\omega t} \\
&\quad +k^{(2)2}\tilde{B}_i e^{ik^{(2)}z}e^{-2i\omega t} + k^{(2)2}\tilde{B}_i^* e^{-ik^{(2)}z}e^{2i\omega t} \\
&= e^{-i\omega t}e^{ik^{(1)}z}\left(\frac{\partial^2}{\partial z^2}\tilde{A}_i + 2ik^{(1)}\frac{\partial}{\partial z}\tilde{A}_i\right) \\
&\quad +e^{i\omega t}e^{ik^{(1)}z}\left(\frac{\partial^2}{\partial z^2}\tilde{A}_i^* + 2ik^{(1)}\frac{\partial}{\partial z}\tilde{A}_i^*\right) \\
&\quad +e^{-i2\omega t}e^{ik^{(2)}z}\left(\frac{\partial^2}{\partial z^2}\tilde{B}_i + 2ik^{(2)}\frac{\partial}{\partial z}\tilde{B}_i\right) \\
&\quad +e^{i2\omega t}e^{ik^{(2)}z}\left(\frac{\partial^2}{\partial z^2}\tilde{B}_i^* + 2ik^{(2)}\frac{\partial}{\partial z}\tilde{B}_i^*\right)
\end{aligned} \tag{A.59}$$

now we equate term with $e^{-i\omega t}$ for RHS and LHS of A.15, the first coupled equation

$$\left(\frac{\partial^2}{\partial z^2}\tilde{A}_i + 2ik^{(1)}\frac{\partial}{\partial z}\tilde{A}_i\right) = -\omega^2\mu \left\{ \begin{array}{c} 2\chi^{(2)}_{ixx}\tilde{B}_x\tilde{A}^*_x + 2\chi^{(2)}_{iyy}\tilde{B}_y\tilde{A}^*_y \\ +2\chi^{(2)}_{izz}\tilde{B}_z\tilde{A}^*_z \\ +\chi^{(2)}_{ixz}\left(\tilde{A}^*_x\tilde{B}_z + \tilde{B}_x\tilde{A}^*_z\right) \\ +\chi^{(2)}_{ixy}\left(\tilde{A}^*_x\tilde{B}_y + \tilde{B}_x\tilde{A}^*_y\right) \\ +\chi^{(2)}_{iyz}\left(\tilde{A}_y\tilde{B}_z + \tilde{B}_y\tilde{A}_z\right) \\ +\chi^{(2)}_{iyx}\left(\tilde{A}^*_y\tilde{B}_x + \tilde{B}_y\tilde{A}^*_x\right) \\ +\chi^{(2)}_{izx}\left(\tilde{A}^*_z\tilde{B}_x + \tilde{B}_z\tilde{A}^*_x\right) \\ +\chi^{(2)}_{izy}\left(\tilde{A}^*_z\tilde{B}_y + \tilde{B}_z\tilde{A}^*_y\right) \end{array} \right\} e^{i\Delta kz} \tag{A.60}$$

and equate term with $e^{-2i\omega t}$ for RHS and LHS, we have another coupled equation

$$\left(\frac{\partial^2}{\partial z^2}\tilde{B}_i + 2ik^{(2)}\frac{\partial}{\partial z}\tilde{B}_i\right) = -4\omega^2\mu \left\{ \begin{array}{c} \chi^{(2)}_{ixx}\tilde{A}^2_x + \chi^{(2)}_{iyy}\tilde{A}^2_y \\ +\chi^{(2)}_{izz}\tilde{A}^2_z + \chi^{(2)}_{ixz}\tilde{A}_x\tilde{A}_z \\ +\chi^{(2)}_{ixy}\tilde{A}_x\tilde{A}_y + \chi^{(2)}_{iyz}\tilde{A}_y\tilde{A}_z \\ +\chi^{(2)}_{iyx}\tilde{A}_y\tilde{A}_x + \chi^{(2)}_{izx}\tilde{A}_z\tilde{A}_x \\ +\chi^{(2)}_{izy}\tilde{A}_z\tilde{A}_y \end{array} \right\} e^{-i\Delta kz} \tag{A.61}$$

and use slowly varying amplitude approximation $\left|\frac{\partial^2}{\partial z^2}\tilde{A}_i\right| \ll \left|2ik^{(1)}\frac{\partial}{\partial z}\tilde{A}_i\right|$ and $\left|\frac{\partial^2}{\partial z^2}\tilde{B}_i\right| \ll \left|2ik^{(1)}\frac{\partial}{\partial z}\tilde{B}_i\right|$, Equations A.60 and A.61 becomes

$$2ik^{(1)}\frac{\partial}{\partial z}\tilde{A}_i = -\omega^2\mu \left\{ \begin{array}{c} 2\chi^{(2)}_{ixx}\tilde{B}_x\tilde{A}^*_x + 2\chi^{(2)}_{iyy}\tilde{B}_y\tilde{A}^*_y \\ +2\chi^{(2)}_{izz}\tilde{B}_z\tilde{A}^*_z \\ +\chi^{(2)}_{ixz}\left(\tilde{A}^*_x\tilde{B}_z + \tilde{B}_x\tilde{A}^*_z\right) \\ +\chi^{(2)}_{ixy}\left(\tilde{A}^*_x\tilde{B}_y + \tilde{B}_x\tilde{A}^*_y\right) \\ +\chi^{(2)}_{iyz}\left(\tilde{A}_y\tilde{B}_z + \tilde{B}_y\tilde{A}_z\right) \\ +\chi^{(2)}_{iyx}\left(\tilde{A}^*_y\tilde{B}_x + \tilde{B}_y\tilde{A}^*_x\right) \\ +\chi^{(2)}_{izx}\left(\tilde{A}^*_z\tilde{B}_x + \tilde{B}_z\tilde{A}^*_x\right) \\ +\chi^{(2)}_{izy}\left(\tilde{A}^*_z\tilde{B}_y + \tilde{B}_z\tilde{A}^*_y\right) \end{array} \right\} e^{i\Delta kz} \tag{A.62}$$

$$2ik^{(2)}\frac{\partial}{\partial z}\tilde{B}_i = -4\omega^2\mu \left\{ \begin{array}{c} \chi^{(2)}_{ixx}\tilde{A}^2_x + \chi^{(2)}_{iyy}\tilde{A}^2_y + \chi^{(2)}_{izz}\tilde{A}^2_z \\ +\chi^{(2)}_{ixz}\tilde{A}_x\tilde{A}_z + \chi^{(2)}_{ixy}\tilde{A}_x\tilde{A}_y + \chi^{(2)}_{iyz}\tilde{A}_y\tilde{A}_z \\ +\chi^{(2)}_{iyx}\tilde{A}_y\tilde{A}_x + \chi^{(2)}_{izx}\tilde{A}_z\tilde{A}_x + \chi^{(2)}_{izy}\tilde{A}_z\tilde{A}_y \end{array} \right\} e^{-i\Delta kz} \tag{A.63}$$

where phase mismatch

$$\Delta k = k^{(2)} - 2k^{(1)} \tag{A.64}$$

Consider $i = x$

$$\frac{\partial \tilde{A}_x}{\partial z} = \frac{i\omega^2 \mu \chi^{(2)}_{xxx}}{k^{(1)}} \tilde{B}_x \tilde{A}^*_x e^{i\Delta kz} \tag{A.65}$$

$$\frac{\partial \tilde{B}_x}{\partial z} = \frac{2i\omega^2 \mu \chi^{(2)}_{xxx}}{k^{(2)}} \tilde{A}^2_x e^{-i\Delta kz} \tag{A.66}$$

A.3 Solving SH Propagation Partial Differential Equation

From Equation 3.38, we have

$$\frac{\partial^2 E^{(2)}_i(z)}{\partial z^2} + k^{(2)2}_i E^{(2)}_i(z) = -\left(\frac{2\omega}{c}\right)^2 \mu^{(2)}_{eff(i)} \chi^{(2)}_i \left\{ \begin{array}{c} \left(\Omega^+_i\right)^2 e^{i2k^{(1)}_i (z-z_{i-1})} \\ + \left(\Omega^-_i\right)^2 e^{-i2k^{(1)}_i (z-z_{i-1})} + 2\Omega^+_i \Omega^-_i \end{array} \right\}$$

Laplace transfrom $(z - z_{i-1}) \to s$

$$\begin{aligned} E^{(2)}_i(s) = & \frac{s\frac{\partial}{\partial z} E^{(2)}_{i-1}}{\left(s^2 + k^{(2)2}_i\right)} + \frac{E^{(2)}_{i-1}}{\left(s^2 + k^{(2)2}_i\right)} \\ & -K \left\{ \begin{array}{c} \frac{\left(\Omega^+_i\right)^2}{\left(s^2+k^{(2)2}_i\right)\left(s-i2k^{(1)}_i\right)} \\ + \frac{\left(\Omega^-_i\right)^2}{\left(s^2+k^{(2)2}_i\right)\left(s+i2k^{(1)}_i\right)} + \frac{2\Omega^+_i \Omega^-_i}{s\left(s^2+k^{(2)2}_i\right)} \end{array} \right\} \end{aligned} \tag{A.67}$$

where $K = \left(\frac{2\omega}{c}\right)^2 \mu^{(2)}_{eff(i)} \chi^{(2)}_i$, Laplace inversion gives

$$\begin{aligned} E^{(2)}_i(z) = & \cos k^{(2)}_i (z - z_{i-1}) \frac{\partial E^{(2)}_{i-1}}{\partial z}|_{z_{i-1}} + \frac{E^{(2)}_{i-1}}{k^{(2)}_i} \sin k^{(2)}_i (z - z_{i-1}) \\ & -K \frac{2\Omega^+_i \Omega^-_i}{k^{(2)2}_i} (1 - \cos k^{(2)}_i (z - z_{i-1})) \\ & -\frac{K}{\left(k^{(2)2}_i - 4k^{(1)2}_i\right)} \left\{ \left(\Omega^+_i\right)^2 e^{i2k^{(1)}_i (z-z_{i-1})} + \left(\Omega^-_i\right)^2 e^{-i2k^{(1)}_i (z-z_{i-1})} \right\} \\ & +\frac{K}{2k^{(2)}_i \left(k^{(2)}_i + 2k^{(1)}_i\right)} \left\{ \left(\Omega^+_i\right)^2 e^{-ik^{(2)}_i (z-z_{i-1})} + \left(\Omega^-_i\right)^2 e^{ik^{(2)}_i (z-z_{i-1})} \right\} \\ & +\frac{K}{2k^{(2)}_i \left(k^{(2)}_i - 2k^{(1)}_i\right)} \left\{ \left(\Omega^+_i\right)^2 e^{ik^{(2)}_i (z-z_{i-1})} + \left(\Omega^-_i\right)^2 e^{-ik^{(2)}_i (z-z_{i-1})} \right\} \end{aligned} \tag{A.68}$$

Write

$$E_i^{(2)-}e^{-ik_i^{(2)}(z-z_{i-1})}+E_i^{(2)+}e^{ik_i^{(2)}(z-z_{i-1})} = \left\{\begin{array}{c}\frac{\partial E_{i-1}^{(2)}}{\partial z}|_{z_{i-1}}\\ +K\frac{2\Omega_i^+\Omega_i^-}{k_i^{(2)2}}\end{array}\right\}\cos k_i^{(2)}(z-z_{i-1}) \quad \text{(A.69)}$$

$$+\frac{E_{i-1}^{(2)}}{k_i^{(2)}}\sin k_i^{(2)}(z-z_{i-1})$$

$$+K\left\{\begin{array}{c}\frac{\left(\Omega_i^-\right)^2}{2k_i^{(2)}\left(k_i^{(2)}-2k_i^{(1)}\right)}\\ +\frac{\left(\Omega_i^+\right)^2}{2k_i^{(2)}\left(k_i^{(2)}-2k_i^{(1)}\right)}\end{array}\right\}e^{ik_i^{(2)}(z-z_{i-1})}$$

$$+K\left\{\begin{array}{c}\frac{\left(\Omega_i^+\right)^2}{2k_i^{(2)}\left(k_i^{(2)}+2k_i^{(1)}\right)}\\ +\frac{\left(\Omega_i^-\right)^2}{2k_i^{(2)}\left(k_i^{(2)}-2k_i^{(1)}\right)}\end{array}\right\}e^{-ik_i^{(2)}(z-z_{i-1})}$$

using Euler equation

$$\cos k_i^{(2)}(z-z_{i-1}) = \frac{1}{2}\left(e^{ik_i^{(2)}(z-z_{i-1})}+e^{-ik_i^{(2)}(z-z_{i-1})}\right) \quad \text{(A.70)}$$

$$\sin k_i^{(2)}(z-z_{i-1}) = \frac{1}{2i}\left(e^{ik_i^{(2)}(z-z_{i-1})}-e^{-ik_i^{(2)}(z-z_{i-1})}\right) \quad \text{(A.71)}$$

therefore, RHS of Equation A.69 becomes

$$\left\{\frac{\partial E_{i-1}^{(2)}}{\partial z}|_{z_{i-1}}+K\frac{2\Omega_i^+\Omega_i^-}{k_i^{(2)2}}\right\}\frac{1}{2}\left(e^{ik_i^{(2)}(z-z_{i-1})}+e^{-ik_i^{(2)}(z-z_{i-1})}\right)$$

$$+\frac{E_{i-1}^{(2)}}{k_i^{(2)}}\frac{1}{2i}\left(e^{ik_i^{(2)}(z-z_{i-1})}-e^{-ik_i^{(2)}(z-z_{i-1})}\right)-K\frac{2\Omega_i^+\Omega_i^-}{k_i^{(2)2}}$$

$$-K\frac{1}{\left(k_i^{(2)2}-4k_i^{(1)2}\right)}\left\{\left(\Omega_i^+\right)^2e^{i2k_i^{(1)}(z-z_{i-1})}+\left(\Omega_i^-\right)^2e^{-i2k_i^{(1)}(z-z_{i-1})}\right\}$$

$$+K\frac{1}{2k_i^{(2)}\left(k_i^{(2)}+2k_i^{(1)}\right)}\left\{\left(\Omega_i^+\right)^2e^{-ik_i^{(2)}(z-z_{i-1})}+\left(\Omega_i^-\right)^2e^{ik_i^{(2)}(z-z_{i-1})}\right\}$$

$$+K\frac{1}{2k_i^{(2)}\left(k_i^{(2)}-2k_i^{(1)}\right)}\left\{\left(\Omega_i^+\right)^2e^{ik_i^{(2)}(z-z_{i-1})}+\left(\Omega_i^-\right)^2e^{-ik_i^{(2)}(z-z_{i-1})}\right\}$$

and further simplify

$$\frac{1}{2}\left\{\frac{\partial E_{i-1}^{(2)}}{\partial z}|_{z_{i-1}}+K\frac{2\Omega_i^+\Omega_i^-}{k_i^{(2)2}}\right\}e^{ik_i^{(2)}(z-z_{i-1})}-\frac{E_{i-1}^{(2)}}{2ik_i^{(2)}}e^{ik_i^{(2)}(z-z_{i-1})}$$
$$+\frac{K}{2k_i^{(2)}}\left\{\frac{\left(\Omega_i^-\right)^2}{\left(k_i^{(2)}+2k_i^{(1)}\right)}+\frac{\left(\Omega_i^+\right)^2}{\left(k_i^{(2)}-2k_i^{(1)}\right)}\right\}e^{ik_i^{(2)}(z-z_{i-1})}$$
$$+\frac{1}{2}\left\{\frac{\partial E_{i-1}^{(2)}}{\partial z}|_{z_{i-1}}+K\frac{2\Omega_i^+\Omega_i^-}{k_i^{(2)2}}\right\}e^{-ik_i^{(2)}(z-z_{i-1})}-\frac{E_{i-1}^{(2)}}{2ik_i^{(2)}}e^{-ik_i^{(2)}(z-z_{i-1})}$$
$$+\frac{K}{2k_i^{(2)}}\left\{\frac{\left(\Omega_i^+\right)^2}{\left(k_i^{(2)}+2k_i^{(1)}\right)}+\frac{\left(\Omega_i^-\right)^2}{\left(k_i^{(2)}-2k_i^{(1)}\right)}\right\}e^{-ik_i^{(2)}(z-z_{i-1})}$$
$$-K\frac{1}{\left(k_i^{(2)2}-4k_i^{(1)2}\right)}\{\left\{\left(\Omega_i^+\right)^2e^{i2k_i^{(1)}(z-z_{i-1})}+\left(\Omega_i^-\right)^2e^{-i2k_i^{(1)}(z-z_{i-1})}\right\}$$
$$-K\frac{2\Omega_i^+\Omega_i^-}{k_i^{(2)2}}$$

equate term with $e^{ik_i^{(2)}(z-z_{i-1})}$ for RHS and LHS of Equation A.69, we have $E_i^{(2)+}$

$$\begin{aligned}E_i^{(2)+} &= \frac{1}{2}(\frac{\partial E_{i-1}^{(2)}}{\partial z}|_{z_{i-1}}+K\frac{2\Omega_i^{(+)}\Omega_i^{(-)}}{k_i^{(2)2}})+\frac{1}{2i}\frac{E_{i-1}^{(2)}}{k_i^{(2)}}\\ &\quad+\frac{K}{2k_i^{(2)}}\left\{\frac{\left(\Omega_i^-\right)^2}{\left(k_i^{(2)}+2k_i^{(1)}\right)}+\frac{\left(\Omega_i^+\right)^2}{\left(k_i^{(2)}-2k_i^{(1)}\right)}\right\}\end{aligned} \tag{A.72}$$

equate term with $e^{-ik_i^{(2)}(z-z_{i-1})}$ for RHS and LHS of Equation A.69, we have $E_i^{(2)-}$

$$\begin{aligned}E_i^{(2)-} &= \frac{1}{2}(\frac{\partial E_{i-1}^{(2)}}{\partial z}|_{z_{i-1}}+K\frac{2\Omega_i^{(+)}\Omega_i^{(-)}}{k_i^{(2)2}})-\frac{1}{2i}\frac{E_{i-1}^{(2)}}{k_i^{(2)}}\\ &\quad+\frac{K}{2k_i^{(2)}}\left\{\frac{\left(\Omega_i^+\right)^2}{\left(k_i^{(2)}+2k_i^{(1)}\right)}+\frac{\left(\Omega_i^-\right)^2}{\left(k_i^{(2)}-2k_i^{(1)}\right)}\right\}\end{aligned} \tag{A.73}$$

We could obtain Equation 3.39

$$\begin{aligned}E_i^{(2)}(z) &= E_i^{(2)-}e^{-ik_i^{(2)}(z-z_{i-1})}+E_i^{(2)+}e^{ik_i^{(2)}(z-z_{i-1})}\\ &\quad+A_i\left\{\left(\Omega_i^+\right)^2e^{i2k_i^{(1)}(z-z_{i-1})}+\left(\Omega_i^+\right)^2e^{-i2k_i^{(1)}(z-z_{i-1})}\right\}\\ &\quad+C_i2\Omega_i^+\Omega_i^-\end{aligned}$$

where $A_i=\frac{-K}{\left(k_i^{(2)2}-4k_i^{(1)2}\right)}, C_i=\frac{-K}{k_i^{(2)2}}$

A.4 Derivation of SH Recursion Transfer Matrix

From Equation 3.60, we could evaluate $j = 2$

$$\begin{bmatrix} E_4^{(2)+} \\ E_4^{(2)-} \end{bmatrix} = Z \begin{bmatrix} E_2^{(2)+} \\ E_2^{(2)-} \end{bmatrix} + Y_4 \tag{A.74}$$

$j = 3$

$$\begin{aligned} \begin{bmatrix} E_6^{(2)+} \\ E_6^{(2)-} \end{bmatrix} &= Z \begin{bmatrix} E_4^{(2)+} \\ E_4^{(2)-} \end{bmatrix} + Y_6 \\ &= Z \left\{ Z \begin{bmatrix} E_2^{(2)+} \\ E_2^{(2)-} \end{bmatrix} + Y_4 \right\} + Y_6 \\ &= Z^2 \begin{bmatrix} E_2^{(2)+} \\ E_2^{(2)-} \end{bmatrix} + ZY_4 + Y_6 \end{aligned} \tag{A.75}$$

$j = 4$

$$\begin{aligned} \begin{bmatrix} E_8^{(2)+} \\ E_8^{(2)-} \end{bmatrix} &= Z \begin{bmatrix} E_6^{(2)+} \\ E_6^{(2)-} \end{bmatrix} + Y_8 \\ &= Z \left\{ Z^2 \begin{bmatrix} E_2^{(2)+} \\ E_2^{(2)-} \end{bmatrix} + ZY_4 + Y_6 \right\} + Y_8 \\ &= Z^3 \begin{bmatrix} E_2^{(2)+} \\ E_2^{(2)-} \end{bmatrix} + Z^2 Y_4 + ZY_6 + Y_8 \end{aligned} \tag{A.76}$$

hence from Equations A.74 to A.76, when we set $j = N$ by induction, we could obtain Equation 3.67. Now, we expand Equation 3.67 and write

$$M_i = A_i \left[B_i F_i - N_i B_i \right] \tag{A.77}$$

$$\vec{J_i} = 2C_i \left[I - N_i \right] \begin{bmatrix} 1 \\ 0 \end{bmatrix} \tag{A.78}$$

$$\vec{J} = \begin{bmatrix} 1 \\ 0 \end{bmatrix} \tag{A.79}$$

$$\vec{I}_i = \begin{bmatrix} \left(\Omega_i^+\right)^2 \\ \left(\Omega_i^-\right)^2 \end{bmatrix} \tag{A.80}$$

$$\vec{E}_i^{(2)} = \begin{bmatrix} E_i^{(2)+} \\ E_i^{(2)-} \end{bmatrix} \tag{A.81}$$

$$\begin{aligned} \begin{bmatrix} E_{2N}^{(2)+} \\ E_{2N}^{(2)-} \end{bmatrix} &= Z^{N-1}\vec{E}_2^{(2)} + \sum_{j=2}^{N} Z^{N-j} Y_{2j} \\ &= Z^{N-1} \begin{Bmatrix} G_2^{-1}N_1 G_0 \vec{E}_0^{(2)} + G_2^{-1}M_1\vec{I}_1 \\ -G_2^{-1}B_2A_2\vec{I}_2 + G_2^{-1}\vec{J}_1\Omega_1^+\Omega_1^- \\ -G_2^{-1}\vec{J}2C_2\Omega_2^+\Omega_2^- \end{Bmatrix} + \sum_{j=2}^{N} Z^{N-j} Y_{2j} \\ &= \begin{Bmatrix} Z^{N-1}G_2^{-1}N_1 G_0 \vec{E}_0^{(2)} + Z^{N-1}G_2^{-1}M_1\vec{I}_1 \\ -Z^{N-1}G_2^{-1}B_2A_2\vec{I}_2 + Z^{N-1}G_2^{-1}\vec{J}_1\Omega_1^+\Omega_1^- \\ -Z^{N-1}G_2^{-1}\vec{J}2C_2\Omega_2^+\Omega_2^- \end{Bmatrix} + \sum_{j=2}^{N} Z^{N-j} Y_{2j} \end{aligned} \tag{A.82}$$

Subsititute Equation 3.59 into Equation 3.57, we have

$$\begin{aligned} \begin{bmatrix} E_t^{(2)+} \\ 0 \end{bmatrix} &= G_0^{-1}G_2Q_2\vec{E}_{2N}^{(2)} + G_0^{-1}A_2B_2F_2\vec{I}_{2N} + G_0^{-1}\vec{J}2C_2\Omega_{2N}^+\Omega_{2N}^- \\ &= G_0^{-1}S^N G_0 \begin{bmatrix} 0 \\ E_0^{(2)-} \end{bmatrix} + G_0^{-1}S^{N-1}N_2M_1\vec{I}_1 \\ &\quad -G_0^{-1}S^{N-1}N_2B_2A_2\vec{I}_2 + G_0^{-1}S^{N-1}N_2\vec{J}_1\Omega_1^+\Omega_1^- \\ &\quad -G_0^{-1}S^{N-1}N_2\vec{J}2C_2\Omega_2^+\Omega_2^- \\ &\quad +G_0^{-1}G_2Q_2\sum_{j=2}^{N} Z^{N-j}Y_{2j} + G_0^{-1}A_2B_2F_2\vec{I}_{2N} \\ &\quad +G_0^{-1}\vec{J}2C_2\Omega_{2N}^+\Omega_{2N}^- \end{aligned} \tag{A.83}$$

We expand $G_0^{-1}G_2Q_2\sum_{j=2}^{N}Z^{N-j}Y_{2j}$

$$
\begin{aligned}
G_0^{-1}G_2Q_2\sum_{j=2}^{N}Z^{N-j}Y_{2j} &= G_0^{-1}G_2Q_2\sum_{j=2}^{N}Z^{N-j}Y_{2j} \\
&= G_0^{-1}G_2Q_2\sum_{j=2}^{N}[Z]^{N-j}\left\{\begin{array}{c} G_2^{-1}N_1B_2F_2A_2\vec{I}_{2(j-1)} \\ +G_2^{-1}M_1\vec{I}_{2j-1} \\ -G_2^{-1}B_2A_2\vec{I}_{2j} \\ +G_2^{-1}N_1\vec{J}2C_2\Omega^{+}_{2(j-1)}\Omega^{-}_{2(j-1)} \\ +G_2^{-1}\vec{J}_1\Omega^{+}_{2j-1}\Omega^{-}_{2j-1} \\ -G_2^{-1}\vec{J}2C_2\Omega^{+}_{2j}\Omega^{-}_{2j}\end{array}\right\}
\end{aligned}
$$

Rearrange the equation and let $N=4$, we have

$$
\begin{aligned}
\begin{bmatrix} E_t^{(2)+} \\ 0 \end{bmatrix} &= G_0^{-1}S^4G_0\begin{bmatrix} E_0^{(2)+} \\ E_0^{(2)-} \end{bmatrix} \\
&\quad +G_0^{-1}\left\{\begin{array}{c} S^3N_2M_1\vec{I}_1+S^2N_2M_1\vec{I}_3 \\ +SN_2M_1\vec{I}_5+N_2M_1\vec{I}_7\end{array}\right\} \\
&\quad +G_0^{-1}\left\{\begin{array}{c} S^3M_2\vec{I}_2+S^2M_2\vec{I}_4 \\ +SM_2\vec{I}_6+M_2\vec{I}_8\end{array}\right\} \\
&\quad +G_0^{-1}\left\{\begin{array}{c} S^3N_2\vec{J}_1\Omega^{+}_1\Omega^{-}_1+S^2N_2\vec{J}_1\Omega^{+}_3\Omega^{-}_3 \\ +SN_2\vec{J}_1\Omega^{+}_5\Omega^{-}_5+N_2\vec{J}_1\Omega^{+}_7\Omega^{-}_7\end{array}\right\} \\
&\quad +G_0^{-1}\left\{\begin{array}{c} S^3\vec{J}_2\Omega^{+}_2\Omega^{-}_2+S^2\vec{J}_2\Omega^{+}_4\Omega^{-}_4 \\ +S\vec{J}_2\Omega^{+}_6\Omega^{-}_6+\vec{J}_2\Omega^{+}_8\Omega^{-}_8\end{array}\right\}
\end{aligned}
$$

This could be written as

$$\begin{aligned}
\begin{bmatrix} E_t^{(2)+} \\ 0 \end{bmatrix} &= G_0^{-1} S^4 G_0 \begin{bmatrix} 0 \\ E_0^{(2)-} \end{bmatrix} \\
&\quad + G_0^{-1} \begin{Bmatrix} S^{4-1} N_2 M_1 \vec{I}_{2(1)-1} + S^{4-2} N_2 M_1 \vec{I}_{2(2)-1} \\ + S^{4-3} N_2 M_1 \vec{I}_{2(3)-1} + S^{4-4} N_2 M_1 \vec{I}_{2(4)-1} \end{Bmatrix} \\
&\quad + G_0^{-1} \begin{Bmatrix} S^{4-1} M_2 \vec{I}_{2(1)} + S^{4-2} M_2 \vec{I}_{2(2)} \\ + S^{4-3} M_2 \vec{I}_{2(3)} + S^{4-4} M_2 \vec{I}_{2(4)} \end{Bmatrix} \\
&\quad + G_0^{-1} \begin{Bmatrix} S N_2 \vec{J}_1 \Omega^+_{2(1)-1} \Omega^-_{2(1)-1} + S^{4-2} N_2 \vec{J}_1 \Omega^+_{2(2)-1} \Omega^-_{2(2)-1} \\ + S^{4-3} N_2 \vec{J}_1 \Omega^+_{2(3)-1} \Omega^-_{2(3)-1} + S^{4-4} N_2 \vec{J}_1 \Omega^+_{2(4)-1} \Omega^-_{2(4)-1} \end{Bmatrix} \\
&\quad + G_0^{-1} \begin{Bmatrix} S^{4-3} \vec{J}_2 \Omega^+_{2(1)} \Omega^-_{2(1)} + S^2 \vec{J}_2 \Omega^+_{2(2)} \Omega^-_{2(2)} \\ + S^{4-3} \vec{J}_2 C_2 \Omega^+_{2(3)} \Omega^-_{2(3)} + S^{4-4} \vec{J}_2 \Omega^+_{2(4)} \Omega^-_{2(4)} \end{Bmatrix}
\end{aligned}$$

and further simplify into N term

$$\begin{aligned}
\begin{bmatrix} E_t^{(2)+} \\ 0 \end{bmatrix} &= G_0^{-1} S^N G_0 \begin{bmatrix} 0 \\ E_0^{(2)-} \end{bmatrix} \\
&\quad + G_0^{-1} \sum_{j=1}^{N} S^{N-j} N_2 M_1 \vec{I}_{2j-1} + G_0^{-1} \sum_{j=1}^{N} S^{N-j} M_2 \vec{I}_{2j} \\
&\quad + G_0^{-1} \sum_{j=1}^{N} S^{N-j} N_2 \vec{J}_1 \Omega^+_{2j-1} \Omega^-_{2j-1} + G_0^{-1} \sum_{j=1}^{N} S^{N-j} \vec{J}_2 \Omega^+_{2j} \Omega^-_{2j} \\
&= G_0^{-1} S^N G_0 \begin{bmatrix} 0 \\ E_0^{(2)-} \end{bmatrix} \\
&\quad + G_0^{-1} \sum_{j=1}^{N} S^{N-j} \begin{Bmatrix} N_2 M_1 \vec{I}_{2j-1} + M_2 \vec{I}_{2j} \\ N_2 \vec{J}_1 \Omega^+_{2j-1} \Omega^-_{2j-1} + \vec{J}_2 \Omega^+_{2j} \Omega^-_{2j} \end{Bmatrix}
\end{aligned}$$

therefore, after rearranging the equation we have Equation 3.68.

A.5 Derivation of Transfer Matrix with Alternative Approach

A.5.1 Linear Part: Fundamental Fields

For $z_{2j-2} < z < z_{2j-1}$

$$E^{*(1)}_{2j-1}(z,t) = \left(\Omega^{*+}_{2j-1} e^{ik_1^{(1)} \Delta z_{2j-2}} + \Omega^{*-}_{2j-1} e^{-ik_1^{(1)} \Delta z_{2j-1}} \right) e^{-i\omega t} \tag{A.84}$$

and for $z_{2j-1} < z < z_{2j}$

$$E_{2j}^{*(1)}(z,t) = \left(\Omega_{2j}^{*+} e^{ik_2^{(1)}\Delta z_{2j-1}} + \Omega_{2j}^{*-} e^{-ik_2^{(1)}\Delta z_{2j}}\right) e^{-i\omega t} \tag{A.85}$$

as we could see from Figure 3.3, the backward complex amplitude Ω_{2j-1}^{-} for $E_{2j-1}^{(1)}(z,t)$ is subjected to phase change from previous layer $(2j-1)$ at right which is described as $e^{-ik_1^{(1)}\Delta z_{2j-1}}$ meanwhile foward complex amplitude Ω_{2j-1}^{+} is subjected to phase change from previous layer $(2j-2)$ at left which is described as $e^{ik_1^{(1)}\Delta z_{2j-2}}$. The same approach applies to $E_{2j}^{(1)}(z,t)$, hence the forward complex amplitude Ω_{2j}^{+} is subjected to phase change from previous layer $(2j-1)$ at left which is described as $e^{ik_2^{(1)}\Delta z_{2j-1}}$ and backward complex amplitude Ω_{2j}^{-} is subjected to phase change from previous layer $(2j)$ which is described as $e^{-ik_2^{(1)}\Delta z_{2j}}$.

Apply Maxwell equation $\nabla \times \mathbf{E}_i^{(1)} = ik_0^{(1)} c\mu_i^{(1)} \mathbf{H}_i^{(1)}$, we have

$$c\mu_{2j-1}^{(1)} H_{2j-1}^{*(1)} = \left(n_1^{(1)} \Omega_{2j-1}^{*+} e^{ik_1^{(1)}\Delta z_{2j-2}} - n_1^{(1)} \Omega_{2j-1}^{*-} e^{-ik_1^{(1)}\Delta z_{2j-1}}\right) e^{-i\omega t} \tag{A.86}$$

and

$$c\mu_{2j}^{(1)} H_{2j}^{*(1)} = \left(n_2^{(1)} \Omega_{2j}^{*+} e^{ik_2^{(1)}\Delta z_{2j-1}} - n_2^{(1)} \Omega_{2j}^{*-} e^{-ik_2^{(1)}\Delta z_{2j}}\right) e^{-i\omega t} \tag{A.87}$$

hence, we obtain the general expression of E and H as

$$E_i^{*(1)}(z,t) = \left(\Omega_{2j-1}^{*+} e^{ik_i^{(1)}(z-z_{i-1})} + \Omega_{2j-1}^{*-} e^{-ik_i^{(1)}(z-z_i)}\right) e^{-i\omega t} \tag{A.88}$$

and

$$c\mu_i^{(1)} H_i^{*(1)}(z,t) = \left(n_i^{(1)} \Omega_i^{*+} e^{ik_i^{(1)}(z-z_{i-1})} - n_i^{(1)} \Omega_i^{*-} e^{-ik_i^{(1)}(z-z_i)}\right) e^{-i\omega t} \tag{A.89}$$

arrange E and H in the matrix,

$$\begin{bmatrix} E_i^{*(1)}(z,t) \\ c\mu_0 H_i^{*(1)}(z,t) \end{bmatrix} = \begin{bmatrix} 1 & 1 \\ \frac{n_i^{(1)}}{\mu_{eff(i)}^{(1)}} & -\frac{n_i^{(1)}}{\mu_{eff(i)}^{(1)}} \end{bmatrix} \begin{bmatrix} \Omega_i^{+}(z,t) \\ \Omega_i^{-}(z,t) \end{bmatrix} \tag{A.90}$$

Consider odd even interface, we have E and H

$$E_{2j-1}^{*(1)}(z,t) = \left(\Omega_{2j-1}^{*+} e^{ik_1^{(1)}(z-z_{2j-2})} + \Omega_{2j-1}^{*-} e^{-ik_1^{(1)}(z-z_{2j-1})}\right) e^{-i\omega t} \tag{A.91}$$

$$E_{2j}^{*(1)}(z,t) = \left(\Omega_{2j}^{*+} e^{ik_2^{(1)}(z-z_{2j-1})} + \Omega_{2j}^{*-} e^{-ik_2^{(1)}(z-z_{2j})}\right) e^{-i\omega t} \tag{A.92}$$

and

$$c\mu_0 H_{2j-1}^{*(1)}(z,t) = \begin{pmatrix} x_1^{(1)}\Omega_{2j-1}^{*+} e^{ik_1^{(1)}\left(z-z_{2j-2}\right)} \\ -x_1^{(1)}\Omega_{2j-1}^{*-} e^{-ik_1^{(1)}\left(z-z_{2j-1}\right)} \end{pmatrix} e^{-i\omega t} \quad (A.93)$$

$$c\mu_0 H_{2j}^{*(1)}(z,t) = \left(x_2^{(1)}\Omega_{2j}^{*+} e^{ik_2^{(1)}\left(z-z_{2j-1}\right)} - x_2^{(1)}\Omega_{2j}^{*-} e^{-ik_2^{(1)}\left(z-z_{2j}\right)} \right) e^{-i\omega t} \quad (A.94)$$

where we define

$$x_i^{(1)} = \frac{n_i^{(1)}}{\mu_{eff(i)}^{(1)}} \quad (A.95)$$

arrange in matrix

$$\begin{aligned} \begin{bmatrix} E_{2j}^{*(1)}\left(z_{2j-1},t\right) \\ c\mu_0 H_{2j}^{*(1)}\left(z_{2j-1},t\right) \end{bmatrix} &= \begin{bmatrix} \Omega_{2j}^{*+} e^{ik_2^{(1)}(0)} + \Omega_{2j}^{*-} e^{-ik_2^{(1)}(-d_2)} \\ x_2^{(1)}\Omega_{2j}^{*+} e^{ik_2^{(1)}(0)} - x_2^{(1)}\Omega_{2j}^{*-} e^{-ik_2^{(1)}(-d_2)} \end{bmatrix} e^{-i\omega t} \quad (A.96) \\ &= \begin{bmatrix} \Omega_{2j}^{*+} + \Omega_{2j}^{*-} e^{ik_2^{(1)}d_2} \\ x_2^{(1)}\Omega_{2j}^{*+} - x_2^{(1)}\Omega_{2j}^{*-} e^{ik_2^{(1)}d_2} \end{bmatrix} e^{-i\omega t} \\ &= \begin{bmatrix} 1 & e^{ik_2^{(1)}d_2} \\ x_2^{(1)} & -x_2^{(1)} e^{ik_2^{(1)}d_2} \end{bmatrix} \begin{bmatrix} \Omega_{2j}^{+} \\ \Omega_{2j}^{*-} \end{bmatrix} e^{-i\omega t} \\ &= \begin{bmatrix} 1 & 1 \\ x_2^{(1)} & -x_2^{(1)} \end{bmatrix} \begin{bmatrix} 1 & 0 \\ 0 & e^{ik_2^{(1)}d_2} \end{bmatrix} \begin{bmatrix} \Omega_{2j}^{*+} \\ \Omega_{2j}^{*-} \end{bmatrix} e^{-i\omega t} \\ &= D_2 W_2 \begin{bmatrix} \Omega_{2j}^{*+} \\ \Omega_{2j}^{*-} \end{bmatrix} e^{-i\omega t} \end{aligned}$$

where

$$W_i = \begin{bmatrix} 1 & 0 \\ 0 & \exp\left(ik_i^{(1)}d_i\right) \end{bmatrix} \quad (A.97)$$

and

$$\begin{bmatrix} E_{2j-1}^{*(1)}\left(z_{2j-1},t\right) \\ c\mu_0 H_{2j-1}^{*(1)}\left(z_{2j-1},t\right) \end{bmatrix} = \begin{bmatrix} \left(\Omega_{2j-1}^{*+}e^{ik_1^{(1)}(d_1)}+\Omega_{2j-1}^{*-}e^{-ik_1^{(1)}(0)}\right) \\ \begin{pmatrix} x_1^{(1)}\Omega_{2j-1}^{*+}e^{ik_1^{(1)}(d_1)} \\ -x_1^{(1)}\Omega_{2j-1}^{*-}e^{-ik_1^{(1)}(0)} \end{pmatrix} \end{bmatrix} e^{-i\omega t} \quad \text{(A.98)}$$

$$= \begin{bmatrix} \Omega_{2j-1}^{*+}e^{ik_1^{(1)}(d_1)}+\Omega_{2j-1}^{*-} \\ x_1^{(1)}\Omega_{2j-1}^{*+}e^{ik_1^{(1)}(d_1)}-x_1^{(1)}\Omega_{2j-1}^{*-} \end{bmatrix} e^{-i\omega t}$$

$$= \begin{bmatrix} e^{ik_1^{(1)}(d_1)}+1 \\ x_1^{(1)}e^{ik_1^{(1)}(d_1)}-x_1^{(1)} \end{bmatrix} \begin{bmatrix} \Omega_{2j-1}^{*+} \\ \Omega_{2j-1}^{*-} \end{bmatrix} e^{-i\omega t}$$

$$= \begin{bmatrix} 1 & 1 \\ x_1^{(1)} & -x_1^{(1)} \end{bmatrix} \begin{bmatrix} e^{ik_1^{(1)}(d_1)} & 0 \\ 0 & 1 \end{bmatrix} \begin{bmatrix} \Omega_{2j-1}^{*+} \\ \Omega_{2j-1}^{*-} \end{bmatrix} e^{-i\omega t}$$

$$= D_1 U_1 \begin{bmatrix} \Omega_{2j-1}^{*+} \\ \Omega_{2j-1}^{*-} \end{bmatrix} e^{-i\omega t}$$

where

$$U_i = \begin{bmatrix} \exp\left(ik_i^{(1)}d_i\right) & 0 \\ 0 & 1 \end{bmatrix} \quad \text{(A.99)}$$

and D_i is the dynamical matrix as defined in previous section. Considering the continuity of the tangential fields at boundary across z_{2j-1}, we have

$$\begin{bmatrix} E_{2j-1}^{*(1)}\left(z_{2j-1},t\right) \\ c\mu_0 H_{2j-1}^{*(1)}\left(z_{2j-1},t\right) \end{bmatrix} = \begin{bmatrix} E_{2j}^{(1)}\left(z_{2j-1},t\right) \\ c\mu_0 H_{2j}^{(1)}\left(z_{2j-1},t\right) \end{bmatrix} \quad \text{(A.100)}$$

and therefore the transfer matrix that relates $\Omega_{2j-1}^{\pm}$ and $\Omega_{2j}^{\pm}$

$$D_1 U_1 \begin{bmatrix} \Omega_{2j-1}^{*+} \\ \Omega_{2j-1}^{*-} \end{bmatrix} = D_2 W_2 \begin{bmatrix} \Omega_{2j}^{*+} \\ \Omega_{2j}^{*-} \end{bmatrix} \quad \text{(A.101)}$$

could be obtained.

Consider even odd interface, we have E and H

$$E_{2j-1}^{*(1)}(z,t) = \left(\Omega_{2j-1}^{*+}e^{ik_1^{(1)}\left(z-z_{2j-2}\right)}+\Omega_{2j-1}^{*-}e^{-ik_1^{(1)}\left(z-z_{2j-1}\right)}\right)e^{-i\omega t} \quad \text{(A.102)}$$

$$E_{2j-2}^{*(1)}(z,t) = \left(\Omega_{2j-2}^{*+}e^{ik_2^{(1)}\left(z-z_{2j-3}\right)}+\Omega_{2j-2}^{*-}e^{-ik_2^{(1)}\left(z-z_{2j-2}\right)}\right)e^{-i\omega t} \quad \text{(A.103)}$$

we could derive

$$\begin{bmatrix} E_{2j-1}^{*(1)}\left(z_{2j-2},t\right) \\ c\mu_0 H_{2j-1}^{(1)}\left(z_{2j-2},t\right) \end{bmatrix} = D_1 W_1 \begin{bmatrix} \Omega_{2j-1}^{*+} \\ \Omega_{2j-1}^{*-} \end{bmatrix} e^{-i\omega t} \quad \text{(A.104)}$$

and

$$\begin{bmatrix} E_{2j-2}^{(1)}\left(z_{2j-2},t\right) \\ c\mu_0 H_{2j-2}^{*(1)}\left(z_{2j-2},t\right) \end{bmatrix} = D_2 U_2 \begin{bmatrix} \Omega_{2j-2}^{*+} \\ \Omega_{2j-2}^{*-} \end{bmatrix} e^{-i\omega t} \tag{A.105}$$

combine Equations A.104 and A.105, we have

$$\begin{bmatrix} E_{2j-2}^{*(1)}\left(z_{2j-2},t\right) \\ c\mu_0 H_{2j-2}^{*(1)}\left(z_{2j-2},t\right) \end{bmatrix} = \begin{bmatrix} E_{2j-1}^{(1)}\left(z_{2j-2},t\right) \\ c\mu_0 H_{2j-1}^{(1)}\left(z_{2j-2},t\right) \end{bmatrix} \tag{A.106}$$

which is written as

$$D_2 U_2 \begin{bmatrix} \Omega_{2j-2}^{*+} \\ \Omega_{2j-2}^{*-} \end{bmatrix} = D_1 W_1 \begin{bmatrix} \Omega_{2j-1}^{*+} \\ \Omega_{2j-1}^{*-} \end{bmatrix} \tag{A.107}$$

further combine Equations A.101 and A.107, transfer matrix that relates $\Omega_{2j}^{*\pm}$ and $\Omega_{2j-2}^{*\pm}$

$$\begin{bmatrix} \Omega_{2j}^{*+} \\ \Omega_{2j}^{*-} \end{bmatrix} == W_2^{-1} D_2^{-1} D_1 U_1 W_1^{-1} D_1^{-1} D_2 U_2 \begin{bmatrix} \Omega_{2j-2}^{*+} \\ \Omega_{2j-2}^{*-} \end{bmatrix} \tag{A.108}$$

could be obtained.

Now, consider boundary between air (left) and layer 1 $(z_0 = 0, z_1 = d_1)$, we have

$$E_1^{*(1)}(0,t) = \left(\Omega_1^{*+} e^{ik_1^{(1)}(z-z_0)} + \Omega_1^{*-} e^{-ik_1^{(1)}(z-z_1)}\right) e^{-i\omega t} \tag{A.109}$$

$$H_1^{*(1)}(0,t) = \frac{1}{c\mu_0^{(1)}} \left(n_0^{(1)} \Omega_i^{*+} - n_0^{(1)} \Omega_i^{*-}\right) e^{-i\omega t} \tag{A.110}$$

and therefore

$$\begin{bmatrix} \Omega_1^{*+} \\ \Omega_1^{*-} \end{bmatrix} = (D_1 W_1)^{-1} D_0 \begin{bmatrix} \Omega_0^{*+} \\ \Omega_0^{*-} \end{bmatrix} \tag{A.111}$$

At the boundary between layer $2N$ (left) and air (right), the transmitted FF field Ω_t^+ is related by

$$E_t^{*(1)}(t) = \Omega_t^{*+} e^{-i\omega t} \tag{A.112}$$

$$H_t^{*(1)}(t) = \frac{1}{c\mu_0^{(1)}} n_t^{(1)} \Omega_t^{*+} e^{-i\omega t} \tag{A.113}$$

For layer $i = 2N$,

$$E_{2N}^{*(1)}(z,t) = \left(\Omega_{2N}^{*+} e^{ik_2^{(1)}(z-z_{2N-1})} + \Omega_{2N}^{*-} e^{-ik_2^{(1)}(z-z_{2N})}\right) e^{-i\omega t} \tag{A.114}$$

$$c\mu_{eff(2)}^{(1)} H_{2N}^{*(1)}(z,t) = \begin{pmatrix} n_2^{(1)} \Omega_{2N}^{*+} e^{ik_2^{(1)}(z-z_{2N-1})} \\ -n_2^{(1)} \Omega_{2N}^{*-} e^{-ik_2^{(1)}(z-z_{2N})} \end{pmatrix} e^{-i\omega t} \tag{A.115}$$

at $z = z_{2N}$, the continuity of E and H gives

$$\begin{aligned}
\begin{bmatrix} e^{ik_2^{(1)}d_2} & 1 \\ e^{ik_2^{(1)}d_2}x_2^{(1)} & -x_2^{(1)} \end{bmatrix} \begin{bmatrix} \Omega_{2N}^{*+} \\ \Omega_{2N}^{*-} \end{bmatrix} &= \begin{bmatrix} 1 & 1 \\ x_t^{(1)} & -x_t^{(1)} \end{bmatrix} \begin{bmatrix} \Omega_t^{*+} \\ 0 \end{bmatrix} \\
D_0 \begin{bmatrix} \Omega_t^{*+} \\ 0 \end{bmatrix} &= D_2U_2 \begin{bmatrix} \Omega_{2N}^{*+} \\ \Omega_{2N}^{*-} \end{bmatrix}
\end{aligned} \tag{A.116}$$

and therefore transfer matrix for N period

$$\begin{aligned}
\begin{bmatrix} \Omega_t^{*+} \\ 0 \end{bmatrix} &= D_0^{-1}D_2U_2 \begin{bmatrix} \Omega_{2N}^{*+} \\ \Omega_{2N}^{*-} \end{bmatrix} \\
&= D_0^{-1}D_2U_2 \left(W_2^{-1}DD_1U_1W_1^{-1}D_1^{-1}D_2U_2\right)^{N-1} \begin{bmatrix} \Omega_2^{*+} \\ \Omega_2^{*-} \end{bmatrix} \\
&= D_0^{-1}L_a^N D_0 \begin{bmatrix} \Omega_0^{*+} \\ \Omega_0^{*-} \end{bmatrix}
\end{aligned} \tag{A.117}$$

is obtained. L_a is transfer matrix for single period developed by alternative method, it is defined as

$$L_a = D_2U_2W_2^{-1}D_2^{-1}D_1U_1W_1^{-1}D_1^{-1} \tag{A.118}$$

A.5.2 Nonlinear Part: Polarization and SH Fields

The interaction of the fundamental wave with medium inside each layer would induce second order nonlinear polarization P_i^{*NL}

$$\begin{aligned}
P_i^{*NL}(z,t) &= \varepsilon_0\chi_i^{(2)} \left(E_i^{*(1)}(z,t)\right)^2 e^{-i2\omega t} \\
&= \varepsilon_0\chi_i^{(2)} \begin{pmatrix} \left(\Omega_i^{*+}\right)^2 e^{i2k_i^{(1)}(z-z_{i-1})} + \left(\Omega_i^{*-}\right)^2 e^{-i2k_i^{(1)}(z-z_i)} \\ +2\Omega_i^{*+}\Omega_i^{*-}e^{ik_i^{(1)}(z_i-z_{i-1})} \end{pmatrix}
\end{aligned} \tag{A.119}$$

expanding 3.37, we have

$$\frac{\partial^2 E_i^{*(2)}(z)}{\partial z^2} + k_i^{(2)2}E_i^{*(2)}(z) = -4\mu_i^{(2)}\varepsilon_i^{(2)}\omega^2\chi_i^{(2)} \begin{pmatrix} \left(\Omega_i^{*+}\right)^2 e^{i2k_i^{(1)}z}e^{-i2k_i^{(1)}z_{i-1}} \\ +\left(\Omega_i^{*-}\right)^2 e^{-i2k_i^{(1)}z}e^{i2k_i^{(1)}z_i} \\ +2\Omega_i^{*+}\Omega_i^{*-}e^{ik_i^{(1)}(z_i-z_{i-1})} \end{pmatrix} \tag{A.120}$$

Using Laplace transform to solve 3.37, we have the general solution of the SH field as

$$\begin{aligned} E_i^{*(2)}(z) &= E_i^{*(2)+} e^{ik_i^{(2)}(z-z_{i-1})} + E_i^{*(2)-} e^{-ik_i^{(2)}(z-z_i)} \\ &+ A_i \left(\Omega_i^{*+}\right)^2 e^{i2k_i^{(1)}(z-z_{i-1})} \\ &+ A_i \left(\Omega_i^{*-}\right)^2 e^{-i2k_i^{(1)}(z-z_i)} \\ &+ C_i 2\Omega_i^{*+}\Omega_i^{*-} e^{ik_i^{(1)}(z_i-z_{i-1})} \end{aligned} \tag{A.121}$$

where $A_i(\omega) = -\left(\frac{2\omega}{c}\right)^2 \frac{\mu_{eff(i)}^{(2)}\chi_i^{(2)}}{k_i^{(2)2}-4k_i^{(1)2}}$, $C_i(\omega) = -\left(\frac{2\omega}{c}\right)^2 \frac{\mu_{eff(i)}^{(2)}\chi_i^{(2)}}{k_i^{(2)2}}$. The magnetic field as obtained from the Maxwell equation $\mathbf{H}_i^{*(2)}(z) = \frac{1}{ik_0^{(2)}c\mu_0\mu_{eff(i)}^{(2)}}\left[\nabla \times \mathbf{E}_i^{*(2)}(z)\right]$ is

$$\begin{aligned} c\mu_0 H_i^{*(2)}(z) &= \frac{n_i^{(2)}}{\mu_{eff(i)}^{(2)}} E_i^{*(2)+} e^{ik_i^{(2)}(z-z_{i-1})} - \frac{n_i^{(2)}}{\mu_{eff(i)}^{(2)}} E_i^{*(2)-} e^{-ik_i^{(2)}(z-z_i)} \\ &+ \frac{2k_0^{(1)}n_i^{(1)}}{k_0^{(2)}\mu_{eff(i)}^{(2)}} A_i \left(\Omega_i^{*+}\right)^2 e^{i2k_i^{(1)}(z-z_{i-1})} \\ &- \frac{2k_0^{(1)}n_i^{(1)}}{k_0^{(2)}\mu_{eff(i)}^{(2)}} A_i \left(\Omega_i^{*-}\right)^2 e^{-i2k_i^{(1)}(z-z_i)} \end{aligned} \tag{A.122}$$

arrange E and H fields in the matrix form, we have

$$\begin{aligned} \begin{bmatrix} E_i^{*(2)}(z) \\ c\mu_0 H_i^{*(2)}(z) \end{bmatrix} &= G_i \begin{bmatrix} E_i^{*(2)+}(z) \\ E_i^{*(2)-}(z) \end{bmatrix} + B_i \begin{bmatrix} A_i \left(\Omega_i^{*+}(z)\right)^2 \\ A_i \left(\Omega_i^{*-}(z)\right)^2 \end{bmatrix} \\ &+ 2C_i \begin{bmatrix} e^{ik_i^{(1)}(z_i-z_{i-1})} \\ 0 \end{bmatrix} \Omega_i^{*+}\Omega_i^{*-} \end{aligned} \tag{A.123}$$

where we define

$$\begin{aligned} E_i^{*(2)+}(z) &= E_i^{*(2)+} e^{ik_i^{(2)}(z-z_{i-1})} \\ E_i^{*(2)-}(z) &= E_i^{*(2)-} e^{-ik_i^{(2)}(z-z_i)} \\ \Omega_i^{*+}(z) &= \left(\Omega_i^{*+}\right) e^{ik_i^{(1)}(z-z_{i-1})} \\ \Omega_i^{*-}(z) &= \left(\Omega_i^{*-}\right) e^{ik_i^{(1)}(z_i-z)} \end{aligned}$$

Consider odd layers $i = 2j-1$

$$\begin{aligned} \begin{bmatrix} E_{2j-1}^{*(2)}(z) \\ c\mu_0 H_{2j-1}^{*(2)}(z) \end{bmatrix} &= G_1 \begin{bmatrix} E_{2j-1}^{*(2)+}(z) \\ E_{2j-1}^{*(2)-}(z) \end{bmatrix} + A_1 B_1 \begin{bmatrix} \left(\Omega_{2j-1}^{*+}(z)\right)^2 \\ \left(\Omega_{2j-1}^{*-}(z)\right)^2 \end{bmatrix} \\ &+ 2C_1 \begin{bmatrix} e^{ik_1^{(1)}d_1} \\ 0 \end{bmatrix} \Omega_{2j-1}^{*+}\Omega_{2j-1}^{*-} \end{aligned} \tag{A.124}$$

and even layers $i = 2j$

$$\begin{aligned}\begin{bmatrix} E_{2j}^{*(2)}(z) \\ c\mu_0 H_{2j}^{*(2)}(z) \end{bmatrix} &= G_2 \begin{bmatrix} E_{2j}^{*(2)+}(z) \\ E_{2j}^{*(2)-}(z) \end{bmatrix} + A_2 B_2 \begin{bmatrix} \left(\Omega_{2j}^{*+}(z)\right)^2 \\ \left(\Omega_{2j}^{*-}(z)\right)^2 \end{bmatrix} \\ &\quad + 2C_2 \begin{bmatrix} e^{ik_2^{(1)} d_2} \\ 0 \end{bmatrix} \Omega_{2j}^{*+} \Omega_{2j}^{*-}\end{aligned} \tag{A.125}$$

where we define

$$\begin{aligned} G_0 &= \begin{bmatrix} 1 & 1 \\ n_{20} & -n_{20} \end{bmatrix} \\ G_i &= \begin{bmatrix} 1 & 1 \\ \frac{n_i^{(2)}}{\mu_{eff(i)}^{(2)}} & -\frac{n_i^{(2)}}{\mu_{eff(i)}^{(2)}} \end{bmatrix} \\ B_i &= \begin{bmatrix} 1 & 1 \\ \frac{2k_0^{(1)} n_i^{(1)}}{k_0^{(2)} \mu_{eff(i)}^{(2)}} & -\frac{2k_0^{(1)} n_i^{(1)}}{k_0^{(2)} \mu_{eff(i)}^{(2)}} \end{bmatrix} = \begin{bmatrix} 1 & 1 \\ \frac{n_i^{(1)}}{\mu_{eff(i)}^{(2)}} & -\frac{n_i^{(1)}}{\mu_{eff(i)}^{(2)}} \end{bmatrix} \end{aligned}$$

Consider the continuity of electric $E(z)$ and magnetic $H(z)$ fields at interface of $z = 2(j-1), z = 2j-1$ and $2j$. At interface $z = 2j-1$, left is odd layer, right is even layer, $j > 0$

$$\begin{bmatrix} E_{2j-1}^{*(2)}\left(z_{2j-1}\right) \\ c\mu_0 H_{2j-1}^{*(2)}\left(z_{2j-1}\right) \end{bmatrix} = \begin{bmatrix} E_{2j}^{*(2)}\left(z_{2j-1}\right) \\ c\mu_0 H_{2j}^{*(2)}\left(z_{2j-1}\right) \end{bmatrix} \tag{A.126}$$

The transfer matrix that relates $E_{2j-1}^{*(2)\pm}$ and $E_{2j}^{*(2)\pm}$ is

$$\begin{aligned} G_1 Q_1 \begin{bmatrix} E_{2j-1}^{*(2)+} \\ E_{2j-1}^{*(2)-} \end{bmatrix} &= G_2 \bar{Q}_2 \begin{bmatrix} E_{2j}^{*(2)+} \\ E_{2j}^{*(2)-} \end{bmatrix} + A_2 B_2 \bar{F}_2 \begin{bmatrix} \left(\Omega_{2j}^{*+}\right)^2 \\ \left(\Omega_{2j}^{*-}\right)^2 \end{bmatrix} \\ &\quad - A_1 B_1 F_1 \begin{bmatrix} \left(\Omega_{2j-1}^{*+}\right)^2 \\ \left(\Omega_{2j-1}^{*-}\right)^2 \end{bmatrix} \\ &\quad + 2C_2 \begin{bmatrix} e^{ik_2^{(1)} d_2} \\ 0 \end{bmatrix} \Omega_{2j}^{*+} \Omega_{2j}^{*-} \\ &\quad - 2C_1 \begin{bmatrix} e^{ik_1^{(1)} d_1} \\ 0 \end{bmatrix} \Omega_{2j-1}^{*+} \Omega_{2j-1}^{*-} \end{aligned} \tag{A.127}$$

where

$$Q_i = \begin{bmatrix} e^{ik_i^{(2)}d_i} & 0 \\ 0 & 1 \end{bmatrix}, \bar{Q}_i = \begin{bmatrix} 1 & 0 \\ 0 & e^{ik_i^{(2)}d_i} \end{bmatrix}$$

$$F_i = P_i^2 = \begin{bmatrix} e^{i2k_i^{(1)}d_i} & 0 \\ 0 & 1 \end{bmatrix}, \bar{F}_i = \begin{bmatrix} 1 & 0 \\ 0 & e^{i2k_i^{(1)}d_i} \end{bmatrix}$$

At interface $z = 2j-2$, left is even layer, right is odd layer, $j > 0$

$$\begin{bmatrix} E^{*(2)}_{2(j-1)}\left(z_{2(j-1)}\right) \\ c\mu_0 H^{*(2)}_{2(j-1)}\left(z_{2(j-1)}\right) \end{bmatrix} = \begin{bmatrix} E^{*(2)}_{2j-1}\left(z_{2(j-1)}\right) \\ c\mu_0 H^{*(2)}_{2j-1}\left(z_{2(j-1)}\right) \end{bmatrix} \tag{A.128}$$

we have transfer matrix that relates $E^{*(2)\pm}_{2j-1}$ and $E^{*(2)\pm}_{2j-2}$

$$\begin{aligned} (G_1\bar{Q}_1)\begin{bmatrix} E^{*(2)+}_{2j-1} \\ E^{*(2)-}_{2j-1} \end{bmatrix} &= G_2Q_2\begin{bmatrix} E^{*(2)+}_{2j-2} \\ E^{*(2)-}_{2j-2} \end{bmatrix} + A_2B_2F_2\begin{bmatrix} \left(\Omega^{*+}_{2j-2}\right)^2 \\ \left(\Omega^{*-}_{2j-2}\right)^2 \end{bmatrix} \\ &\quad + 2C_2\begin{bmatrix} e^{ik_2^{(1)}d_2} \\ 0 \end{bmatrix}\Omega^{*+}_{2j-2}\Omega^{*-}_{2j-2} \\ &\quad - A_1(B_1\bar{F}_1)\begin{bmatrix} \left(\Omega^{*+}_{2j-1}\right)^2 \\ \left(\Omega^{*-}_{2j-1}\right)^2 \end{bmatrix} \\ &\quad - 2C_1\begin{bmatrix} e^{ik_1^{(1)}d_1} \\ 0 \end{bmatrix}\Omega^{*+}_{2j-1}\Omega^{*-}_{2j-1} \end{aligned} \tag{A.129}$$

At (input) interface between air at left and layer 1 at right, we obtain

$$\begin{aligned} (G_1\bar{Q}_1)\begin{bmatrix} E^{*(2)+}_{1} \\ E^{*(2)-}_{1} \end{bmatrix} &= G_0\begin{bmatrix} 0 \\ E^{*(2)-}_{0} \end{bmatrix} - A_1(B_1\bar{F}_1)\begin{bmatrix} \left(\Omega^{*+}_{1}\right)^2 \\ \left(\Omega^{*-}_{1}\right)^2 \end{bmatrix} \\ &\quad - 2C_1\begin{bmatrix} e^{ik_1^{(1)}d_1} \\ 0 \end{bmatrix}\Omega^{*+}_{1}\Omega^{*-}_{1} \end{aligned} \tag{A.130}$$

At (output) interface between layer $2N$ at left and air at right (setting $j = N+1$),

$$\begin{aligned} G_0\begin{bmatrix} E^{*(2)+}_{t} \\ 0 \end{bmatrix} &= G_2Q_2\begin{bmatrix} E^{*(2)+}_{2N} \\ E^{*(2)-}_{2N} \end{bmatrix} + A_2B_2F_2\begin{bmatrix} \left(\Omega^{*+}_{2N}\right)^2 \\ \left(\Omega^{*-}_{2N}\right)^2 \end{bmatrix} \\ &\quad + 2C_2\begin{bmatrix} e^{ik_2^{(1)}d_2} \\ 0 \end{bmatrix}\Omega^{*+}_{2N}\Omega^{*-}_{2N} \end{aligned} \tag{A.131}$$

To connect the first and second layer, set $j = 1$

$$
\begin{aligned}
G_2\bar{Q}_2\begin{bmatrix} E_2^{*(2)+} \\ E_2^{*(2)-} \end{bmatrix} &= G_1Q_1\begin{bmatrix} E_1^{*(2)+} \\ E_1^{*(2)-} \end{bmatrix} - A_2B_2\bar{F}_2\begin{bmatrix} \left(\Omega_2^{*+}\right)^2 \\ \left(\Omega_2^{*-}\right)^2 \end{bmatrix} \\
&\quad + A_1B_1F_1\begin{bmatrix} \left(\Omega_1^{*+}\right)^2 \\ \left(\Omega_1^{*-}\right)^2 \end{bmatrix} - 2C_2\begin{bmatrix} e^{ik_2^{(1)}d_2} \\ 0 \end{bmatrix}\Omega_2^{*+}\Omega_2^{*-} \\
&\quad + 2C_1\begin{bmatrix} e^{ik_1^{(1)}d_1} \\ 0 \end{bmatrix}\Omega_1^{*+}\Omega_1^{*-}
\end{aligned} \tag{A.132}
$$

Eliminate $\begin{bmatrix} E_1^{*(2)+} \\ E_1^{*(2)-} \end{bmatrix}$, we relate the input $E_0^{*(2)+}$ and reflected $E_0^{*(2)-}$ fields with the fields in the second layer

$$
\begin{bmatrix} E_2^{*(2)+} \\ E_2^{*(2)-} \end{bmatrix} = (G_2\bar{Q}_2)^{-1}N_1G_0\begin{bmatrix} 0 \\ E_0^{*(2)-} \end{bmatrix} + (G_2\bar{Q}_2)^{-1}\{O_1 - W_2\} \tag{A.133}
$$

where

$$
X_{2j-2} = \left(A_2N_1B_2F_2\begin{bmatrix} \left(\Omega_{2j-2}^{*+}\right)^2 \\ \left(\Omega_{2j-2}^{*-}\right)^2 \end{bmatrix} + 2C_2N_1\begin{bmatrix} e^{ik_2^{(1)}d_2} \\ 0 \end{bmatrix}\Omega_{2j-2}^{*+}\Omega_{2j-2}^{*-}\right)
$$

$$
O_{2j-1} = \begin{pmatrix} A_1[B_1F_1 - N_1(B_1\bar{F}_1)]\begin{bmatrix} \left(\Omega_{2j-1}^{*+}\right)^2 \\ \left(\Omega_{2j-1}^{*-}\right)^2 \end{bmatrix} \\ +2C_1(I-N_1)\begin{bmatrix} e^{ik_1^{(1)}d_1} \\ 0 \end{bmatrix}\Omega_{2j-1}^{*+}\Omega_{2j-1}^{*-} \end{pmatrix}
$$

$$
W_{2j} = \left(A_2(B_2\bar{F}_2)\begin{bmatrix} \left(\Omega_{2j}^{*+}\right)^2 \\ \left(\Omega_{2j}^{*-}\right)^2 \end{bmatrix} + 2C_2\begin{bmatrix} e^{ik_2^{(1)}d_2} \\ 0 \end{bmatrix}\Omega_{2j}^{*+}\Omega_{2j}^{*-}\right)
$$

By combining Equations A.127 and A.129, the transfer matrix of transmission and reflection SH electric fields at $z = 2(j-1)$ and $2j$ could be related by eliminating $\begin{bmatrix} E_{2j-1}^{*(2)+} \\ E_{2j-1}^{*(2)-} \end{bmatrix}$

giving the recursion relation

$$\begin{aligned}
\begin{bmatrix} E_{2j}^{*(2)+} \\ E_{2j}^{*(2)-} \end{bmatrix} &= (G_2\bar{Q}_2)^{-1}N_1G_2Q_2 \begin{bmatrix} E_{2j-2}^{*(2)+} \\ E_{2j-2}^{*(2)-} \end{bmatrix} \\
&+A_2(G_2\bar{Q}_2)^{-1}N_1B_2F_2 \begin{bmatrix} \left(\Omega_{2j-2}^{*+}\right)^2 \\ \left(\Omega_{2j-2}^{*-}\right)^2 \end{bmatrix} \\
&+A_1\left[(G_2\bar{Q}_2)^{-1}B_1F_1-(G_2\bar{Q}_2)^{-1}N_1(B_1\bar{F}_1)\right] \begin{bmatrix} \left(\Omega_{2j-1}^{*+}\right)^2 \\ \left(\Omega_{2j-1}^{*-}\right)^2 \end{bmatrix} \\
&-A_2(G_2\bar{Q}_2)^{-1}(B_2\bar{F}_2) \begin{bmatrix} \left(\Omega_{2j}^{*+}\right)^2 \\ \left(\Omega_{2j}^{*-}\right)^2 \end{bmatrix} \\
&+2C_2(G_2\bar{Q}_2)^{-1}N_1 \begin{bmatrix} e^{ik_2^{(1)}d_2} \\ 0 \end{bmatrix} \Omega_{2j-2}^{*+}\Omega_{2j-2}^{*-} \\
&+2C_1(G_2\bar{Q}_2)^{-1}[I-N_1] \begin{bmatrix} e^{ik_1^{(1)}d_1} \\ 0 \end{bmatrix} \Omega_{2j-1}^{*+}\Omega_{2j-1}^{*-} \\
&-2C_2(G_2\bar{Q}_2)^{-1} \begin{bmatrix} e^{ik_2^{(1)}d_2} \\ 0 \end{bmatrix} \Omega_{2j}^{*+}\Omega_{2j}^{*-}
\end{aligned} \tag{A.134}$$

where

$$N_1 = G_1Q_1(G_1\bar{Q}_1)^{-1} = G_1Q_1\bar{Q}_1^{-1}G_1^{-1}$$

We write the recursion relation A.134 as

$$\begin{bmatrix} E_{2j}^{*(2)+} \\ E_{2j}^{*(2)-} \end{bmatrix} = Z \begin{bmatrix} E_{2(j-1)}^{*(2)+} \\ E_{2(j-1)}^{*(2)-} \end{bmatrix} + Y_{2j} \tag{A.135}$$

and also define

$$Z = (G_2\bar{Q}_2)^{-1}N_1G_2Q_2$$

$$
\begin{aligned}
Y_{2j} &= (G_2\bar{Q}_2)^{-1}[X_{2j-2}+O_{2j-1}-W_{2j}] \qquad \text{(A.136)}\\
&= A_2(G_2\bar{Q}_2)^{-1}N_1B_2F_2\begin{bmatrix}\left(\Omega_{2j-2}^{*+}\right)^2\\ \left(\Omega_{2j-2}^{*-}\right)^2\end{bmatrix}\\
&\quad +A_1(G_2\bar{Q}_2)^{-1}\left[B_1F_1-N_1(B_1\bar{F}_1)\right]\begin{bmatrix}\left(\Omega_{2j-1}^{*+}\right)^2\\ \left(\Omega_{2j-1}^{*-}\right)^2\end{bmatrix}\\
&\quad -A_2(G_2\bar{Q}_2)^{-1}(B_2\bar{F}_2)\begin{bmatrix}\left(\Omega_{2j}^{*+}\right)^2\\ \left(\Omega_{2j}^{*-}\right)^2\end{bmatrix}\\
&\quad +2C_2(G_2\bar{Q}_2)^{-1}N_1\begin{bmatrix}e^{ik_2^{(1)}d_2}\\ 0\end{bmatrix}\Omega_{2j-2}^{*+}\Omega_{2j-2}^{*-}\\
&\quad +2C_1(G_2\bar{Q}_2)^{-1}\left[I-N_1\right]\begin{bmatrix}e^{ik_1^{(1)}d_1}\\ 0\end{bmatrix}\Omega_{2j-1}^{*+}\Omega_{2j-1}^{*-}\\
&\quad -2C_2(G_2\bar{Q}_2)^{-1}\begin{bmatrix}e^{ik_2^{(1)}d_2}\\ 0\end{bmatrix}\Omega_{2j}^{*+}\Omega_{2j}^{*-}
\end{aligned}
$$

By induction, for $j=N$

$$
\begin{bmatrix}E_{2N}^{*(2)+}\\ E_{2N}^{*(2)-}\end{bmatrix}=Z\begin{bmatrix}E_{2(N-1)}^{*(2)+}\\ E_{2(N-1)}^{*(2)-}\end{bmatrix}+Y_{2N}=Z^{N-1}\begin{bmatrix}E_2^{*(2)+}\\ E_2^{*(2)-}\end{bmatrix}+\sum_{j=2}^{N}Z^{N-j}Y_{2j} \qquad \text{(A.137)}
$$

Eliminate

$$
\begin{bmatrix}E_2^{*(2)+}\\ E_2^{*(2)-}\end{bmatrix}=(G_2\bar{Q}_2)^{-1}N_1G_0\begin{bmatrix}E_0^{*(2)+}\\ E_0^{*(2)-}\end{bmatrix}+(G_2\bar{Q}_2)^{-1}\{O_1-W_2\}
$$

we have

$$
\begin{aligned}
\begin{bmatrix}E_{2N}^{*(2)+}\\ E_{2N}^{(2)-}\end{bmatrix} &= Z^{N-1}(G_2\bar{Q}_2)^{-1}N_1G_0\begin{bmatrix}E_0^{*(2)+}\\ E_0^{*(2)-}\end{bmatrix} \qquad \text{(A.138)}\\
&\quad +Z^{N-1}(G_2\bar{Q}_2)^{-1}\{O_1-W_2\}+\sum_{j=2}^{N}Z^{N-j}Y_{2j}
\end{aligned}
$$

substitute A.131 into A.138

$$
\begin{aligned}
G_0 \begin{bmatrix} E_t^{*(2)+} \\ 0 \end{bmatrix} &= (G_2Q_2)\,Z^{N-1}(G_2\bar{Q}_2)^{-1}N_1G_0 \begin{bmatrix} E_0^{*(2)+} \\ E_0^{*(2)-} \end{bmatrix} \\
&\quad + (G_2Q_2)\,Z^{N-1}(G_2\bar{Q}_2)^{-1}\{O_1 - W_2\} + \sum_{j=2}^{N} Z^{N-j}Y_{2j} \\
&\quad + A_2B_2F_2 \begin{bmatrix} \left(\Omega_{2N}^{*+}\right)^2 \\ \left(\Omega_{2N}^{*-}\right)^2 \end{bmatrix} \\
&\quad + 2C_2 \begin{bmatrix} e^{ik_2^{(1)}d_2} \\ 0 \end{bmatrix} \Omega_{2N}^{*+}\Omega_{2N}^{*-}
\end{aligned} \tag{A.139}
$$

define

$$
\begin{aligned}
S^N &= G_2Q_2Z^{N-1}(G_2\bar{Q}_2)^{-1}N_1 \\
&= G_2Q_2((G_2\bar{Q}_2)^{-1}N_1G_2Q_2)^{N-1}(G_2\bar{Q}_2)^{-1}N_1 = (N_2N_1)^N
\end{aligned}
$$

after mathematical manipulation, we have final recursion for SH electric fields

$$
\begin{aligned}
\begin{bmatrix} E_t^{*(2)+} \\ 0 \end{bmatrix} &= G_0^{-1}S^NG_0 \begin{bmatrix} E_0^{*(2)+} \\ E_0^{*(2)-} \end{bmatrix} \\
&\quad + \sum_{j=1}^{N} S^{N-j} \left(\begin{array}{l}
A_1[N_2B_1F_1 - S(B_1\bar{F}_1)] \begin{bmatrix} \left(\Omega_{2j-1}^{*+}\right)^2 \\ \left(\Omega_{2j-1}^{*-}\right)^2 \end{bmatrix} \\
+2C_1(N_2 - S) \begin{bmatrix} e^{ik_1^{(1)}d_1} \\ 0 \end{bmatrix} \Omega_{2j-1}^{*+}\Omega_{2j-1}^{*-} \\
+A_2(B_2F_2 - N_2(B_2\bar{F}_2)) \begin{bmatrix} \left(\Omega_{2j}^{*+}\right)^2 \\ \left(\Omega_{2j}^{*-}\right)^2 \end{bmatrix} \\
+2C_2(I - N_2) \begin{bmatrix} e^{ik_2^{(1)}d_2} \\ 0 \end{bmatrix} \Omega_{2j}^{*+}\Omega_{2j}^{*-}
\end{array} \right)
\end{aligned}
$$

$$
\begin{aligned}
r_s &= \frac{n_i\cos\theta_i - n_t\cos\theta_t}{n_i\cos\theta_i + n_t\cos\theta_t} \\
t_s &= \frac{2n_i\cos\theta_i}{n_i\cos\theta_i + n_t\cos\theta_t} \\
r_p &= \frac{n_i\cos\theta_t - n_t\cos\theta_i}{n_i\cos\theta_t + n_t\cos\theta_i} \\
t_p &= \frac{2n_i\cos\theta_i}{n_i\cos\theta_t + n_t\cos\theta_i}
\end{aligned}
$$

REFERENCES

Agate, B., Brown, C., Sibbett, W., & Dholakia, K. (2004). Femtosecond optical tweezers for *in-situ* control of two-photon fluorescence. *Opt. Exp.*, *12*(13), 3011-3017.

Agrawal, G. P. (1995). *Nonlinear fiber optics*. Academic Press.

Amstrong, J. A., Bloembergen, N., Drucuing, J., & Pershan, P. S. (1962). Interactions between light waves in a nonlinear dielectric. *Phys. Rev.*, *32*(6), 1918-1939.

Anlage, S. M. (2011). The physics and applications of superconducting metamaterials. *J. Opt.*, *13*(2), 024001.

Arahira, S., Namekata, N., Kishimoto, T., Yaegashi, H., & Inoue, S. (2011). Generation of polarization entangled photon pairs at telecommunication wavelength using cascaded $\chi^{(2)}$ processes in a periodically poled linbo$_3$ ridge waveguide. *Opt. Exp.*, *19*(17), 16032-16043.

Argyros, A., Manos, S., Large, M. C., McKenzie, D. R., Cox, G. C., & Dwarte, D. M. (2002). Electron tomography and computer visualisation of a three-dimensional photonic crystal in a butterfly wing-scale. *Micron.*, *33*(5), 483-487.

Aryeh, B. Y. (2005). Superresolution effects obtained by negative refraction lens. *J. Mod. Opt.*, *52*(13), 1871-1883.

Ashkin, A. (1970). Acceleration and trapping of particles by radiation pressure. *Phys. Rev. Lett.*, *24*(4), 156-159.

Ashkin, A. (1980). Applications of laser radiation pressure. *Science*, *210*(4474), 1081-1088.

Bahabad, A., Cohen, O., Murnane, M. M., & Kapteyn, H. C. (2008). Quasi-phase-matching and dispersion characterization of harmonic generation in the perturbative regime using counterpropagating beams. *Opt. Exp.*, *16*(20), 15923-15931.

Baqir, M. A., & Choudhury, P. K. (2012). On the energy flux through a uniaxial chiral metamaterial made circular waveguide under PMC boundary. *J. Electromagnet. Wave*, *26*, 2165–2175.

Bardeen, J. (1958). Two-fluid model of superconductivity. *Phys. Rev. Lett.*, *1*(11), 399-400.

Barnes, N. (1973). Coherent (visible) light emission from Ga($As_{1-x}P_x$) junctions. *J. Appl. Phys.*, *44*(1), 230-237.

Bass, M., Franken, P. A., Hill, A. E., Peters, C. W., & Weinreich, G. (1962). Optical mixing. *Phys. Rev. Lett.*, *8*, 18–18.

Berlein, J. D., & Ahmed, F. (1987). Observation and poling of ferroelectric domains in ktiopo$_4$. *Appl. Phys. Lett.*, *51*(17), 1322-1324.

Bethune, D. S. (1989). Optical harmonic generation and mixing in multilayer media: analysis using optical transfer matrix techniques. *J. Opt. Soc. Am. B*, *6*(5), 910-916.

Bhat, N. A. R., & Sipe, J. E. (2001). Optical pulse propagation in nonlinear photonic crystals. *Phys. Rev. E*, *64*(5), 056604.

Bierlein, J. D., & Vanherzeele, H. (1989). Second harmonic generation in left-handed metamaterials. *J. Opt. Soc. Am. B*, *6*(4), 622-633.

Biris, C. G., & Panoiu, N. C. (2010). Second harmonic generation in metamaterials based on homogeneous centrosymmetric nanowires. *Phys. Rev. B*, *81*(19), 195102.

Biro, L. P., Balint, Z., Kertesz, K., Vertesy, Z., Mark, G. I., Horvath, Z. E., et al. (2003). Role of photonic-crystal-type structures in the thermal regulation of a Lycaenid butterfly sister species pair. *Phys. Rev. E*, *67*(2), 021907.

Bloembergen, N. (1992). *Nonlinear optics*. Addison-Wesley.

Boardman, A. (2011). Pioneers in metamaterials: John Pendry and Victor Veselago. *J. Opt.*, *13*(19), 020401.

Bordenave, E., Abraham, E., Jonusauskas, G., Oberle, J., & Rulliere, C. (2002). Longitudinal imaging in biological tissues with a single laser shot correlation system. *Opt. Exp.*, *10*(1), 35-40.

Born, M., & Wolf, E. (1999). *Principles of optics*. Pergamon Press.

Boulanger, B., Fejer, M. M., Blachman, R., & Bordui, P. F. (1994). Study of ktiopo$_4$ gray-tracking at 1064, 532, and 355 nm. *Appl. Phys. Lett.*, *65*(19), 2401-2403.

Boyd, R. W., & Sipe, J. E. (1994). Nonlinear optical susceptibilities of layered composite materials. *J. Opt. Soc. Am. B*, *11*(2), 297-303.

Brewer, R. G. (1967). Frequency shifts in self-focused light. *Phys. Rev. Lett.*, *19*(1), 8-10.

Byod, R. W. (2003). *Nonlinear optics*. Academic Press.

Campagnola, P. J., Wei, M., Lewis, A., & Loew, L. M. (1999). High-resolution nonlinear optical imaging of live cells by second harmonic generation. *Biophys. J.*, *77*(6), 3341–3349.

Cao, H., Hall, D. B., Torkelson, J. M., & Cao, C. Q. (2000). Large enhancement of second harmonic generation in polymer films by microcavities. *Appl. Phys. Lett.*, *76*(5), 538-540.

Cao, P. F., Zhang, X. P., & Cheng, Q. Q., L.and Meng. (2009). Far field imaging research based on multilayer positive- and ngative -refractive index media under off-axis illumination. *Prog Electromagn Res*, *98*, 283-298.

Chang, Y., Wen, J., Wang, H., & Li, B. (1992). Refractive index measurement and second harmonic generation in a series of $LiNbO_3$: Mg (5 mol%) crystals. *Chinese Phys. Lett.*, *9*(8), 427-430.

Chen, H., Ran, L., Huangfu, J., Zhang, X., Chen, K., Grzegorczyk, T. M., et al. (2003). T-junction waveguide experiment to characterize left-handed properties of metamaterials. *J. Appl. Phys.*, *94*(6), 3712-3716.

Chen, H., Ran, L., Huangfu, J., Zhang, X., Chen, K., Grzegorczyk, T. M., et al. (2004). Left-handed materials composed of only S-shaped resonators. *Phys. Rev. E*, *70*(5), 057605.

Chen, H., Wu, B., Zhang, B., & Kong, J. A. (2007). Electromagnetic wave interactions with a metamaterial cloak. *Phys. Rev. Lett.*, *99*(6), 063903.

Chen, H., Wu, B. I., & Kong, J. A. (2006). Review of electromagnetic theory in left-handed materials. *J. of Electromagn. Waves and Appl.*, *20*(15), 2137–2151.

Chen, T., Li, S., & Sun, H. (2012). Metamaterials application in sensing. *Sensor*, *12*(3), 2742-2765.

Chen, Y. Y., Huang, Z. M., Wang, Q., Li, C. F., & Shi, J. L. (2005). Photon tunnelling in one-dimensional metamaterial photonic crystals. *J. Opt. A*, *7*(9), 519-524.

Cheung, A. C., Rank, D. M., Chiao, R. Y., & Townes, C. H. (1968). Phase modulation of *q*-switched laser beams in small-scale filaments. *Phys. Rev. Lett.*, *20*(15), 786-789.

Choudhury, P. K., & Lakhtakia, A. (2008). The future of optoelectronics technology. *Asian J. Phys.*, *17*(2), 181-183.

Chow, J., Town, G., Eggleton, B., Ibsen, M., Sugden, K., & Bennion, I. (1996). Multiwavelength generation in an erbium-doped fiber laser using in-fiber comb filters. *IEEE Photonics Techn. Lett.*, *8*(1), 60-62.

Clausen, C. B., Kivshar, Y. S., Bang, O., & Christiansen, P. L. (1999). Quasiperiodic envelope solitons. *Phys. Rev. Lett.*, *83*(23), 4740–4743.

Cook, D. M. (1975). *The theory of the electromagnetic field*. Prentice Hall.

Corkum, P. (2000). Laser physics: Attosecond pulses at last. *Nature*, *403*, 845-846.

Cowan, A. R., & Young, J. F. (2002). Mode matching for second-harmonic generation in photonic crystal waveguides. *Phys. Rev. B*, *65*(8), 085106.

D'Aguanno, G., Centini, M., Scalora, M., Sibilia, C., Dumeige, Y., Vidakovic, P., et al. (2001). Photonic band edge effects in finite structures and applications to $\chi^{(2)}$ interactions. *Phys. Rev. E*, *64*(1), 016609.

Dantzig, N. A. van, Planken, P. C. M., & Bakker, H. J. (1998). Far-infrared second-harmonic generation and pulse characterization with the organic salt dast. *Opt. Lett.*, *23*(6), 466-468.

Davey, R. P., Langford, N., & Ferguson, A. I. (1991). Subpicosecond pulse generation from erbium doped fibre laser. *Electron. Lett.*, *27*(9), 726-728.

De, A. K., Roy, D., & Goswami, D. (2011). Two-photon fluorescence diagnostics of femtosecond laser tweezers. *Curr. Sci.*, *101*(7), 935-938.

Dekker, R., Usechak, N., Forst, M., & Driessen, A. (2007). Ultrafast nonlinear all-optical processes in silicon-on-insulator waveguides. *J. Phys. D: Appl. Phys.*, *40*(14), R249–R271.

DeMaria, A. J., Ferrar, C. M., & Danielson, G. E. (1966). Mode locking of a Nd^{3+}-doped glass laser. *Appl. Phys. Lett.*, *8*(1), 22-24.

Denz, C., Flach, S., & Kivshar, Y. S. (2008). *Nonlinearities in periodic structures and metamaterials*. Springer.

Diels, J. C., & Rudolph, W. (1996). *Ultrashort laser pulse phenomena*. Academic Press.

Dong, J. W., Zheng, H. H., Lai, Y., Wang, H. Z., & Chan, C. T. (2011). Metamaterial slab as a lens, a cloak, or an intermediate. *Phys. Rev. B*, *83*(11), 115124.

Dou, S. X., Josse, D., & Zyss, J. (1993). Near-infrared pulsed optical parametric oscillation in N-(4-nitrophenyl)-L-prolinol at the 1-ns time scale. *J. Opt. Soc. Am. B*, *10*(9), 1708-1715.

Driscoll, T. A., Hoffman, H. J., Stone, R. E., & Perkins, P. E. (1986). Efficient second-harmonic generation in KTP crystals. *J. Opt. Soc. Am. B*, *16*(5), 683-686.

Du, Q. G., Ren, F. F., Kam, C. H., & Sun, X. W. (2009). Second-harmonic generation in photonic crystal with a pair of epsilon-negative and mu-negative defects. *Opt. Exp.*, *17*(8), 6682-6687.

Dudley, J. M., Genty, G., & Coen, S. (2006). Supercontinuum generation in photonic crystal fiber. *Rev. Mod. Phys.*, *78*(4), 1135-1184.

Eghlidi, M. H., Mehrany, K., & Rashidian, B. (2006). Improved differential-transfer-matrix method for inhomogeneous one-dimensional photonic crystals. *J. Opt. Soc. B*, *23*(7), 1451-1459.

Engheta, N. (2002). An idea for thin subwavelength cavity resonators using metamaterials with negative permittivity and permeability. *IEEE Antennas and Wireless Propagation Lett.*, *1*(1), 10-13.

Enkrich, C., Wegener, M., Linden, S., Burger, S., Zschiedrich, L., Schmidt, F., et al. (2005). Magnetic metamaterials at telecommunication and visible frequnecies. *Phys. Rev. Lett.*, *95*(20), 203901.

Faccio, D., & Bragheri, F. (2005). Localization of light and second-order nonlinearity enhancement in weakly disordered one-dimensional photonic crystals. *Phys. Rev. E*, *71*(5), 057602.

Faccio, D., Bragheri, F., & Cherchi, M. (2004). Optical Bloch-mode-induced quasi phase matching of quadratic interactions in one-dimensional photonic crystals. *J. Opt. Soc. Am. B*, *21*(2), 296-301.

Fan, T. Y., & Byer, R. L. (1987). Modeling and CW operation of a quasi-three-level 946 nm Nd: YAG laser. *IEEE J. Quantum Electron.*, *23*(5), 605 - 612.

Fejer, M. M., Magel, G. A., Jundt, D. H., & Byer, R. L. (1992). Quasi-phase-matched second harmonic generation: Tuning and tolerances. *IEEE J. Quantum Electron.*, *28*(11), 2631-2654.

Feng, J., Tian, X., Li, Y., & Zhang, K. (2008). Generation of a squeezing vacuum at a telecommunication wavelength with periodically poled $linbo_3$. *Appl. Phys. Lett.*, *92*(22), 221102.

Ferreira, M. F. S. (2011). *Nonlinear effects in optical fibers*. Academic Press.

Frances, J., Neipp, C., Marquez, A., Belendez, A., & Pascual, I. (2011). Analysis of reflection gratings by means of a matrix method approach. *Prog Electromagn Res*, *118*, 167-183.

Franken, P. A., Hill, A. E., & Weinreich, G. (1961). Generation of optical harmonics. *Phys. Rev. Lett.*.

Franken, P. A., & Ward, J. F. (1963). Optical harmonics and nonlinear phenomena. *Rev. Mod. Phys.*, *35*(1), 23–39.

Fu, C., Zhang, Z. M., & Tanner, D. B. (2002). Radiative properties of multilayer thin flims with positive and negative refractive indexes. In *ASME International Mechanical Congress and Exposition* (p. 1-2). Louisiana, United States: ASME.

Ganeev, R. A., Hutchinson, C., Witting, T., Frank, F., Okell, W. A., Zair, A., et al. (2012). High-order harmonic generation in graphite plasma plumes using ultrashort laser pulses: a systematic analysis of harmonic radiation and plasma conditions. *J. Phys. B: At. Mol. Opt. Phys.*, *45*(16), 165402.

Gehr, R. J., Fischer, G. L., Boyd, R. W., & Sipe, J. E. (1996). Nonlinear optical response of layered composite materials. *Phys. Rev. A*, *53*(4), 2792–2798.

Gentile, M., Hentschel, M., Taubert, R., Guo, H., Giessen, H., & Fiebig, M. (2011). Investigation of the nonlinear optical properties of metamaterials by second harmonic generation. *Appl. Phys. B*, *105*(1), 149-162.

Geusic, J. E., Marcos, H. M., & Van Uitert, L. G. (1964). Laser oscillations in nd-doped yttrium aluminium, yttrium gallium and gadolinium garnets. *Appl. Phys. Lett.*, *4*(10), 182-184.

Ghiradella, H. (1991). Light and color on the wing: structural colors in butterflies and moths. *Appl. Opt.*, *30*(24), 3492-3500.

Gokkavas, M., Guven, K., Bulu, I., Aydin, K., Penciu, R. S., Kafesaki, M., et al. (2006). Experimental demonstration of a left-handed metamaterial operating at 100 GHz. *Phys. Rev. B*, *73*(19), 193103.

Gong, M., Zhang, H., Kang, H., Wang, D., Huang, L., Yan, P., et al. (2008). A chamfered-edge-pumped planar waveguide solid-state laser. *Laser Phys. Lett.*, *5*(7), 518-521.

Gralak, B., Enoch, S., & Tayeb, G. (2000). Anomalous refractive properties of photonic crystals. *J. Opt. Soc. Am. A*, *17*(6), 1012-1020.

Grynko, Y., Meier, T., Linden, S., Niesler, F. B. P., Wegener, M., & Foerstner, J. (2012). Near-field coupling and second-harmonic generation in split-ring resonator arrays. In *AIP Conf. Proc. 1475* (p. 128-130). Bad Honnef, Germany.

Guida, G., Lustrac, A. de, & Priou, A. (2003). An introduction to photonic band gap (PBG) materials. *Prog. Electromag. Res.*, *41*, 1-20.

Guo, H. (2007). *Nonlinear photonic crystals - a study of the microstructure designs and parametric processes*. Unpublished doctoral dissertation, National University of Singapore, Singapore.

Guo, S., & Sacharia, A. (2003). Full vector wave calculation of photonic band structures in face-centered-cubic dielectric media. *Opt. Exp.*, *11*(2), 167-175.

Guven, K., Saenz, E., Gonzalo, R., Ozbay, E., & Tretyakov, S. (2008). Electromagnetic cloaking with canonical spiral inclusions. *New J. Phys.*, *10*, 115037.

Haertle, D., Jazbinsek, M., Montemezzani, G., & Gunter, P. (2005). Nonlinear optical coefficients and phase-matching conditions in $Sn_2P_2S_6$. *Opt. Exp.*, *13*(10), 3765-3776.

Hall, R. N., Fenner, G. E., Kingsley, J. D., Soltys, T. J., & Carlson, R. O. (1962). Coherent light emission from GaAs junctions. *Phys. Rev. Lett.*, *9*(9), 366–368.

Hanson, F. (1995). Efficient operation of a room-temperature Nd:YAG 946-nm laser pumped with multiple diode arrays. *Opt. Lett.*, *20*(2), 148-150.

Hao, J., Ren, Q., An, Z., Huang, X., Chen, Z., Qiu, M., et al. (2009). Optical metamaterial for polarization control. *Phys. Rev. A*, *80*(2), 023807.

Hao, J., Yuan, Y., Ran, L., Jiang, T., Kong, J. A., Chan, C. T., et al. (2007). Manipulating electromagnetic wave polarizations by anisotropic metamaterials. *Phys. Rev. Lett.*, *99*(6), 063908.

Hao, J., & Zhou, L. (2008). Electromagnetic wave scatterings by anisotropic metamaterials: generalized 4×4 transfer matrix method. *Phys. Rev. B*, *77*(9), 094201.

Hao, J. M., Qiu, M., & Zhou, L. (2010). Manipulate light polarizations with metamaterials: From microwave to visible. *Front. Phys.*, *5*(3), 291-307.

Ho, K. M., Chan, C. T., & Soukoulis, C. M. (1990). Existence of a photonic gap in periodic dielectric structures. *Phys. Rev. Lett.*, *65*(25), 3152–3155.

Holonyak, N., & Bevacqua, S. F. (1962). Coherent (visible) light emission from $Ga(As_{1-x}P_x)$ junctions. *Appl. Phys. Lett.*, *1*(4), 82-83.

Huang, Z., Tu, C., Zhang, S., Li, Y., Lu, F., Fan, Y., et al. (2010). Femtosecond second-harmonic generation in periodically poled lithium niobate waveguides written by femtosecond laser pulses. *Opt. Lett.*, *35*(6), 877-879.

Hui, R., & Mecozzi, A. (1992). Phase noise of four-wave mixing in semiconductor lasers. *Appl. Phys. Lett.*, *60*(20), 2454-2456.

Hum, D. S., & Fejer, M. M. (2007). Quasi-phasematching. *C. R. Phys.*, *8*(2), 180–198.

Huttunen, A., & Torma, P. (2002). Band structures for nonlinear photonic crystals. *J. Appl. Phys.*, *91*(7), 3988-3991.

Ibrahim, A.-B. M. A., Choudhury, P. K., & Alias, M. S. B. (2005). Analytical design of photonic band-gap fibers and their dispersion characteristics. *Optik*, *26*(4), 169-174.

Ikuta, R., Kusaka, Y., Kitano, T., Kato, H., Yamamoto, T., Koashi, M., et al. (2011). Wide-band quantum interface for visible-to-telecommunication wavelength conversion. *Nat. Commun.*, *2*, 537.

Iliew, R., Etrich, C., Perstsch, T., & Lederer, F. (2008). Slow-light enhanced collinear second-harmonic generation in two-dimensional photonic crystals. *Phys. Rev. B*, *77*(11), 115124.

Iliew, R., Etrich, C., Perstsch, T., Lederer, F., & Kivshar, Y. S. (2010). Huge enhancement of backward second-harmonic generation with slow light in photonic crystals. *Phys. Rev. A*, *81*(2), 023820.

Ishikawa, A., Tanaka, T., & Kawata, S. (2005). Negative magnetic permeability in the visible light region.

Phys. Rev. Lett., *95*(23), 237401.

Ito, H., Takyu, C., & Inaba, H. (1991). Fabrication of periodic domain grating in $LiNbO_3$ by electron beam writing for application of nonlinear optical processes. *Electron. Lett.*, *27*(14), 1221-1222.

Jaque, D., Capmany, J., & Garcia Sole, J. (1999). Red, green, and blue laser light from a single $Nd:YAl_3(BO_3)_4$ crystal based on laser oscillation at 1.3 μm. *Appl. Phys. Lett.*, *75*(3), 325-327.

Jeong, J., & Lee, B. (1999). Section-wise-exact coupled-mode theory of waveguide quasi-phase-matched second-harmonic generation. *IEEE J. Quantum Electron.*, *35*(10), 1434-1446.

Joannopoulos, J. D., Johnson, S. G., Winn, J. N., & Meade, R. D. (2008). *Photonic crystals:molding the flow of light*. Princeton University Press.

John, S., & Wang, J. (1990). Quantum electrodynamics near a photonic band gap: Photon bound states and dressed atoms. *Phys. Rev. Lett.*, *64*, 2418–2421.

Juhasz, T., Djotyan, G., Loesel, F. H., Kurtz, R. M., Horvath, C., Bille, J. F., et al. (2000). Applications of femtosecond lasers in corneal surgery. *Laser Phys.*, *10*(2), 495–500.

Juhasz, T., Loesel, F. H., Kurtz, R. M., Horvath, C., Bille, J. F., & Mourou, G. A. (1999). Corneal refractive surgery with femtosecond lasers. *IEEE Sel. Topics in Quantum Electron.*, *5*(4), 902-910.

Kalra, Y., & Sinha, R. K. (2006). Photonic band gap engineering in 2D photonic crystals. *Pramana-J. Phys.*, *67*(6), 1155-1164.

Kang, H. X., Zhang, H., Yan, P., Wang, D. S., & Gong, M. (2008). An end-pumped nd:yag planar waveguide laser with an optical to optical conversion efficiency of 58%. *Laser Phys. Lett.*, *5*(12), 879-881.

Kano, H., & Hamaguchi, H. (2003). Characterization of a supercontinuum generated from a photonic crystal fiber and its application to coherent raman spectroscopy. *Opt. Lett.*, *28*(23), 2360-2362.

Katsidis, C. C., & Siapkas, D. I. (2002). General transfer-matrix method for optical multilayer systems with coherent, partically coherent, and incoherent interference. *Appl. Opt.*, *41*(19), 3978-3987.

Keeler, G. A., Nelson, B. E., Agarwal, D., Christof, D., Noah, C., Bhatnagar, A., et al. (2003). The benefits of ultrashort optical pulses in optically interconnected systems. *IEEE Sel. Topics in Quantum Electron.*, *9*(2), 477-485.

Keller, U. (2003). Recent developments in compact ultrafast lasers. *Nature*, *424*, 831-838.

Kenanakis, G., Shen, N. H., Mavidis, C., Katsarakis, N., Kafesaki, M., Soukoulis, C. M., et al. (2012). Microwave and thz sensing using slab-pair-based metamaterials. *Physica B*, *407*(20), 4070-4074.

Khanarian, G., Norwood, R. A., Haas, D., Feuer, B., & Karim, D. (1990). Phase-matched second-harmonic generation in a polymer waveguide. *Appl. Phys. Lett.*, *57*(10), 977-979.

Khorasani, S., & Rashidian, B. (2002). Modified transfer matrix method for conducting interfaces. *J. Opt. A: Pure Appl. Opt.*, *4*, 251–256.

Kim, J. H., & Yoon, C. S. (2002). Domain switching characteristics and fabrication of periodically poled potassium niobate for second -harmonic generation. *Appl. Phys. Lett.*, *81*(18), 3332-3334.

Klarskov, P., Isomaki, A., Hansen, K. P., & Andersen, P. E. (2011). Supercontinuum generation for coherent anti-stokes Raman scattering microscopy with photonic crystal fibers. *Opt. Exp.*, *19*(27), 26672-26683.

Klein, J. J., & Nigam, B. P. (1964). Birefringence of the vacuum. *Phys. Rev.*, *135*(5B), B1279–B1280.

Klein, M. W., Enkrich, C., Wegener, M., & Linden, S. (2006). Second-harmonic generation from magnetic

metamaterials. *Science*, *313*(5786), 502-504.

Klein, M. W., Enkrich, C., Wegener, M., Soukoulis, C. M., & Linden, S. (2006). Single-slit split-ring resonators at optical frequencies: limits of size scaling. *Opt. Lett.*, *31*(9), 1259-1261.

Klein, M. W., Wegener, M., Feth, N., & Linden, S. (2007). Experiments on second- and third-harmonic generation from magnetic metamaterials. *Opt. Exp.*, *15*(8), 5238-5247.

Knight, J. C. (2000). Anomalous dispersion in photonic crystal fiber. *IEEE Photonics Technol. Lett.*, *12*(7), 807-809.

Knippels, G. M. H., Mols, R. F. X. A. M., Meer, A. F. G. van der, Oepts, D., & Amersfoort, P. W. van. (1995). Intense far-infrared free-electron laser pulses with a length of six optical cycles. *Phys. Rev. Lett.*, *75*(9), 1755-1758.

Kong, J. A. (2002). Electromagnetic wave interaction with stratified negative isotropic media. *Prog. Electromag. Res.*, *35*, 1-52.

Kong, Y., Chen, X., & Zhu, T. (2010). Intensity modulation on polarization coupling and frequency conversion in periodically poled lithium niobate. *Appl. Phys. B*, *102*(1), 101-107.

Korn, G., Thoss, A., Stiel, H., Vogt, U., Richardson, M., Elsaesser, T., et al. (2002). Ultrashort 1-kHz laser plasma hard x-ray source. *Opt. Lett.*, *27*(10), 866-868.

Korobkin, J., D.V. (1995). Anomalous dispersion in Er^{3+} and Yb^{3+}-doped fibers. *J. Lightwave Techn.*, *13*(2), 191-195.

Korte, F., Adams, S., Egbert, A., Fallnich, C., Ostendorf, A., Nolte, S., et al. (2000). Sub-diffraction limited structuring of solid targets with femtosecond laser pulses. *Opt. Exp.*, *7*(2), 41-49.

Korte, F., Serbin, J., Koch, J., Egbert, A., Fallnich, C., Ostendorf, A., et al. (2003). Towards nanostructuring with femtosecond laser pulses. *Appl. Phys. A*, *77*(2), 229-235.

Kosmidou, E. P., & Tsiboukis, T. D. (2003). An fdtd analysis of photonic crystal waveguides comprising third-order nonlinear materials. *Optical and Quantum Electronics*, *35*(10), 167-175.

Kowalczyk, T. C., Singer, K. D., & Cahill, P. A. (1995). Anomalous-dispersion phase-matched second-harmonic generation in a polymer waveguide. *Opt. Lett.*, *20*(22), 2273-2275.

Krausz, F., Brabec, T., Wintner, E., & Schmidt, A. J. (1989). Mode locking of a continuous wave Nd:glass laser pumped by a multistripe diode laser. *Appl. Phys. Lett.*, *55*(23), 2386-2388.

Kuroda, K., Toga, Y., Satoh, T., Shimura, T., Ashihara, S., Takahashi, Y., et al. (2010). Generation of mid/far-infrared ultrashort pulses in organic crystals. *J. Phys: Conf. Ser.*, *206*(1), 012014.

Lavrinenko, A., Borel, P., Frandsen, L., Thorhauge, M., Harpøth, A., Kristensen, M., et al. (2004). Comprehensive fdtd modelling of photonic crystal waveguide components. *Opt. Exp.*, *12*(2), 234-248.

Lazar, B., & Sterian, P. (2008). Band gaps in 2d photonic crystals with hexagonal symmetry. *J. Optoelectronics and Adv. Materials*, *10*(11), 2882-2889.

Lee, C. M., Shim, W. S., Moon, Y., & Seo, C. H. (2012). Design of ultra-wide band-pass filter based on metamaterials applicable to microwave photonics. *J. Opt. Soc. Korea*, *16*(3), 288-291.

Lee, D., & Wong, N. C. (1993). Stabilization and tuning of a doubly resonant optical parametric oscillator. *J. Opt. Soc. Am. B*, *10*(9), 1659-1667.

Lee, H. M., & Wu, J. C. (2010). Transmittance spectra in one-dimensional superconductor-dielectric photonic crystal. *J. Appl. Phys.*, *107*(9), 09E149.

Leung, K. M., & Liu, Y. F. (1990). Full vector wave calculation of photonic band structures in face-

centered-cubic dielectric media. *Phys. Rev. Lett.*, *65*(21), 2646–2649.

Leuthold, J., Koos, C., & Freude, W. (2010). Nonlinear silicon photonics. *Nature Photonics*, *4*, 535 - 544.

Li, J. J., Li, Z. Y., & Zhang, D. Z. (2007). Second harmonic generation in one-dimensional nonlinear photonic crystal solved by the transfer matrix method. *Phys. Rev. E*, *75*(5), 056606.

Li, J. J., Li, Z. Y., & Zhang, D. Z. (2008). Nonlinear frequency conversion in two-dimensional nonlinear photonic crystal solved by plane-wave-based transfer-matrix method. *Phys. Rev. B*, *77*(19), 195127.

Li, Z. Y. (2005). Principles of the plane-wave transfer-matrix method for photonic crystals. *Science and Technology of Advanced Materials*, *6*(7), 837–841.

Li, Z. Y., & Lin, L. L. (2003). Photonic band structures solved by a plane-wave-based transfer-matrix method. *Phys. Rev. E*, *67*(4), 046607.

Lim, E. J., Fejer, M. M., & Byer, R. L. (1989). Second-harmonic generation of green light in periodically poled planar lithium niobate waveguide. *Electron. Lett.*, *25*(3), 174-179.

Lim, S. C. (2002). Magnetic second-harmonic generation of an antiferromagnetic film. *J. Opt. Soc. Am. B*, *19*(6), 1401-1410.

Lin, L. L., Li, Z. Y., & Ho, K. M. (2003). Lattice symmetry applied in transfer-matrix methods for photonics crystals. *J. Appl. Phys.*, *94*(2), 811-821.

Lin, S. Y., Chow, E., Hietala, V., Villeneuve, P. R., & Joannopoulos, J. D. (1998). Experimental demonstration of guiding and bending of electromagnetic waves in a photonic crystal. *Science*, *282*(5387), 274-276.

Lin, S. Y., Fleming, J. G., Hetherington, D. L., Smith, B. K., Biswas, R., Ho, K. M., et al. (1998). A three-dimensional photonic crystal operating at infrared wavelengths. *Nature*, *394*, 251-253.

Linden, D. S., Orlando, T. P., & Lyons, W. G. (1994). Modified two-fluid model for superconductor surface impedance calculation. *IEEE Trans. on Applied Superconductivity*, *4*(3), 136-142.

Liu, H., Gong, M., Wushouer, X., & Gao, S. (2010). Compact corner-pumped Nd:YAG/YAG composite slab 1319 nm/1338 nm laser. *Laser Phys. Lett.*, *7*(2), 124-129.

Liu, J., Xue, L., Wang, Z., Kai, G., Liu, Y., Zhang, W., et al. (1995). Anomalous dispersion in photonic crystal fiber. *IEEE J. Quantum Electron.*, *42*(9), 961-968.

Liu, K., & Chen, X. (2009). Evolution of the optical polarization in a periodically poled superlattice with an external electric field. *Phys. Rev. A*, *80*(6), 063808.

Loesel, F. H., Niemz, M. H., Bille, J. F., & Juhasz, T. (1996). Laser-induced optical breakdown on hard and soft tissues and its dependence on the pulse duration: experiment and model. *IEEE J. Quantum Electron.*, *32*(10), 1717-1722.

Luo, C., Johnson, S. G., Joannopoulos, J. D., & Pendry, J. B. (2003). Negative refraction without negative index in metallic photonic crystals. *Opt. Exp.*, *11*(7), 746-754.

Ma, D. L., Ren, M. L., Dou, J. H., & Li, Z. Y. (2010). Giant enhancement of second harmonic generation at photonic band gap edges. *Chin. Phys. Lett.*, *27*(11), 114209.

Maiman, T. H. (1960). Stimulated optical radiation in ruby. *Nature*, *187*, 493-494.

Maker, P., Terhune, R. W., Nisenoff, M., & Savage, C. M. (1962). Effects of dispersion and focusing on the production of optical harmonics. *Phys. Rev. Lett.*, *8*(1), 21-22.

Makino, T. (1995). Transfer matrix method with applications to distributed feedback optical devices. *Prog Electromagn Res*, *10*, 271-319.

Maksimovic, M. (2008). *Optical resonances in multilayer structures*. Unpublished doctoral dissertation, University of Twente, Enschede, The Netherlands.

Mallick, S. B., Agrawal, M., & Peumans, P. (2010). Optimal light trapping in ultra-thin photonic crystal crystalline silicon solar cells. *Opt. Exp.*, *18*(6), 5691-5706.

Mark, J., Liu, L. Y., Hall, K. L., Haus, H. A., & Ippen, E. P. (1989). Femtosecond pulse generation in a laser with a nonlinear external resonator. *Opt. Lett.*, *14*(1), 48-50.

Markos, P., & Soukoulis, C. M. (2001). Transmission studies of left-handed materials. *Phys. Rev. B*, *65*(3), 033401.

Marks, D. L., Oldenburg, A. L., Reynolds, J. J., & Boppart, S. A. (2002). Study of an ultrahigh-numerical-aperture fiber continuum generation source for optical coherence tomography. *Opt. Lett.*, *27*(22), 2010-2012.

Marques, R., Martel, J., Mesa, F., & Medina, F. (2002). Left-handed-media simulation and transmission of EM waves in subwavelength split-ring-resonator-loaded metallic waveguides. *Phys. Rev. Lett.*, *89*(18), 183901.

Martin, F., Bonache, J., Falcone, F., Sorolla, M., & Marques, R. (2003). Split ring resonator-based left-handed coplanar waveguide. *Appl. Phys. Lett.*, *83*(22), 4652-4654.

Matias, I. R., Del Villar, I., Arregui, F. J., & Claus, R. O. (2003). Development of an optical refractometer by analysis of one-dimensional photonic bandgap structures with defects. *Opt. Lett.*, *28*(13), 1099-1101.

Maywar, D. N., Nakano, Y., & Agrawal, G. P. (2000). 1.31-to-1.55 μm wavelength conversion by optically pumping a distributed feedback amplifier. *IEEE Photon. Technol. Lett.*, *12*(7), 858-860.

McCall, M. W., Lakhtakia, A., & Weiglhofer, W. S. (2002). The negative index of refraction demystified. *Eur. J. Phys.*, *23*(3), 353-360.

McCall, S. L., Platzman, P. M., Dalichaouch, R., Smith, D., & Schultz, S. (1991). Microwave propagation in two-dimensional dielectric lattices. *Phys. Rev. Lett.*, *67*(15), 2017–2020.

McIntosh, K. A., Mahoney, L. J., Molvar, K. M., McMahon, O. B., Verghese, S., Rothschild, M., et al. (1997). Three-dimensional metallodielectric photonic crystals exhibiting resonant infrared stop bands. *Appl. Phys. Lett.*, *70*(2), 2937-2939.

Meade, R. D., Brommer, K. D., Rappe, A. M., & Joannopoulos, J. D. (1992). Existence of a photonic band gap in two dimensions. *Appl. Phys. Lett.*, *61*(4), 495-497.

Mekis, A., Chen, J. C., Kurland, I., Fan, S., Villeneuve, P. R., & Joannopoulos, J. D. (1996). High transmission through sharp bends in photonic crystal waveguides. *Phys. Rev. Lett.*, *77*, 3787–3790.

Miller, R. C. (1964). Optical harmonic generation in single crystal $BaTiO_3$. *Phys. Rev.*, *134*(5A), A1313–A1319.

Milonni, P. W., & Eberly, J. H. (2010). *Laser phyiscs*. John Wiley and Sons.

Mokhtar, M. R. (2005). *Bragg grating filters for optical networks*. Unpublished doctoral dissertation, University of Southampton, Southampton, United Kingdom.

Moss, C. D., Grzegorczyk, T. M., Zhang, Y., & Kong, J. A. (2002). Numerical studies of left handed metamaterials. *Prog. Electromag. Res.*, *35*, 315-334.

Myers, L. E., Eckardt, R. C., Fejer, M. M., Byer, R. L., & Bosenberg, W. R. (1996). Multigrating quasi-phase-matched optical parametric oscillator in periodically poled $LiNbO_3$. *Opt. Lett.*, *21*(8), 591-593.

Nedialkov, N. N., Imamova, S. E., & Atanasov, P. A. (2004). Ablation of metals by ultrashort laser pulses.

J. Phys. D.: Appl. Phys., *37*(4), 638-643.

Neviere, M., Popov, E., Reinisch, R., & Vitrant, G. (2000). *Electromagnetic resonances in nonlinear optics*. Gordon and Breach Science Publishers.

Ni, P., Ma, B., Wang, X., Cheng, B., & Zhang, D. (2003). Second-harmonic generation in two-dimesnional periodically poled lithium niobate using second-order quasiphase matching. *Appl. Phys. Lett.*, *82*(24), 4230-4232.

Noda, S., Tomoda, K., Yamamoto, N., & Chutinan, A. (2000). Full three-dimensional photonic bandgap crystals at near-infrared wavelengths. *Science*, *289*(5479), 604-606.

Noda, S., Yamamoto, N., Kobayashi, H., Okano, M., & Tomoda, K. (1999). Optical properties of three-dimensional photonic crystals based on iii–v semiconductors at infrared to near-infrared wavelengths. *Appl. Phys. Lett.*, *75*(7), 905-907.

Notomi, M. (2000). Theory of light propagation in strongly modulated photonic crystals: Refractionlike behavior in the vicinity of the photonic band gap. *Phys. Rev. B*, *62*(16), 10696.

Notomi, M. (2010). Manipulating light with strongly modulated photonic crystals. *Reports on Progress in Physics*, *73*(9), 096501.

Okada, M., Takizawa, K., & Ieiri, S. (1976). Second harmonic generation by periodic laminar structure of nonlinear optical crystal. *Opt. Commun.*, *18*(3), 331-334.

Okada, M., Takizawa, K., & Ieiri, S. (1985). Current induced periodic ferroelectric domain structures in $LiNbO_3$ applied for efficient nonlinear optical frequency mixing. *Appl. Phys. Lett.*, *47*(11), 1125-1127.

Okawachi, Y., Sharping, J. E., Xu, C., & Gaeta, A. L. (2006). Large tunable optical delays via self-phase modulation and dispersion. *Opt. Exp.*, *14*(25), 12022-12027.

Ooi, C. H. R., & Au Yeung, T. C. (1999). Polariton gap in a superconductor-dielectric superlattice. *Phys. Lett. A*, *259*(5), 413-419.

Ooi, C. H. R., Au Yeung, T. C., Kam, C. H., & Lim, T. K. (2000). Photonic band gap in a superconductor-dielectric superlattice. *Phys. Rev. B*, *61*(9), 5920-5923.

Ooi, C. H. R., & Gong, Q. (2011). Temperature dependent resonances in superconductor photonic crystal. *J. Appl. Phys.*, *110*(6), 063513.

Ooi, C. H. R., & Kam, C. H. (2010). Echo and ringing of optical pulse in finite photonic crystal with superconductor and dispersive dielectric. *J. Opt. Soc. Am. B*, *27*(3), 458-463.

Ooi, C. H. R., & Ng, K. F. (2011). Switching the negative refractive index and surface wavevector of superconducting metamaterials. In *IEEE 2nd International Conference on Photonics* (p. 1-3). Sabah, Malaysia: IEEE.

Oraizi, H., & Asfahi, M. (2007). Transfer matrix method with applications to distributed feedback optical devices. *Prog Electromagn Res*, *74*, 217-240.

Owens, D. (2010). *Linear and nonlinear optical properties of metal-dielectric multilayer structures*. Unpublished doctoral dissertation, Georgia Institute of Technology, Georgia, United States of America.

Ozbay, E. (2010). Photonic metamaterials: Science meets magic. *IEEE Photonics J.*, *2*(2), 249-252.

Ozbay, E., Abeyta, A., Tuttle, G., Tringides, M., Biswas, R., Chan, C. T., et al. (1994). Measurement of a three-dimensional photonic band gap in a crystal structure made of dielectric rods. *Phys. Rev. B*, *50*(3), 1945-1948.

Ozbay, E., Michel, E., Tuttle, G., Biswas, R., Ho, K. M., Bostak, J., et al. (1994). Terahertz spectroscopy

of three-dimensional photonic band-gap crystals. *Opt. Lett.*, *19*(15), 1155-1157.

Ozbay, E., Michel, E., Tuttle, G., Biswas, R., Sigalas, M., & Ho, K. M. (1994). Micromachined millimeter-wave photonic band-gap crystals. *Appl. Phys. Lett.*, *64*(16), 2059-2061.

Padilla, W. J., Basov, D., & Smith, D. R. (2006). Negative refractive index metamaterials. *Materialstoday*, *9*(7-8), 28-35.

Pan, T., Zhuang, F., & Li, Z. (2003). Absolute photonic band gaps in a two-dimensional photonic crystal with hollow anisotropic rods. *Solid State Commun.*, *129*(2004), 501-506.

Parimi, P. V., Lu, W. T., Vodo, P., Sokoloff, J., Derov, J. S., & Sridhar, S. (2004). Negative refraction and left-handed electromagnetism in microwave photonic crystals. *Phys. Rev. Lett.*, *92*(12), 127401.

Parker, A. R. (2002). Natural photonic engineers. *Material Today*, *5*(9), 26-31.

Parmigiani, F., Finot, C., Mukasa, K., Ibsen, M., Roelens, M. A., Petropoulos, P., et al. (2006). Ultra-flat SPM-broadened spectra in a highly nonlinear fiber using parabolic pulses formed in a fiber Bragg grating. *Opt. Exp.*, *14*(17), 7617-7622.

Paul, H. (2004). *Introduction to quatum optics*. Cambridge University Press.

Pendry, J. B. (2000). Negative refraction makes a perfect lens. *Phys. Rev. Lett.*, *85*(18), 3966–3969.

Pendry, J. B. (2004). Negative refraction. *Contemporary Physics*, *45*(3), 191-202.

Pendry, J. B., Holden, A. J., Robbins, D. J., & Stewart, W. J. (1999). Magnetsim from conductors and enhanced nonlinear phenomena. *IEEE Trans. Microwave Theory and Techniques*, *47*(11), 2075-2084.

Pendry, J. B., Holden, A. J., Stewart, W. J., & Youngs, I. (1996). Extremely low frequency plasmons in metalic mesostructures. *Phys. Rev. Lett.*, *76*(25), 4773-4776.

Pendry, J. B., Holdent, A. J., Robbins, D. J., & Stewart, W. J. (1998). Low frequency plasmons in thin-wire structures. *J. Phys.: Condens. Matter*, *10*(22), 4785-4809.

Pendry, J. B., & Smith, D. R. (1991). Reversing light with negative refraction. *Phys. Today*, *57*(6), 37-43.

Plihal, M., & Maradudin, A. A. (1991). Photonic band structure of two-dimensional systems: The triangular lattice. *Phys. Rev. B*, *44*(16), 8565–8571.

Plihal, M., Shambrook, A., Maradudin, A. A., & Sheng, P. (1991). Two-dimensional photonic band structures. *Opt. Commun.*, *80*, 199-204.

Pliska, T., Cho, W. R., Meier, J., Le Duff, A. C., Ricci, V., Otomo, A., et al. (2000). Comparative study of nonlinear-optical polymers for guided-wave second-harmonic generation at telecommunication wavelengths. *J. Opt. Soc. Am. B*, *17*(9), 1554-1564.

Popov, A. K., Shalaev, M. I., Slabko, V. V., Myslivets, S. A., & Nefedov, I. S. (2013). Nonlinear backward-wave photonic metamaterials. *Adv. Sci. Technol.*, *77*, 246-252.

Popov, A. K., & Shalaev, V. M. (2006). Negative-index metamaterials: second-harmonic generation, Manley-Rowe relations and parametric amplification. *Appl. Phys. B*, *84*(1-2), 131-137.

Popov, A. K., Slabko, V. V., & Shalaev, V. M. (2006). Second harmonic generation in left-handed metamaterials. *Laser Phys. Lett.*, *3*(6), 293-297.

Powers, P. E., Ellingson, R. J., Pelouch, W. S., & Tang, C. L. (1993). Recent advances of the Ti: sapphire-pumped high-repetition-rate femtosecond optical parametric oscillator. *J. Opt. Soc. Am. B*, *10*(11), 2162-2167.

Quimby, R. S. (2006). *Photonics and lasers: An introduction*. John Wiley and Sons.

Rahman, F. A., Choudhury, P. K., Kumar, D., & Yusoff, Z. (2009). An analytical investigation of four-layer dielectric optical fibers with Au nano-coating a comparison with three-layer optical fibers. *Prog. Electromag. Res.*, *90*, 269-286.

Rajinder, S. (2002). C.V. Raman and discovery of the Raman effect. *Phys. in Perspective*, *4*(4), 399-420.

Ramakhrishna, S. A. (2005). Physics of negative refractive index material. *Rep. Prog. Phys.*, *68*(2), 449-551.

Rauh, H., & Genenko, Y. A. (2008). The effect of a superconducting surface layer on the optical properties of a dielectric photonic composite. *J. Phys.: Condens. Matter*, *20*(14), 145203.

Reid, D. T. (2001). Toward attosecond pulses. *Science*, *291*(5510), 1191-1192.

Ren, M. L., & Li, Z. Y. (2009). Giant enhancement of second harmonic generation in nonlinear photonic crystals with distributed bragg reflector mirrors. *Opt. Exp.*, *17*(17), 14502-14510.

Ribbing, C. G., Hogstrom, H., & Rung, A. (2006). Studies of polaritonic gaps in photonic crystals. *Appl. Opt.*, *45*(7), 1575-1582.

Rose, A., Huang, D., & Smith, D. R. (2000). Controlling the second harmonic in a phase-matched negative-index metamaterial. *Phys. Rev. Lett.*, *107*(6), 063902.

Rose, A., & Smith, D. R. (2011). Overcoming phase mismatch in nonlinear metamaterials. *Opt. Mat. Exp.*, *1*(7), 1232-1243.

Roychoudhuri, C. (2008). *Fundamentals of photonics*. SPIE Press.

Rudnick, J., & Stern, E. A. (1971). Second-harmonic radiation from metal surfaces. *Phys. Rev. B*, *4*(12), 4274–4290.

Rusu, M. (2006). *Frequency conversion using ultrashort fiber lasers*. Unpublished doctoral dissertation, Tampere University of Technology, Tampere, Finland.

Sajeev, J. (1987). Strong localization of photons in certain disordered dielectric superlattices. *Phys. Rev. Lett.*, *58*(23), 2486-2489.

Saleh, B. E. A., & Teich, M. C. (1991). *Fundamental of photonics*. John Wiley and Sons.

Sargsjan, G., Stamm, U., Unger, C., Zschocke, W., & Ledig, M. (1991). Characteristics of a neodymium-doped fiber laser mode-locked with a linear external cavity. *Opt. Commun.*, *89*(6), 480-486.

Scalora, M., Bloemer, M. J., Manka, A. S., Dowling, J. P., Bowden, C. M., Viswanathan, R., et al. (1997). Pulsed second-harmonic generation in nonlinear, one-dimensional, periodic structures. *Phys. Rev. A*, *56*(4), 3166–3174.

Schurig, D., Mock, J. J., Justice, B. J., Cummer, S. A., Pendry, J. B., Starr, A. F., et al. (2006). Metamaterial electromagnetic cloak at microwave frequencies. *Science*, *314*(5801), 977-980.

Scully, M. O., & Zubairy, M. S. (1997). *Quatum optics*. Cambridge University Press.

Shadrivov, I. V., Zharov, A. A., & Kivshar, Y. S. (2006). Second-harmonic generation in nonlinear left-handed metamaterials. *J. Opt. Soc. Am. B*, *23*(3), 529-534.

Shah, L., Tawney, J., Richardson, M., & Richardson, K. (2004). Self-focusing during femtosecond micromachining of silicate glasses. *IEEE J. Quantum Electron.*, *40*(1), 57-68.

Shah, L., Tawney, J., Richardson, M., & Richardson, K. (2005). Single-pulse femtosecond laser machining of glass. *J. Opt. A: Pure Appl. Opt.*, *7*(4), 162-168.

Shalaev, V. M. (2007). Optical negative-index metamaterials. *Nat. Photonics*, *1*, 41-48.

Sharmal, K. K. (2006). *Optics principle and applications*. Elsevier.

Shelby, R. A., Smith, D. R., Nemat-Nasser, S. C., & Schultz, S. (2001). Microwave transmission through a two-dimensional, isotropic, left-handed metamaterial. *Appl. Phys. Lett.*, *78*(4), 489-491.

Shelby, R. A., Smith, D. R., & Schultz, S. (2001). Experimental verification of a negative index of refraction. *Science*, *292*, 77-79.

Shen, H. B., Wang, Q. P., Zhang, Y. X., Liu, Z. J., Bai, F., Gao, L., et al. (2013). A frequency-doubled Nd:YAG/KTP laser at 561 nm with diode side-pumping. *Laser Phys.*, *23*(3), 035402.

Shen, Y. R. (1984). *The principles of nonlinear optics*. John Wiley and Sons.

Shen, Y. R. (1989). Surface properties probed by second-harmonic and sum-frequency generation. *Nature*, *337*, 519 - 525.

Shenoyu, M. R., Thyagarajan, K., & Ghatak, A. K. (1988). Numerical analysis of optical fibers using matrix approach. *IEEE J. Lightwave Techn.*, *6*(8), 1285-1291.

Shi, B., Jiang, Z. M., & Wang, X. (2001). Defective photonic crystals with greatly enhanced second-harmonic generation. *Opt. Lett.*, *26*(15), 1194-1196.

Shi, Y., Poulsen, C., Sejka, M., & Poulsen, O. (1994). Mode-locked Pr3+-doped silica fiber laser with an external cavity. *J. Lightwave Techn.*, *12*(5), 749-753.

Shields, J. H., & Ellis, J. W. (1956). Dispersion of birefringence of quartz in the near infrared. *J. Opt. Soc. Am.*, *46*(4), 263-265.

Shimizu, F. (1967). Frequency broadening in liquids by a short light pulse. *Phys. Rev. Lett.*, *19*(19), 1097-1100.

Shvets, G. (2003). Photonic approach to making a material with a negative index of refraction. *Phys. Rev. B*, *67*(3), 035109.

Sievenpiper, D. F., Sickmiller, M. E., & Yablonovitch, E. (1996). 3D wire mesh photonic crystal. *Phys. Rev. Lett*, *76*(14), 2480–2483.

Sihvola, A. (2007). Metamaterials in electromagnetics. *Metamaterials*, *1*(1), 2–11.

Sipe, J. E., & Boyd, R. W. (1992). Nonlinear susceptibility of composite optical materials in the Maxwell Garnett model. *Phys. Rev. A*, *46*(3), 1614–1629.

Smart, R. N., & Steel, W. H. (1959). Birefringence of quartz and calcite. *J. Opt. Soc. Am.*, *127*(7), 710-712.

Smith, D. R., & Kroll, N. (2000). Negative refractive index in left-handed materials. *Phys. Rev. Lett.*, *85*(14), 2933–2936.

Smith, D. R., Padilla, W. J., Vier, D. C., Nemat-Nasser, S. C., & Schultz, S. (2000). Composite medium with smiltaneously negative permeability and permittivity. *Phys. Rev. Lett.*, *84*(18), 4184-4187.

Smolyaninov, I. I., Smolyaninova, V. N., Kildishev, A. V., & Shalaev, V. M. (2009). Anisotropic metamaterials emulated by tapered waveguides: Application to optical cloaking. *Phys. Rev. Lett.*, *102*(21), 213901.

Soljacic, M., & Joannopoulos, J. D. (2004). Enhancement of nonlinear effects using photonic crystals. *Nature Materials*, *3*, 211 - 219.

Soljacic, M., Johnson, S. G., Fan, S., Ibanescu, M., Ippen, E., & Joannopoulos, J. D. (2002). Photonic-crystal slow-light enhancement of nonlinear phase sensitivity. *J. Opt. Soc. Am. B*, *19*(9), 2052-2059.

Sorokin, E., Ober, M. H., Sorokina, I., Wintner, E., Schmidt, A. J., Zagumennyi, A. I., et al. (1993). Femtosecond solid-state lasers using Nd^{3+}-doped mixed scandium garnets. *J. Opt. Soc. Am. B*, *10*(8), 1436-1442.

Soukoulis, C. M. (1996). *Photonic band gap materials*. Kluwer.

Soukoulis, C. M., Linden, S., & Wegener, M. (2007). Negative refractive index at optical wavelengths. *Science*, *315*(5808), 47-49.

Soukoulis, C. M., & Wegener, M. (2011). Past achievements and future challenges in the development of three-dimensional photonic metamaterials. *Nat. Photonics*, *5*, 523–530.

Spielmann, C., Burnett, N. H., Sartania, S., Koppitsch, R., Schnürer, M., Kan, C., et al. (1997). Generation of coherent X-rays in the water window using 5-femtosecond laser pulses. *Science*, *278*(5538), 661–664.

Spielmann, C., Krausz, F., Brabec, T., Wintner, E., & Schmidt, A. J. (1991). Femtosecond passive mode locking of a solid-state laser by a dispersively balanced nonlinear interferometer. *Appl. Phys. Lett.*, *58*(22), 2470-2472.

Stolen, R. H., & Lin, C. (1978). Self-phase-modulation in silica optical fibers. *Phys. Rev. A*, *17*(4), 1448–1453.

Sun, W., He, Q., Hao, J., & Zhou, L. (2011). A transparent metamaterial to manipulate electromagnetic wave polarizations. *Opt. Exp.*, *36*(6), 927-929.

Szilagyi, A., Hordvik, A., & Schlossberg, H. (1976). A quasi-phase-matching technique for efficient optical mixing and frequency doubling. *J. Appl. Phys.*, *47*(5), 2025-2032.

Takada, A., & Miyazawa, H. (1990). 30 Ghz picosecond pulse generation from actively mode-locked erbium-doped fibre laser. *Electron. Lett.*, *26*(3), 216-217.

Tang, S., Cho, D. J., Xu, H., Wu, W., Shen, Y. R., & Zhou, L. (2011). Nonlinear responses in optical metamaterials: theory and experiment. *Opt. Exp.*, *19*(19), 18283-18293.

Torres, J., Coquillat, D., Legros, R., Lascaray, J. P., Teppe, F., Scalbert, D., et al. (2004). Giant second-harmonic generation in a one-dimensional GaN photonic crystal. *Phys. Rev. B*, *69*(8), 085105.

Troparevsky, M. C., Sabau, A. S., Lupini, A. R., & Zhang, Z. (2010). Transfer-matrix formalism for the calculation of optical response in multilayer systems: from coherent to incoherent interference. *Opt. Exp.*, *18*(24), 24715-24721.

Tunyagi, A. R. (2004). *Non-collinear second harmonic generation in strontium barium niobate*. Unpublished doctoral dissertation, Universität Osnabrück, Osnabrück,Germany.

Tuong, P. V., Park, J. W., Lam, V. D., Jang, W. H., Choi, E. H., Nikitov, S., et al. (2012). Negative refractive index at the third-order resonance of flower-shaped metamaterial. *J. Lightwave Techn.*, *30*(22), 3451-3455.

Urata, Y., & Wada, S. (2005). 808-nm diode-pumped continuous-wave Tm:GdVO4 laser at room temperature. *Appl. Opt.*, *44*(15), 3087-3092.

Usuki, T., Sakuma, Y., Hirose, S., Takemoto, K., Yokoyama, N., Miyazawa, T., et al. (2006). Single-photon generator for optical telecommunication wavelength. *J. Phys.: Conf. Ser.*, *38*(1), 140-143.

Vardeny, Z. V., & Raikh, M. (2007). Light localized on the lattice. *Nature*, *446*, 37-38.

Veselago, V., Braginsky, L., Shklover, V., & Hafner, C. (2006). Negative refractive index materials. *J. Comput. Theor. Nanosci.*, *3*(2), 1-30.

Veselago, V. G. (1968). The electrodynamics of substances with simultaneously negative values of ε and

μ. *Sov. Phys. Usp.*, *10*(4), 509-514.

Villeneuve, P. R., & Piche´, M. (1992). Photonic band gaps in two-dimensional square and hexagonal lattices. *Phys. Rev. B*, *46*(8), 4969–4972.

Voronin, E. S., & Strizhevskii, V. L. (1979). Parametric up-conversion of infrared radiation and its applications. *Opt. Lett.*, *127*(22), 99-133.

Wang, R. L., Wang, R., Liu, R. J., Lu, X. H., Zhao, J., & Li, Z. Y. (2013). Origin of shape resonance in second-harmonic generation from metallic nanohole arrays. *Sci. Rep.*, *3*, 2358.

Wang, Z. Y., Chen, X. M., He, X. Q., & Fan, S. L. (2009). Photonic crystal narrow filters with negative refractive index structural defects. *Prog Electromagn Res*, *80*, 421-430.

Wang, Z. Y., Chen, X. M., He, X. Q., Fan, S. L., & Yan, W. Z. (2008). Photonic crystal narrow filters with negative refractive index structural defects. *Prog Electromagn Res*, *80*, 421-430.

Wigley, P. G. J., French, P. M. W., & R., T. J. (1990). Mode locking of a continuous wave neodymium doped fibre laser with a linear external cavity. *Electron. Lett.*, *26*(16), 1238-1239.

Wiltshire, M. C. K. (2001). Bending of light in the wrong way. *Science*, *292*(5514), 60-61.

Wongkasem, N., & Akyurtlu, A. (2006). Novel broadband terahertz negative refractive index metamaterials: Aanalysis and experiment. *Prog Electromagn Res*, *64*, 205-218.

Wu, C. J., & Chen, Y. L. (2011). Microwave properties of a high-temperature superconductor and ferromagnetic bilayer structure. *Prog Electromagn Res*, *111*(23), 433-445.

Wu, C. J., Liu, C. L., & Yang, T. J. (2011). Investigation of photonic band structure in a one-dimensional superconducting photonic crystal. *J. Opt. Soc. Am B*, *4*(11), 2089-2094.

Wu, Z., Hu, X., Yu, Z., Hu, W., Xu, F., & Lu, Y. (2010). Nonlinear plasmonic frequency conversion through quasiphase matching. *Phys. Rev. B*, *82*(15), 155107.

Xu, H., He, Q., Xiao, S., Xi, B., Hao, J., & Zhou, L. (2011). Tight-binding analysis of coupling effects in metamaterials. *J. Appl. Phys.*, *109*(2), 023103.

Xu, L., Chang, D., Niu, H., & Jia, S. (1989). Raman scattering and fluorescent spectra of $KTiOPO_4$ (KTP) crystal. *Chin. Phys. Lett.*, *6*(5), 225-228.

Xu, P., Ji, S. H., Zhu, S. N., Yu, S. Q., Sun, J., Wang, H. T., et al. (2004). Conical second harmonic generation in a two-dimensional $\chi^{(2)}$ photonic crystal: A hexagonally poled $LiTaO_3$ crystal. *Phys. Rev. Lett.*, *93*(13), 1133904.

Xu, Y. Z., Ren, X. M., Wang, Z. N., Zhang, X., & Huang, Y. Q. (2007). Flat supercontinuum generation at 1550nm in a dispersion-flattened microstructure fibre using picosecond pulse. *Chin. Phys. Lett.*, *24*(3), 734-737.

Yablonovitch, E. (1987). Inhibited spontaneous emission in solid-state physics and electronics. *Phys. Rev. Lett.*, *58*(20), 2059–2062.

Yablonovitch, E., & Gmitter, T. J. (1989). Photonic band structure: The face-centered-cubic case. *Phys. Rev. Lett.*, *63*(18), 1950–1953.

Yablonovitch, E., & Gmitter, T. J. (1990). Photonic band structure: The face-centered-cubic case. *J. Opt. Soc. Am. A*, *7*, 1792-1800.

Yablonovitch, E., Gmitter, T. J., & Leung, K. M. (1991). Photonic band structure: The face-centered-cubic case employing nonspherical atoms. *Phys. Rev. Lett.*, *67*(17), 2295–2298.

Yablonovitch, E., Gmitter, T. J., Meade, R. D., Rappe, A. M., Brommer, K. D., & Joannopoulos, J. D.

(1991). Donor and acceptor modes in photonic band structure. *Phys. Rev. Lett.*, *67*(24), 3380–3383.

Yamada, M., Nada, N., Satoh, M., & Watanabe, K. (1993). First-order quasi-phase matched $LiNbO_3$ waveguide periodically poled by applying an external field for efficient blue second-harmonic generation. *Appl. Phys. Lett.*, *62*(5), 435-436.

Yariv, A., & Yeh, P. (1977). Electromagnetic propagation in periodic stratified media. I birefringence, phase matching, and x-ray laser. *J. Opt. Soc. Am.*, *67*(4), 438-448.

Yariv, A., & Yeh, P. (1984). *Optical waves in crystal*. John Wiley and Sons.

Yee, K. S. (1966). Numerical solution of initial boundary value problems involving maxwell's equations in isotropic media. *IEEE Trans. Antennas Propag.*, *14*(3), 302-307.

Yeh, P. (1988). *Optical waves in layered media*. John Wiley and Sons.

Yeh, P., Yariv, A., & Hong, C. S. (1977). Electromagnetic propagation in periodic stratified media. I general theory. *J. Opt. Soc. Am.*, *67*(4), 423-438.

Yu, J., Shen, Y., Liu, X., Fu, R., Zi, J., & Zhu, Z. (2004). Absorption in one-dimensional metallic-dielectric photonic crystals. *J. Phys.: Condens. Matter*, *16*(7), L51-L56.

Yu, Y. J., Jin, G. Y., Wang, C., Chen, X. Y., Hao, D. W., & Guo, J. X. (2009). All-solid-state continuous-wave doubly resonant all-intracavity cyan laser at 500.8 nm by sum-frequency-mixing in double-crystal RTP generation. *Laser Phys. Lett.*, *6*(7), 513-516.

Yuffa, A. J., & Scales, J. A. (2012). Linear response law and causality in electrodynamics. *Eur. J. Phys.*, *33*(6), 1635-1650.

Zhang, C., Wei, H., Zhu, Y. Y., Wang, H. T., Zhu, S. N., & Ming, N. B. (2001). Third-harmonic generation in a general two-component quasi-periodic optical superlattice. *Opt. Lett.*, *26*(12), 899-901.

Zhou, B. K., Kane, T. J., Dixon, G. J., & Byer, R. L. (1985). Efficient, frequency-stable laser-diode-pumped Nd:YAG laser. *Opt. Lett.*, *10*(2), 62-64.

Zhou, D., & Biswas, R. (2008). Photonic crystal enhanced light-trapping in thin film solar cells. *J. Apply. Phys.*, *103*(9), 093102.

Zhou, S., Li, H., Fu, S., & Wang, X. (2009). Second harmonic generation from an antiferromagnetic film in one-dimensional photonic crystals. *Phys. Rev. B*, *80*(20), 205409.

Zhu, H., Zhang, G., C., H., Y., W., Huang, L., Chen, J., et al. (2007). Diode-side-pumped 131 W, 1319 nm single-wavelength cw Nd:YAG laser. *Appl. Opt.*, *46*(3), 384-388.

Zhu, S., Zhu, Y., & Ming, N. (1997). Quasi–phase-matched third-harmonic generation in a quasi-periodic optical superlattice. *Science*, *278*(5339), 843-846.

Ziolkowski, R. W., & Heyman, E. (2001). Wave propagation in media having negative permittivity and permeability. *Phys. Rev. E*, *64*(5), 056625.